Exploration of Bronzaphyrin – A 26π hexaphyrin[2.0.0.2.0.0] near infrared dye: Synthesis, structure & aromatic switching

A Thesis Submitted for the Degree of

DOCTOR OF PHILOSOPHY

By

M. V. Nanda Kishore

School of Chemistry
University of Hyderabad
Hyderabad-500 046
INDIA

November 2018

Dedicated

to

My Guruji

and

My family

TABLE OF CONTENTS

DECLARATION

I hereby declare that the matter embodied in the thesis entitled **"*Exploration of bronzaphyrin – A 26π hexaphyrin(2.0.0.2.0.0) near infrared dye: Synthesis, structure and aromatic switching*"** is the result of investigations carried out by me in the School of Chemistry, University of Hyderabad, Hyderabad, India under the supervision of **Prof. Pradeepta K. Panda** and it has not been submitted elsewhere for the award of any degree or diploma or membership, etc. This work is also free from plagiarism. I hereby agree that my thesis can be deposited in Shodhganga/INFLIBNET.

In keeping with the general practice of reporting scientific investigations, due acknowledgements have been made wherever the work described is based on the findings of other investigators. Any omission or error that might have occurred by oversight or error is sincerely regretted.

November 2018 **M. V. Nanda Kishore**

UNIVERSITY OF HYDERABAD
Central University (P.O.), Hyderabad-500046, INDIA

Pradeepta K. Panda
Professor
School of Chemistry

Tel: 91-40-23134818 (Office)
Fax: 91-40-23012460
E-mail: pkpsc@uohyd.ernet.in
pradeepta.panda@uohyd.ac.in

CERTIFICATE

This is to certify that the work described in this thesis entitled "***Exploration of bronzaphyrin – A 26π hexaphyrin(2.0.0.2.0.0) near infrared dye: Synthesis, structure and aromatic switching***" has been carried out by Mr. M. V. Nanda Kishore, holding the Reg. No. 08CHPH21 under my supervision, for partial fulfilment for the award of Doctor of Philosophy in Chemistry and the same has not been submitted elsewhere for any degree, which is a plagiarism free thesis.

Part of thesis have been:

A. Published in following journals

1) Kishore, M. V. N.; Panda, P. K. *Eur. J. Org. Chem*. **2017**, 5197; (**Chapter-3**).
2) Kishore, M. V. N.; Panda, P. K. *Chem. Commun.* **2018**, *54*, 13135; (**Chapter-3**).

B. Presented in the following conferences

1. APSC-2018; **2.** ICCCS-8, 2017; **3.** Chemfest-2015; **4**. NDCS-2012; **5**. Chemfest-2012; **6**. NDCS-2010.

Prof. Pradeepta K. Panda
(Thesis Supervisor)

Dean
School of Chemistry

PREFACE

The present thesis entitled "***Exploration of bronzaphyrin – A 26π hexaphyrin(2.0.0.2.0.0) near infrared dye: Synthesis, structure and aromatic switching***" is divided into five chapters. Basically, it describes the synthesis and exploration of bronzaphyrin, an expanded porphyrin. Although different kinds of expanded porphyrins pertaining to the number of pyrroles and/or meso positions and their combinations are well explored, there is still much scope in their effective synthesis, analyzing photophysical aspects, understanding structural diversities and investigating their NLO properties. In this aspect, the current work, presented in this thesis highlights the hassle-free synthesis of several novel bronzaphyrins, a 26π-aromatic expanded porphyrin displaying intense near infrared absorptions, which was ignored for more than two decades in spite of its early promise. Herein, the brief content included in the thesis is presented below.

In **chapter 1,** a brief description about various synthetic routes, structural features, conformational flexibilities along with aromaticity switching in expanded porphyrins. **Chapter 2** provides the information about the materials and methods used in the course of the investigation. In **chapter 3**, we have demonstrated an efficient one pot synthesis of acetylene and butadiyne bridged bipyrroles utilizing a modified Sonogashira coupling. The butadiyne bridge of one of the bipyrroles was employed in synthesizing terpyrroles, thereby demonstrating a much facile route in achieving the latter ones, which were then finally utilized in synthesizing dithia and all-aza bronzaphyrins. Solid state structural characterization done for the first time for this class of macrocycles revealed intriguing structural diversities and have showed the effect of substituents on both the periphery and inner core of the macrocycles. In **chapter 4**, we have successfully synthesized first aromatic tetrathiabronzaphyrin with an intense NIR absorption and emission, which shows switching between aromatic and nonaromatic systems via a radical intermediate. Finally, the **chapter 5** summarizes the findings of the present investigation.

November 2018 **M. V. Nanda Kishore**

Acknowledgement

I would like to acknowledge all the people who have helped me directly or indirectly to carry out my Ph.D. work in University of Hyderabad.

At first I would like to express my sincere and special gratitude to my supervisor **Prof. Pradeepta K. Panda** for his kind guidance, and encouragement. Especially his patience and way of logical thinking and analysis helped me in all the time of research work.

I would like to thank the former and present Deans, School of Chemistry, for their constant support and for allowing me to use the available facilities. I am extremely thankful individually to all the faculty members including doctoral committee members Prof. R. Balamurugan and Prof. K. Muralidharan of the School for their kind help and cooperation at various stages of my stay in the campus. I also thank all the non-teaching staff of the School of Chemistry, ACRHEM and CIL for their assistance on various occasions.

Council of Scientific and Industrial Research (CSIR), India is gratefully acknowledged for providing me the Junior and Senior research fellowships. In addition, SERB and DST-CERI, India are also greatly acknowledged for financial support.

I would like to thank our collaborator Prof. Dongho Kim for his contribution in required computational work. My sincere and special thanks also extends to Prof. M. V. Rajasekharan for his help in EPR studies.

I would also like to thank Prof. V. G. Anand (IISER, Pune) along with his research group (Dr. T. Y. Gopalakrishna) for helping in NICS and HOMA calculations.

A special thanks goes to all my lab mates, where I have been lucky enough to enjoy each of their company like a family member- Dr. Naren, Dr. Sanjeev, Dr. Tridib, Dr. Ritwik, Dr. Brijesh, Dr. Anup, Sathish, Obaiah, Vikranth, Prameela, Nagamaiah, Sameeta, Sipra, Jyotsna, Ishfaq, Jeladhara, Dr. Raju, Dr. Ujwal, Dr. Kurumurthy, Dr. Manasi, Dr. Chandrashekhar, Dr. Rahul, Dr. Sandip, Dr. Chinnayyaswami, Shamimul, Dr. Rajesh, Pramod, Rajasekhar, Samatha, Sateesh, Mahesh, Vidyasagar, Shantimoy, Sauradip, Srinivas, Sabhapati, Suganya, Ranjith, Muan, Dr. Bishnu, Jaypal, Chandu, Prasad, Preeti, Ramprasad, Rupinder, Arpita, Sajal, Swayam Prakash, Gopi sudheer, Sravan, Resma, Simran, Rajdeep, Shubham, Sreedhar, Shuvanker, Avinash, Bhargavi, Nitya, Apoorva, Rajneesh, Malobi, Anupam, Raza, Priya, Prem, Raviteja, Nitish, Arnab and Chitrak.

My pleasant association with some friends both in my M.Sc. and Ph.D. tenure inside and outside UOH such as Dr. Rajagopal reddy, Dr. Gangadhar, Dr. Ashwin kumar, Dr. Srinivas, Dr. Shivaji, Dr. Rajashekhar, Dr. Vanaja, Dr. Murali, Dr. Vikas, Dr. Raveendrababu, Dr. Naveen, Dr. Ramu, Dr. Sashikanth, Dr. Umakanth, Raghu Vijay, Dr. Karunakar, Dr. Venkatesh, Ganesh, Dr. Pavan, Durgaprasad is unforgettable.

I would like to thank all my seniors, juniors and friends from school of chemistry, whose names are not mentioned due to limited space.

I would like to thank all teachers in different educational levels, Veera manohar, Prabhakar Reddy, Mohan Rao, Prabhakar Rao, Ravindranath. I would also thank my childhood and college friends Bhavani, Murali, Sreenath, Satish, Vishnu, Varun, Mahesh, Amar, Revanth, Siva, Naresh, Wazeed, Srikanth, Aditya, Goutham, Manohar, Manasa, Rajesh, Bharath, Ashwin, Praveen, Mani, Bheem, Sudheer, Saidulu, Saida Rao, Ravi, Sharath, Naidu, Nagaraj, Chakri and all members of dynamic block.

Finally, I would like to express my love and gratitude to my parents M. Rama Chandra Moorthy and M. Janaki Lakshmi, and family members Sesha Phani Sarma, Vasudha Bhargavi, Neelesh, Chinmai, Muni Sankar, Kowsik, Neelima, Ananya, madam for their unconditional love and blessings and my deepest gratitude for the families of my uncles Chalapathi and Prasad. They made me what I am today and I owe everything to them. Dedicating this thesis to them is a minor recognition for their persistent support and love.

November 2018 **M. V. Nanda Kishore**

University of Hyderabad

LIST OF ABBREVIATIONS

abs	absorbance
AcOH	Acetic acid
Ac_2O	Acetic anhydride
anhyd	anhydrous
aq.	aqueous
atm	atmosphere
Å	Angstrom
a.u.	arbitrary unit
$BF_3.OEt_2$	Borontrifluoride diethyletherate
bp	boiling point
B_2Pin_2	Bis(pinacoleto)diboron
t-Bu	tert-butyl
CCDC	Cambridge Crystallographic Data Centre
CMSD	Centre for Modelling, Simulation & Design
CIF	Crystallographic information file
cm	Centimeter (s)
conc.	Concentrated
CuCl	Copper(I)chloride
CV	Cyclic voltammetry
d	Doublet
dd	Doublet of doublet
δ	chemical shift in parts per million
°	Degree
°C	Degree Celsius
DBU	1,8-Diazabicyclo[5.4.0]undec-7-ene
DCE	1,2-Dichloroethane
DCM	Dichloromethane
DFT	Density Functional Theory
diff.	Diffraction
DMF	Dimethylformamide
DMSO	Dimethylsulphoxide

DNA	Deoxyribonucleic acid
D_2O	Deuterium oxide
DPV	Differential pulse voltammetry
dt	Doublet triplet
dtbpy	4,4′-Di-*tert*-butyl-2,2′-dipyridyl
E	Energy
ε	Epsilon (molar extinction coefficient)
e.g.	For example
EPR	Electron paramagnetic resonance
eq.	Equivalent
Equiv.	Equivalent
eV	Electron volt
ESI	Electrospray Ionization
et al.	and others
etc	et cetera (and other similar things)
EtOH	Ethanol
fl	fluorescence
FT	Fourier transform
g	gram
GOF	Goodness of fit
h	Hour (s)
H-bond	hydrogen bond
HBr	Hydrobromic acid
HCl	Hydrochloric acid
HOMA	Harmonic oscillator model of aromaticity
HOMO	Highest occupied molecular orbital
HPLC	High-performance liquid chromatography
HRMS	High resolution-mass spectrometry
Hz	Hertz
I_2	Iodine
i.e.	that is
IPA	Isopropanol

IR	Infrared
J	coupling constant (in NMR)
KBr	Potassium bromide
K_2CO_3	Potassium carbonate
KF	Potassium fluoride
KI	Potassium iodide
KO_2	Potassium superoxide
KOH	Potassium hydroxide
L	Liter
LC	liquid chromatography
lit.	Literature
log	Logarithm
LUMO	Lowest unoccupied molecular orbital
µ	micro
M	moles per liter
m	meta (structure); multiplet (NMR); milli (unit)
mA	milliampere
MeOH	Methanol
mg	milligram
$MgSO_4$	Magnesium sulfate
MHz	megahertz
min	Minute (s)
mL	milliliter
mp	melting point
MnO_2	Manganese dioxide
MS	mass spectrometry
MSA	Methanesulfonic acid
m/z	mass to charge ratio (in mass spectrometry)
MTBE	Methyl *tert*-butylether
NaOAc	Sodium acetate
NaCl	Sodium chloride
Na_2CO_3	Sodium carbonate

NaH	Sodium hydride
Na_2S	Sodium sulfide
Na_2SO_4	Sodium sulfate
$Na_2S_2O_3$	Sodium thiosulfate
$Na_2S_2O_4$	Sodium dithionite
NBS	N-bromosuccinimide
NH_4Cl	Ammonium chloride
NICS	Nucleus independent chemical shift
NLO	Nonlinear optical
nm	nanometer (s)
NMR	Nuclear magnetic resonance
N,N-DMAc	N,N-dimethylacetamide
N,N-DMBz	N,N-dimethylbenzamide
ns	nanosecond (s)
o	ortho
ORTEP	Oak Ridge thermal ellipsoid Plot
p	para
Pd/C	Palladium(0) on activated carbon (charcoal)
i-Pr	isopropyl
$POCl_3$	Phosphorous oxychloride
PPh_3	Triphenyl phosphene
ppm	parts per million
p-TSA	*p*-Toluenesulfonic acid
q	quartet
rt	room temperature
s	singlet
sat.	saturated
t	triplet
TD-DFT	Time dependent density functional theory
TEA	Triethylamine
TFA	Trifluoroacetic acid
THF	Tetrahydrofuran

$TiCl_4$	Titanium tetrachloride
TLC	Thin layer chromatography
TMS	Tetramethylsilane
TMSA	Trimethylsilylacetylene
TOSMIC	Tosylmethylisocyanide
TPA	Two photon absorption
UV-vis-NIR	Ultraviolet-visible-near infrared
viz.	namely
vs	versus (against)
w.r.t.	with respect to
XRD	X-ray diffraction
Z	Formula units in the unit cell
Zn	Zinc

CHAPTER 1

Introduction

1.1 Porphyrins

Porphyrins are the macrocyclic dyes well known for their pivotal role in most of the biological processes such as photosynthesis (Chlorophyll a), oxygen storage and transport (Heme B), as cofactor in DNA synthesis (Vitamin B_{12}) to name a few (Figure 1.1). As life heavily relies on these processes porphyrins are often called "pigments of life".[1] The name porphyrin comes from the Greek word *'porphyros'* meaning purple. Apart from its multiple biological functions, its absorption and emission properties, strong aromaticity and ability of binding to most of the metals in the periodic table made it as the most widely studied macrocycle among all ring systems present.[2]

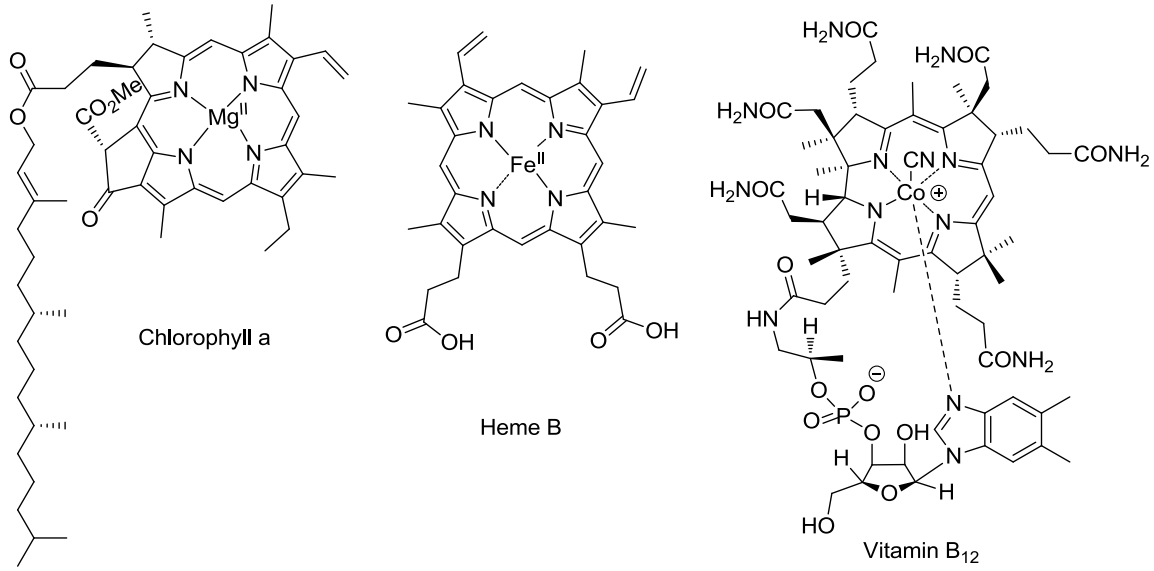

Figure 1.1 Structures of some biologically important porphyrins

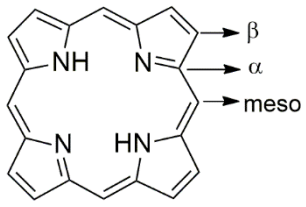

Figure 1.2 Porphyrin

A porphyrin skeleton (Figure 1.2) generally consists of four pyrrole subunits along with four methine bridges connected in a coplanar fashion at their α-carbon atoms to give almost a square planar geometry. Porphyrins contain 22π electrons of which 18π electrons are in conjugation giving it a strong absorption band in near UV region termed to be Soret band.[3] Understanding of porphyrins began as early as 1840s[4] creating a lot of interest to study its photophysical, optical, chemical and biological properties involving wide variety of fields such as optoelectronics, material chemistry, catalysis, as photosensitizers in photodynamic therapy etc. This vital role in different fields led to a new research area in developing more synthetic systems such as contracted, isomeric, expanded, inverted,

confused and core modified porphyrins that bear similar resemblance to naturally occurring macrocycles but being chemically quite different.[2]

1.2 Nomenclature

The terms α and β have been defined to indicate the 2,5 and 3,4 positions of pyrrole whereas "*meso*" or meso like term has been used for the bridging carbon atoms. Traditionally they are more popularized by their trivial names which have been coined by their creators based on their color or structural features. The suffix "phyrin" or "rin" has been used generally at the end which was started initially by R. B. Woodward by naming a pentapyrrolic macrocycle as "Sapphyrin" due to its blue sapphire color in its solid state.[5] Different groups led by Sessler also followed this trend by naming porphyrins in a similar fashion such as rubyrin, amethyrin, orangarin, platyrin etc.[6]

The systematic nomenclature of porphyrin analogues for the first time was defined by Franck and Nonn which has been divided into three parts.[7] The first part, a square-bracketed prefix indicates the number of π electrons in conjugation pathway followed by second part, a core name indicating the number of heterocyclic subunits and the third part, a round-bracketed suffix which indicates the number of bridging carbon atoms between the heterocyclic subunits starting from the largest unit. Hence according to this nomenclature porphyrin **1.1** (Figure 1.2) can be termed as [18]porphyrin-(1.1.1.1) indicating the 18π electron conjugation pathway with four separated meso carbon atoms bridging four pyrroles. Similarly, as shown in Figure 1.3, porphycene **1.2**, an isomer of porphyrin was termed [18]porphyrin-(2.0.2.0), sapphyrin **1.3** as [22]pentaphyrin-(1.1.1.1.0) and rubyrin **1.4** as [26]hexaphyrin-(1.1.0.1.1.0).

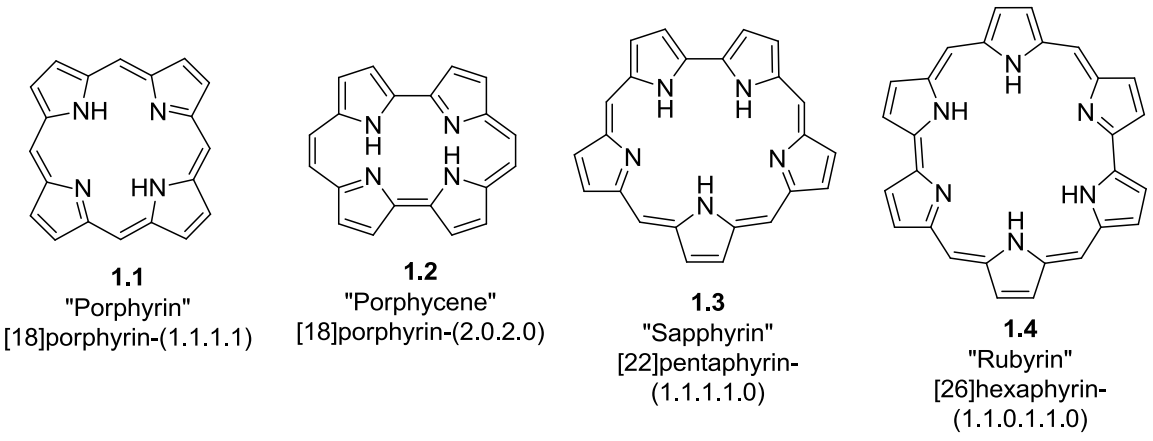

Figure 1.3 Nomenclature of some porphyrins according to Franck's approach.

Porphyrins can be broadly listed into three categories: contracted, isomeric and expanded porphyrins. An elaborative discussion will be done only for expanded porphyrins as this thesis will be mainly focusing on them.

1.3 Contracted porphyrins

Synthesis of first contracted porphyrin, corrole **1.5** (Figure 1.4) (one meso carbon less than porphyrin) was reported by Johnson and coworkers in 1964 while trying to synthesize Vitamin B_{12}.[8] Though corrole is an 18π system similar to that of porphyrin, it acts as a trianionic ligand by stabilizing metals in their higher oxidation state and the metal-nitrogen bonds are also more covalent in metallocorroles than those in metalloporphyrins. Synthetic chemistry of corroles started on a high note after 1999, when two independent research groups led by Zeev Gross[9] and Roberto Paolesse[10] reported one pot synthesis of meso substituted corroles from pyrrole and corresponding aromatic aldehydes. Due to unique stabilization of high valent transition metals and very rich photophysical properties corroles find their major use in materials chemistry as well as stress-induced diseases and in cancer theranostics.[11]

Subporphyrin **1.6**, the true congener of contracted porphyrin (removing one pyrrole and one meso carbon each), was reported by Osuka and coworkers in 2006.[12] Obtained by the templated synthesis, this molecule has a 14π electron conjugation pathway with boron atom sitting slightly above the macrocyclic plane leading to a bowl shape. Synthesis of boron-free subporphyrin is still a challenge, though to some extent a boron free analogous compound, subpyriporphyrin **1.7** containing one pyridine in place of a pyrrole ring was reported by Latos-Grażyński following a "2+1" approach.[13]

Triphyrins can be dated back to 1964, where Badger et al. reported heteroatom bridged macrocycles containing 18π conjugation pathway.[14] These systems were later developed by Vogel and Cava groups using McMurry coupling from their corresponding 2,5-diformyl precursors. Later, Latos-Grażyński and Yamada groups demonstrated triphyrin **1.8** synthesis and rich coordination chemistry by isolating their freebase structures.[15]

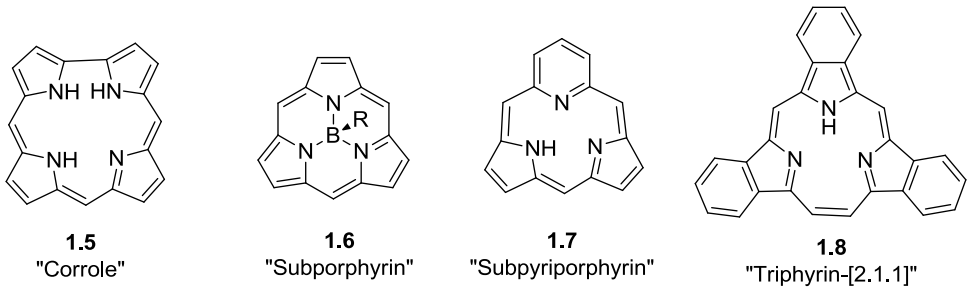

1.5 "Corrole" **1.6** "Subporphyrin" **1.7** "Subpyriporphyrin" **1.8** "Triphyrin-[2.1.1]"

Figure 1.4 Some examples of contracted porphyrins.

1.4 Isomeric porphyrins

Porphyrinic isomers can be classified into two categories. The first of its kind will be having the same N_4 core but only differ in the arrangement of pyrrole-linking carbon atoms, for example, porphycene, corrphycene, hemiporphycene etc., while the other category contains minimum one of its pyrrole ring confused or inverted to give an N_3C core.[16]

The first constitutional isomer of porphyrin was reported in 1986 by an annulene chemist Vogel and coworkers, which has been termed porphycene due to its close resemblance to both porphyrin and acene.[17] It is the most stable porphyrin isomer and got wide spread attention due to its interesting photophysical properties.[18a] The reduced symmetry of the porphycene causes a bathochromic shift and a very large ΔLUMO gap leading to its more intensified Q bands in the absorption spectrum when compared to normal porphyrin.[18] This aspect stimulated a number of researchers to explore its utility as a potential photosensitizer for photodynamic therapy (PDT), material chemistry, catalysis and solar cells.[19] Corrphycene **1.9**,[20] hemiporphycene **1.10**,[21] and isoporphycene **1.11**[22] (Figure 1.5) reported later by both Vogel and Sessler groups did not receive much attention owing to their synthetic difficulties.

N-confused porphyrin **1.12** was first reported in 1994 by two independent groups, Furuta and Latos-Grażyński.[23] Further improvement in terms of yield was developed by Lindsey and coworkers in 1999 by using methanesulfonic acid.[24] Their unique role in supramolecular chemistry in terms of its confusion of pyrrole ring in coordination chemistry, its anion binding ability and as sensitizer for singlet oxygen generation created a lot of interest. Apart from these carbaporphyrinoids,[25] where one or more pyrrole rings replaced with cyclopentadiene, benzene or azulene, and core modified porphyrinoids **1.13**[26] were also developed.

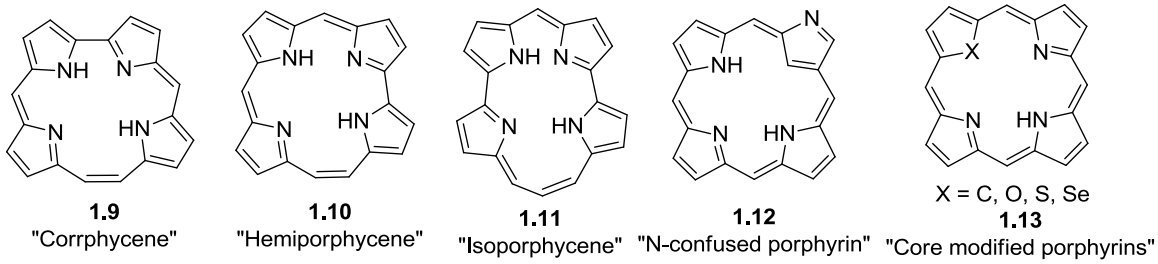

1.9 "Corrphycene" **1.10** "Hemiporphycene" **1.11** "Isoporphycene" **1.12** "N-confused porphyrin" **1.13** "Core modified porphyrins"

Figure 1.5 Some examples of isomeric porphyrins.

1.5 Expanded porphyrins

According to a review in 2003 by Sessler, expanded porphyrins can be defined as "macrocycles that contain pyrrole, furan, thiophene, or other heterocyclic subunits linked together either directly or through one or more spacer atoms in such a manner that the internal ring pathway contains a minimum of 17 atoms."[27] The serendipitous discovery of expanded porphyrin was reported by Woodward and coworkers in 1966 while trying to synthesize Vitamin B_{12} although full report was published only in 1983.[5] The rational synthesis of sapphyrin was then reported by Johnson and his coworkers in 1972.[28] Later on, the groups of LeGeoff, Franck and Vogel developed the stretched systems like platyrins **1.14**,[29] vinylogous porphyrins **1.15**[7] (Figure 1.6) and acetylene-cumulene porphyrinoids.[30] The pentapyrrolic and hexapyrrolic systems, pentaphyrin and hexaphyrin **1.16** were first reported by Gossauer's group[31] and was later developed in a one pot synthesis by Osuka and his coworkers.[32] But the major contribution in exploring different expanded porphyrins such as texaphyrins **1.17**,[33] improved synthesis of sapphyrins,[34] rubyrins,[35] rosarins,[36] turcasarin **1.18**[37] came from Sessler and his coworkers. Combined efforts from all the groups have led to renaissance in expanded porphyrin chemistry demonstrating their potential utility in anion recognition, MRI (magnetic resonance imaging) contrasting agents, in photodynamic therapy (PDT), understanding aromaticity and as non-linear optical (NLO) materials.[38]

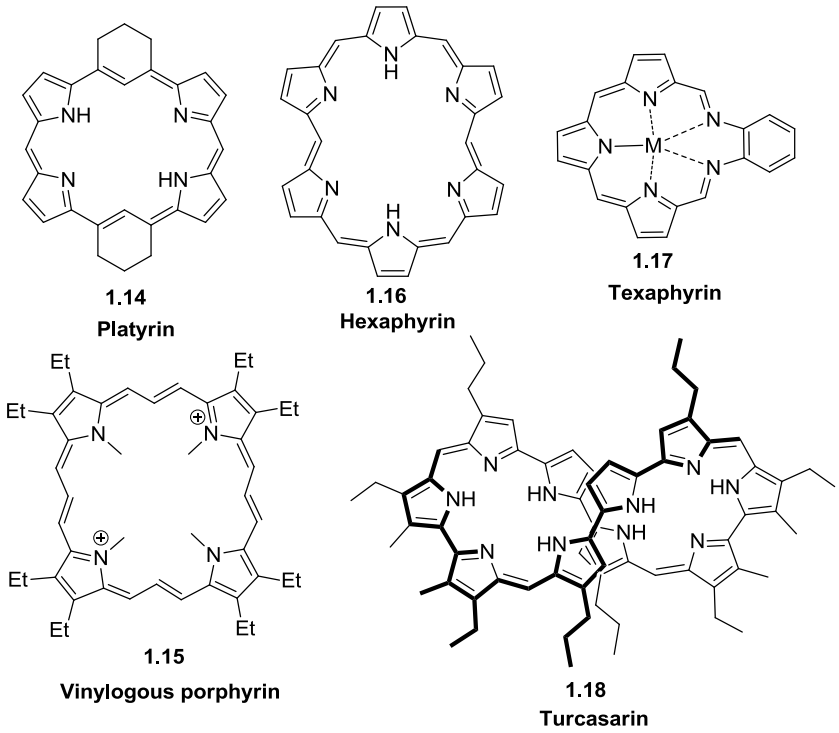

Figure 1.6 Some examples of expanded porphyrins.

1.5.1 Synthesis

Early stages of research in expanded porphyrins were mainly focused on β-substituted derivatives synthesized mainly by either acid-catalyzed condensation or oxidative coupling reactions. Meso aryl substituted expanded porphyrins were later stabilized by introducing electron withdrawing substituents.[38] Rather than discussing about the synthesis of different expanded porphyrins, here it will be accounted keeping in view different methodologies employed during their synthesis. Though a large number of expanded porphyrins have been reported since the past few decades, the ways of achieving the target molecules i.e. different types of reactions used to obtain them were very less. Here we have classified them into different categories and for each category few examples have been discussed.

1.5.1.1 MacDonald condensation

Using dipyrrylmethanes as intermediates MacDonald's group developed an efficient condensation reaction for synthesizing meso-unsubstituted porphyrins.[39] This methodology gained much attention after Johnson and coworkers reported the first rational synthesis of sapphyrin in a "3 + 2" approach involving tripyrromethane diacid and bifuran dialdehyde, as shown in Scheme 1.[28] This approach was later extended to "4

+ 1" systems as well, albeit in lesser yields by Woodward's group.[5] Improved yields were later reported by Lash et.al using dilute aq. ferric chloride as oxidizing agent.[40]

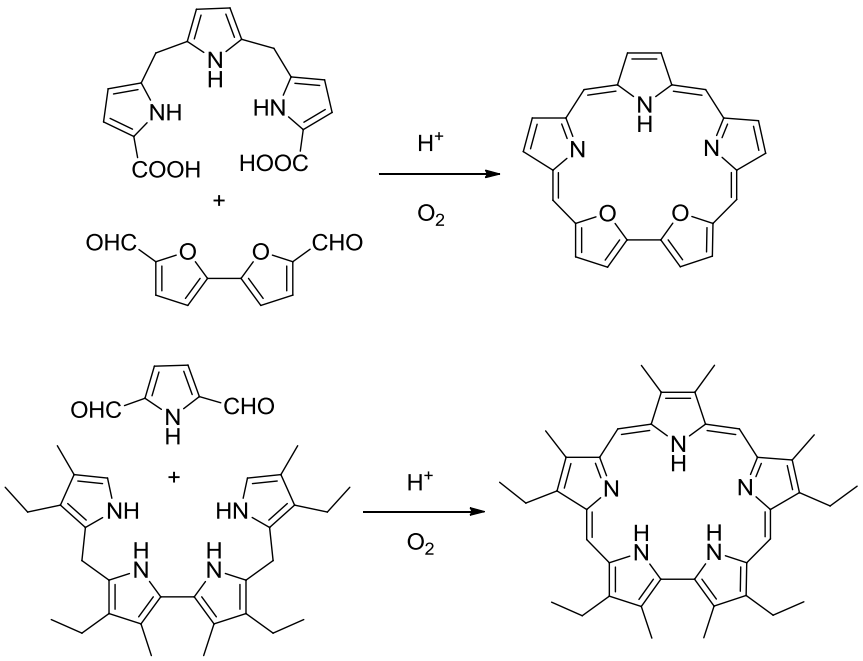

Scheme 1 Rational synthesis of sapphyrins showing "3+2" and "4+1" approaches.

Turcasarin, a giant decapyrrolic system, was reported by Sessler's group, which involves a "3 + 2 + 3 + 2" type MacDonald condensation of terpyrrole and bipyrrole dialdehyde (Scheme 2).[37]

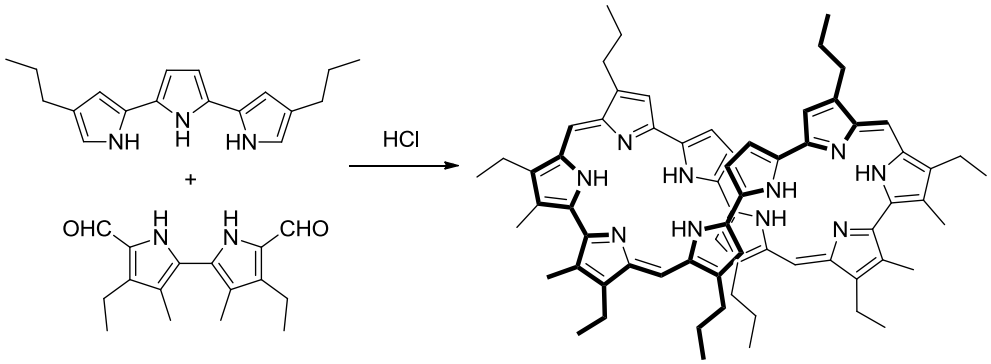

Scheme 2 Synthesis of turcasarin.

1.5.1.2 Rothemund synthesis

A modified Rothemund synthesis was first employed by Gossauer and coworkers in synthesizing hexaphyrin.[31] While the MacDonald condensation always yields an even number of subunits in an expanded porphyrin, Sessler and his coworkers utilized Rothemund method in synthesizing rosarin, an expanded porphyrin with odd number of bipyrrolic units, as shown in Scheme 3.[36]

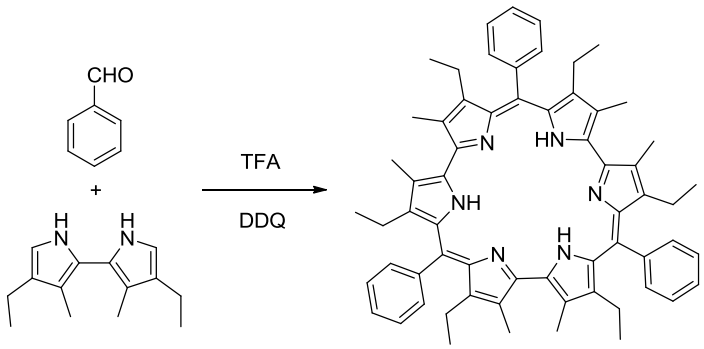

Scheme 3 Synthesis of rosarin using modified Rothemund reaction.

Setsune and his coworkers replacing the benzaldehyde with bulky 2,6-dichlorobenzaldehyde able to isolate a number of giant expanded porphyrins, including hexadecaphyrin (route A, Scheme 4). By using an alternate novel synthetic strategy, where the bipyrrole was replaced with diazafulvene, they could able to succeed in preparing super expanded porphyrin containing 24 pyrrole rings displaying zigzag-shaped folding conformations (route B, Scheme 4) but still hexadecaphyrin remains the largest structurally characterized expanded porphyrin till date.[41]

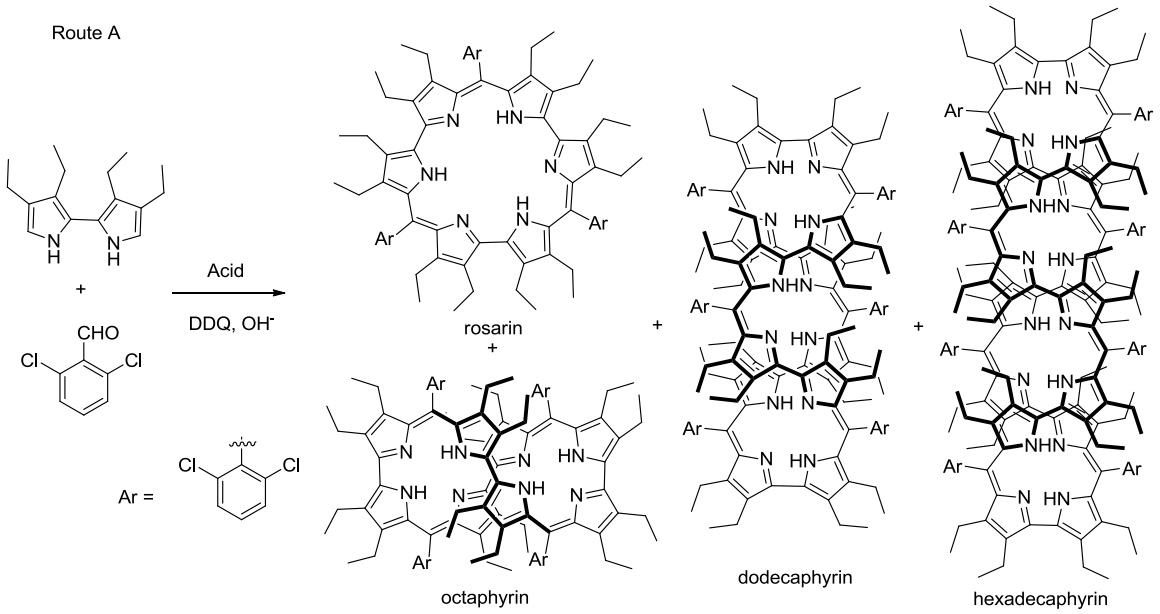

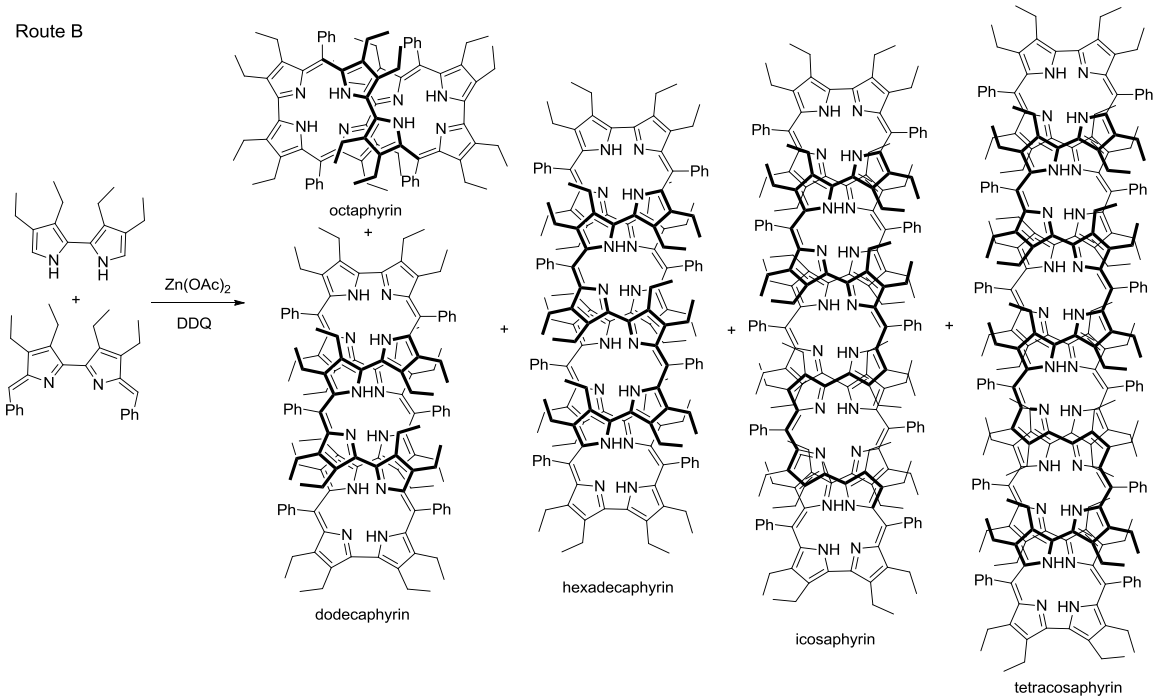

Scheme 4 Synthesis of giant expanded porphyrins using modified Rothemund reaction (route A) and diazafulvene approach (route B).

Later, Osuka's group developed one pot synthesis of meso-aryl substituted expanded porphyrins using Rothemund-Lindsey protocol involving $BF_3.OEt_2$ catalyzed condensation of pyrrole and pentafluorobenzaldehyde (Scheme 5).[32]

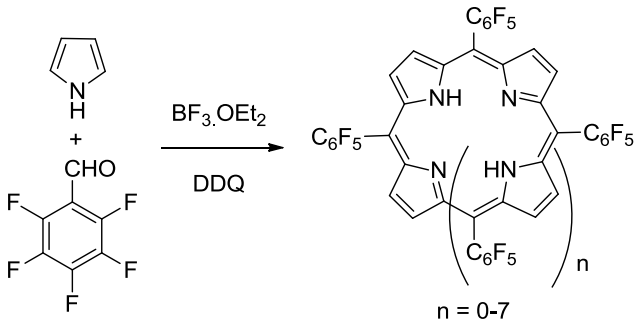

Scheme 5 One pot **s**ynthesis of meso aryl expanded porphyrins.

Recently, Lee and his coworkers have condensed in Rothemund fashion using a structurally rigid naphthobipyrrole with pentafluorobenzaldehyde to give both rubyrin and inverted sapphyrin macrocycles, as shown in Scheme 6.[42]

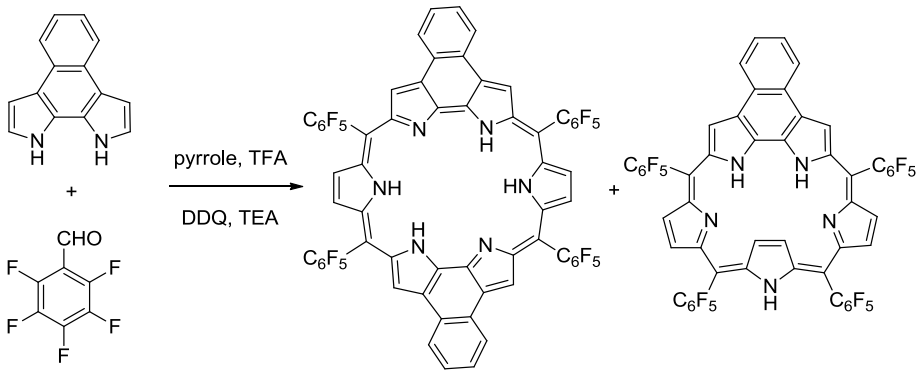

Scheme 6 Synthesis of rubyrin and inverted sapphyrin.

1.5.1.3 Oxidative coupling

Chandrashekar and coworkers inspired by the synthesis of sapphyrin in Rothemund synthesis[43] reacted modified tripyrranes under proper acid catalyst to undergo oxidative coupling to yield rubyrin for the first time (Scheme 7).[44]

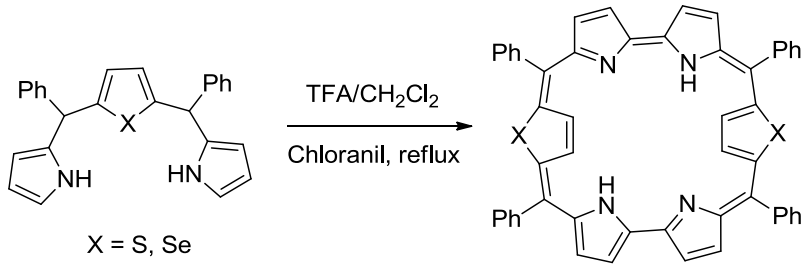

Scheme 7 Synthesis of rubyrin by oxidative coupling.

Later, Sessler's group employed the oxidative coupling in presence of sodium dichromate in synthesizing [32]octaphyrin(1.0.0.0.1.0.0.0) from a linear tetrapyrrolic precursor, as shown in Scheme 8.[45]

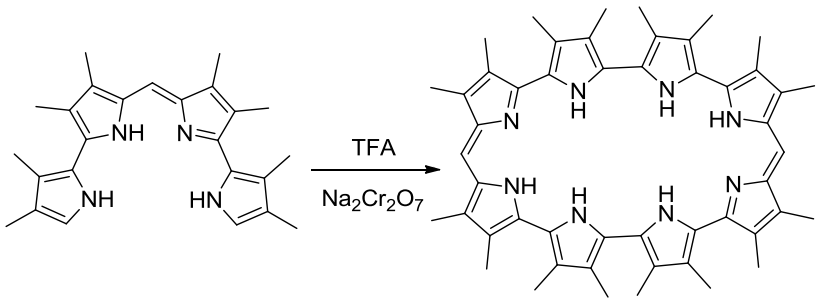

Scheme 8 Synthesis of [32]octaphyrin by oxidative coupling.

The same group utilizing the template based methodology synthesized cyclo[8]pyrroles under carefully optimized biphasic conditions (bipyrroles in CH_2Cl_2 and $FeCl_3$ in 1M H_2SO_4), as shown in Scheme 9,[46] which was later applied by Panda and coworkers to obtain structurally rigid cyclo[4]naphthobipyrroles.[47]

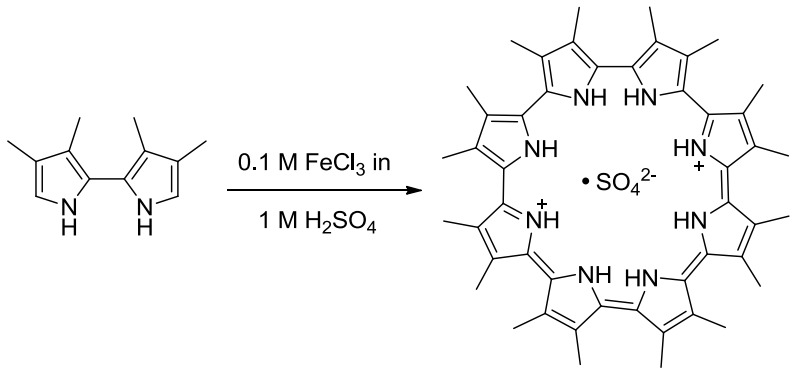

Scheme 9 Synthesis of cyclo[8]pyrrole by oxidative coupling strategy.

1.5.1.4 McMurry coupling

The first porphyrinic isomer, porphycene was synthesized employing this methodology (generated Ti^0 by using $Zn/TiCl_4$) by Vogel's group.[17] Later, they extended this procedure in synthesizing expanded porphycenes with ethylene and acetylene bridges (Scheme 10).[30]

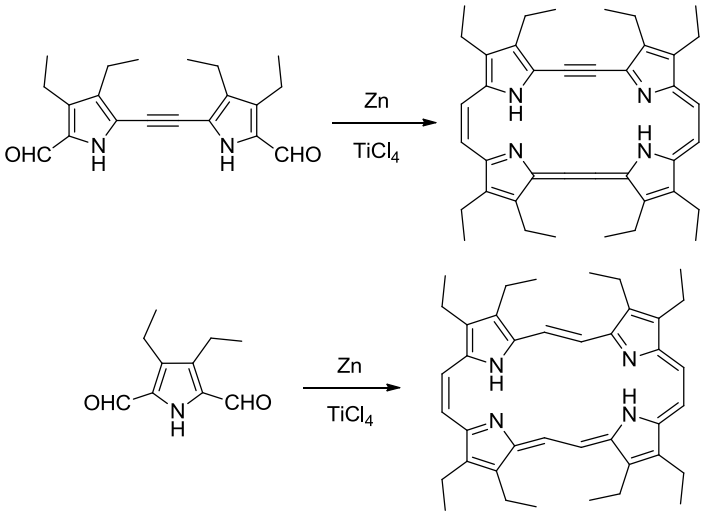

Scheme 10 Synthesis of stretched porphycenes.

Ibers, Johnson and coworkers utilized this approach to develop bronzaphyrins from their corresponding terpyrrole precursor, as shown in Scheme 11.[48]

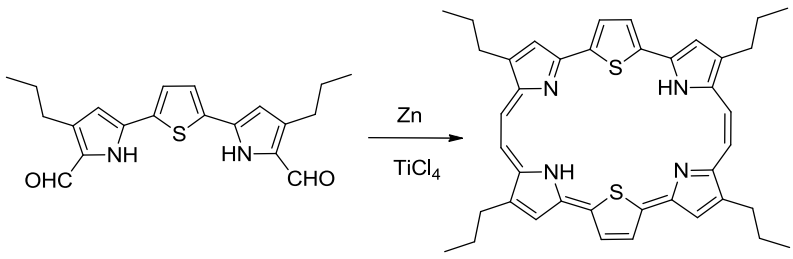

Scheme 11 Synthesis of bronzaphyrin from its terpyrrole precursor.

Recently, Rana et al. applied this strategy in synthesizing stable expanded porphycenes showing diradicaloid and tetraradicaloid characters.[49]

1.5.1.5 Other synthetic methods

A one pot synthesis of indene incorporated aromatic hexaphyrin was reported by Peterson and his coworkers due to an unexpected *in situ* annulation during "2 + 2" condensation of *β*-alkyl-substituted dipyrromethanes with 2-ethynylbenzaldehyde (Scheme 12).[50]

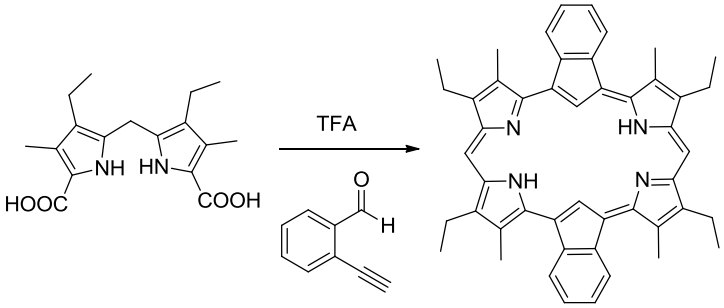

Scheme 12 One pot synthesis of indene expanded porphyrin.

An electrochemical synthesis, involving less expensive and no toxic reagents, was developed as an alternative to chemical oxidative coupling by Bucher and Sessler's group in synthesizing core modified cyclo[9]pyrrole, as shown in Scheme 13.[51]

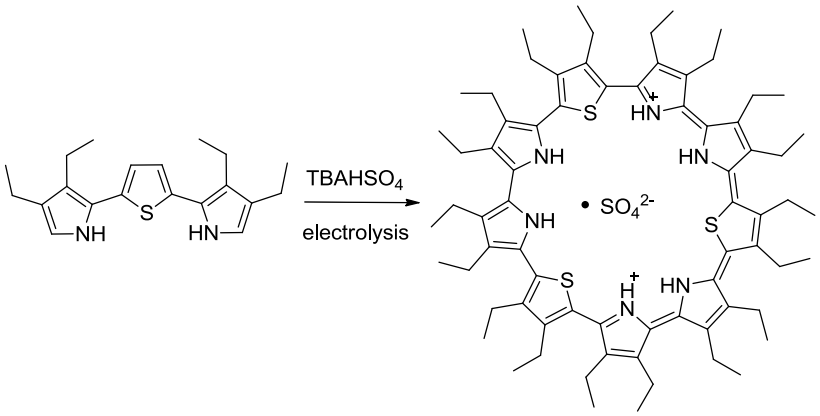

Scheme 13 Electrochemical synthesis of cyclo[9]pyrrole.

Umetani et al. applying ring expansion strategy utilized Fritsch–Buttenberg–Wiechell rearrangement for transforming tetrabromoporphoquinodimethane into an antiaromatic [20]porphyrin(2.1.2.1), as shown in Scheme 14.[52]

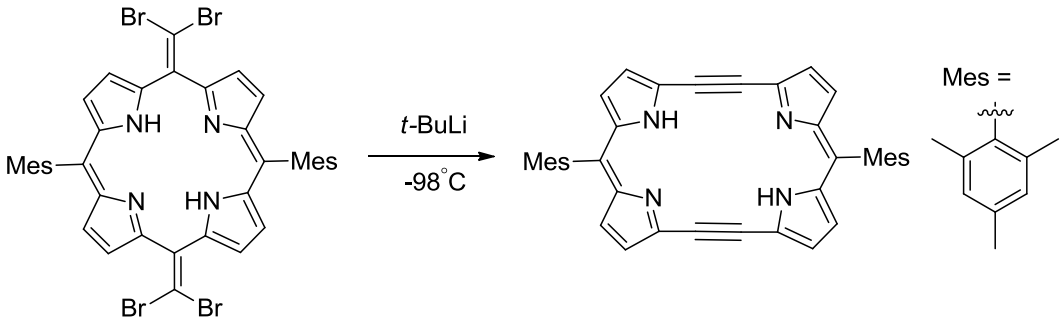

Scheme 14 Synthesis of antiaromatic [20]porphyrin(2.1.2.1).

1.5.2 Structural aspects

Understanding the structural diversity and flexibility of expanded porphyrins could be very much useful and instrumental in designing or redesigning of macrocyclic frameworks for their utility in appropriate fields. For example, designing an expanded porphyrin to bind multiple ions through different coordinating compartments adjacent to one another may give intriguing possibilities for generating synergic effects.[53] Expanded porphyrins are widely considered to share two structural features: 1) a large and flexible π-conjugated electronic network leading to good solubility, high aromaticity (anti) and unique photophysical properties, including absorption and fluorescence in near infrared (NIR) region and 2) amine-imine interconvertible pyrrole subunits arranged regularly to attain a facile interconversion between variable π-electronic states, metal coordination, anion binding and intra/intermolecular hydrogen bonding interactions.[38]

The conformational flexibility of expanded porphyrins, which directs the electronic, optical and coordination properties, depends on the following factors: 1) intrinsic structural constraints arising from a conjugated cyclic structure, 2) peripheral substituents at the meso and/or β-positions, 3) intra/intermolecular hydrogen bonding, 4) the temperature, 5) solvent polarity and 6) aromatic versus antiaromatic characters of electronic π-system.[38] It also depends on the nature and number of heteroatoms present in the cavity and protonation by acids.[54] The conformational changes in meso aryl sapphyrin were first reported for the neutral and protonated states by Latos-Grażyński's group, as shown in Figure 1.7.[55]

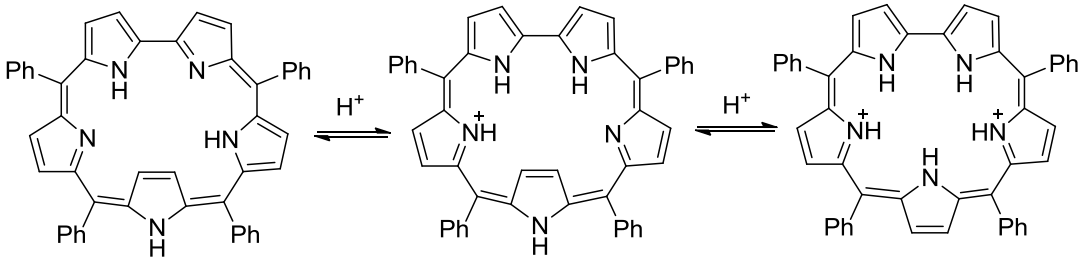

Figure 1.7 Protonation induced conformational switching in meso-tetraphenylsapphyrin.

It is indeed observed that β-alkyl substituted sapphyrins, both free base and its protonated forms, exhibit normal structure, in which all the nitrogens will be pointing inward towards the macrocyclic core, while the meso-aryl substituted sapphyrins show structural diversity by also exhibiting inverted structure, wherein, the nitrogen atom of the pyrrole ring opposite to the bipyrrole unit, points outward from the macrocyclic core.[53] For instance, the structurally rigid naphthobipyrrole substituted β-alkyl sapphyrin doesn't

show any changes upon protonation but the meso aryl substituted sapphyrin undergoes flipping of pyrrole opposite to the naphthobipyrrole moiety upon mono protonation (Figure 1.8).[56]

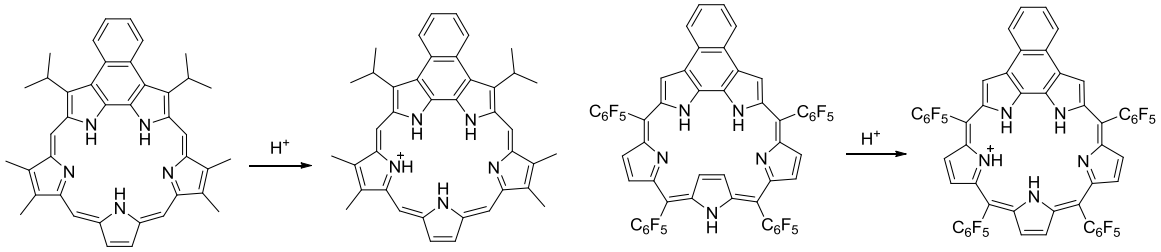

Figure 1.8 Conformational switching in naphthobipyrrole substituted sapphyrins.

Interestingly, it was also observed that the molecular geometry of macrocyclic cation strongly depends on the choice of the acid. The below example of inverted rubyrin containing inverted bipyrrole (one of the pyrrole of the bipyrroles are inverted), when treated with HCl converts to normal form having a bowl like structure with all nitrogens pointing into the cavity but on treatment with TFA it adopts a rectangular conformation in which the two bridged pyrrole rings point outward from the macrocyclic core (Figure 1.9).[57]

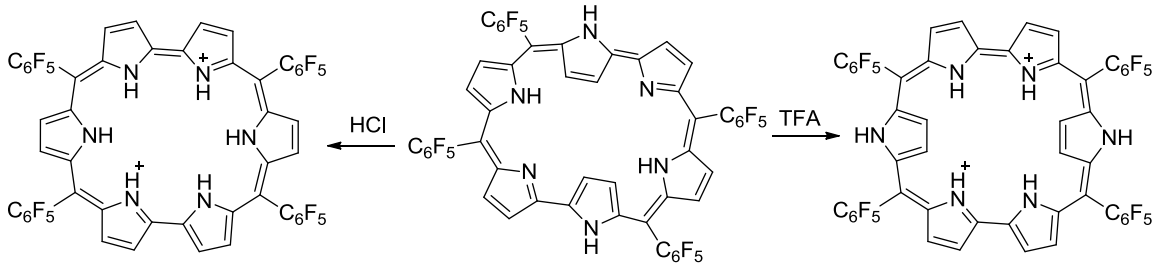

Figure 1.9 Conformational switching in rubyrin upon protonation with HCl and TFA.

Conformational switching due to temperature difference was first reported in case of tetratolyl unsymmetrical dithiasapphyrin (Figure 1.10). The equilibrium between the normal and inverted forms is temperature dependant in the range of 193-342 K and the dominant fraction is inverted form in the entire range with a molar fraction of 0.87 at 298 K.[58]

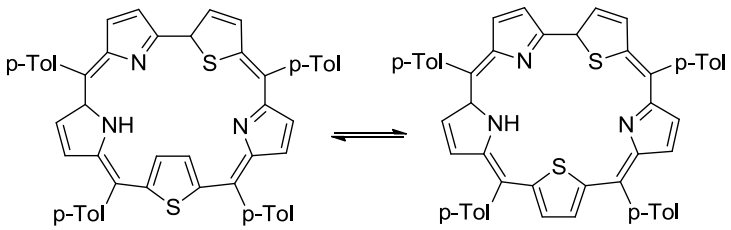

Figure 1.10 Conformational switching due to effect of temperature.

Perhaps the widely studied macrocycle for its conformational switching is hexaphyrin(1.1.1.1.1.1), probably owing to its remarkable fluxionality due to the presence of six meso-carbon bridges when compared to contracted hexaphyrins. It exists in a variety of possible conformers, of which five have been detected experimentally (Figure 1.11). The list includes three nearly planar structures and two twisted ones.[53]

Gossauer and coworkers reported in their first seminal work on β-alkylated [26]hexaphyrin(1.1.1.1.1.1), where the macrocycle assumed to form dumbbell shape (Type-I conformer) inferred from its characteristic ^{1}H NMR spectrum.[31] This dumbbell shape is not only restricted to β-alkyl derivatives and was also observed in case of tetraaryl substituted hexaphyrins. If all the meso positions are occupied then it adopts a rectangular core (Type-II conformer), in which the central pyrrole of longer sides will be inverted while the other four pyrroles point inward towards the macrocyclic core for effe-

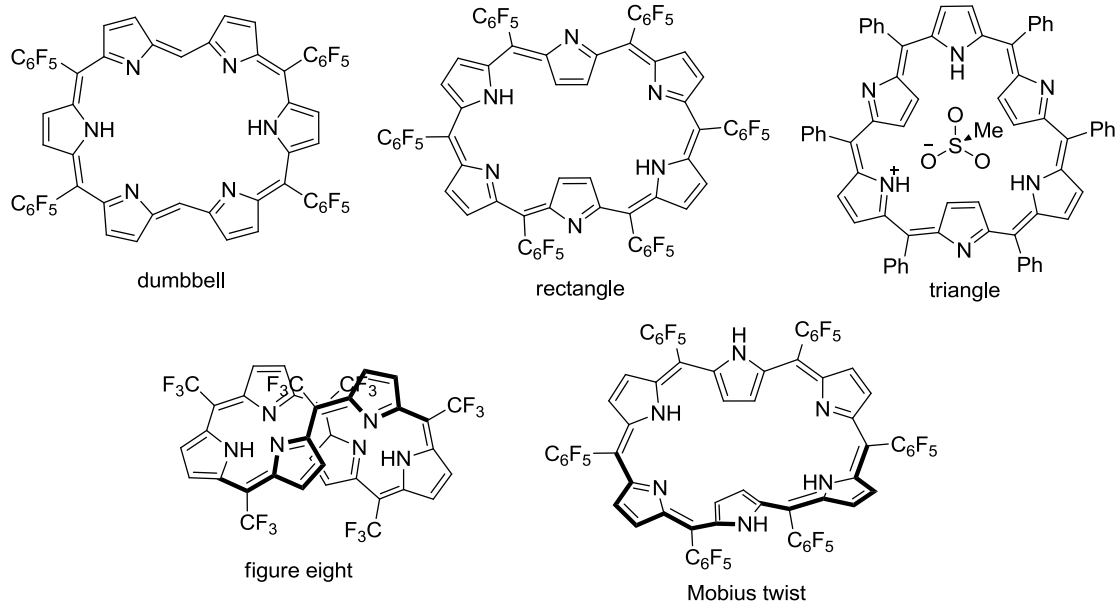

Figure 1.11 Various conformations of hexaphyrins.

ctive intramolecular hydrogen bonding.[32] The dumbbell shaped conformer is apparently preferred over rectangular core because of more hydrogen bonding interactions from thermodynamic point of view but can be disfavored because of inwardly pointed meso substituents which can cause steric congestion. The triangular conformer was first reported when a meso phenyl hexaphyrin was mono protonated with methanesulfonic acid as a rare case[59] but was later observed in case of triply N-confused hexaphyrin and their lactams.[60] Figure eight structure was seen only when bulky substituents such as trifluoromethyl-CF_3 were placed at the meso and/or β-positions.[61] To explain the diatropicity of [28]hexaphyrin, Osuka and coworkers speculated the presence of Möbius

strip conformer in equilibrium with rectangular form and was observed at lower temperature limits revealing the chemical shift patterns consistent with Möbius topology.[38,53] Overall expanded porphyrins show intriguing structural diversities that can be controlled by placing suitable substituents at meso and/or β-positions.

1.5.3 Aromaticity

Understanding aromaticity is a basic concept in organic chemistry towards explaining the stability of benzene molecule, since its discovery by Faraday in 1825 and its proposed resonance structure by Kekulé in 1865. Huckel's rule has been the sole criteria for defining aromaticity for most of the decades, which states that only cyclic conjugated molecular systems with [4n+2] π-electrons having a closed shell configuration will be aromatic and [4n] π-electrons will be antiaromatic with an open shell configuartion. On the contrary, Möbius aromaticity predicts an aromatic circuit for [4n] π-electrons with a singly twisted Möbius topology (Figure 1.12).[62] This simple and intriguing concept was first proposed by Heilbronner in 1964 and by Zimmerman in 1966. However, attaining chemically stable Möbius aromatic molecules with two conflicting structural elements, a twisted Möbius topology and a cyclic conjugated [4n] π-electron system, is an ardent task.[63]

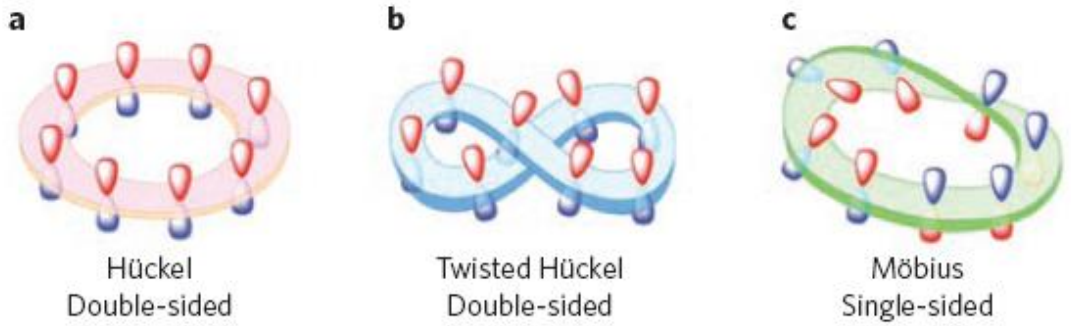

Figure 1.12 Schematic representations of topologies of π-conjugated systems.

The seminal work on this concept was reported by Herges and his coworkers on a [16]annulene that has moderate aromatic character with a twisted Möbius topology.[64] After the report of Sondheimer's group, showing the similarities between the [18]annulene and porphyrin, intrerpretation of porphyrin as multiple-bridged aromatic diaza[18]annulene and its aromaticity was described using Huckel's theory of [4n+2] cyclic conjugated π-electrons.[65] The versatile conformational flexibilities of expanded porphyrins like planar, figure-eight and helical structures are useful in determining the aromatic and antiaromatic properties in various conformations. The potential utility of

expanded porphyrins in implementing Möbius aromatic nature was reported by Latos-Grażyński in 2007 by synthesizing A,D-di-p-benzi[28]hexaphyrin.[66] Structural elucidation of this macrocycle revealed a Möbius twisted form with a single sided strap having 1,4-phenylene rings that could easily rotate in solution (Figure 1.13). This structural flexibility led them to record temperature dependent ^{1}H NMR study to reveal

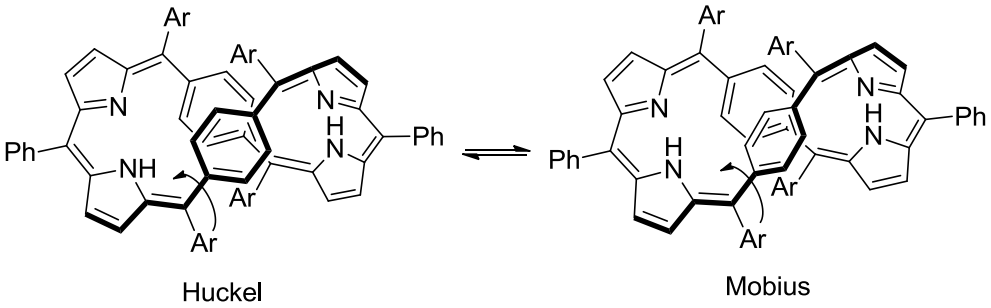

Figure 1.13 Conformational switching of p-benzihexaphyrin.

the conformational switch between Möbius and Huckel topologies. Subsequently, Osuka and coworkers synthesized different large annulenic systems to alleviate the distortion associated with Möbius topology (Figure 1.14).[67]

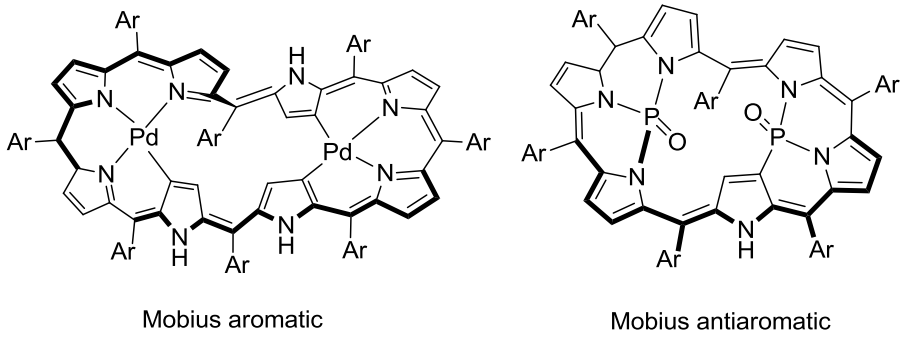

Figure 1.14 Large annulenic systems with Möbius topology.

Conformational changes associated with [28]hexaphyrin is not only limited to temperature, where it fluctuates between rectangular Huckel character to twisted Möbius topology, but also observed in case of protonation. Titration of [28]hexaphyrin with TFA (trifluoroacetic acid) led to monoprotonated derivative with a single Möbius aromatic species showing a diatropic ring current. But, on the other hand, titration with strong acid MSA (methanesulfonic acid) resulted in a diprotonated species associated with large structural change of going to nearly planar triangular conformation, displaying Huckel antiaromatic character, as shown in Figure 1.15.[68]

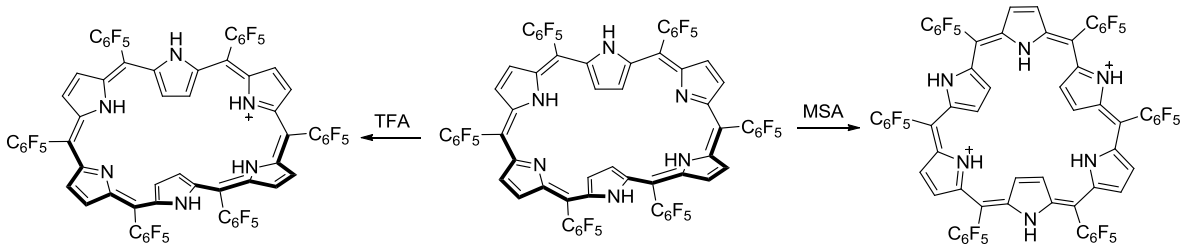

Figure 1.15 Protonation of [28]hexaphyrin with TFA and MSA.

1.5.4 Photophysical properties

It has been evident form the studies that expanded porphyrins containing more number of heterocyclic rings leading to a structural distortion hindering the delocalization of π-electrons along the molecular framework. While the absorption bands of planar expanded porphyrins show a continuous red shift, some of the larger expanded porphyrin analogues with distorted topologies, exhibit ill-defined and broad absorption spectra. The overall molecular structure plays a vital role in determining the electronic structures of expanded porphyrins through the extent of π-conjugation.[69] In general, aromaticity was evaluated by means of structural measures such as bond-length equalization (HOMA - Harmonic Oscillator Model of Aromaticity) and molecular planarity, its magnetic properties including ^{1}H NMR chemical shifts and NICS (Nucleus Independent Chemical Shift) values. Kim and coworkers have outlined the importance of considering photophysical properties in determining the aromatic/antiaromatic character of expanded porphyrins.[38]

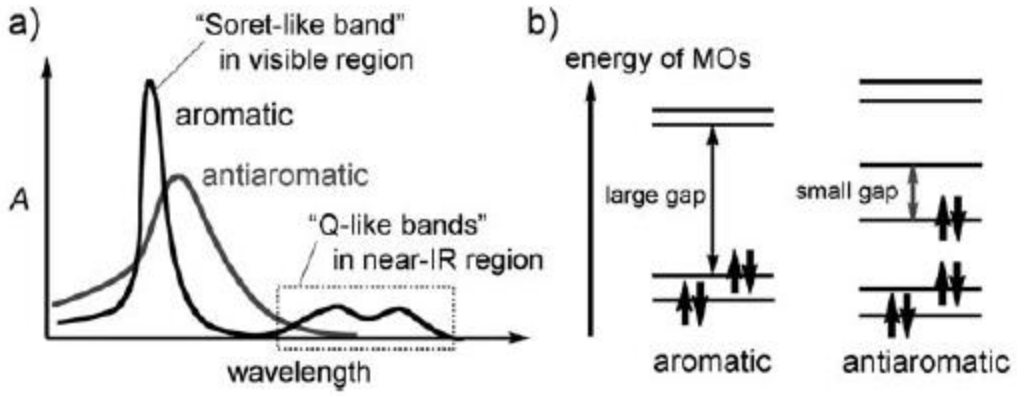

Figure 1.16 Typical UV/Vis/NIR (near infrared) absorption spectra and molecular orbital (MO) diagrams of aromatic/antiaromatic expanded porphyrins.

The common phtophysical characteristics (Figure 1.16a) exhibited by aromatic expanded porphyrins are: 1) a sharp Soret-like absorption band in the visible region and distinct Q-like bands in the NIR region, 2) a weak but detectable fluorescence in the NIR (near infrared) region, 3) a relatively long excited-state lifetime and 4) a large TPA cross-

section value. On the contrary, antiaromatic expanded porphyrins have: 1) a broad and ill-defined absorption spectrum without Q-like bands in the NIR region, 2) no fluorescence, 3) a very short excited-state lifetime, and 4) a relatively small TPA cross-section value.[38] These characteristic features can be attributable to the electronic structures of these compounds. While the aromatic expanded porphyrins show a wide HOMO-LUMO gap (Figure 1.16b), the antiaromatic congeners exhibit a narrow HOMO-LUMO gap. The HOMO/HOMO-1 and LUMO/LUMO+1 levels are almost degenerate in case of aromatic systems where as there is no degeneracy in case of antiaromatic systems.[38]

One more fascinating tool to assess the aromaticity/antiaromaticity is to study the induced current density which is helpful in visualizing a diatropic or paratropic ring current in expanded porphyrins.[70] Recently, Kim and coworkers sought insight into this relationship between structure and electronic character through more sophisticated and theoretical methods by deploying appropriate light sources and detection methods. These methods provide them to measure linear and NLO phenomenon in the NIR region, such as steady-state and time resolved absorption and emission spectra, and femtosecond two-photon absorption (TPA) measurements in a variety of expanded porphyrins, exploring the relationship between structural features including topology and photophysical properties.[71]

1.5.5 Organic Radicals

Stabilizing organic radicals has generated a lot of interest not only for their intriguing structures and pure scientific interest but also possible applications in both basic and applied chemistry, such as organic magnets, organic batteries and optical materials.[38] As they are highly reactive and short-lived, organic radicals are generally stabilized either by steric protection and/or delocalization of unpaired electron through effective conjugation. They are also stabilized by placing suitable heteroatoms such as nitrogen and sulfur adjacent to the radical center.[63] Recent studies explored the radical-stabilizing abilities of expanded porphyrins emulating a general strategy by utilizing the appropriate conjugative positions.[72]

Porphyrinoid-based radicals were classified into four categories according to the origin of the radical: 1) one electron oxidized/reduced, 2) substituent centered, 3) non-innocent ligands and 4) Kekulé/non-Kekulé type diradicaloids. It is inferred that not only delocalization and steric protection but also moderate redox potentials should be required

to prevent facile oxidation and reduction of radical itself. As they have unique open shell electronic configurations, characterization of porphyrinoid-radicals with NMR spectroscopy is difficult because of their fast electronic relaxations. At this juncture one electron oxidizing or reducing agents can be employed for the characterizations. ESR spectroscopy is also a handy tool in assessing porphyrinoid radicals as they display isotropic signals around $g = 2$ without hyperfine structures.[72]

Isolation of first expanded porphyrin based monoradicaloid was reported by Osuka's group in 2008. During the synthesis of *meso*-free [26]hexaphyrin, they could able to separate a byproduct which was NMR inactive, ESR active and having broad and low energy absorption bands in the NIR region.[73] In 2010, the same group dematalated the di-Ni(II) complex of *meso*-free [26]hexaphyrin to yield a meso,meso-dioxygenated hexaphyrin which was characterized as a non-Kekulé singlet biradicaloid due to its temperature dependent ESR intensity and magnetic susceptibility features (Figure 1.17).[74]

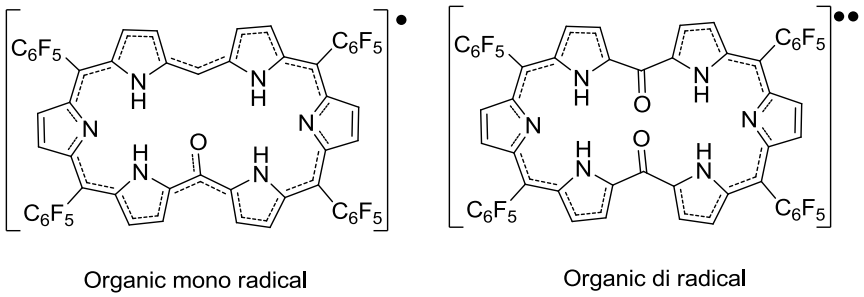

Figure 1.17 *meso*-oxygenated and *meso*-dioxygenated [26]hexaphyrins.

First example of a distorted nonplanar, figure eight, stable π-radical was observed in a bis-Pd(II) hexaphyin complex (Figure 1.18). Theoretical studies show the spin distribution along the twisted macrocycle rather than on its Pd(II) centers and has been characterized by both EPR and magnetic susceptibility measurments.[75]

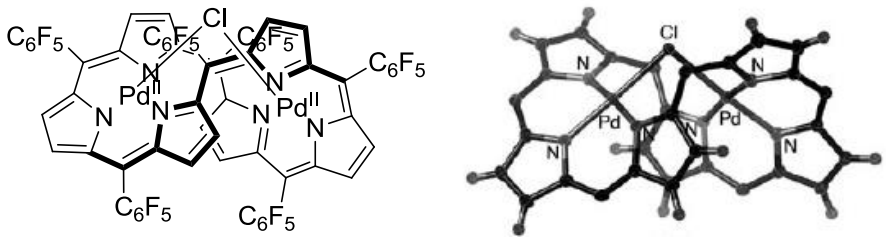

Figure 1.18 Bis-Pd(II)-[26]hexaphyrin complex and its crystal structure (C_6F_5 omitted for clarity).

Very interesting redox switching between a 24π-antiaromatic and 26π-aromatic annulated rosarian through a 25π-radical species was reported by Ishida et al (Figure 1.19). The structurally rigid, planar 24π-antiaromatic rosarin upon protonation with either HCl or HBr led to a stable triprotonated monoradical dication, which could be further converted

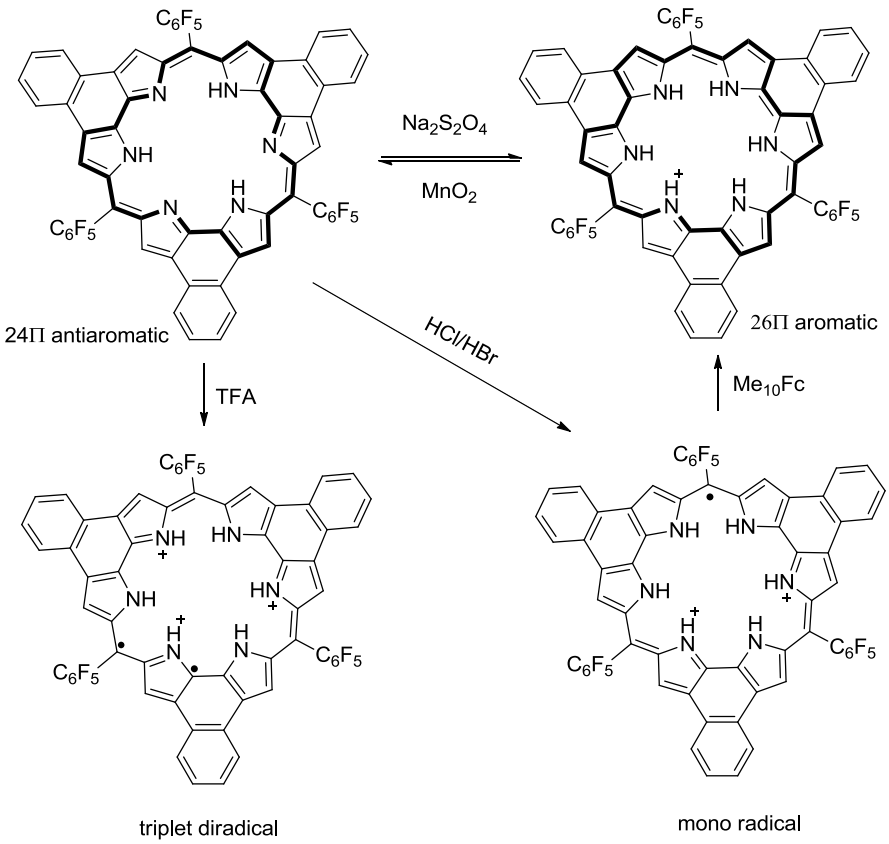

Figure 1.19 Protonation induced radical generation in annulated rosarin.

to triprotonated monocationic rosarian by reducing with decamethyl ferrocene. The annulated rosarin on treatment with TFA at low temperature yields triprotonated ground state triplet diradicaloid species.[76]

1.5.6 Applications

As the result of incessant research on expanded porphyrins, endowed with tremendous topological and photophysical properties, they find application in wide range of fields. Few applications corresponding to different fields will be discussed here.

The Schiff base expanded porphyrins, texaphyrins, and first reported by Sessler and coworkers in 1988, exhibit rich coordination chemistry owing to their strong binding interaction between the imine moieties and various metals. They have successfully explored them for various medical applications in the form of magnetic resonance

imaging (MRI) contrasting agents as well as anticancer agents; motexafin gadalonium (MGd), a water-soluble texaphyrin Gd^{III} complex, being the most promising one (Figure 1.20).[33,77]

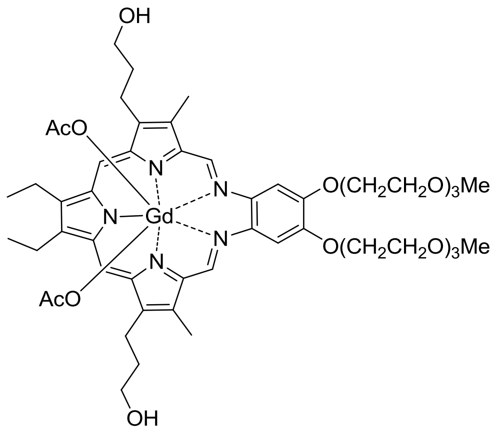

Figure 1.20 Structure of motexafin gadalonium (MGd).

Meso-aryl-[26]hexaphyrin(1.1.1.1.1.0), a contracted hexaphyrin (Figure 1.21), reported by Wong and coworkers, had been found to be highly sensitive near-infrared fluorescent chemodosimeter selective for Hg^{2+} ions even in the presence of other alkali and alkaline earth metal ions.[78] Ikawa, Furuta and coworkers have synthesized doubly N-confused hexaphyrin Zn(II) complex (Figure 1.21), which shows fluorescence quenching on subsequent addition of double-stranded DNA (dsDNA), probably owing to the further formation of a ternary complex.[79]

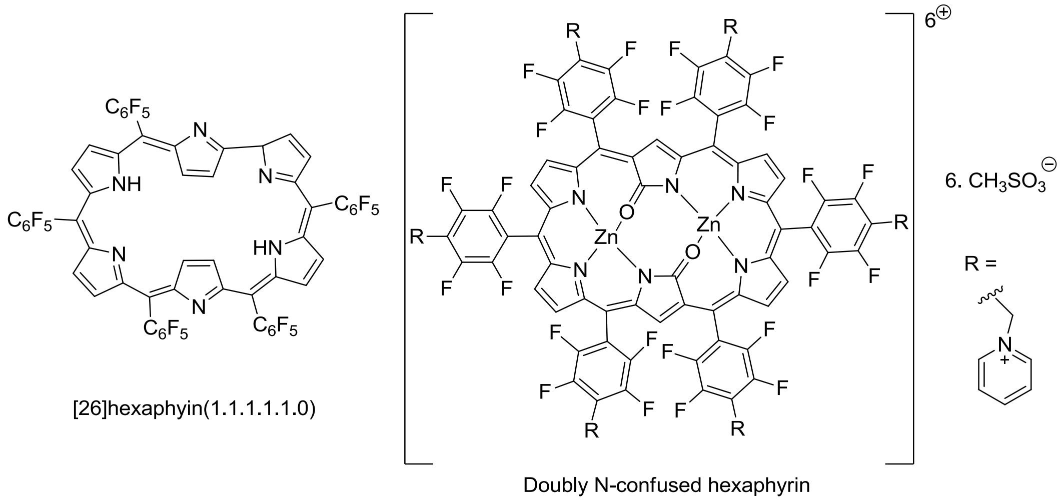

Figure 1.21 Structures of *meso*-aryl-[26]hexaphyrin(1.1.1.1.1.0) and doubly N-confused hexaphyrin Zn(II) complex.

Mane et al. have showed the application of expanded porphyrins, boryl oxasmaragdyrins (Figure 1.22), macrocycle with five heterocyclic rings, as sensitizers in dye sensitized

solar cells (DSCs). By modulating the periphery of boryl oxasmaragdyrins through molecular engineering approach they evaluated photophysical, electrochemical and photovoltaic properties which revealed that the number and position of the donor–acceptor groups play an important role in their photovoltaic performance.[80]

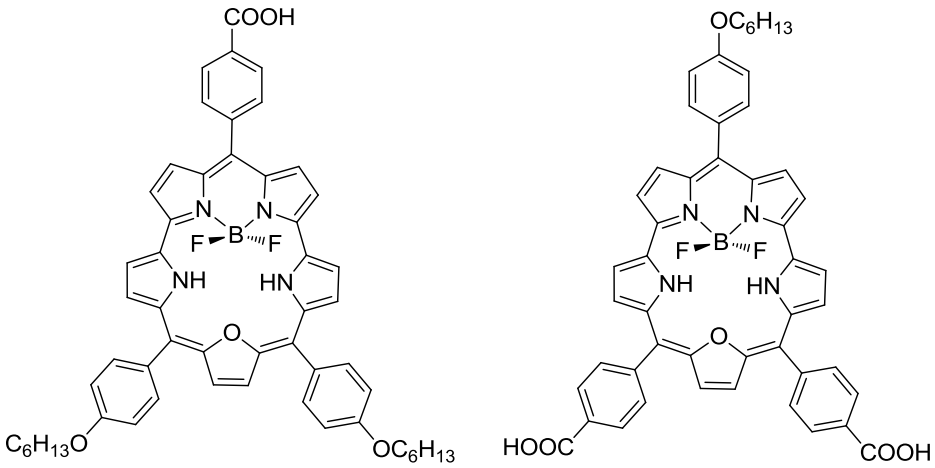

Figure 1.22 Examples of boryl smaragdyrins used in DSCs.

Imahori and his coworkers synthesized multiple fluorine atoms incorporated *meso*-aryl hexaphyrin (Figure 1.23) as a theranostic agent, which under NIR (near infrared) illumination showed intense photothermal effect and weak photodynamic effect causing ablation of cancer cells more effectively than the photodynamic effect of indocyanine green (ICG). Visualization of tumors was also achieved by ^{19}F MRI due to the presence of multiple fluorine atoms.[81]

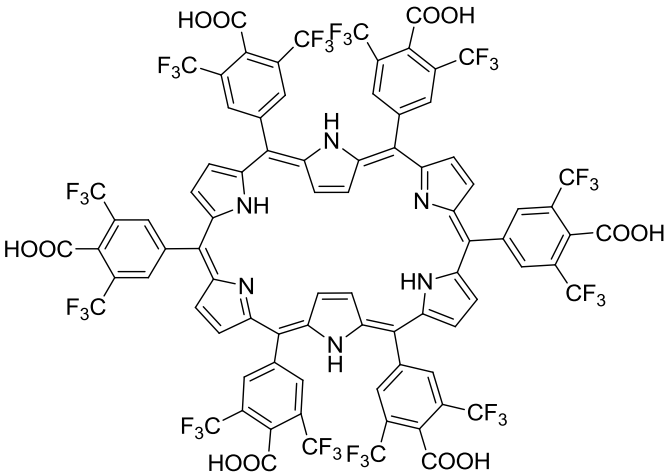

Figure 1.23 Hexaphyin as a theranostic agent for photothermal therapy.

1.6 Scope of the present work:

From the brief discussion above, one can see how expanded porphyrins came to limelight by showcasing their wide range of applications ranging from biomedical to sensing and material to optoelectronics. Although different kinds of expanded porphyrins pertaining to the number of pyrroles and/or meso positions and their combinations are well explored, there is still much scope in their effective synthesis, analyzing photophysical aspects, understanding structural diversities and investigating their NLO properties. Keeping this in mind, our group reported in the past, several fascinating works on expanded porphyrins like cyclo[8]pyrroles,[47] acetylene cumulene porphyrinoids[82] and sapphyrins.[56a,83] In this aspect, the current work, presented in this thesis highlights the hassle-free synthesis of several novel bronzaphyrins, a 26π-aromatic expanded porphyrin displaying intense near infrared absorptions, which was ignored for more than two decades in spite of its early promise. A glance at its early chemistry reveals tedious synthetic procedures and little known structural and photophysical aspects,[48,84] through different approaches. The present work also enlists the first structural determination done for this class of macrocycles along with their rich structural diversities, which will be discussed in the following chapters. It also demonstrates the intriguing photophysical properties of bronzaphyrins along with the computational studies for better understanding.

1.7 References

1. Battersby, A. R.; Fookes, C. J. R.; Matcham, G. W. J.; McDonald, E. *Nature* **1980**, *285*, 17.
2. (a) *The Porphyrin Handbook* (Eds.: K. M. Kadish; K. M. Smith; R. Guilard) Academic Press, San Diego, **2000**. (b) *Handbook of Porphyrin Science* (Eds.: K. M. Kadish; K. M. Smith; R. Guilard) World Scientific Publishing, Singapore, **2010**.
3. With, T. K. *Int. J. Biochem.* **1980**, *11*, 189.
4. Dolphin, D. *The Porphyrins, Structure and Synthesis Part A* **1978**, *1*, 29.
5. Bauer, V. J.; Clive, D. L. J.; Dolphin, D.; Paine III, J. B. P.; Harris, F. L.; King, M. M.; Loder, J.; Wang, S.-W. C.; Woodward, R. B. *J. Am. Chem. Soc.* **1983,** *105*, 6429.
6. Sessler, J. L.; Weghorn, S. J. *Expanded, Contracted and Isomeric Porphyrins* Pergamon, New York, **1997**.
7. Franck, B.; Nonn, A. *Angew. Chem., Int. Ed. Engl*. **1995**, *34*, 1795.
8. Johnson, A. W.; Kay, I. T. *Proc. Chem. Soc. London* **1964**, 89.
9. Gross, Z.; Galili, N.; Saltsman, I *Angew. Chem., Int. Ed.* **1999**, *38*, 1427.
10. Paolesse, R.; Jaquinod, L.; Nurco, D. J.; Mini, S.; Sagone, F.; Boschi, T.; Smith, K. M. *Chem. Commun.* **1999**, 1307.
11. Teo, R. D.; Hwang, J. Y.; Termini, J.; Gross, Z.; Gray, H. B. *Chem. Rev.* **2017**, *117*, 2711.
12. Inokuma, Y.; Kwon, J. H.; Ahn, T. K.; Yoo, M.-C.; Kim, D.; Osuka, A. *Angew. Chem., Int. Ed.* **2006**, *45*, 961.
13. Myśliborski, R.; Latos-Grażyński, L.; Szterenberg, L.; Lis, T. *Angew. Chem., Int. Ed.* **2006**, *45*, 3670.
14. Badger, G. M.; Elix, J. A.; Lewis, G. E. *Proc. Chem. Soc.* **1964**, 82.
15. Shimiju, S. *Chem. Rev.* **2017**, *117*, 2730.
16. Srinivasan, A.; Furuta, H. *Acc. Chem. Res.* **2005**, *38*, 10.
17. Vogel, E.; Köcher, M.; Schmickler, H.; Lex, J. *Angew. Chem., Int. Ed. Engl.* **1986**, *25*, 257.
18. (a) Waluk, J. *Chem. Rev.* **2017**, *117*, 2447. (b) Sarma, T.; Panda, P. K. *Chem. Rev.* **2017**, *117*, 2785. (c) Mack, J. *Chem. Rev.* **2017**, *117*, 3444.
19. Anguera, G.; Sanchez-Garcia, D. *Chem. Rev.* **2017**, *117*, 2481.
20. (a) Sessler, J. L.; Brucker, E. A.; Weghorn, S. J.; Kister, M.; Schäfer, M.; Lex, J.; Vogel, E. *Angew. Chem. Int. Ed. Engl.* **1994**, *33*, 2308. (b) Aukauloo, M. A.; Guilard, R. *New. J. Chem*. **1994**, *18*, 1205.
21. (a) Callot, H. J.; Rohrer, A.; Tschamber, T. *New. J. Chem*. **1995**, *19*, 155. (b) Vogel, E.; Bröring, M.; Weghorn, S. J.; Scholz, P.; Deponte, R.; Lex, J.; Schmickler, H.; Schaffner, K.; Braslavsky, S. E.; Müller, M.; Pörting, S.; Sessler, J. L.; Fowler, C. J. *Angew. Chem. Int. Ed*. **1997**, *36*, 1651.
22. (a) Vogel, E. *J. Heterocyclic Chem*. **1996**, *33*, 1461. (b) Vogel, E.; Scholz, P.; Demuth, R.; Erben, C.; Bröring, M.; Schmickler, H.; Lex, J.; Hohlneicher, G.; Bremm, D.; Wu, Y.-D. *Angew. Chem. Int. Ed*. **1999**, *38*, 2919.

23. (a) Furuta, H.; Asano, T.; Ogawa, T. *J. Am. Chem. Soc.* **1994**, *116*, 767. (b) Chmielewski, P. J.; Latos-Grażyński, L.; Rachlewicz, K.; Glowiak, T. *Angew. Chem., Int. Ed. Engl.* **1994**, *33*, 779.
24. Geier, G. R., III; Haynes, D. M.; Lindsey, J. S. *Org. Lett.* **1999**, *1*, 1455.
25. Lash, T. D. *Chem. Rev.* **2017**, *117*, 2313.
26. Chatterjee, T.; Shetti, V. S.; Sharma, R.; Ravikanth, M. *Chem. Rev.***2017**, *117*, 3254.
27. Sessler, J. L.; Seidel, D. *Angew. Chem. Int. Ed.* **2003**, *42*, 5134.
28. Broadhurst, M. J.; Grigg, R.; Johnson, A. W. *J. Chem. Soc. Perkin Trans. 1* **1972**, 1124.
29. Berger, R. A.; LeGeoff, E. *Tetrahedron Lett.* **1978**, *19*, 4225.
30. (a) Jux, N.; Koch, P.; Schmickler, H.; Lex, J.; Vogel, E. *Angew. Chem., Int. Ed. Engl.* **1990**, *29*, 1385. (b) Vogel, E.; Jux, N.; Rodriguez-Val, E.; Lex, J.; Schmickler, H. *Angew. Chem., Int. Ed. Engl.* **1990**, *29*, 1387.
31. (a) Rexhausen, H.; Gossauer, A. *J. Chem. Soc. Chem. Commun.* **1983**, 275. (b) Charriere, R.; Jenny, T. A.; Rexhausen, H.; Gossauer, A. *Heterocycles* **1993**, *36*, 1561.
32. Shin, J.-Y.; Furuta, H.; Yoza,K.; Igarashi, S.; Osuka, A. *J. Am. Chem. Soc.* **2001**, *123*, 7190.
33. Sessler, J. L.; Murai, T.; Lynch, V.; Cyr, M. *J. Am. Chem. Soc.* **1988**, *110*, 5586.
34. Sessler, J. L.; Cyr, M. J.; Lynch, V.; McGhee, E.; Ibers, J. A. *J. Am. Chem. Soc.* **1990**, *112*, 2810.
35. Sessler, J. L.; Morishima, T.; Lynch, V. *Angew. Chem., Int. Ed. Engl.* **1991**, *30*, 977.
36. Sessler, J. L.; Weghorn, S. J.; Morishima, T.; Rosingana, M.; Lynch, V.; Lee, V. *J. Am. Chem. Soc.* **1992**, *114*, 8306.
37. Sessler, J. L.; Weghorn, S. J.; Lynch, V.; Johnson, M. R. *Angew. Chem., Int. Ed. Engl.* **1994**, *33*, 1509.
38. Saito, S.; Osuka, A. *Angew. Chem., Int. Ed.* **2011**, *50*, 4342.
39. Arsenault, G. P.; Bullock, E.; MacDonald, S. F. *J. Am. Chem. Soc.* **1960**, *82*, 4384.
40. Richter, D. T.; Lash, T. D. *Tetrahedron Lett.* **1999**, *40*, 6735.
41. (a) Setsune, J.-i.; Katakami, Y.; Iizuna, N. *J. Am. Chem. Soc.* **1999**, *121*, 8957. (b) Setsune, J.-i.; Maeda, S. *J. Am. Chem. Soc.* **2000**, *122*, 12405.
42. Kee, S.-Y.; Lim, J. M.; Kim, S.-J.; Yoo, J.; Park, J.-S.; Sarma, T.; Lynch, V. M.; Panda, P. K.; Sessler, J. L.; Kim, D.; Lee, C.-H. *Chem. Commun.* **2011**, *47*, 6813.
43. Chmielewski, P. J.; Latos-Grażyński, L.; Rachlewicz, K. *Chem. Eur. J.* **1995**, *1*, 68.
44. Narayanan, S. J.; Sridevi, B.; Chandrashekar, T. K.; Vij, A.; Roy, R. *Angew. Chem., Int. Ed.* **1998**, *37*, 3394.
45. Sessler, J. L.; Seidel, D.; Lynch, V. *J. Am. Chem. Soc.* **1999**, *121*, 11257.
46. Seidel, D.; Lynch, V.; Sessler, J. L. *Angew. Chem., Int. Ed. Engl.* **2002**, *41*, 1422.

47. Sarma, T.; Panda, P. K. *Chem. Eur. J.* **2011**, *17*, 13987.
48. Johnson, M. R.; Miller, D. C.; Bush, K.; Becker, J. J.; Ibers, J. A. *J. Org. Chem.* **1992**, *57*, 4414.
49. Rana, A.; Hong, Y.; Gopalakrishna, T. Y.; Phan, H.; Herng, T. S.; Yadav, P.; Ding, J.; Kim, D.; Wu, J. *Angew. Chem., Int. Ed. Engl.* **2018**, *57*, 12534.
50. Peterson, G. R.; Bampos, N. *Angew. Chem. Int. Ed.* **2010**, *49*, 3930.
51. Bui, T.-T.; Iordache, A.; Chen, Z.; Roznyatovskiy, V. V.; Saint-Aman, E.; Lim, J. M.; Lee, B. S.; Ghosh, S.; Moutet, J.-C.; Sessler, J. L.; Kim, D.; Bucher, C. *Chem. Eur. J.* **2012**, *18*, 5853.
52. Umetani, M.; Tanaka, T.; Kim, T.; Kim, D.; Osuka, A. *Angew. Chem. Int. Ed.* **2016**, *55*, 8095.
53. Szyszko, B.; Białek, M. J.; Pacholska-Dudziak, E.; Latos- Grażyński, L. *Chem. Rev.* **2017**, *117*, 2839.
54. Misra, R.; Chandrashekar, T. K. *Acc. Chem. Res.* **2008**, *41*, 265.
55. Rachlewicz, K.; Sprutta, N.; Latos-Grażyński, L.; Chmielewski, P. J.; Szterenberg, L. *J. Chem. Soc., Perkin Trans. 2* **1998**, 959.
56. (a) Sarma, T.; Anusha, P. T.; Pabbathi, A.; Rao, S. V.; Panda, P. K. *Chem. Eur. J.* **2010**, *20*, 15561. (b) Shetti, V. S.; Kee, S.-Y.; Lee, C. H. *Chem. Asian J.* **2014**, *9*, 734.
57. Shimizu, S.; Taniguchi, R.; Osuka, A. *Angew. Chem., Int. Ed.* **2005**, *44*, 2225.
58. Sprutta, N.; Latos- Grażyński, L. *Org. Lett.* **2001**, *3*, 1933.
59. Xie, Y.-S.; Yamaguchi, K.; Toganoh, M.; Uno, H.; Suzuki, M.; Mori, S.; Saito, S.; Osuka, A.; Furuta, H. *Angew. Chem., Int. Ed.* **2009**, *48*, 5496.
60. Lim, J. M.; Lee, J. S.; Chung, H. W.; Bahng, H. W.; Yamaguchi, K.; Toganoh, K.; Furuta, H.; Kim, D. *Chem. Commun.* **2010**, *46*, 4357.
61. Shimizu, S.; Aratani, N.; Osuka, A. *Chem. Eur. J.* **2006**, *12*, 4909.
62. Yoon, Z. S.; Osuka, A.; Kim, D. *Nat. Chem.* **2009**, *1*, 113.
63. Tanaka, T.; Osuka, A. *Chem. Rev.* **2017**, *117*, 2584.
64. Ajami, D.; Oeckler, O.; Simon, A.; Herges, R. *Nature* **2003**, *426*, 819.
65. Bröring, M. *Angew. Chem., Int. Ed.* **2011**, *50*, 2436.
66. Stępień, M.; Latos-Grażyński, L.; Sprutta, N.; Chwalisz, P.; Szterenberg,L. *Angew. Chem., Int. Ed.* **2007**, *46*, 7869.
67. (a) Mori, S.; Osuka, A. *J. Am. Chem. Soc.* **2005**, *127*, 8030. (b) Tanaka, Y.; Saito, S.; Mori, S.; Aratani, N.; Shinokubo, H.; Shibata, N.; Higuchi, Y.; Yoon, Z. S.; Kim, K. S.; Noh, S. B.; Park, J. K.; Kim, D.; Osuka, A. *Angew. Chem., Int. Ed.* **2008**, *47*, 681.
68. (a) Ishida, S.-i.; Higashino, T.; Mori, S.; Mori, H.; Aratani, N.; Tanaka, T.; Lim, J. M.; Kim, D.; Osuka, A. *Angew. Chem., Int. Ed.* **2014**, *53*, 3427. (b) Sung, Y. M.; Oh, J.; Cha, W.-Y.; Kim, W.; Lim, J. M.; Yoon, M.-C.; Kim, D. *Chem. Rev.* **2017**, *117*, 2257.
69. Shin, J.-Y.; Kim, K. S.; Yoon, M.-C.; Lim, J. M.; Yoon, Z. S.; Osuka, A.; Kim, D. *Chem. Soc. Rev.*, **2010**, *39*, 2751.
70. (a) E. Steiner, P. W. Fowler, *Org. Biomol. Chem.* **2004**, *2*, 34. (b) Geuenich, D.; Hess, K.; Köhler, F.; Herges, R. *Chem. Rev.* **2005**, *105*, 3758.

71. Lim, J. M.; Yoon, Z. S.; Shin, J.-Y.; Kim, K. S.; Yoon, M.-C.; Kim, D. *Chem. Commun.*, **2009**, 261.
72. Shimizu, D.; Osuka, A. *Chem. Sci.* **2018**, *9*, 1408.
73. Koide, T.; Kashiwazaki, G.; Suzuki, M.; Furukawa, K.; Yoon, M.-C.; Cho, S.; Kim, D.; Osuka, A. *Angew. Chem., Int. Ed.* **2008**, *47*, 9661.
74. Koide, T.; Furukawa, K.; Shinokubo, H.; Shin, J.-Y.; Kim, K. S.; Kim, D.; Osuka, A. *J. Am. Chem. Soc.* **2010**, *132*, 7246.
75. Rath, H.; Tokuji, S.; Aratani, N.; Furukawa, K.; Lim, J. M.; Kim, D.; Shinokubo, H.; Osuka, A. *Angew. Chem., Int. Ed.* **2010**, *49*, 1489.
76. (a) Ishida, M.; Kim, S.-J.; Preihs, C.; Ohkubo, K.; Lim, J. M.; Lee, B. S.; Park, J. S.; Lynch, V. M.; Roznyatovskiy, V. V.; Sarma, T.; Panda, P. K.; Lee, C.-H.; Fukuzumi, S.; Kim, D.; Sessler, J. L. *Nat. Chem.* **2013**, *5*, 15. (b) Fukuzumi, S.; Ohkubo, K.; Ishida, M.; Preihs, C.; Chen, B.; Borden, W. T.; Kim, D.; Sessler, J. L. *J. Am. Chem. Soc.* **2015**, *137*, 9780.
77. (a) Sessler, J. L.; Hemmi, G.; Mody, T. D.; Murai, T.; Burrell, A.; Young, S. W. *Acc. Chem. Res.* **1994**, *27*, 43. (b) Young, S.W.; Fan, Q.; Harriman, A.; Sessler, J. L.; Dow, W. C.; Mody, T. D.; Hemmi, G. W.; Hao, Y.; Miller, R. A. *Proc. Natl. Acad. Sci. USA* **1996**, *93*, 6610. (c) Zahedi Avval, F.; Berndt, C.; Pramanik, A.; Holmgren, A. *Biochem. Biophys. Res. Commun*. **2009**, *379*, 775.
78. Zhu, X.-J.; Fu, S.-T.; Wong, W.-K.; Guo, J.-P.; Wong, W.-Y. *Angew. Chem., Int. Ed.* **2006**, *45*, 3150.
79. Ikawa, Y.; Katsumata, S.; Sakashita, R.; Furuta, H. *Chem. Lett.* **2014**, *43*, 1929.
80. (a) Mane, S. B.; Hu, J-Y.; Chang, Y.-C.; Luo, L.; Diau, E. W.-G.; Hung, C.-H. *Chem. Commun.*, **2013**, *49*, 6882. (b) Mane, S. B.; Hung, C.-H. *Chem. Eur. J.* **2015**, *21*, 4825.
81. Higashino, T.; Nakatsuji, H.; Fukuda, R.; Okamoto, H.; Imai, H.; Matsuda, T.; Tochio, H.; Shirakawa, M.; Tkachenko, N. V.; Hashida, M.; Murakami, T.; Imahori, H. *ChemBioChem* **2017**, *18*, 951.
82. Rana, A.; Lee, S.; Kim, D.; Panda, P. K. *Chem. Eur. J.* **2015**, *21*, 12129.
83. Rana, A. Kumar, B. S.; Panda, P. K. *Org. Lett.* **2015**, *17*, 3030.
84. (a) Miller, D. C.; Johnson, M. R.; Ibers, J. A. *J. Org. Chem.* **1994**, *59*, 2877. (b) Johnson, M. R. *J. Org. Chem.* **1997**, *62*, 1168Z. (c) Hu, C. Scordilis-Kelley, M. P. Cava, *Tetrahedron Lett.* **1993**, *34*, 1879. (d) Hu, Z.; Atwood, J. L.; Cava, M. P. *J. Org. Chem.* **1994**, *59*, 8071. (e) Kozaki, M.; Parakka, J.; Cava, M. P. *J. Org. Chem.* 1996, **61**, 3657. (f) Ellinger, F.; Gieren, A.; Hübner, Th.; Lex, J.; Lucchesini, F.; Merz, A.; Neidlein, R.; Salbeck, J. *Monatsh. für Chemie* **1993**, *124*, 931.

CHAPTER 2

Materials and methods

This chapter provides a detailed account of the chemicals used, instrumentation and methods followed for various studies. Also, the procedures used for the purification of solvents and chemicals are described. Further, we have elaborated about the synthetic procedures of known compounds employed during the course of our investigations.

2.1 General experimental

2.1.1 Solvents

2.1.1.1 Solvent for reactions[1]

Chloroform, acetonitrile, DCM, DCE and DMF were dried by distillation over calcium hydride. THF was dried by passing through column of activated alumina, followed by distillation over sodium metal, in presence of benzophenone as indicator. MeOH was dried by using activated magnesium turnings with I_2. Toluene, hexane and benzene were refluxed with sodium and benzophenone until blue color persists and distilled before use. Pyridine and triethylamine were dried over KOH pellets and distilled before use. $POCl_3$ was distilled before use.

2.1.1.2 NMR solvents

Chloroform-*d*, DMSO-d_6, methanol-d_4, toluene-d_8, TFA-*d* and D_2O were purchased from Sigma Aldrich/Acros Organics/Cambridge isotope Inc. and directly used for spectroscopic purpose.

2.1.1.3 Solvents for optical measurement

$CHCl_3$ (spectroscopy grade) were purchased from Merck and used as such.

2.1.2 Reagents

Thiophene, B_2Pin_2, $[Ir(COD)(OMe)]_2$, dtbpy, CuCl, chloranil, NaH, KO_2, CaH_2, benzophenone, $PdCl_2(PPh_3)_2$ and $Pd(OAc)_2$ were bought from Sigma-Aldrich® and used as such. THF was purchased from Finar chemicals. DCE, NBS, DMF, DCM, $CHCl_3$, DMSO, MeOH, ethylene glycol, isopentanol, fumaric acid, TOSMIC, periodic acid and 2-methoxyethanol were purchased from Merck/SRL/Finar/Avra. $TiCl_4$, Zn powder, PPh_3 and sodium were purchased from Finar chemicals. All the inorganic salts, mineral acids, KI, NaOH, $MgSO_4.7H_2O$, K_2CO_3, Na_2SO_4, anhydrous $MgSO_4$, sodium dithionite, KOH, $Na_2S_2O_3.5H_2O$, $NaHCO_3$ and solvents used for the routine laboratory work, were purchased from Merck, India. $POCl_3$ was purchased from Chemlab, India.

2.2 Chromatography

Thin layer chromatography was performed on pre-coated TLC Silica gel 60 F_{254} on aluminum sheet, purchased from Merck. Column chromatography was carried out on silica gel (100-200 mesh) purchased from Merck/SRL/Dessica, India.

2.3 Characterization and instrumentation

All the instrumentation facilities have been provided by School of Chemistry and ACRHEM at University of Hyderabad, Hyderabad, India for the thesis work. Nuclear magnetic resonance (NMR) spectra were recorded on Bruker 400 MHz and 500 MHz FT-NMR spectrometer operating at ambient temperature. In $CDCl_3$, TMS (δ = 0 ppm) was used as internal standard for ^{1}H NMR spectra and for other deuterated solvents, solvent residual peak was taken as standard. Similarly, for ^{13}C NMR spectra solvent peak was taken as standard for all deuterated solvent for calibration purpose. Mass spectral data were collected by Bruker Maxis HRMS by ESI techniques and LCMS were recorded by Shimadzu-LCMS-2010 mass spectrometer both by positive and negative ionization method. Melting points were determined by a Lab India MR-VIS$^+$ visual melting point apparatus and uncorrected. IR spectra were recorded on NICOLET 5700 FT-IR spectrometer by either using KBr pellet or neat sample.

UV-vis spectra were documented on Perkin Elmer Lambda 35 and Lambda 750 UV-VIS-NIR spectrophotometer. Fluorescence spectra were measured on Horiba Zobin Yovan Fluoromax-4 and Fluorolog-3-221 spectrofluorometer equipped with Hamamatsu H10330-75 TE cooled NIR detector working at -60 °C. For the observation of steady-state emission spectra in the (NIR) region, a photomultiplier tube module (H10330-75, Hamamatsu), a lock-in amplifier (5210, EG&G) combined with a chopper and a CW He-Cd laser (Omnichrome 74, Melles Griot) for the 442 nm excitation were used. All steady-state measurements were carried out by using a quartz cuvette with a path length of 1 cm at ambient temperatures. EPR measurements were performed on Bruker EMX and JEF-FA series microX spectrometers.

Some of the crystallographic data were collected on BRUKER SMART-APEX CCD diffractometer, Mo−K_α (λ = 0.71073 Å) radiation was used to collect X-ray reflections from the single crystal. The remaining data were collected on BRUKER APEX-II CCD microfocus diffractometer, Mo−K_α (λ = 0.71073 Å) radiation was used to collect X-ray reflections from the single crystal. Data reduction was performed using Bruker SAINT[2] software. Intensities for absorption were corrected using SADABS,[3] and SADABS

2014/5,[3] refined using SHELXL-97,[4a] SHELXL-2014/7[4b] with anisotropic displacement parameters for non-H atoms. Hydrogen atoms on O and N were experimentally located in difference electron density maps. All C−H atoms were fixed geometrically using HFIX command in SHELX-TL. A check of the final CIF file using PLATON[5] did not show any missed symmetry. Further, some of the remaining crystallographic data were collected on Oxford Gemini A Ultra diffractometer with dual source, where Mo-K_α (λ = 0.71073 Å) and Cu-K_α (λ = 1.54184 Å) radiations were used to collect the X-ray reflections of the crystal. Data reduction was performed using CrysAlis^{Pro} 171.33.55 software.[6] Structures were solved and refined using Olex2-1.0, with anisotropic displacement parameters for non-H atoms. Hydrogen atoms on N were located from the Fourier map in all of the crystal structures. All C–H atoms were fixed geometrically. Empirical absorption correction was done using spherical harmonics, implemented in SCALE3 ABSPACK scaling algorithm. A check of the final CIF file using PLATON[5] did not show any missed symmetry.

2.4 Computational studies

Quantum mechanical calculations were performed with Gaussian 09 program[7] provided by CMSD facility of University of Hyderabad. All calculations were done by Density functional theory (DFT) with restricted Becke's three-parameter hybrid exchange functional and the Lee-Yang-Parr correlation functional (B3LYP) was used. The 6-31+G(d,p) basis set was used for all atoms. For all the performed calculations, input was taken from the crystal structures coordinates. The molecular orbitals were visualized using Gauss view 5.

2.5 Preparation of starting materials

2.5.1 Synthesis of ethyl 2-isocyanoacetate 2.4[8]

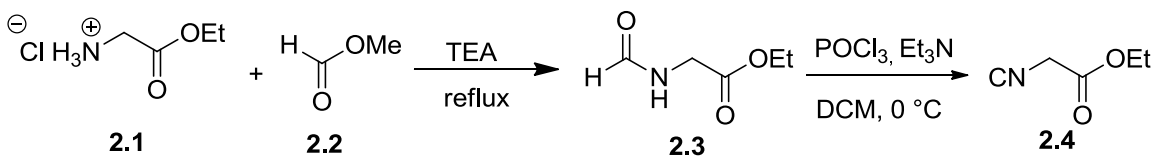

Scheme 1 Synthesis of **2.4.**

A. A three necked round bottomed flask fitted with a mechanical stirrer, a pressure equalizing dropping funnel, and a reflux condenser bearing a calcium chloride drying tube is charged with (69.5 g, 0.5 mol) of glycine ethyl ester hydrochloride and methyl formate (265 mL, 4.25 mol). Triethylamine (76 mL, 0.55 mol) was added to the suspension at reflux condition and further refluxed for 24 h. The mixture was cooled to room temperature and filtered through a buchner funnel. The filtrate was concentrated on a rotary evaporator and the remaining liquid is distilled under reduced pressure yielding N-formyl glycine ethyl ester as colorless liquid. Yield obtained 44 g (67%); reported yield 79%.

B. A three-necked, round-bottomed flask equipped with a thermometer, a mechanical stirrer, and a pressure-equalizing dropping funnel bearing a nitrogen inlet was charged with *N*-formyl glycine ethyl ester **2.3** (22 g, 0.165 mol), triethylamine (58 mL, 0.41 mol), and DCM (170 mL). The resulting solution is stirred and cooled to 0 °C to −2 °C in an ice–salt bath, and phosphorus oxychloride (16 mL, 0.165 mol) was added dropwise over 15–20 min while the temperature is maintained at 0 °C. The mixture becomes reddish brown as it was stirred and cooled at 0 °C for additional 2 h. The ice–salt bath was removed and replaced by an ice-water bath. Anhyd sodium bicarbonate (33 g, 0.39 mol) in water (225 mL) was added dropwise in stirring condition at a rate such that the temperature of the mixture was maintained at 25–30 °C. The two-phase mixture was stirred for another 30 min, after which water was added until the volume of the aqueous layer brought to 1 L. The aqueous layer was separated and extracted with DCM. The DCM solution was washed with brine solution and dried over anhyd potassium carbonate. Evaporation of the solvent under reduced pressure and distillation of the remaining brown oil afforded ethyl-2-isocyanoacetate. Yield obtained 14 g (75%); reported yield 76%.

2.5.2 Synthesis of 4-acetoxy-3-nitrohexane 2.8[9]

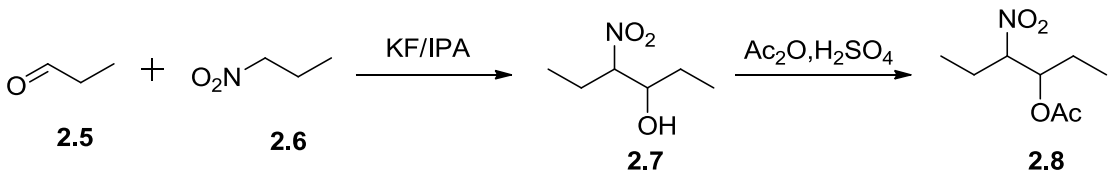

2.5 **2.6** **2.7** **2.8**

Scheme 2 Synthesis of **2.8**.

A. Propionaldehyde **2.5** (30 mL, 0.45 mol) and IPA (62 mL) were taken in a three-necked, round-bottomed flask fitted with a mechanical stirrer, thermometer, dropping funnel, and drying tube. To the stirred solution, finely ground KF (1.2 g, 0.021 mol) was added. 1-Nitropropane **2.6** (40 mL, 0.45 mol) was then added dropwise with stirring, and the temperature was kept below 40 °C. The mixture was stirred for an additional 18 h. The solid residue then removed by filtration and the filtrate was concentrated under reduced pressure. The remaining liquid is distilled using Kugelrorh distillation apparatus under reduced pressure yielding 4-nitro-3-hexanol **2.7** and used directly in the next step. Yield obtained: 38 g (57%); reported yield: 65%.

B. 4-Nitro-3-hexanol **2.7** (38 g, 0.26 mol) was taken in a three-necked, round-bottomed flask fitted with thermometer and dropping funnel. Few drops of conc. H_2SO_4 were added. The reaction mixture was stirred in an ice bath and Ac_2O (24.6 mL, 0.26 mol) was added in portions, keeping the temperature below 60°C. After complete addition of the acetic anhydride, reaction mixture was stirred for 1 h. The lower boiling compounds (Ac_2O and AcOH) were removed under reduced pressure in rotary evaporator and then purified using Kugelrorh distillation apparatus under reduced pressure yielding **2.8**. Yield obtained: 30 g (62%); reported yield: 90%.

2.5.3 Synthesis of ethyl 3,4-diethyl-1H-pyrrole-2-carboxylate 2.9a[10]

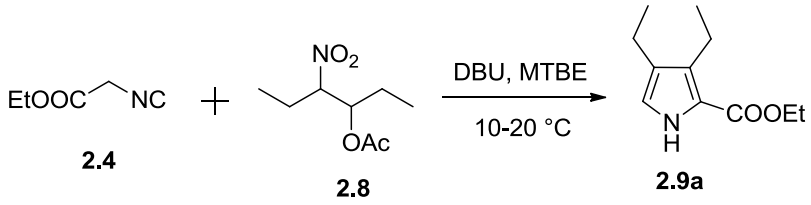

Scheme 2.3 Synthesis of **2.9a**.

Under nitrogen atmosphere, DBU (76 mL, 0.51 mol) was added to a stirred mixture of ethyl isocyanoacetate **2.4** (29.5 g, 0.26 mol), 4-acetoxy-3-nitrohexane **2.8** (49.4 g, 0.26 mol) in MTBE (75 mL) over a period of 90 min maintaining a temperature of 10–20 °C. The reaction mixture was stirred at 20 °C for 2 h. To the stirred mixture was added MTBE (111 mL), water (94 mL), NaCl (6.6 g) and concentrated HCl (34 mL) and the stirred mixture was warmed to 35–40 °C and allowed to settle. The MTBE solution containing the product was washed with saturated aq. Na_2CO_3 solution. Evaporation of

the solvent under reduced pressure produced the crude product, which was then purified using Kugelrorh distillation apparatus under reduced pressure yielding **2.9a**. Yield obtained: 41.7 g (82%); reported yield: 99%.

2.5.4 Synthesis of benzyl 3,4-diethyl-1H-pyrrole-2-carboxylate 2.9b[11]

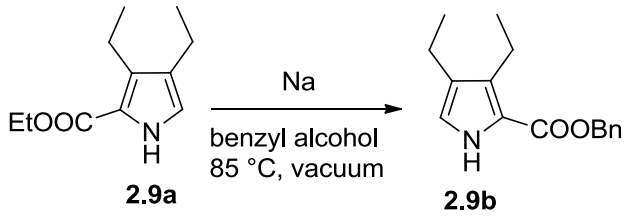

Scheme 2.4 Synthesis of **2.9b**.

Sodium (0.235 g, 10.24 mmol) along with dry benzyl alcohol (20 mL) was taken in a two- neck round bottom flask and stirred in nitogen for some time. Then compound **2.9a** (2 g, 10.24 mmol) was added to the reaction mixture and later stirred under vacuum at 85 °C for 4 h. Completion of reaction was confirmed by TLC. Then the excess benzyl alcohol was removed by Kugelrohr distillation under high vacuum at 100 °C. The crude product was then dissolved in DCM, washed with saturated NH_4Cl solution (50 mL) and finally with water (50 mL) to give **2.9b** as brown oil. Yield obtained: 2.06 g (78%), reported yield: 100%.

2.5.5 Synthesis of 3, 4-diethylpyrrole 2.10[9]

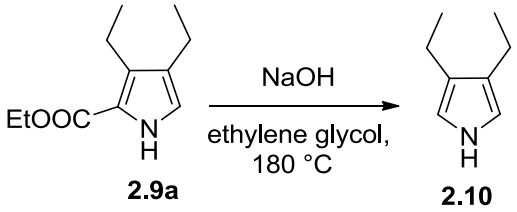

Scheme 2.5 Synthesis of **2.10**.

To the compound **2.9a** (7.8 g, 4 mmol) was added sodium hydroxide (2.46 g, 6.2 mmol) and dry ethylene glycol (30 mL). The contents are held at reflux under nitrogen for 1 h, cooled, transferred to a separatory funnel, and diluted with water (150 mL) and hexane (100 mL). The layers are separated, and the aqueous layer is extracted further with hexane (2 × 50 mL). The hexane layers are combined, dried over anhyd $MgSO_4$, and concentrated under reduced pressure. The residue is subjected to Kugelrohr distillation under high vacuum to yield **2.10**. Yield obtained: 4.05 g (82%); reported yield: 40%.

2.5.6 General procedure for the synthesis of 2-benzoyl/acyl/formyl-3,4-diethylpyrroles 2.9c-e

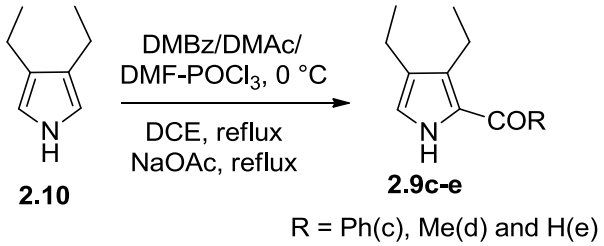

Scheme 2.6 Synthesis of **2.9c-e**.

To a three-neck round bottom flask having a dropping funnel and a reflux condenser N,N-dimethylbenzamide (DMBz) (3.3 g, 22 mmol)/N,N-DMAc (3.1 mL, 33 mmol)/DMF (1.7 mL, 22 mmol) was added. The flask was immersed in an ice bath, $POCl_3$ (2 mL, 22 mmol)/ (3.1 mL, 33 mmol)/ (2 mL, 22 mmol) was added slowly through syringe. The ice bath was removed and the complex was stirred for another 24 h/15 min/15 min at room temperature. DCE (5 mL) was added and the ice bath was replaced. When the internal temperature has been lowered to 5 °C, 3,4-diethylpyrrole (2.46 g, 20 mmol)/ (3.69 g, 30 mmol)/(2.46 g, 20 mmol) dissolved in DCE (20 mL) was added slowly to cooled reaction mixture. After the addition was complete, the ice bath was replaced with heating mantle. The mixture was refluxed for 4 h, then cooled to 25-30 °C and a saturated solution of sodium acetate (9 g, 110 mmol)/ (13.5 g, 165 mmol)/ (9 g, 110 mmol) was added slowly to the reaction mixture. The reaction mixture was again refluxed for 4 h, during which period there was a copious evolution of HCl gas. After the completion of reaction, it was extracted thrice with DCM. The combined organic layers were washed with saturated aq sodium carbonate solution and dried over anhyd sodium carbonate. The crude product was purified via column chromatography using silica gel with 20% EtOAc + 80% hexane as eluent to get the desired products.

2.9c Yield: 3.8 g, 84%; pale yellow liquid; FTIR data (in cm^{-1}): 3282, 2972, 1660; ^1H NMR (400 MHz, $CDCl_3$ δ in ppm): 8.76 (s, 1H), 7.66 (m, 2H), 7.52 (m, 1H), 7.46 (m, 2H), 6.81 (d, *J* = 2.8 Hz, 1H), 2.50 (m, 4H), 1.22 (t, *J* = 7.6 Hz , 3H), 1.01 (t, *J* = 7.6 Hz, 3H); ^{13}C NMR (100 MHz, $CDCl_3$ δ in ppm): 186.5, 140.2, 134.1, 131.0, 128.3, 128.0, 121.6, 18.3, 18.0, 15.4, 14.7; HRMS m/z calculated for $[M+Na]^+$ $C_{15}H_{17}NONa$: 250.1208, found 250.1210.

2.9d Yield: 4.7 g, 95%; off-white crystalline solid; mp 96-98 °C ; FTIR data (in cm^{-1}): 3203, 2967, 1615; ^{1}H NMR (400 MHz, $CDCl_3$ δ in ppm) : 9.04 (s, 1H), 6.76 (d, *J* = 3.2 Hz, 1H), 2.76 (q, *J* = 7.6 Hz, 2H), 2.47 (s, 3H), 2.45 (q, *J* = 7.6 Hz, 2H), 1.2 (m, 6H); ^{13}C NMR (100 MHz, $CDCl_3$ δ in ppm): 187.6, 131.6, 128.9, 127.3, 121.0, 27.2, 18.6, 17.8, 15.8, 14.7; HRMS m/z calculated for $[M+H]^+$ $C_{10}H_{16}NO$:166.1232 found 166.1229.

2.9e Yield: 2.8 g, 92%; reported yield: 98%.[12]

2.5.7 General procedure for the synthesis of iodopyrrole derivatives 2.11a-e

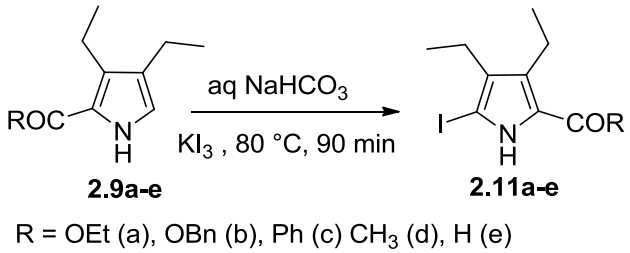

Scheme 2.7 Synthesis of **2.11a-e**.

To sodium bicarbonate solution (3.125 g, 38 mmol in 58.5 mL water) in a two-neck round bottom flask bearing a reflux condenser with a nitrogen inlet and a pressure equalizing dropping funnel, the corresponding pyrrole derivative **2.9a-e** (10 mmol) in DCE was added and heated at 90 °C. To this, KI_3 solution (KI - 3.65 g, 22 mmol + I_2 - 2.79 g, 11 mmol in 30 mL water) was added dropwise and stirred for 90 min at 80 °C. Later, the reaction mixture was extracted twice with DCM. The organic layer was washed with saturated sodium thiosulphate solution and dried over anhyd sodium sulfate. The solvent was evaporated on a rotary evaporator and the crude product was subsequently purified by column chromatography using silica gel with 10% EtOAc + 90% hexane as eluent to obtain the pure compounds.

2.11a Yield: 2.73 g, 85%; reported yield: 85%.[13]

2.11b Yield: 3 g, 78%; white solid; mp 94-95 °C; FTIR data (in cm^{-1}): 3266, 2964, 1671; ^{1}H NMR (400 MHz, $CDCl_3$ δ in ppm): 8.94 (s, 1H), 7.38 (m, 5H), 5.31, (s, 2H), 2.77 (q, J = 7.6 Hz, 2H), 2.38 (q, J = 7.6 Hz, 2H), 1.13 (t, J = 7.6 Hz, 3H), 1.08 (t, J = 7.6 Hz, 3H); ^{13}C NMR (100 MHz, $CDCl_3$ δ in ppm): 160.0, 136.1, 133.7, 131.7, 128.6, 128.3, 122.8, 73.1, 66.0, 19.8, 18.8, 15.8, 15.5; HRMS calcd. for $[M+H]^+$ $C_{16}H_{19}NO_2I$:384.0461, found 384.0461.

2.11c Yield: 2.9 g, 83%; yellow solid; mp 120-121 °C ; FTIR data (in cm^{-1}): 3237, 2963, 1604; ^1H NMR (400 MHz, $CDCl_3$ δ in ppm): 9.05 (s, 1H), 7.66 (m, 2H), 7.54 (m, 1H), 7.46 (m, 2H), 2.52 (q, J = 7.6 Hz, 2H), 2.42 (q, J = 7.6 Hz, 2H), 1.11 (t, J = 7.6 Hz, 3H), 0.99 (t, J = 7.6 Hz, 3H); ^{13}C NMR (100 MHz, $CDCl_3$ δ in ppm): 185.3, 139.5, 134.3, 132.4, 131.3, 128.4, 128.1, 76.8, 19.8, 18.8, 15.8, 15.3; HRMS calcd. for $[M+H]^+$ $C_{15}H_{17}NOI$: 354.0355, found 354.0359.

2.11d Yield: 2.4 g, 83%; off-white solid; mp 118-120 °C; FTIR data (in cm^{-1}): 3238, 2964, 1621; ^1H NMR (400 MHz, $CDCl_3$ δ in ppm): 9.29 (s, 1H), 2.77 (q, J = 7.6 Hz, 2H), 2.46 (s, 3H), 2.39 (q, J = 7.6 Hz, 2H), 1.20 (t, J = 7.6 Hz, 3H), 1.09 (t, J = 7.6 Hz, 3H); ^{13}C NMR (100 MHz, $CDCl_3$ δ in ppm): 186.4, 133.4, 132.0, 131.8, 76.8, 27.0, 19.7, 19.2, 16.3, 15.4; HRMS calcd. for $[M+H]^+$ $C_{10}H_{15}NOI$: 292.0198, found 292.0199.

2.11e Yield: 1.94 g, 70%: reported yield: 89%.[12]

2.5.8 Synthesis of 2-(4,4,5,5-tetramethyl-1,3,2-dioxaborolan-2-yl)-thiophene 2.13[14]

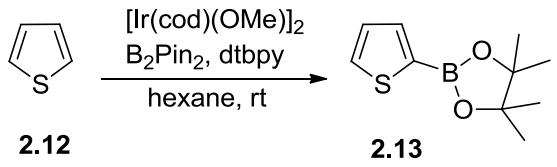

Scheme 2.8 Synthesis of **2.13**.

$[Ir(cod)(OMe)]_2$ (72 mg, 0.107mmol), dtbpy (60 mg, 0.224 mmol) and B_2Pin_2 (3.68 g, 14.43 mmol) were placed in a two-necked round bottomed flask and was evacuated for 1 h. Dry hexane (50 mL) was added under nitrogen atmosphere to get a bright red color solution of the active catalyst. To this solution, thiophene **2.12** (12.1 mL, 0.144 mol) was added via syringe under nitrogen atmosphere and the reaction mixture was stirred for 0.5 h. Then the organic layer was separated after washing with brine solution by ethyl acetate. The solvent was evaporated under reduced pressure in rotary evaporator and purified using Kugelrorh distillation apparatus under reduced pressure. Yield obtained: 3.1 g (51%); reported yield: 57%.

2.6 Summary

A brief account of various solvents and chemicals used in the synthesis and different techniques and other physical and computational methods employed for characterization

in our investigation, is given in this chapter. All reported compounds are synthesized and characterized by following reported procedure, which are employed as starting materials for the dissertation work, were also described here.

2.7 References

1. Armarego, W. L. F.; Chai, C. In *Purification of laboratory chemicals*, sixth edition, Elsevier, Burlington, **2003**.
2. SAINT, version 6.45 /8/6/03, Bruker AXS, **2003**.
3. Sheldrick, G. M. *SADABS*, Program for Empirical Absorption Correction of Area Detector Data, University of Göttingen, Germany, **1997**.
4. SHELXL -Version 2014/7, Program for the Solution and Refinement of Crystal Structures, University of Göttingen, Germany, 1993-2014, Sheldrick, G. M. *Acta Cryst.* **2008**, *A64*, 112.
5. (a) Spek, A. L. *PLATON*, *A Multipurpose Crystallographic Tool*, Utrecht University, Utrecht, the Netherlands, **2002**. (b) Spek, A. L. *J. Appl. Cryst.* **2003**, *36*, 7.
6. Oxford Diffraction (**2008**). CrysAlis CCD and CrysAlis RED. Versions 1.171.33.55. Oxford Diffraction Ltd, Yarnton, Oxfordshire, England.
7. Gaussian 09, Revision C.01, Frisch, M. J.; Trucks, G. W.; Schlegel, H. B.; Scuseria, G. E.; Robb, M. A.; Cheeseman, J. R.; Scalmani, G.; Barone, V.; Mennucci, B.; Petersson, G. A.; Nakatsuji, H.; Caricato, M.; Li, X.; Hratchian, H. P.; Izmaylov, A. F.; Bloino, J.; Zheng, G.; Sonnenberg, J. L.; Hada, M.; Ehara, M.; Toyota, K.; Fukuda, R.; Hasegawa, J.; Ishida, M.; Nakajima, T.; Honda, Y.; Kitao, O.; Nakai, H.; Vreven, T.; Montgomery Jr., J. A.; Peralta, J. E.; Ogliaro, F.; Bearpark, M.; Heyd, J. J.; Brothers, E.; Kudin, K. N.; Staroverov, V. N.; Keith, T.; Kobayashi, R.; Normand, J.; Raghavachari, K.; Rendell, A.; Burant, J. C.; Iyengar, S. S.; Tomasi, J.; Cossi, M.; Rega, N.; Millam, J. M.; Klene, M.; Knox, J. E.; Cross, J. B.; Bakken, V.; Adamo, C.; Jaramillo, J.; Gomperts, R.; Stratmann, R. E.; Yazyev, O.; Austin, A. J.; Cammi, R.; Pomelli, C.; Ochterski, J. W.; Martin, R. L.; Morokuma, K.; Zakrzewski, V. G.; Voth, G. A.; Salvador, P.; Dannenberg, J. J.; Dapprich, S.; Daniels, A. D.; Farkas, O.; Foresman, J. B.; Ortiz, J. V.; Cioslowski, J.; Fox, D. J. *Gaussian, Inc.*, Wallingford CT, **2010**.
8. Hartman, G. D.; Weinstock, L. M. *Org. Synth.* **1979**, *59*, 183.
9. Sessler, J. L.; Mozaffari, A.; Johnson, M. R. *Org. Synth.* **1992**, *70*, 68.

10. Bhattacharya, A.; Cherukuri, S.; Plata, R. E.; Patel, N.; Tamez, V. Jr.; Grosso, J. A.; Peddicord, M.; Palaniswamy, V. A. *Tetrahedron Lett.* **2006**, *47*, 5481.
11. Boudif, A.; Momenteau, M. *J. Chem. Soc., Perkin Trans.* 1, **1996**, 1235.
12. Rana, A.; Lee, S.; Kim, D.; Panda, P. K. *Chem. Eur. J.* **2015**, *21*, 12129.
13. Shevchuk, S. V.; Davis, J. M.; Sessler, J. L. *Tetrahedron Lett.* **2001**, *42*, 2447.
14. Ishiyama, T.; Takagi, J.; Nobuta, Y.; Miyaura, N. *Org. Synth.* **2005**, *82*, 126.

2.8 ^{1}H NMR, ^{13}C NMR, IR and HRMS spectra

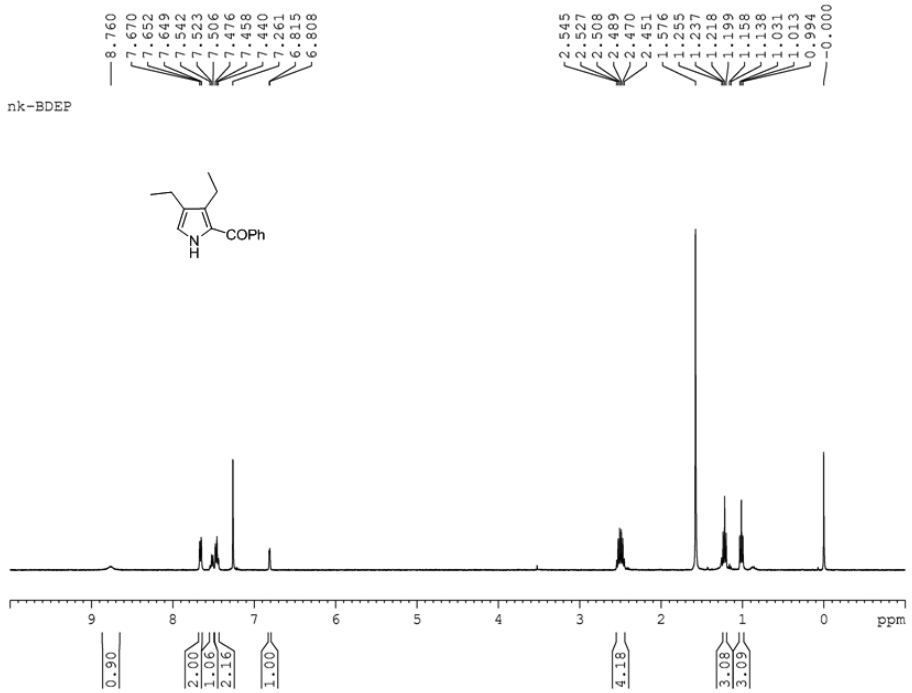

Figure 2.1 ^{1}H NMR spectrum of **2.9c** in $CDCl_3$.

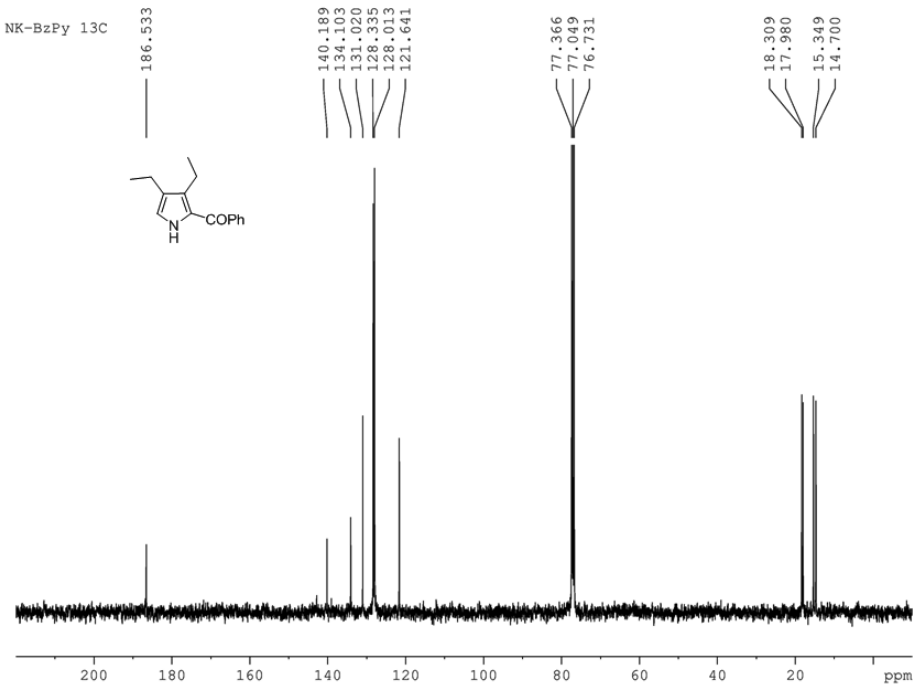

Figure 2.2 ^{13}C NMR spectrum of **2.9c** in $CDCl_3$.

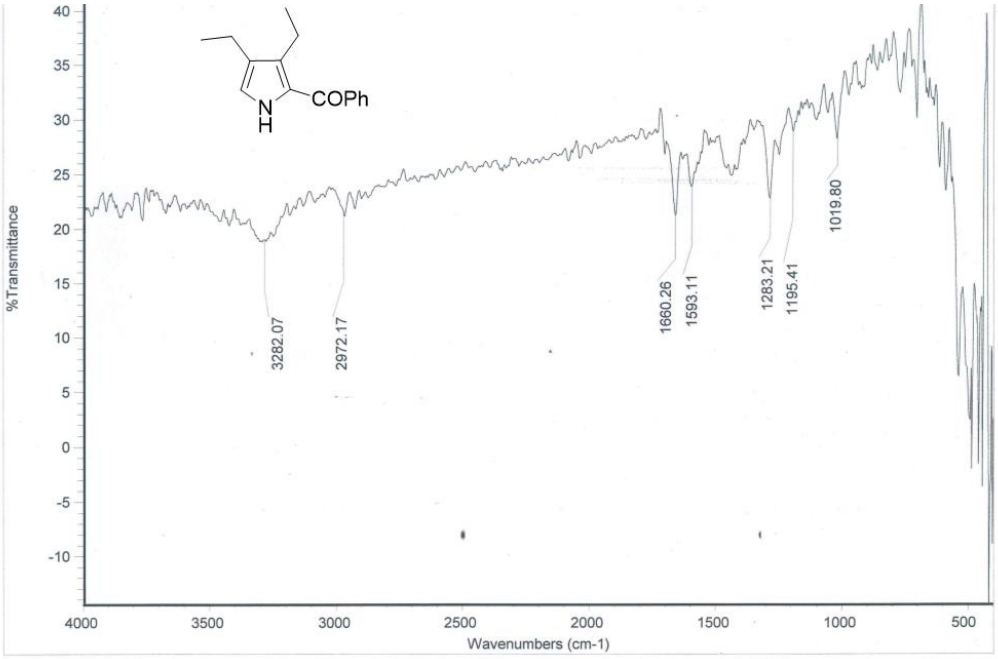

Figure 2.3 IR spectrum of **2.9c**.

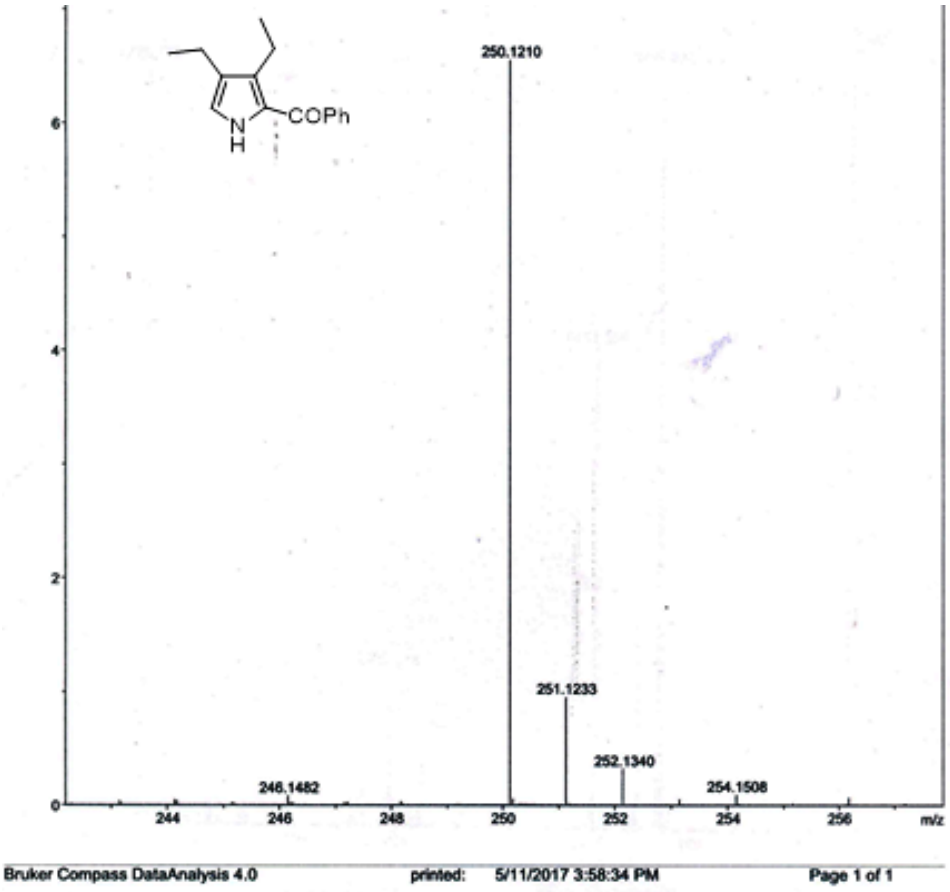

Figure 2.4 HRMS spectrum of **2.9c** for $[M+Na]^+$ $C_{15}H_{17}NONa$: 250.1208, found 250.1210.

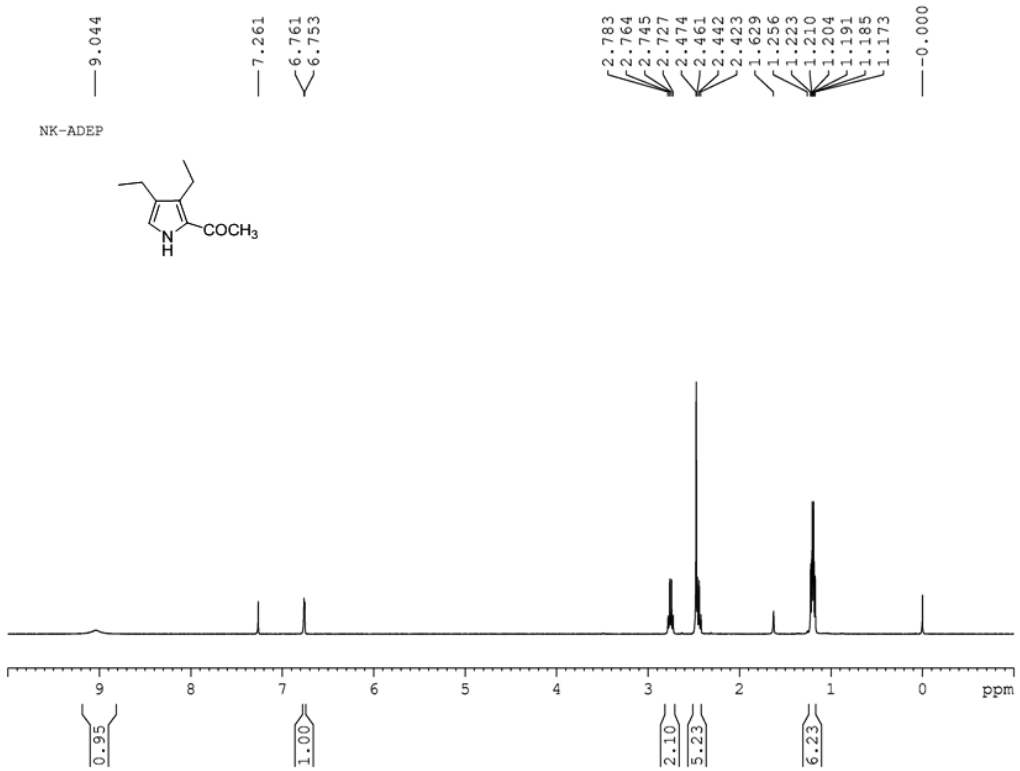

Figure 2.5 ^{1}H NMR spectrum of **2.9d** in $CDCl_3$.

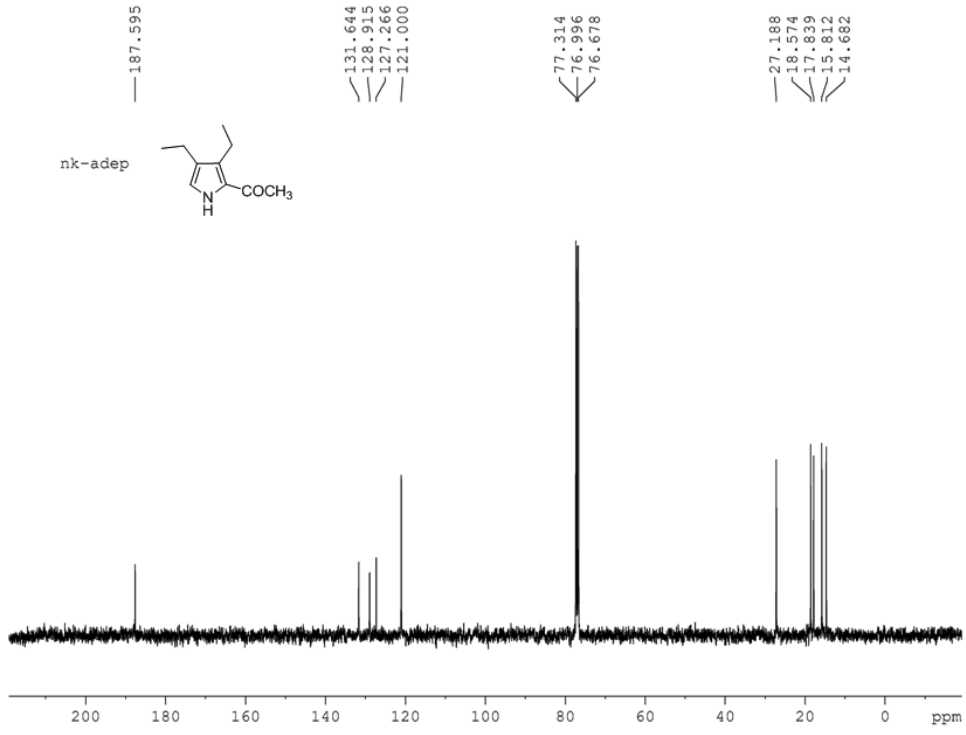

Figure 2.6 ^{13}C NMR spectrum of **2.9d** in $CDCl_3$.

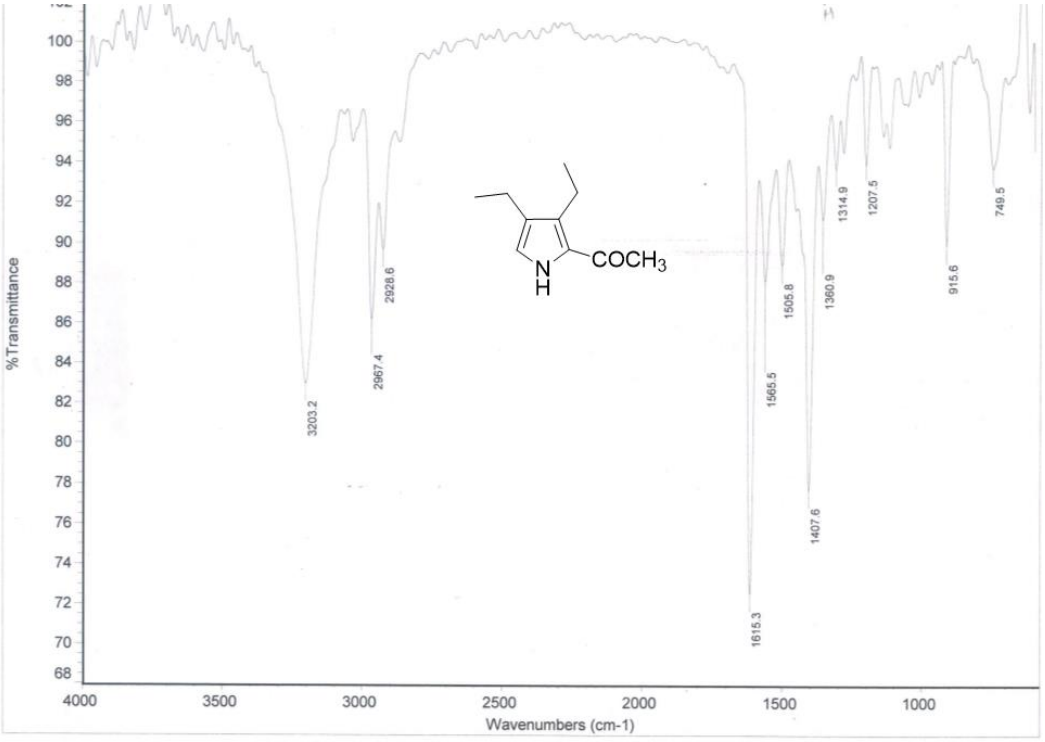

Figure 2.7 IR spectrum of **2.9d**.

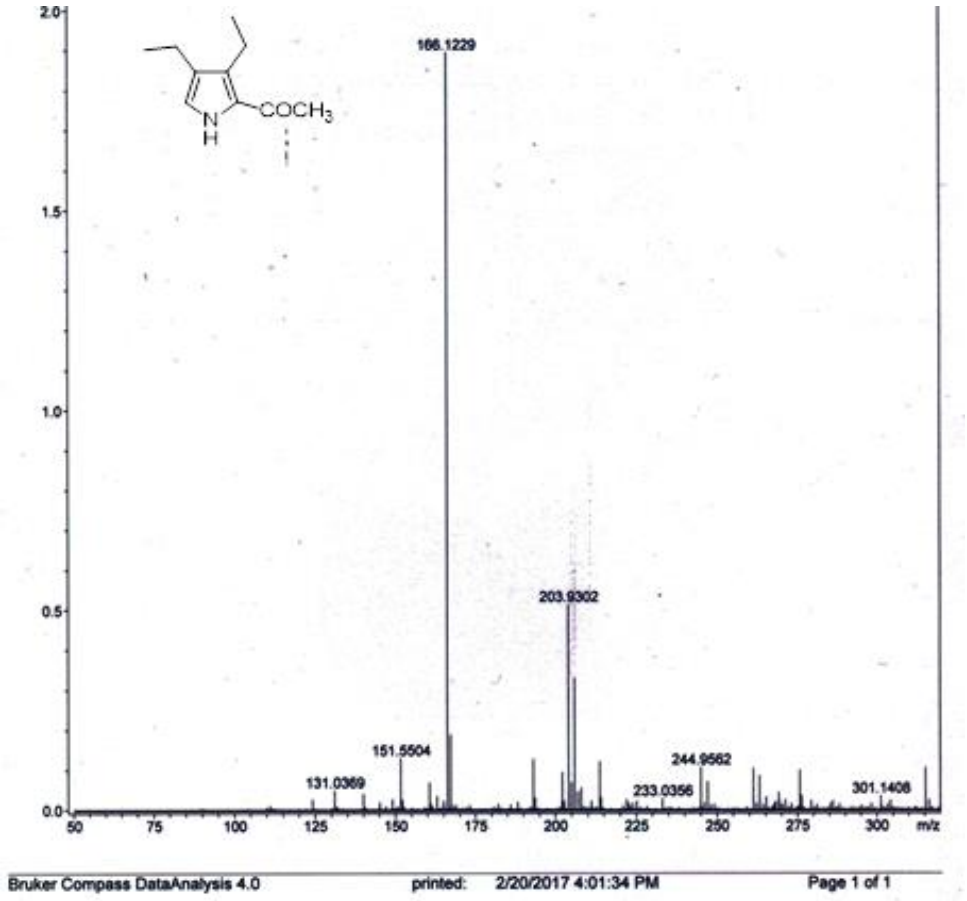

Figure 2.8 HRMS spectrum of **2.9d** for $[M+H]^+$ $C_{10}H_{16}NO$:166.1232 found 166.1229.

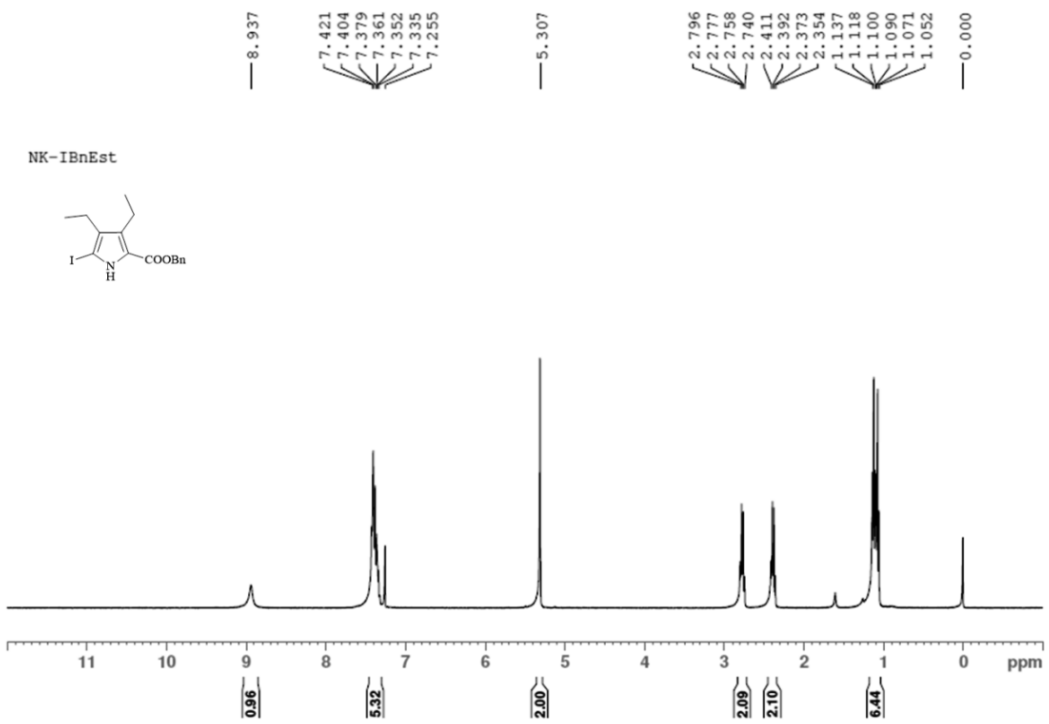

Figure 2.9 ^{1}H NMR spectrum of **2.11b** in $CDCl_3$.

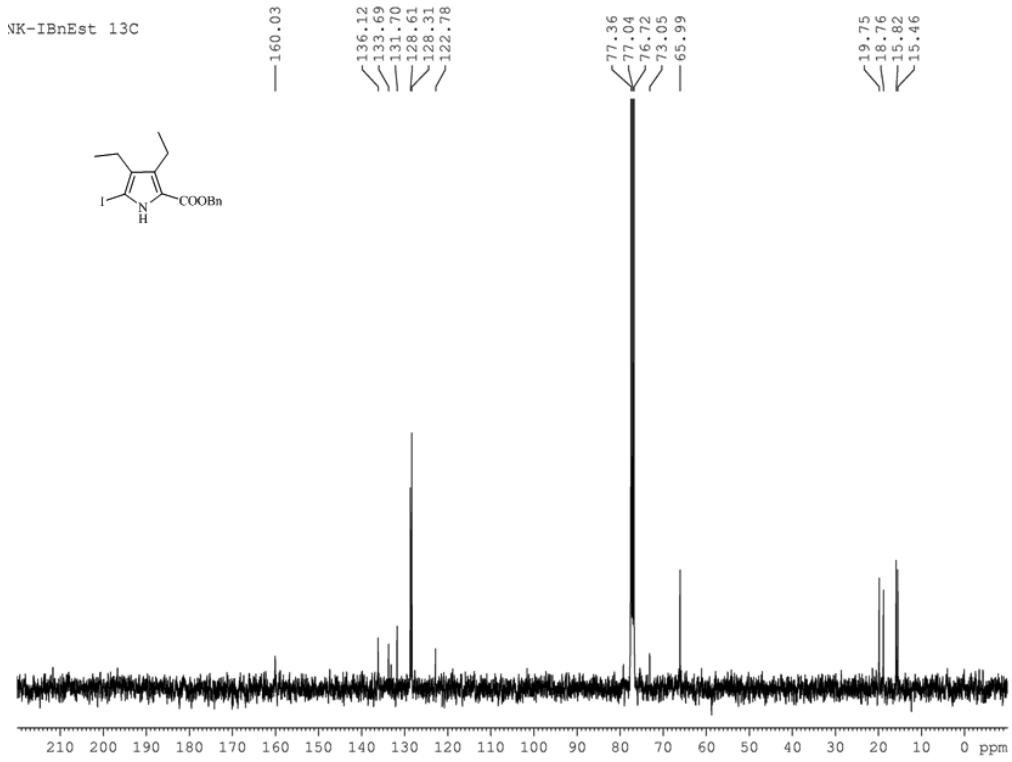

Figure 2.10 ^{13}C NMR spectrum of **2.11b** in $CDCl_3$.

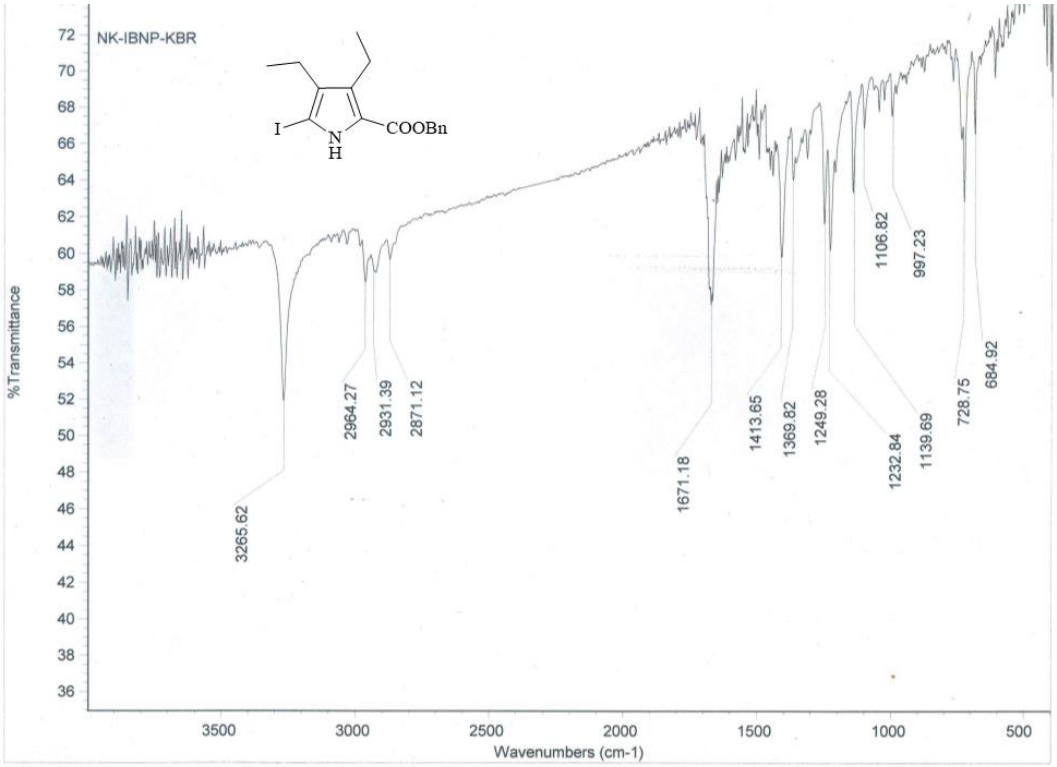

Figure 2.11 IR spectrum of **2.11b**.

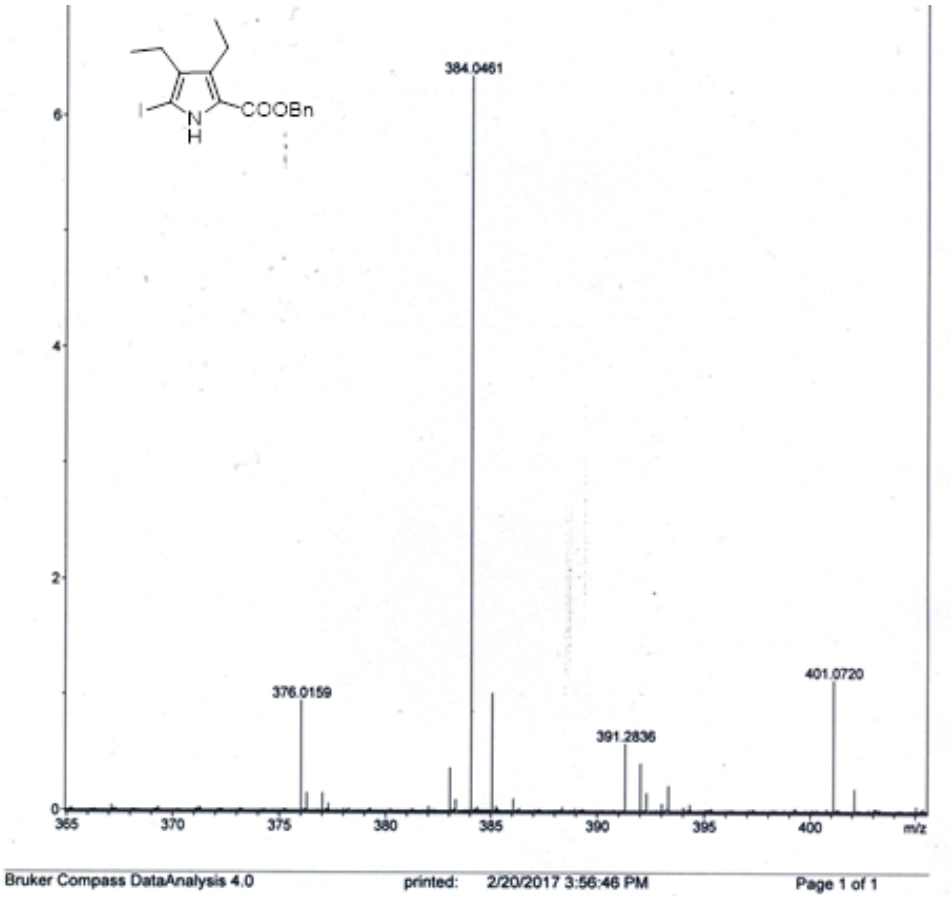

Figure 2.12 HRMS Spectrum of **2.11b** for $[M+H]^+$ $C_{16}H_{19}NO_2I$:384.0461, found 384.0461.

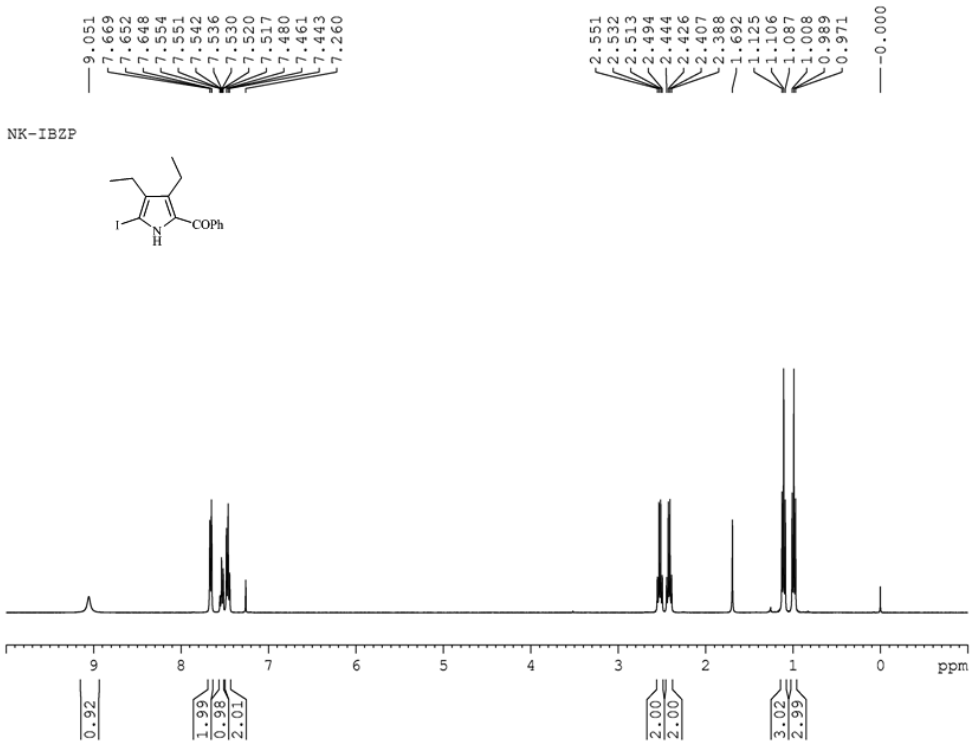

Figure 2.13 ^{1}H NMR spectrum of **2.11c** in $CDCl_3$.

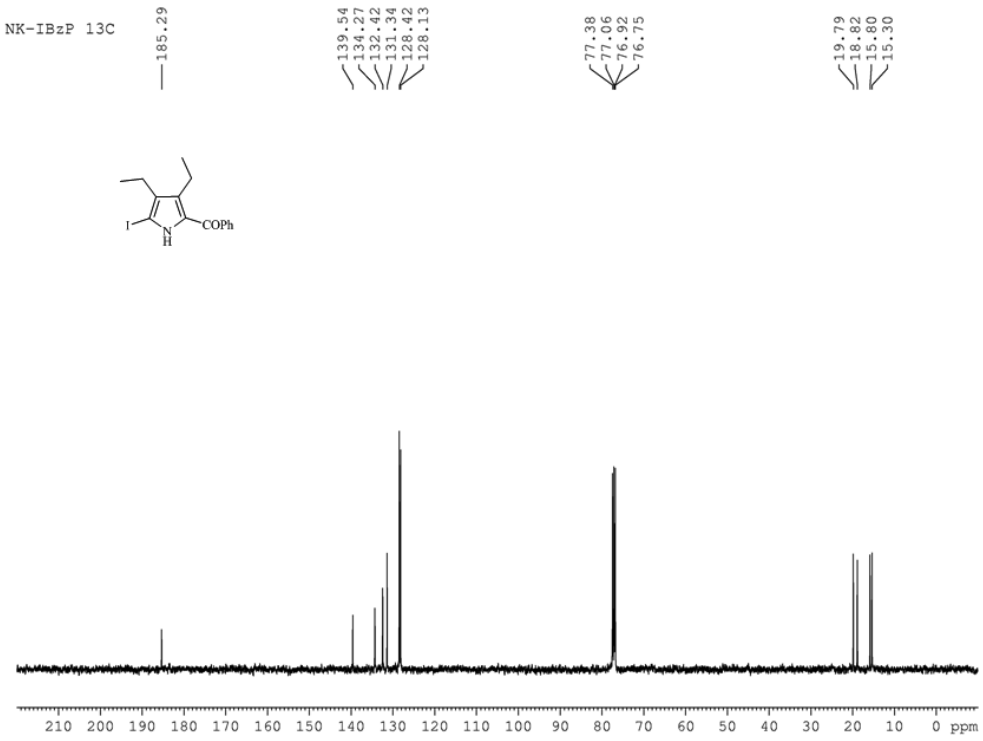

Figure 2.14 ^{13}C NMR spectrum of **2.11c** in $CDCl_3$.

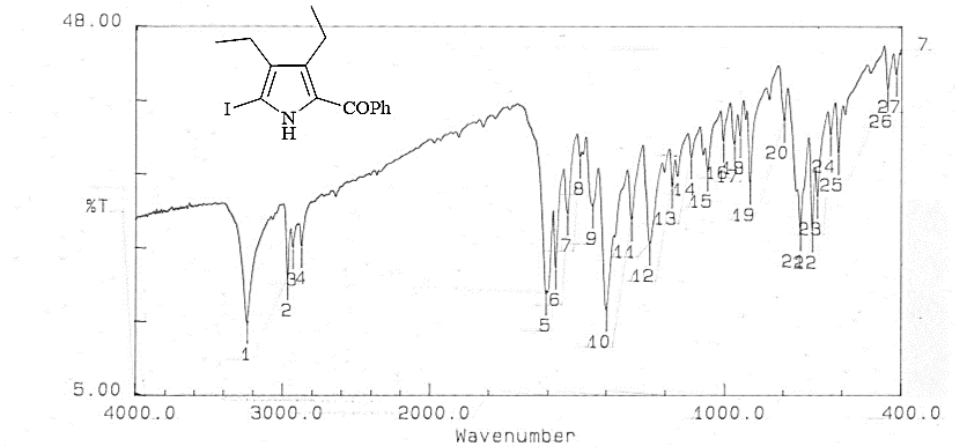

Condition

upper 48.00 lower 5.00 depth 2.00

Peak table

1:	3236.84 (13.6)	2:	2962.93 (18.7)	3:	2928.21 (22.3)	4:	2868.41 (22.5)
5:	1604.92 (17.0)	6:	1572.13 (20.0)	7:	1531.62 (26.3)	8:	1489.18 (32.9)
9:	1446.74 (27.1)	10:	1398.52 (15.0)	11:	1313.64 (25.6)	12:	1251.91 (22.8)
13:	1176.68 (29.4)	14:	1113.03 (32.8)	15:	1057.09 (31.4)	16:	1003.07 (34.7)
17:	966.42 (34.4)	18:	947.13 (35.3)	19:	912.41 (29.9)	20:	796.67 (37.1)
21:	740.73 (24.5)	22:	700.22 (24.3)	23:	682.86 (28.2)	24:	638.50 (35.5)
25:	611.49 (33.3)	26:	445.60 (40.8)	27:	416.66 (42.5)		

Figure 2.15 IR spectrum of **2.11c**.

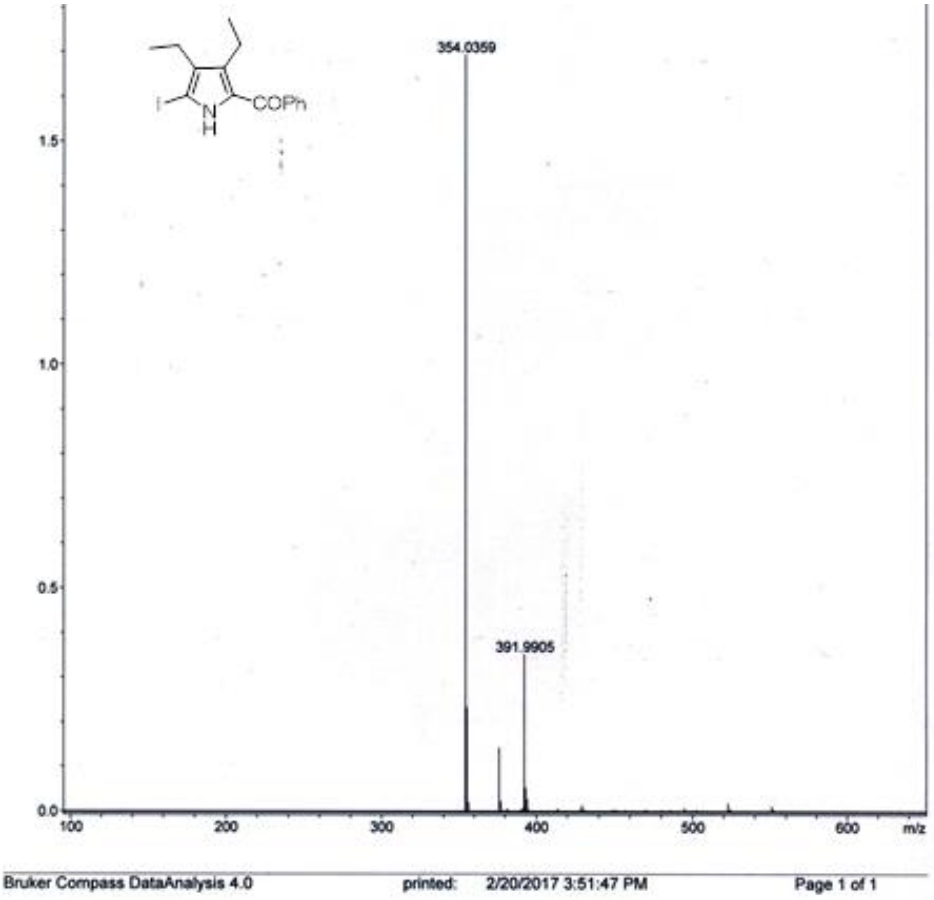

Figure 2.16 HRMS spectrum of **2.11c** for $[M+H]^+$ $C_{15}H_{17}NOI$:354.0355, found 354.0359.

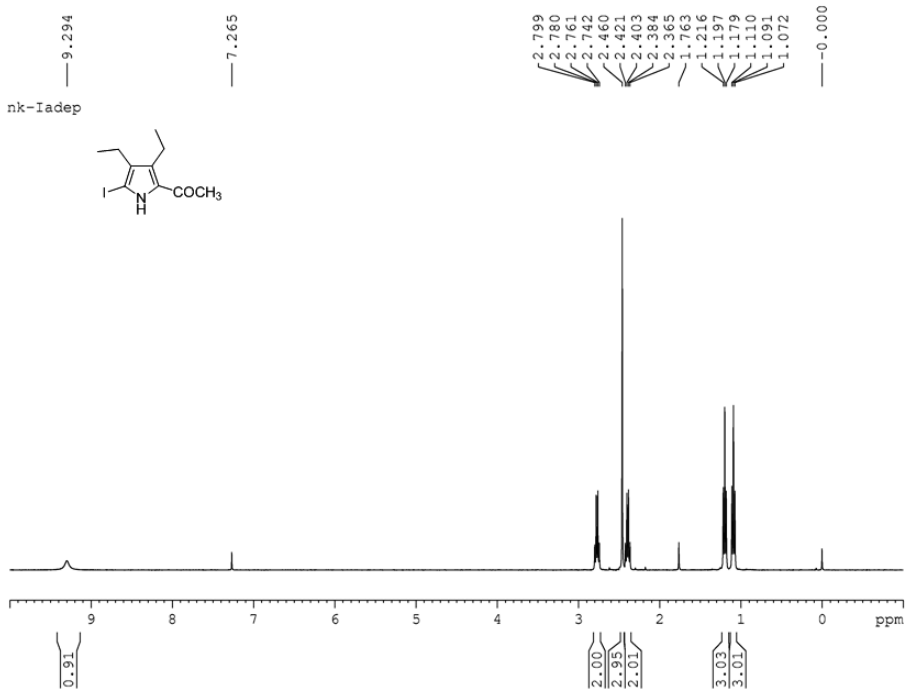

Figure 2.17 ^{1}H NMR spectrum of **2.11d** in $CDCl_3$.

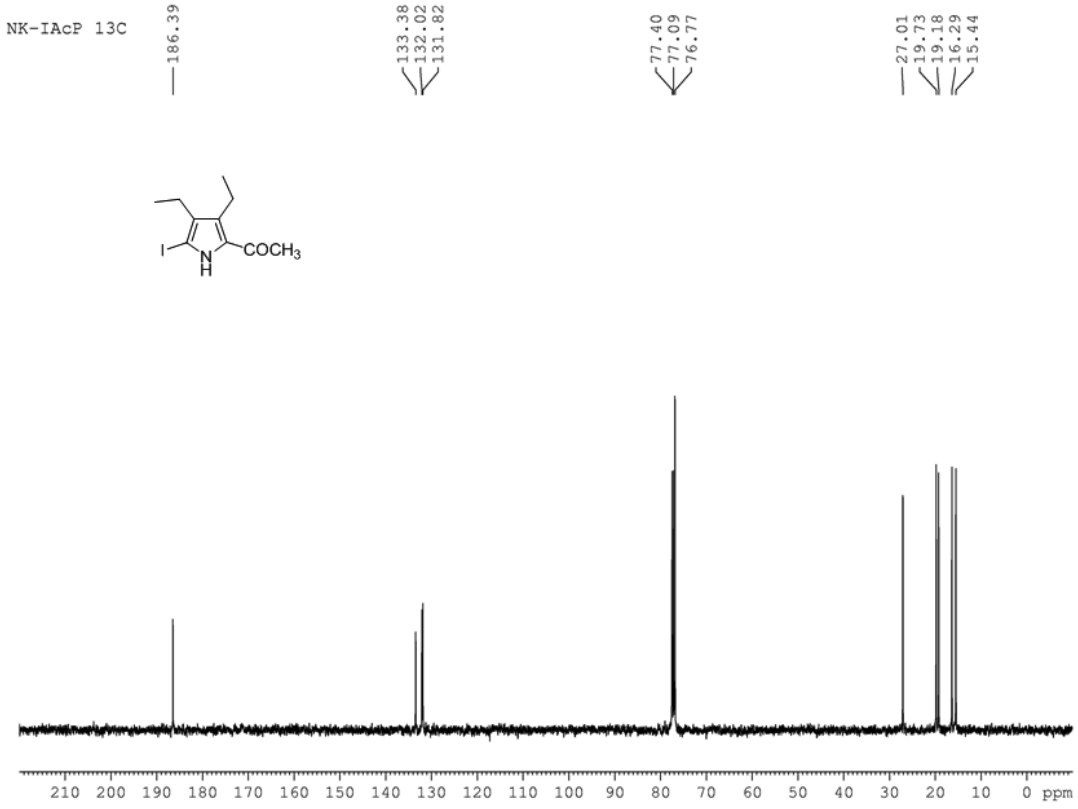

Figure 2.18 ^{13}C NMR spectrum of **2.11d** in $CDCl_3$.

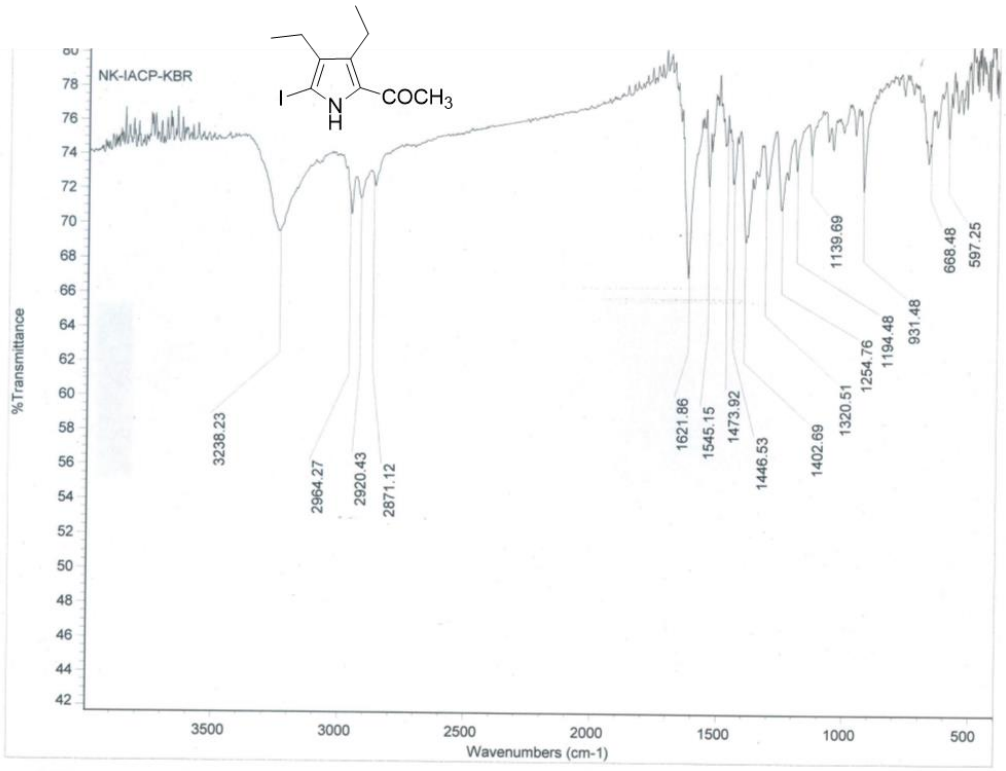

Figure 2.19 IR spectrum of **2.11d**.

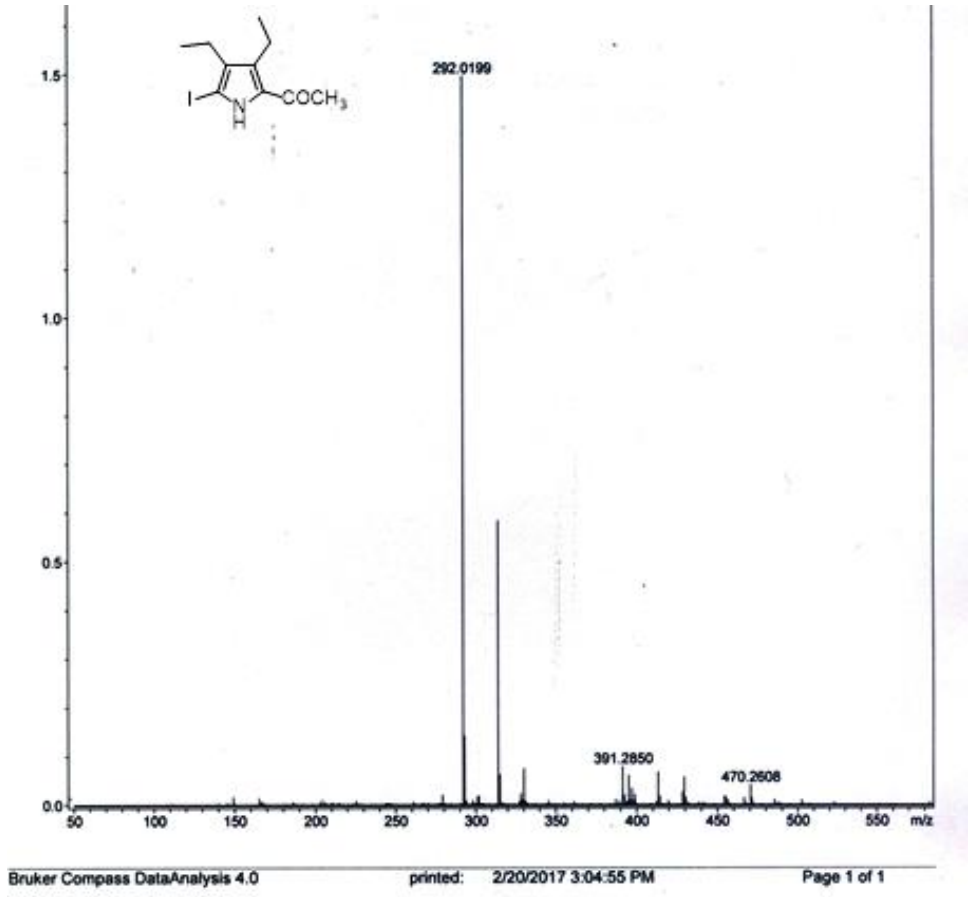

Figure 2.20 HRMS spectrum of **2.11d** for $[M+H]^+$ $C_{10}H_{15}NOI$:292.0198, found 292.0199.

CHAPTER 3

Dithia and all-aza bronzaphyrins

3.1 Introduction

Expanded porphyrins endowed with rigid bridging moieties, and in particular acetylene, have shown quite intriguing structural and photophysical properties, due to increased effective conjugation between the bridging units.[1] The first expanded porphyrin containing an acetylene bridged bipyrrole **3.1** (Figure 3.1) dates back to 1990,[1a] where Vogel and coworkers have reported an acetylene-cumulene porphyrinoid, inspired from the work on 1,2,8,9-tetradehydro[14]annulene by Sondheimer et al.[2] Later they extended their strategy to synthesize butadiyne-cumulene bridged expanded porphyrin **3.2** (Figure 3.1).[1c] As expected, these acetylene-cumulene porphyrinoids show pronounced bathochromic shifts compared to porphycene but their application was highly limited as photosensitizer in photodynamic therapy (PDT), due to poor singlet oxygen generation ability.[1c] Though lesser yields of acetylene bridged bipyrroles reported by Vogel were improvised by Kim and coworkers,[3] it remained a tedious task in synthesizing these systems, which involve three steps: i) Pd/Cu-co-catalyzed Sonogashira coupling of iodo pyrroles with trimethylsilylacetylene (TMSA), ii) followed by deprotection of the silyl protecting group and iii) another Sonogashira coupling to generate the monoacetylene-bridged bipyrrole derivatives or Pd-catalyzed oxidative coupling to yield the diacetylene (butadiyne)-bridged bipyrrole derivatives. Due to this ardent task, only very few groups incorporated acetylene bridge in synthesizing expanded porphyrins (Figure 3.1)[4a-c] and even demonstrated their utilities by converting them to heterocyclic systems.[4d,e] However, there are no reports showcasing the utility of diacetylene bridged bipyrrole by its success-

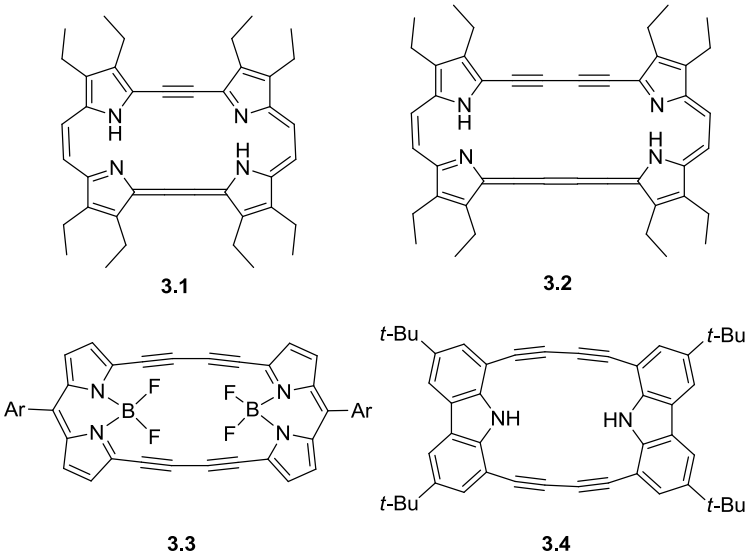

Figure 3.1 Examples of acetylene bridged expanded porphyrins.

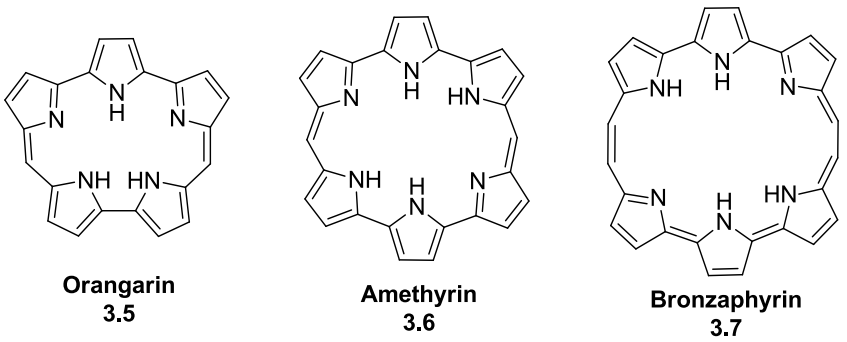

Figure 3.2 Some examples of terpyrrole containing expanded porphyrins.

ful conversion to terpyrrole moiety, as the latter has been well explored in synthesizing novel expanded porphyrins such as orangarin **3.5**,[5] amethyrin **3.6**[5,6] and in particular bronzaphyrin **3.7**[7] (Figure 3.2) and there are only very few reports regarding the synthetic methodology of terpyrroles, albeit with tedious approach.[8] Bronzaphyrin, unlike other hexapyrrolic systems endowed with *meso*-bridges hexaphyrin **3.8**,[9] rubyrin **3.9**[10] and rosarin **3.10**[11] (Figure 3.3) was the least explored in the last few decades, despite showing much intense red-shifted near-infrared (NIR) bands (only cyclo[6]pyrrole **3.11**[12] with no meso bridges display very intense Q-type absorption bands like bronzaphyrin). Bronzaphyrin, coined due to its characteristic bronze color in chloroform solution, is an aromatic [26]hexaphyrin(2.0.0.2.0.0) first reported by Johnson et al. as dithia derivative in 1992,[7a] using a modified Merrill and LeGoff method as shown in Scheme 3.1.

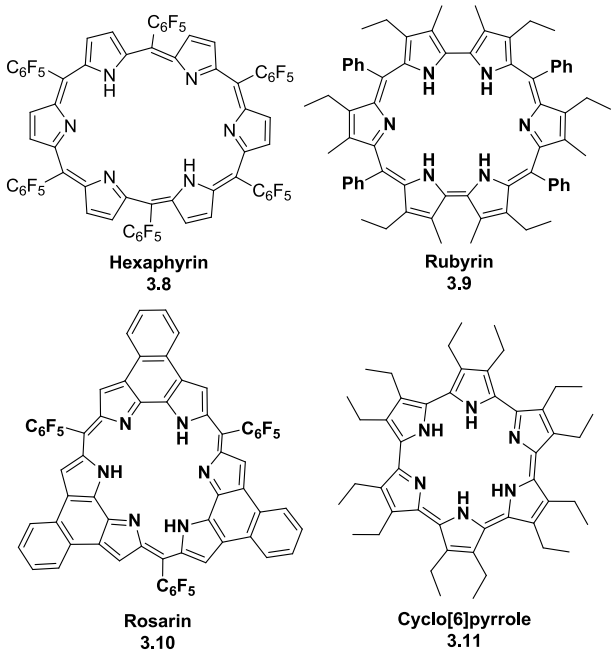

Figure 3.3 Examples of hexaphyrin, rubyrin, rosarian and cyclo[6]pyrrole.

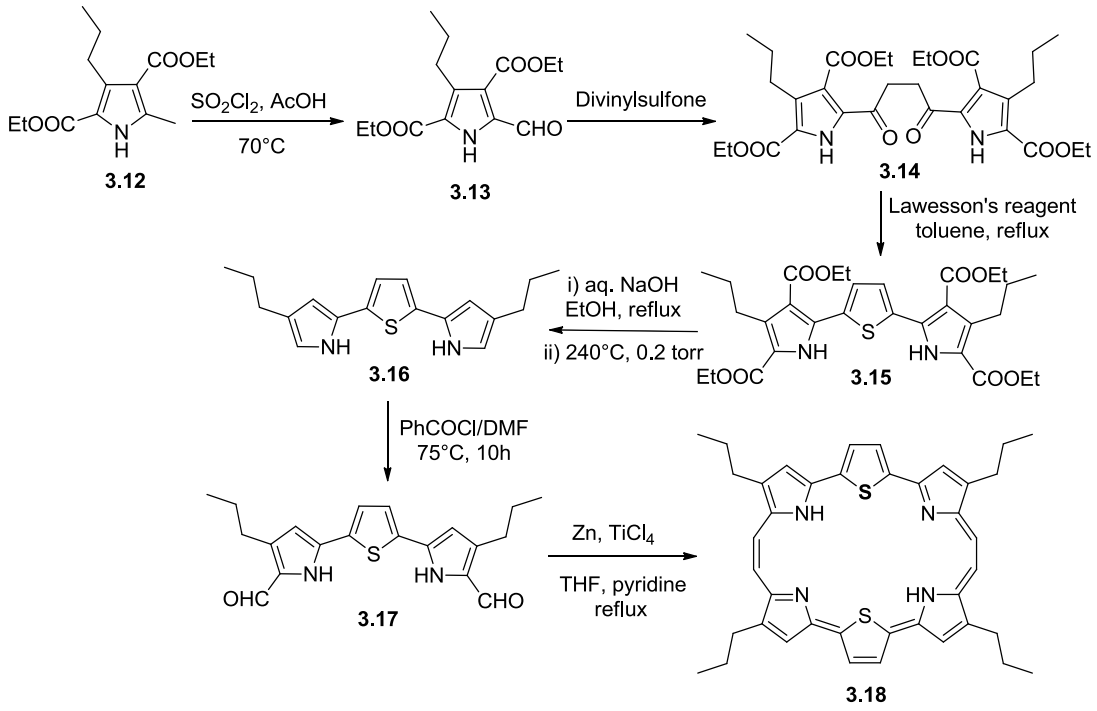

Scheme 3.1 Synthesis of dithiabronzaphyrin **3.18**.

Diethyl-5-methyl-3-propylpyrrole-2,4-dicarboxylate was treated with sulfuryl chloride in acetic acid at 70°C to give the corresponding aldehyde derivative, which was further coupled with divinyl sulfone using Stetter's method to yield dipyrrolylbutanedione derivative in high purity. This dione was then treated with Lawesson's reagent in refluxing toluene to give thiophene substituted terpyrrole tetraester, which was later decarboxylated and then formylated using benzoyl chloride/DMF at 75°C for 10 h. The diformylated product thus obtained was later employed in reductive coupling (McMurry coupling), to give dithiabronzaphyrin **3.18** in 28% yield. The macrocycle obtained was confirmed to be aromatic by means of both ^{1}H-NMR (diamagnetically shielded pyrrolic NH proton) and UV-Vis-NIR spectroscopy (characteristic Soret and Q bands).

Later Cava's group in 1993, employed three derivatives of thiophene substituted terpyrroles towards synthesizing bronzaphyrins, utilizing the same McMurry coupling (Scheme 3.2).[7d] However, among the three, only hexathia derivative **3.20** was able to be oxidized to show the characteristic features of bronzaphyrin, albeit in highly acidic condition, as a dicationic form, in presence of conc. H_2SO_4.[7e]

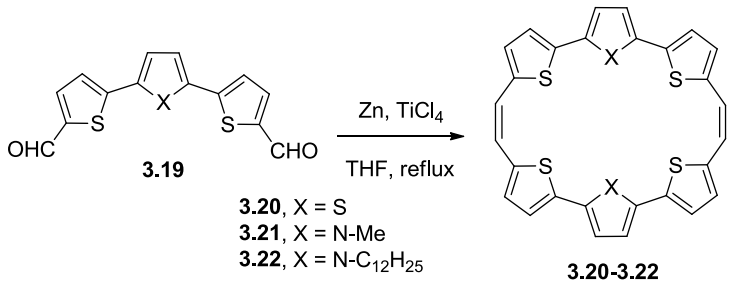

Scheme 3.2 Synthesis of reduced bronzaphyrins reported by Cava's group.

Johnson and Ibers's group, employed condensation of a mixture of thiophene and furan substituted terpyrrole aldehydes to yield both homo and hetero coupling products of dithiabronzaphyrin, **3.18** and oxobronzaphyrin **3.24** respectively (Scheme 3.3).[7b] However, they were unable to isolate the other homo coupled product, dioxobronzaphyrin. The oxobronzaphyrin shared similar aromatic characteristics to that of dithiabronzaphyrin.

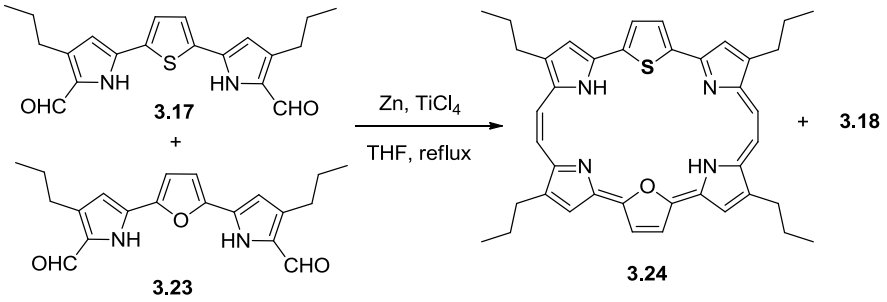

Scheme 3.3 Synthesis of oxobronzaphyrin **3.24**.

Meanwhile, Cava and coworkers attempt in cyclizing N-alkyl bridged bis-terpyrroles to yield bronzaphyrins ended up in isolating their corresponding reduced derivatives as shown in Scheme 3.4.[7f]

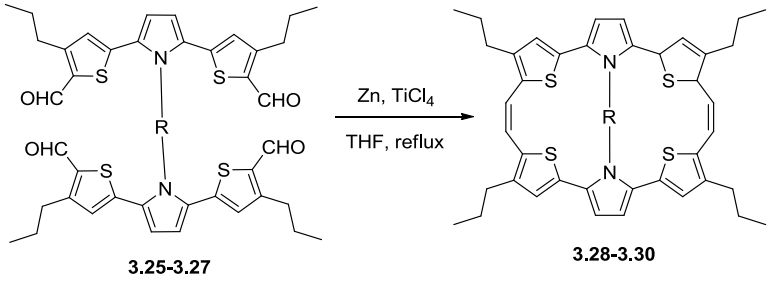

Scheme 3.4 Synthesis of bridged reduced bronzaphyrins reported by Cava's group.

Finally the last report on bronzaphyrin came in 1997[7c] and was reported by Johnson, capitalizing the mixed condensation reaction, which he performed under Ibers's group. He reacted a mixture of thiophene substituted and hexyl chain incorporated aza terpyrrole aldehydes to yield both homo and hetero coupling products of dithiabronzaphyrin (bronzaphyrin SS), **3.18** and bronzaphyrin NS, **3.32**, respectively (Scheme 3.5). Long hexyl chain is required to make the aza terpyrrole aldehyde soluble in THF. Isolation of the other homo coupled product all aza bronzaphyrin NN was not done apparently due to its unstable nature.

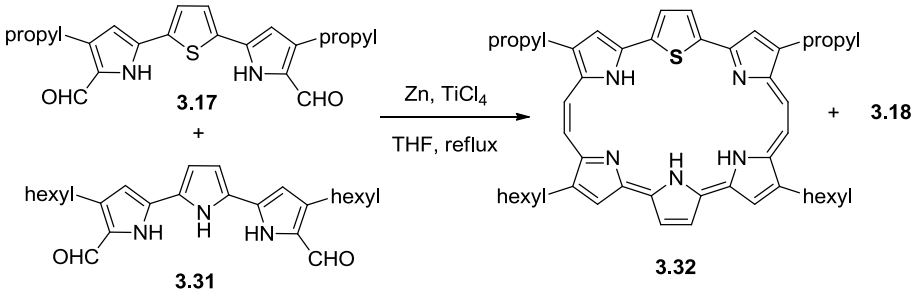

Scheme 3.5 Synthesis of bronzaphyrin NS **3.32**.

Due to these extreme solubility issues and synthetic difficulties, the work on bronzaphyrin probably has been abandoned in its infant stage, in spite of its promising rich photophysical properties and hitherto, unknown structural characteristics.

3.2 Research goal

As emphasized before, we wanted to explore much more convenient and easy synthesis in a one-pot approach to simplify the tedious three step process of synthesizing diacetylene bridged bipyrrole and successfully convert it to terpyrroles. Furthermore, as shown in the retrosynthetic scheme below (Scheme 3.6), these terpyrroles will be utilized in exploring novel bronzaphyrin (all-aza and dithia) derivatives and assess their stabilities, structural and photophysical properties.

In this regard, we opted for 3,4-dialkyl substituted pyrrole, and in particular, ethyl 3,4-diethyl pyrrole-2-carboxylate as the starting material, to combat the solubility issues. The ester protecting group comes handy, as it can be deprotected easily at any stage when required. Introduction of ethyl groups at all β-positions of bronzaphyrin will not only enhance the solubility of the macrocycle but also affect its structural aspects. The benzyl moiety employed for the protection of central pyrrole not only helps in stabilizing the molecule, but also sterically less crowded and may help in attaining alternate structural

features. In addition, the benzyl moieties can be deprotected as per our convenience. We have also anticipated that though dithiabronzaphyrin derivative may be similar to its reported macrocyclic core but the substitution at the inner β-positions might play an important factor in its structural and photophysical properties, as many thiophene containing macrocycles are prone to structural changes depending on the type of substitution and environment.

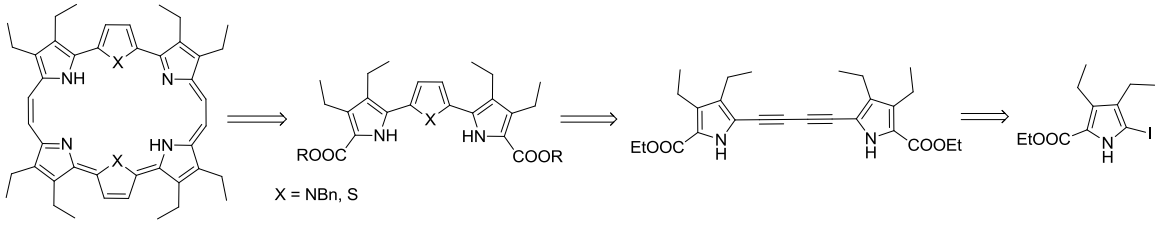

Scheme 3.6 Retrosynthetic approach of novel bronzaphyrin derivatives.

3.3 Results and discussion

3.3.1 Synthesis and characterization of diacetylene bridged bipyrroles

Motivation for the synthesis of diacetylene bridged bipyrroles came from our attempts to synthesize monoacetylene bridged bipyrroles, following the one-pot synthetic methodology developed for symmetrical bisarylethynes by Mio et al. involving a modified Sonogashira coupling reaction.[13] During the synthesis of monoacetylene bridged bipyrrole **3.34a**, we always ended up with a new compound, which could not be suppressed by modulation of reaction conditions (Scheme 3.7). Successful isolation and characterization of this new compound showed ^{1}H NMR very similar to monoacetylene bridged bipyrrole (Figure 3.4) but ^{13}C NMR spectrum showed an additional peak (Figure 3.5), which was later assumed to be extra C≡C bond after confirmation by mass spectrometry analysis (**3.34a**: 413.2440 and **3.35a**: 437.2427).

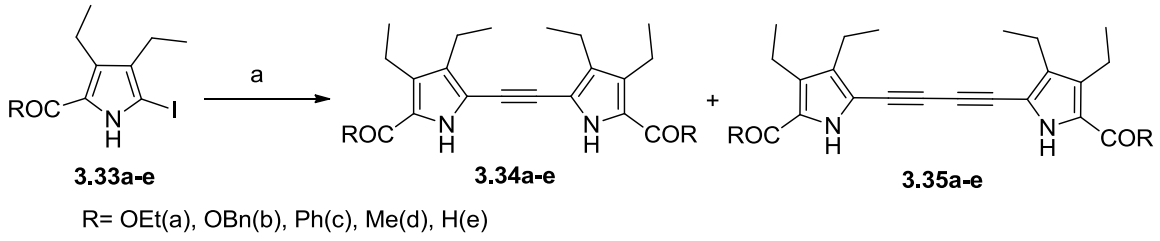

Scheme 3.7 Synthesis of mono and diacetylene bridged bipyrrole derivatives, a) $PdCl_2(PPh_3)_2$ (6 mol %), CuI (10 mol %), acetonitrile, DBU (6 equiv), TMSA (0.5 equiv), water (40 mol %), 24 h, rt.

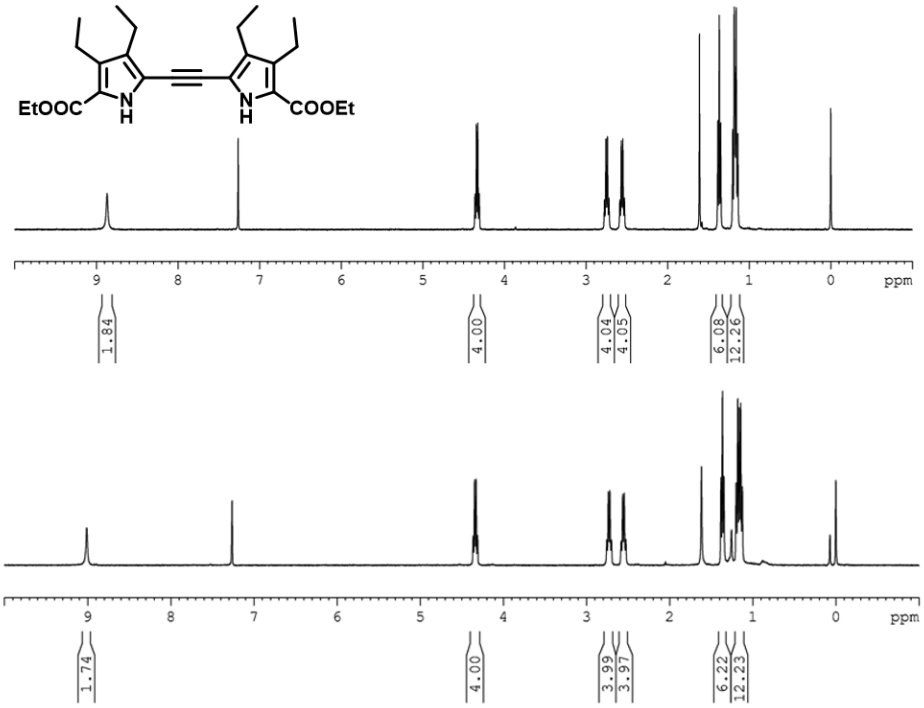

Figure 3.4 ^{1}H NMR spectrum of **3.34a** (top) and **3.35a** (bottom) in $CDCl_3$.

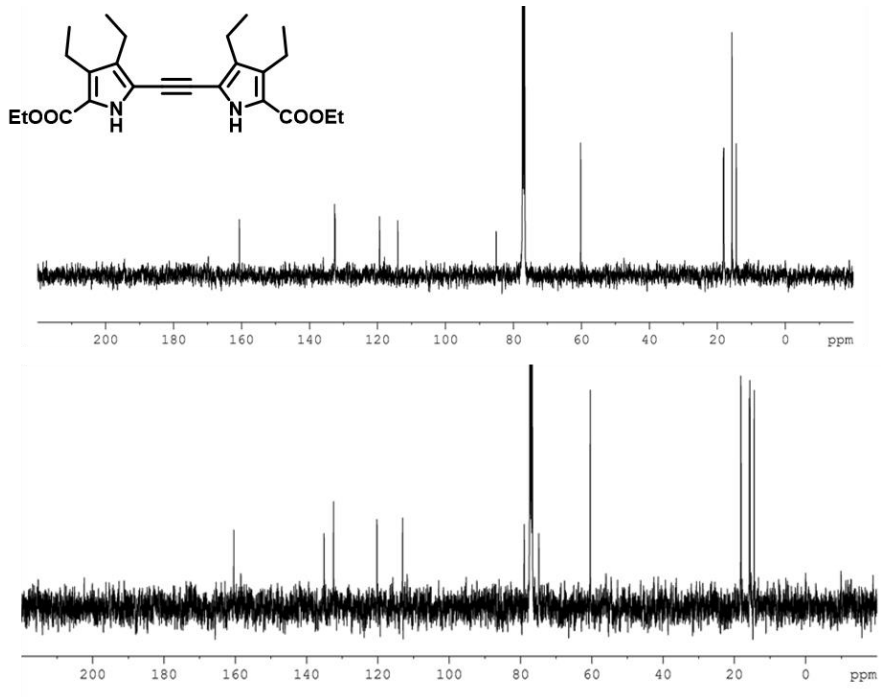

Figure 3.5 ^{13}C NMR spectrum of **3.34a** (top) and **3.35a** (bottom) in $CDCl_3$.

Finally, the identity of the molecular structure was unequivocally resolved, once the single crystal was obtained by slow evaporation of a dichloromethane solution of **3.35a**, through X-ray diffraction analysis, revealing both pyrrole rings in opposite directions, yet in same plane (Figure 3.6). Whereas, in case of monoacetylene bridged bipyrrole **3.34a**

(crystal obtained in same procedure as that of **3.35a**), the pyrroles were pointed in the same direction but with angular distortions of around 33° between the two pyrrolic planes.

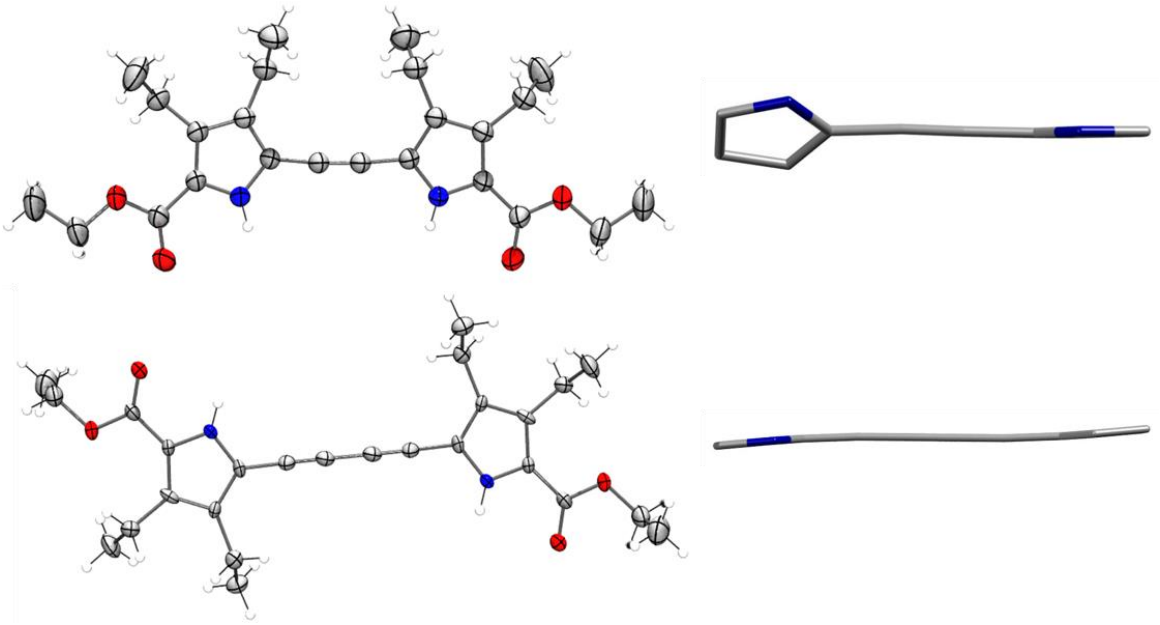

Figure 3.6 ORTEP diagrams of **3.34a** (top) and **3.35a** (bottom). Thermal ellipsoids are scaled up to the 35% probability level. Color code: gray = carbon, white = hydrogen, blue = nitrogen, and red = oxygen.

Following Scheme 3.7, we could able to isolate the corresponding diacetylene bridged derivatives in most of the cases (Table 1), which can be attributed to oxidative coupling in presence of traces of oxygen present in the reaction medium. Inspired by this outcome, we wanted to modify our reaction conditions to obtain diacetylene bridged bipyrroles, exclusively. For this we increased the quantity of trimethylsilylacetylene (TMSA) to 1.2 eq and left it open to aerial atmosphere after Sonogashira coupling (Scheme 3.8). Under these conditions we could able to isolate diacetylene bridged bipyrrole **3.35a** in 72% yield after column chromatography.

Table 1: Yields of compounds **3.34a-e** and **3.35a-e** from Scheme 3.7.

entry	**R**	**(% yield)**	
		3.34	**3.35**
1	OEt (a)	71	7
2	OBn (b)	65	13
3	Ph (c)	58	22
4	Me (d)	52	18
5	H (e)	44	-

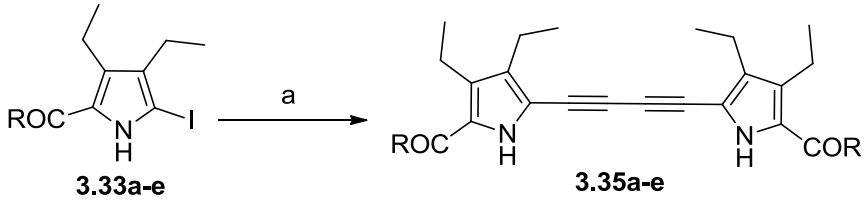

3.33a-e **3.35a-e**

R= OEt(a), OBn(b), Ph(c), Me(d), H(e)

Scheme 3.8 Synthesis of diacetylene bridged bipyrrole derivatives, a) (i) $PdCl_2(PPh_3)_2$ (6 mol %), CuI (10 mol %), THF, DBU (6 equiv), TMSA (1.2 equiv), 16 h, rt. (ii) water (40 mol %), 24 h, rt.

Table 2: Yields of compounds **3.35a-e** from Scheme 3.8.

entry	**R**	**3.35 (% yield)**
1	OEt (a)	72
2	OBn (b)	67
3	Ph (c)	61
4	Me (d)	54
5	H (e)	31

Further, this protocol was utilized in synthesizing different diacetylene bridged bipyrroles **3.35b-e** in good yields, 31-67% (Table 2). Low yield obtained in case of **3.35e** may be attributed to the strong deactivating nature of formyl group situated at the α-position of diethylpyrrole moiety. A scale up reaction of even up to 10g of **3.33a** did not decrease the yield much (60%). While the probable mechanism of this one-pot reaction involves an *in situ* Sonogashira coupling of TMSA in the first step followed by base-mediated deprotection of the TMS group in the second step, and oxidative Glaser coupling of the thus-formed acetylenic pyrrole in the third step.

3.3.2 Synthesis of bronzaphyrins from diacetylene bridged bipyrrole

It has been well noted from literature that a diacetylene bridge can be successfully converted into heterocyclic subunits such as pyrrole, thiophene or furan.[14] Hence we wished to convert the diacetylene bridged bipyrrole into thiophene substituted terpyrrole, which can be further employed in synthesizing similarly reported dithiabronzaphyrin. Employing sodium sulphide in presence of 2-methoxyethanol, we could able to convert diacetylene bridged bipyrrole **3.35a** into the thiophene bridged terpyrrole.[14d] However, owing to high basic condition and temperature, we could obtain the terpyrrole as a sodium salt, which upon treatment with HCl yielded the diacid derivative **3.36** in 90% yield (Scheme 3.9). However, this diacid derivative **3.36** when subjected to decarboxylation and then subsequent formylation led to diminished yield.

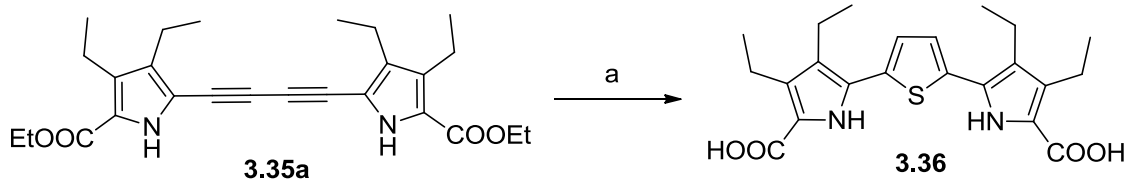

Scheme 3.9 Synthesis of thiophene bridged terpyrrole diacid **3.36**. a) Na_2S, THF, 2-methoxyethanol, 70°C.

Hence, we opted for direct approach of converting diacid to dialdehyde using Clezy protocol,[15] thereby isolating thiophene substituted terpyrrole dialdehyde **3.37** in a reasonable yield of around 38% (Scheme 3.10).

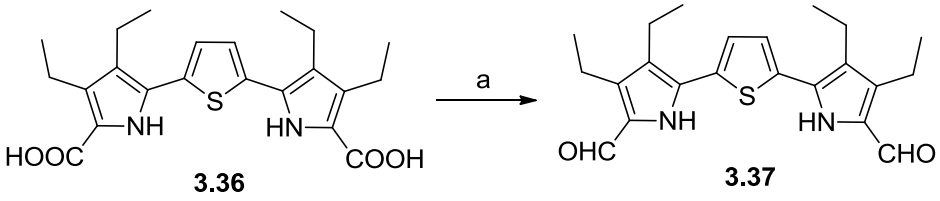

Scheme 3.10 Synthesis of thiophene bridged terpyrrole dialdehyde **3.37**. a) TFA, triethylorthoformate, rt.

Having the terpyrrole dialdehyde **3.37** in hand, we employed the reported Ibers's reaction conditions,[7a] which include a reductive McMurry coupling of dialdehyde to form a nonconjugated and reduced bronzaphyrin macrocycle, which was oxidized by stirring under aerial condition of the chloroform solution, and successfully isolated dithiabronzaphyrin **3.38** in 24% yield (Scheme 3.11).

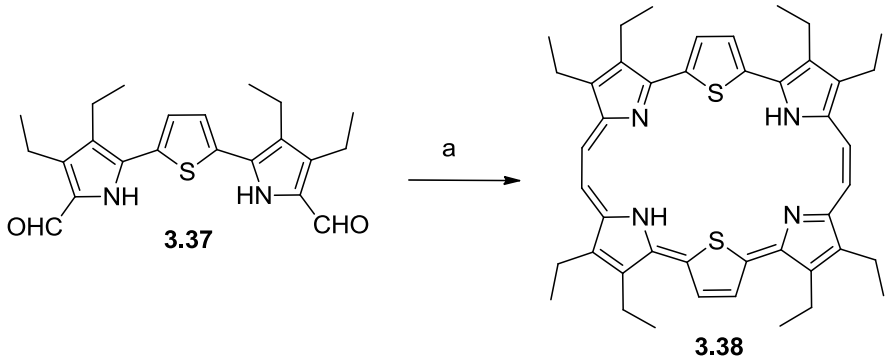

Scheme 3.11 Synthesis of dithiabronzaphyrin **3.38**. a) (i) Zn, $TiCl_4$, THF, pyridine, reflux, 16 h, (ii) oxidation in $CHCl_3$ (air), rt.

Utilizing the conditions employed by Osuka,[14b] we could able to synthesize N-benzyl terpyrrole diester **3.39**, albeit in lesser yield. This prompted us to tune the experimental

conditions and we found decreasing the time and temperature from reflux condition to 140°C resulted in optimal yield (62%) of **3.39** as thick gel (Scheme 3.12). The N-benzyl

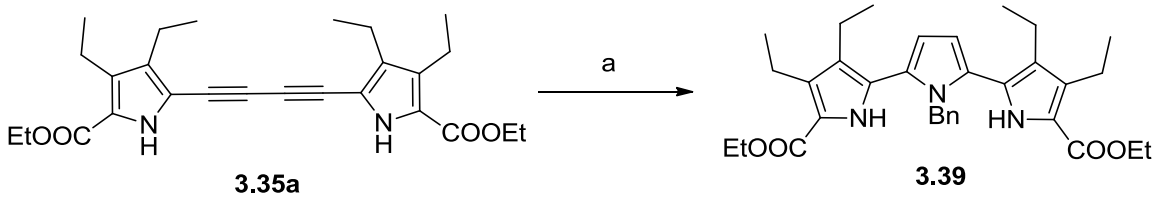

Scheme 3.12 Synthesis of N-benzyl terpyrrole ester **3.39**. a) CuCl, benzyl amine, mesitylene, 140°C.

terpyrrole diester **3.39** thus obtained was subjected to base mediated deprotection of the ester groups to give the crude N-benzyl terpyrrole, which was further formylated under Vilsmeier-Haack condition to give the corresponding N-benzyl terpyrrole dialdehyde **3.40** in 69% yield (Scheme 3.13). Owing to the N-benzyl moiety and four ethyl groups at the periphery, the terpyrrole dialdehyde **3.40** was highly soluble in organic solvents, which was not observed in previous reports of terpyrrole dialdehydes.

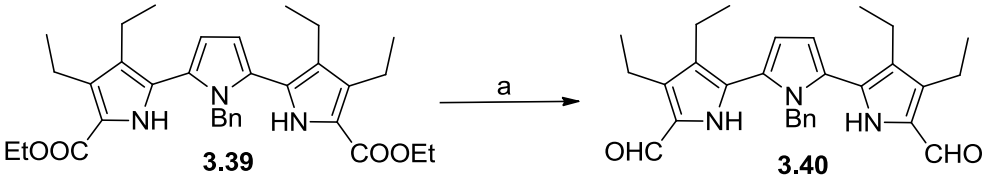

Scheme 3.13 Synthesis of N-benzyl terpyrrole dialdehyde **3.40**. a) (i) NaOH, ethylene glycol, reflux; (ii) DMF, $POCl_3$, DCE, reflux; (iii) aq. NaOAc, reflux.

Crystal structure of **3.40** (obtained from slow evaporation of its chloroform solution) showcases all pyrroles aligned in same direction but the central pyrrole twisting to about 47° from the remaining pyrroles of terpyrrole moiety (Figure 3.7). The terpyrrole dialdehyde **3.40** was finally subjected to McMurry coupling following Ibers's condition.[7a] After the completion of reaction, we could able to observe much red shifted absorption bands in UV-Vis-NIR spectroscopy similar to bronzaphyrin, however, we failed to isolate the title compound through column chromatography. At this juncture, we envisioned to isolate the reduced bronzaphyrin obtained from the reductive coupling of N-benzyl terpyrrole dialdehyde **3.40** immediately after workup and carry out oxidation later. Fortunately, we succeeded in isolating **3.41**, albeit, in very low yield as a bright orange fluorescent spot through column chromatography (Scheme 3.14).

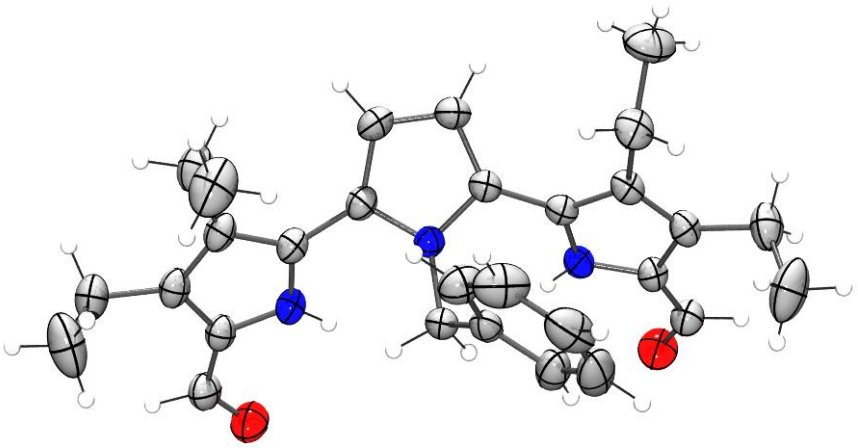

Figure 3.7 ORTEP diagram of **3.40**. Thermal ellipsoids are scaled up to the 35% probability level. Color code: gray = carbon, white = hydrogen, blue = nitrogen, and red = oxygen.

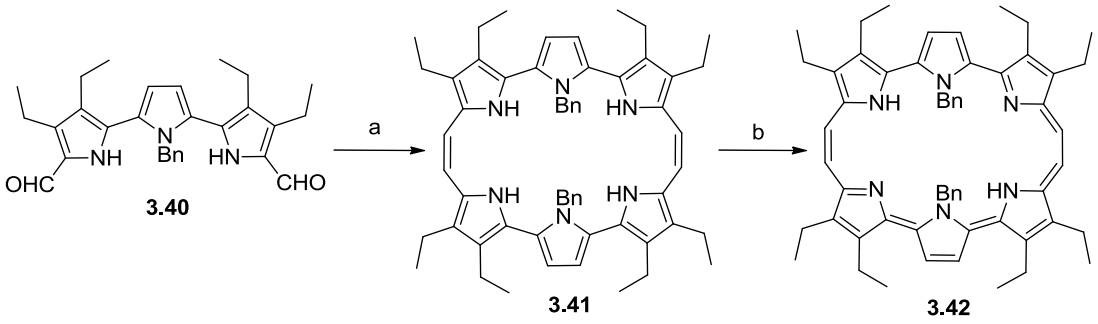

Scheme 3.14 Synthesis of all azabronzaphyrin **3.42**. a) Zn, $TiCl_4$, THF, reflux, 16 h. b) oxidation in $CHCl_3$ (HCl or $HClO_4$), rt.

The ^{1}H NMR spectroscopy of **3.41** (Figure 3.8) revealed a perfect non-aromatic compound having four NH protons, *meso* and β-protons resonating around 6-8 ppm and a

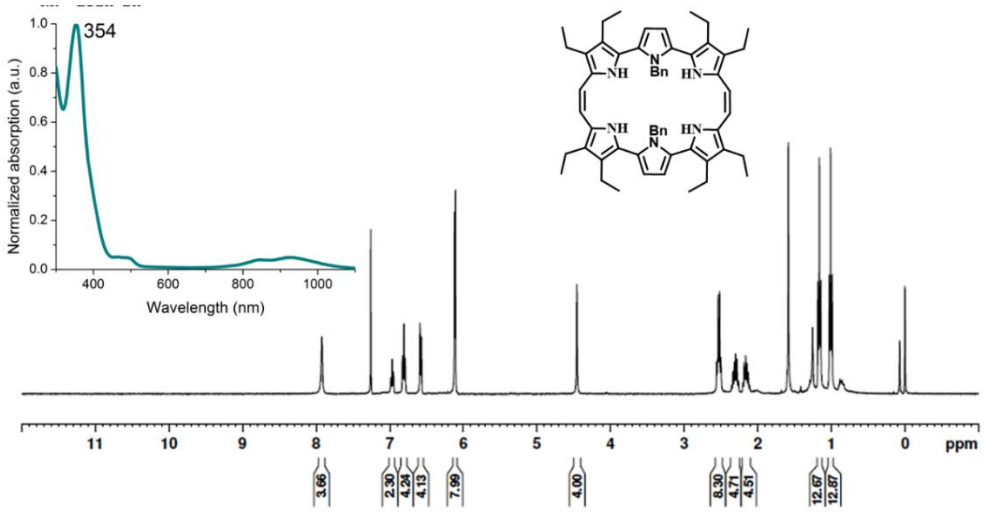

Figure 3.8 ^{1}H NMR spectrum of **3.41** in $CDCl_3$ (in set: absorption spectrum in chloroform).

sharp single peak arising at 354 nm in absorption spectrum, confirming a nonconjugated system. The compound thus obtained was dissolved in chloroform and left for oxidation (treating with dil. $HCl/HClO_4$) and subsequently poured onto a short silica gel column and eluted with 10% MeOH/chloroform mixture. This led to successful isolation of the desired bronzaphyrin **3.42** as a dichloride salt (in case of $HClO_4$) in 4% or monochloride salt (in case of HCl) in 3% yields. Both the bronzaphyrins **3.38** and **3.42** display typical bronze color in chloroform solution and were well characterized by UV-Vis-NIR and NMR spectroscopies, HRMS and also by XRD analysis.

3.3.3 ^{1}H NMR studies

Interestingly, the ^{1}H NMR spectrum of octaethyl substituted dithiabronzaphyrin **3.38** revealed to be much more different from the reported tetrapropyl substituted dithiabronzaphyrin **3.18**. Dithiabronzaphyrin **3.38** showed a sharp singlet at -0.5 ppm (four protons) and a broad singlet (two protons) at 6.5 ppm. During a D_2O exchange study, we could able to observe exchanging of protons resonating at 6.5 ppm and hence could be attributed to pyrrolic NHs, which led us to anticipate inversion of the thiophene moieties in the macrocyclic system and as a consequence, their β-protons resonating in the shielded region (Figure 3.9). For checking the flexibility of this flipped thiophene ring, we have conducted a high temperature ^{1}H NMR experiment in toluene-d_8. We found

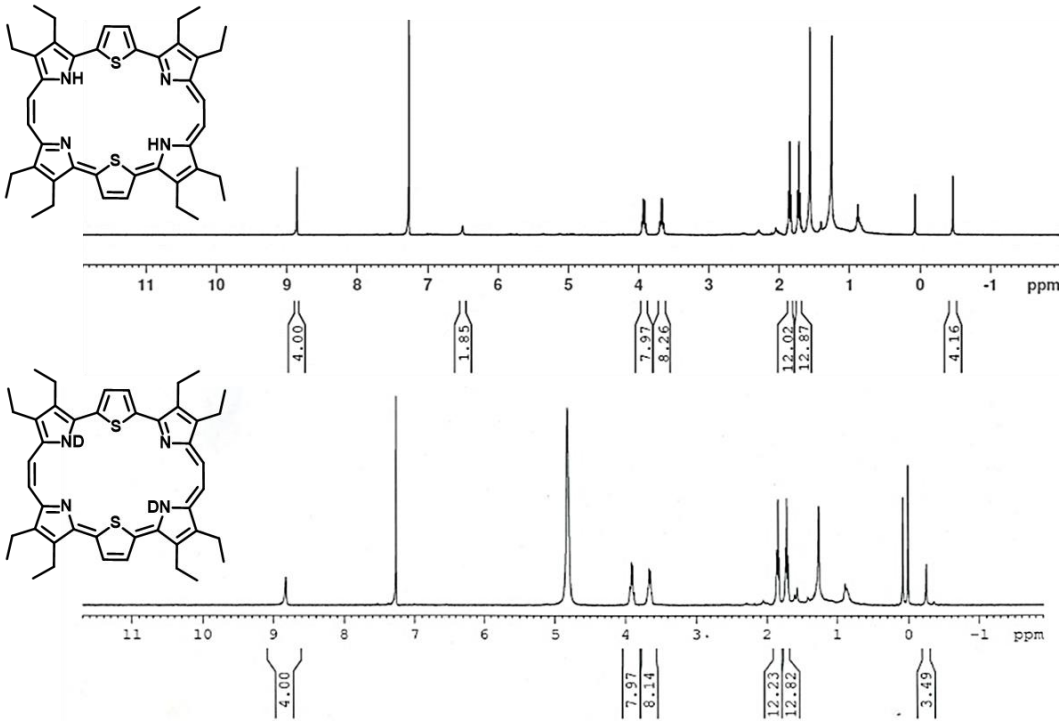

Figure 3.9 ^{1}H NMR spectra of **3.38** in $CDCl_3$ (top) and $CDCl_3$ + D_2O (bottom).

that the molecule is stable even at 80 °C and there is not much shift in the shielded peak resonating in the negative region (Figure 3.10). The inversion of the thiophene rings in dithiabronzaphyrin **3.38** can be ascribed to the steric repulsion between the pyrrolic inner *β*-ethyl moieties and *β*-protons of thiophene at the periphery (hence not observed in case of tetraalkyl analogue **3.18**), whereas, the downfield shift of the pyrrolic NHs, not noticed in case of analogous bronzaphyrins (**3.18, 3.24** and **3.32**) reported so far, may be ascribed

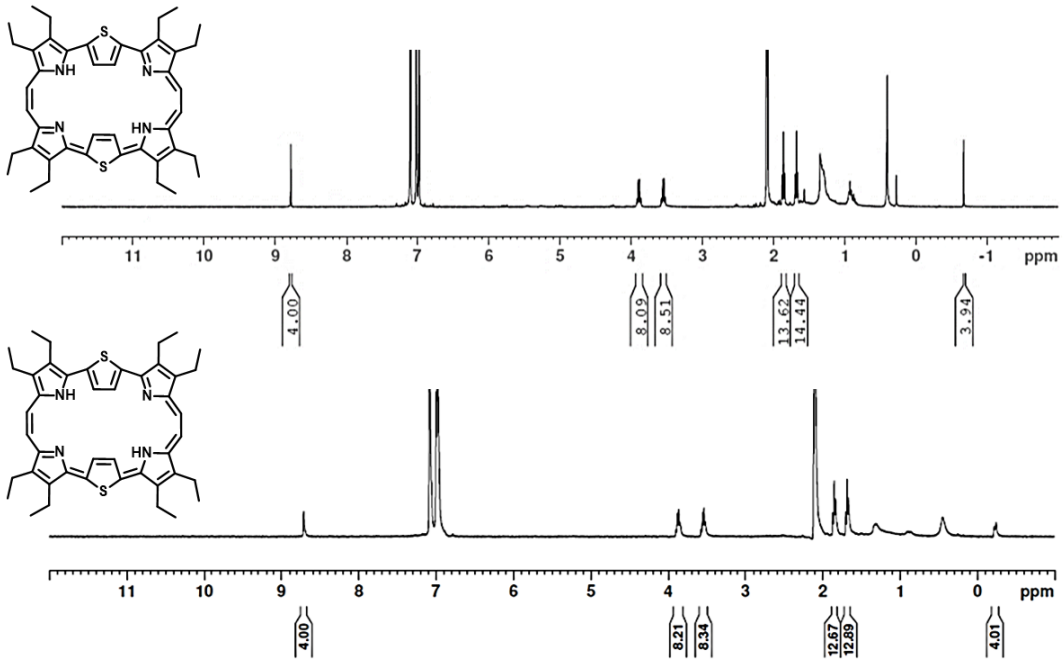

Figure 3.10 ^{1}H NMR spectrum of **3.38** in toluene-d_8 at rt (top) and at 80 °C (bottom).

to strong NH…N hydrogen bonding as noticed in porphycenes.[16] The reason might be attributed to the close proximity of the opposite pyrrolic units caused by the inversion of thiophene moieties. Further evidence via computational analysis for this phenomenon will be discussed in separate section. Having failed to protonate dithiabronzaphyrin **3.38** with small amounts of acid, we added large excess of TFA (50 μL) to the $CDCl_3$ solution of the freebase to obtain ^{1}H NMR spectrum of the completely protonated compound. The pyrrolic NH protons were seen resonating along with the β-protons of thiophene in the shielded region at -1.7 ppm, undergoing a large upfield shift from around 8 ppm, which was confirmed by D_2O study (Figure 3.11). This demonstrates the structural rigidity of the macrocycle, as protonation does not yield flipping back of thiophene rings into normal conformation, which has been observed in some cases of expanded porphyrins.[17] In addition, difficulty aroused in protonation of dithiabronzaphyrin **3.38** might be due to the

strong NH…N hydrogen bonding, whereas, shielding of the NH signals can be attributed to the lack of NH…N hydrogen bonding upon protonation.

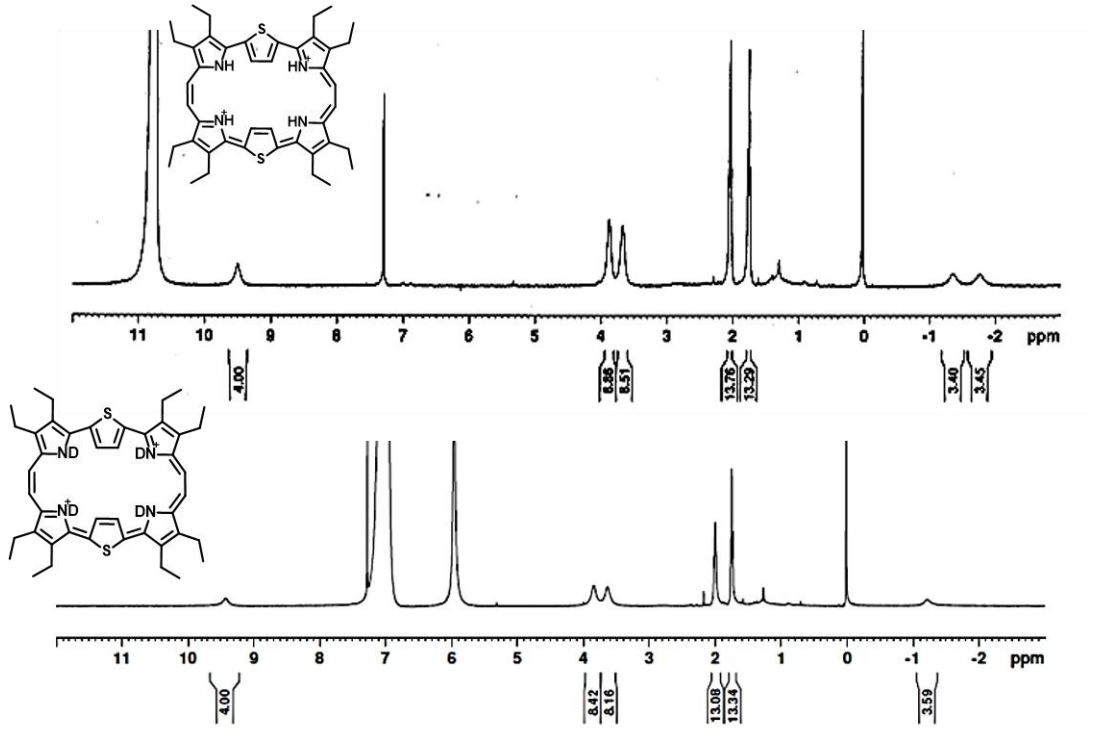

Figure 3.11 ^{1}H NMR spectrum of **3.38** in $CDCl_3$ + TFA (top) and $CDCl_3$ + TFA + D_2O (bottom).

Characterization of all-aza bronzaphyrin **3.42** dichloride salt by ^{1}H NMR spectroscopy failed not only due to its lack of solubility but also initial studies revealing it's paramagnetic nature (Figure 3.12). However, the monochloride salt shows a much clear ^{1}H NMR spectrum with ten protons, highly upfield shifted due to their close proximity to diamagnetic ring current, and resonating in the negative region (-2 ppm to -7 ppm) proba-

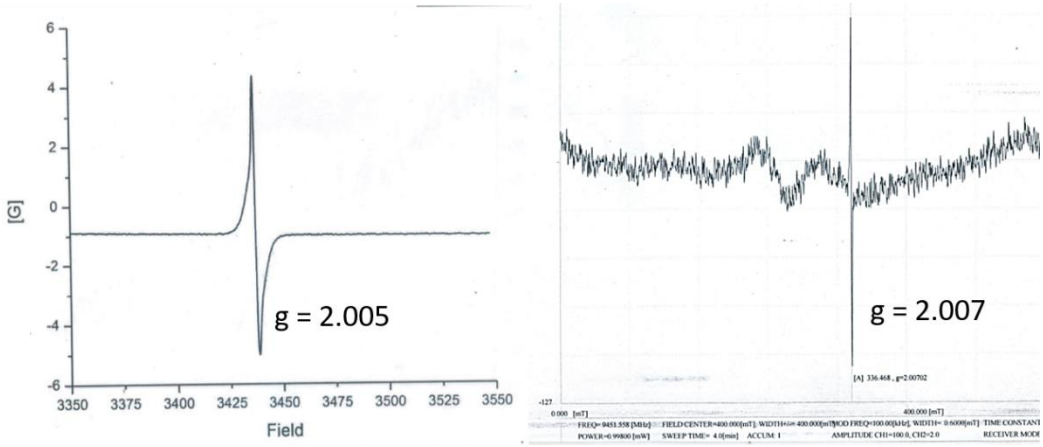

Figure 3.12 EPR spectra of **3.42** dichloride salt (left) and freebase (right).

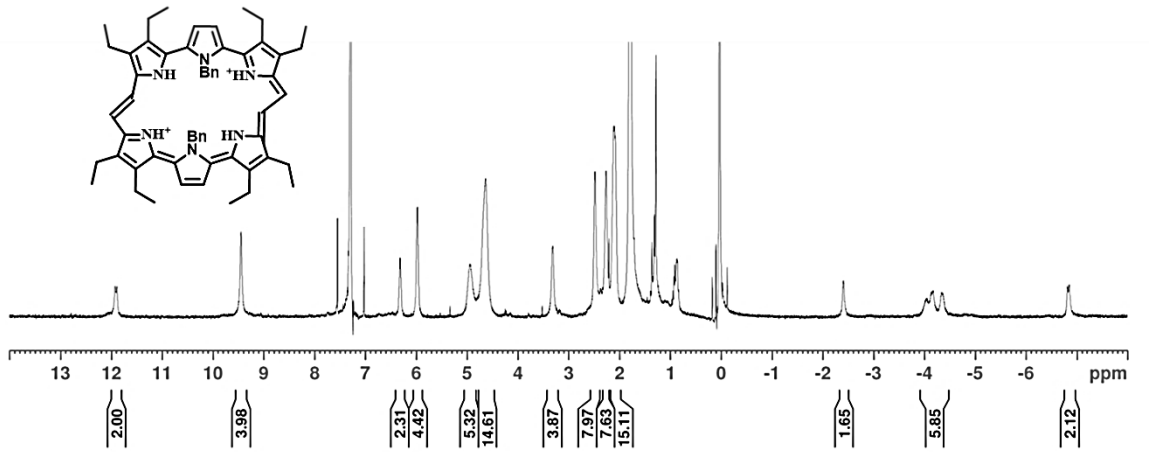

Figure 3.13 ^{1}H NMR spectrum of **3.42.H$_2^{2+}$** (monochloride salt) in $CDCl_3$.

bly comprising two sets of benzylic protons, four pyrrolic NH protons and two meso protons (which was previously observed in *trans* conformation of vinylogous porphyrins), as shown in Figure 3.13. The other two meso protons and β-protons were found to resonate at 11.9 and 9.4 ppm, respectively. As expected, the *ortho*-CH protons of benzene are upfield shifted due to their close interaction with the ring current. The compound obtained was very less and we couldn't proceed to perform further studies of D_2O exchange and protonation. Initial studies of freebase bronzaphyrin, obtained either by aerobic oxidation of **3.41** in chloroform or by washing the dichloride salt with potassium carbonate solution, revealed to be paramagnetic in nature making it to be NMR inactive. The stabilization of *trans* conformation compared to *cis* will be explained in the section of DFT studies.

3.3.4 UV-Vis-NIR and fluorescence studies

UV-Vis-NIR absorption spectral study of both the bronzaphyrins **3.38** and **3.42** revealed much intense and quite red-shifted Q-bands compared to analogous bronzaphyrins (**3.18, 3.24** and **3.32**). For example, dithiabronzaphyrin **3.38** (in chloroform) shows clearly separated broad Soret bands at 467 and 548 nm ($\varepsilon = 3.0 \times 10^4$ and 1.2×10^4, respectively), as shown in Figure 3.14, but **3.18** (in THF) shows a slightly separated Soret bands at 460 and 501 nm ($\varepsilon = 1.9 \times 10^5$ and 8.9×10^4, respectively). The Q-bands of dithiabronzaphyrin **3.38** displayed a completely different pattern with two less resolved peaks at 867 and 904 nm, with a broad shoulder on the higher energy side, whereas, **3.18** exhibited four Q transitions with first at 745 nm, two slightly resolved peaks at 780 and 790 nm, and a distinct sharp band at 859 nm. Strikingly, **3.38** depicts a much more

strengthening of Q bands, almost reaching up to 80%, when compared to the higher energy Soret band and a much red shifted absorption, with lowest energy band bathochro-

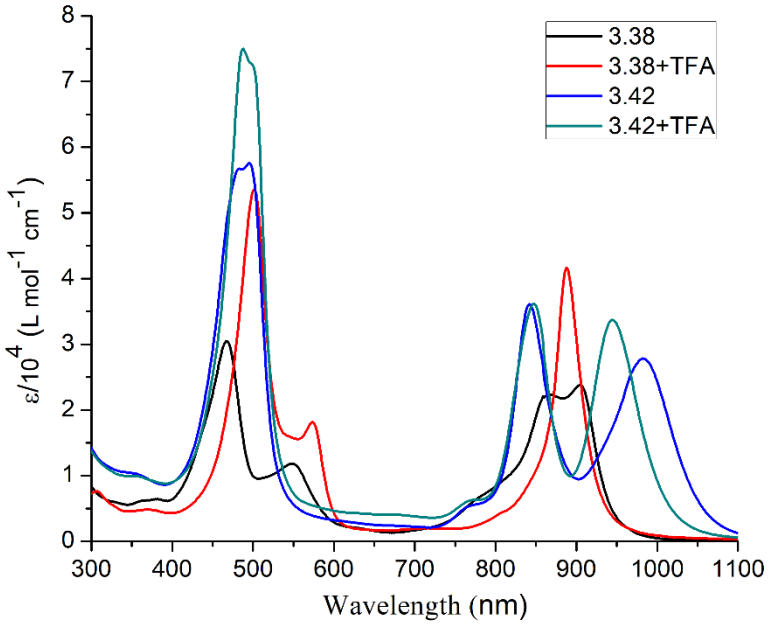

Figure 3.14 UV-Vis-NIR absorption spectra of bronzaphyrins **3.38** and **3.42** along with their protonated analogues measured in chloroform.

mically shifted close to 45 nm with respect to (w.r.t.) **3.18**, owing to the strong sensitivity towards inner substituents that compel the thiophene rings to inverted position. On the other hand, the all-aza bronzaphyrin **3.42** exhibited an intense broad Soret band (owing to merger of two bands at 483 and 495 nm) with two intense NIR Q bands at 842 and 982 nm (ε = 3.6 x 10^4 and 2.8 x 10^4, respectively), whose tail reaches up to 1100 nm. Surprisingly, all-aza macrocycle **3.42** did not undergo much change upon protonation with TFA, except blue shift of the lowest energy band, indicating possibly its core is not much affected during the process.

We subjected bronzaphyrin **3.38** for protonation study using TFA, as protonation of expanded porphyrins often leads to interesting structural and photophysical alterations.[17] UV-Vis-NIR spectroscopic titration study revealed dithiabronzaphyrin **3.38** was in need of large quantity of acid for diprotonation (Figure 3.15). Due to lack of tautomerism, this protonated species displayed enhancement of intensity of the peaks with large red-shifted Soret bands (502 and 572 nm) and slightly blue-shifted sharp Q-band at 887 nm (Figure 3.14)

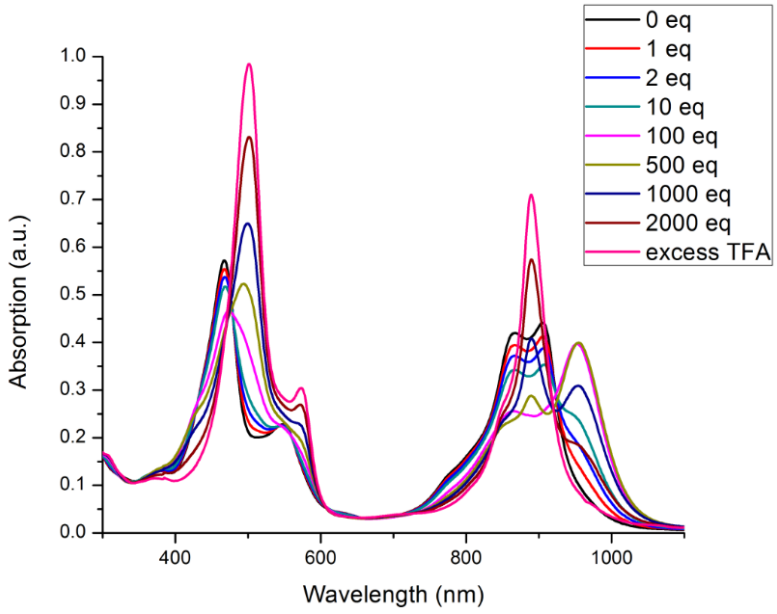

Figure 3.15: Acidometric titration spectra of **3.38** in chloroform with TFA.

Both the bronzaphyrins **3.38** and **3.42** exhibit weak NIR emission with corresponding peak maxima at 959 and 1022 nm as shown in Figure 3.16.

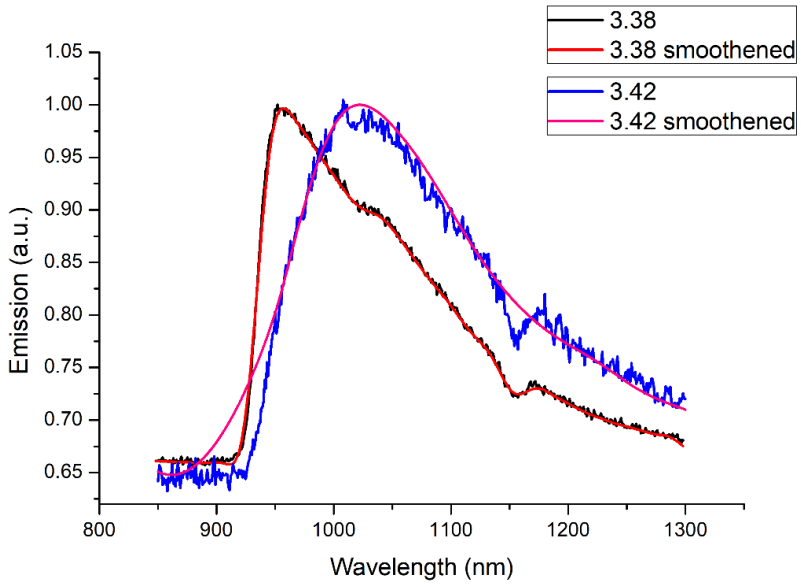

Figure 3.16: Emission spectra of bronzaphyrins **3.38** and **3.42** with peak maxima at 959 and 1022 nm (λ_{ex} = 490 nm with slit widths of 14 nm).

3.3.5 X-ray crystal structure analysis

After several attempts, we could able to grow diffraction grade crystals for both the bronzaphyrins **3.38** and **3.42**. Dithiabronzaphyrin **3.38** was isolated in both freebase and protonated forms, whereas, all-azabronzaphyrin **3.42** was isolated as its dichloride and

monochloride salts. While the freebase dithiabronzaphyrin **3.38** was crystalized from highly concentrated chloroform solution containing pyridine, the protonated bronzaphyrin **3.38.H$_2^{2+}$** was obtained by slow evaporation of TFA mixed chloroform solution. Interestingly, both the structures exhibit rich structural features of this class of macrocycles, ignored over more than two decades since its inception. For example, the crystal structure of dithiabronzaphyrin **3.38** (Figure 3.17) confirmed the flipping of thiophene rings, as expected from the ^{1}H NMR spectroscopy, and the deviation of thiophene rings w.r.t. the mean macrocyclic plane is 29.6°. Further, due to strong N-H...N hydrogen bonding (N-N distance across the meso-bridges 2.61 Å), the macrocycle takes a rectangular core with the four pyrrolic moieties and the bridging C-C units residing almost in one plane, with dihedral angles of 1.3° and 6.4°. Crystal structure of the protonated dithiabronzaphyrin **3.38.H$_2^{2+}$** also displays flipping of thiophene rings with a deviation of 29.2° w.r.t. the mean macrocyclic plane, confirming the evidence from the ^{1}H NMR spectroscopy and found to be flipping away from the core, as they doesn't revert back to normal conformation upon protonation (Figure 3.18).

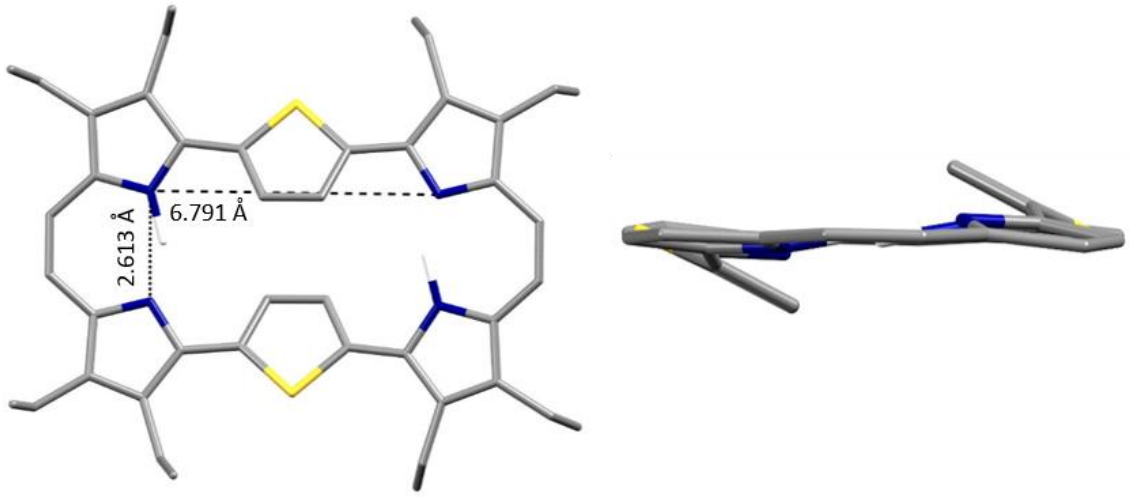

Figure 3.17 Molecular structures of **3.38** top (left) and side (right) views. All at 50% probability level. All hydrogens in the structures and ethyl groups in side views were omitted for clarity. Grey = Carbon, blue = Nitrogen and yellow = Sulphur.

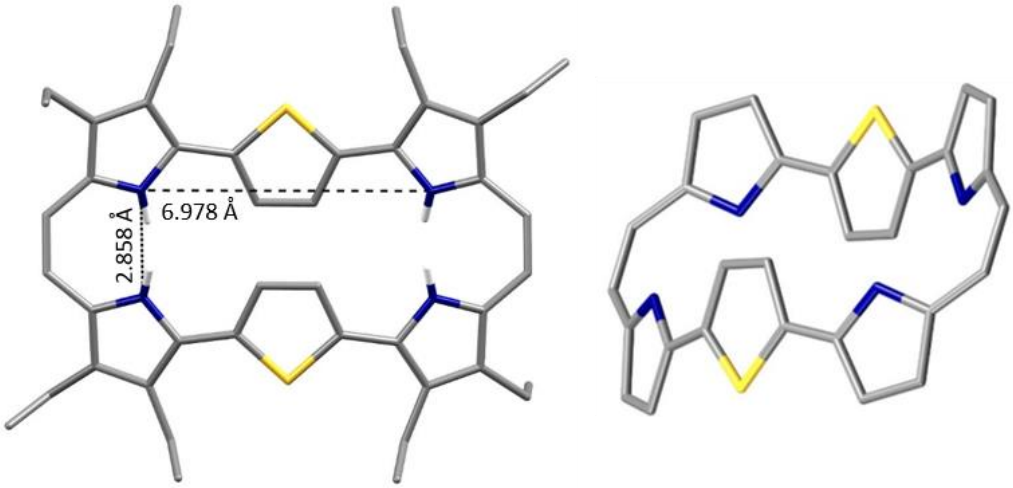

Figure 3.18 Molecular structures of **3.38.H$_2^{2+}$** top (left) and side (right) views. All at 50% probability level. All hydrogens in the structures and ethyl groups in side views were omitted for clarity. Grey = Carbon, blue = Nitrogen and yellow = Sulphur.

The packing diagram displays the macrocycle coordinating to four hydrogen bridged open dimeric trifluoroacetate ions i.e., $[(CF_3COO)_2H]^-$ via hydrogen bonds (Figure 3.19). Overall it showcases layers of macrocycles forming a stacked network through anion bridging. As far as we know, this type of unique coordination mode involving dimeric anions has no precedence in expanded porphyrin chemistry.[18] Formation of this open dimeric trifluoroacetate ions may be due to the presence of large excess of TFA, used to overcome the strong N-H…N hydrogen bonds in freebase **3.38** for completing the protonation. As a result, the thiophenes now become coplanar with the two pyrroles of the

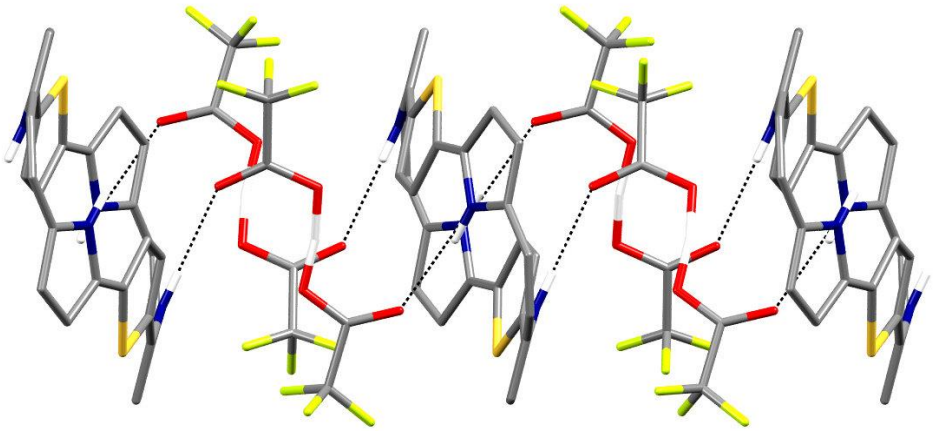

Figure 3.19 Crystal packing diagram of the TFA salt of **3.38**. All hydrogens and ethyl groups in the structures were omitted for clarity. Grey = Carbon, blue = Nitrogen, yellowish green = Fluorine, yellow = Sulphur and red = Oxygen.

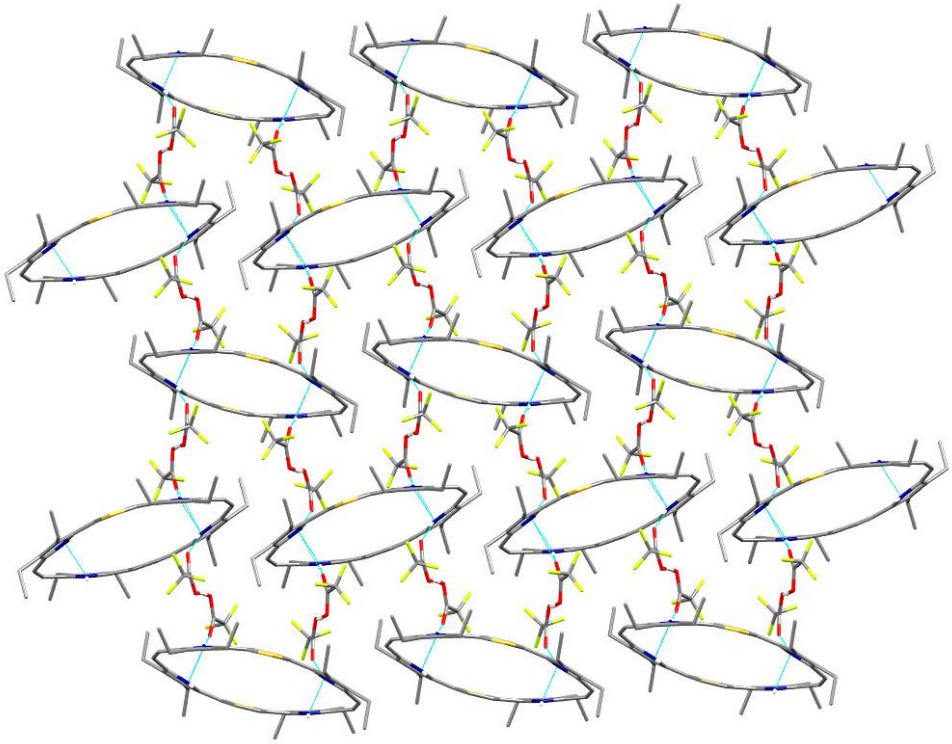

Figure 3.20 Crystal packing diagram showing anion bridged network of the TFA salt of **3.38**. All hydrogens in the structures were omitted for clarity. Grey = Carbon, blue = Nitrogen, yellowish green = Fluorine, yellow = Sulphur and red = Oxygen.

terpyrrole units (dihedral angle of only 3°), whereas in case of freebase, the thiophenes make a dihedral angle of 22° w.r.t. the mean plane of the two pyrroles of the terpyrrolic moiety (excluding Hs and ethyl Cs). This makes the terpyrrolic moieties appear as two steps of a ladder with much enhanced deviation from the plane of the bridging C-C units (16.2° and 17.5°). In addition, both the N-N distances increased slightly due to the effect of protonation providing the overall macrocycle an oval shape (Figure 3.20).

Dichloride salt of all azabronzaphyrin **3.42** was crystalized by slow evaporation of mixture of dichloromethane and tetrachloroethane, whereas, monochloride salt was obtained from TFA added chloroform solution. Interestingly, both structures revealed trans-alkene bridged meso double bonds indicating rich structural diversities that this class of macrocycles could adopt, which is a rare phenomenon in expanded porphyrin chemistry. This trans conformation leads to stretching of macrocycle to assume a rhombus type core with N-N distances of 4.76 and 4.78 Å, respectively (Figure 3.21). As expected, the benzyl groups were protruded out of the mean macrocyclic plane, keeping

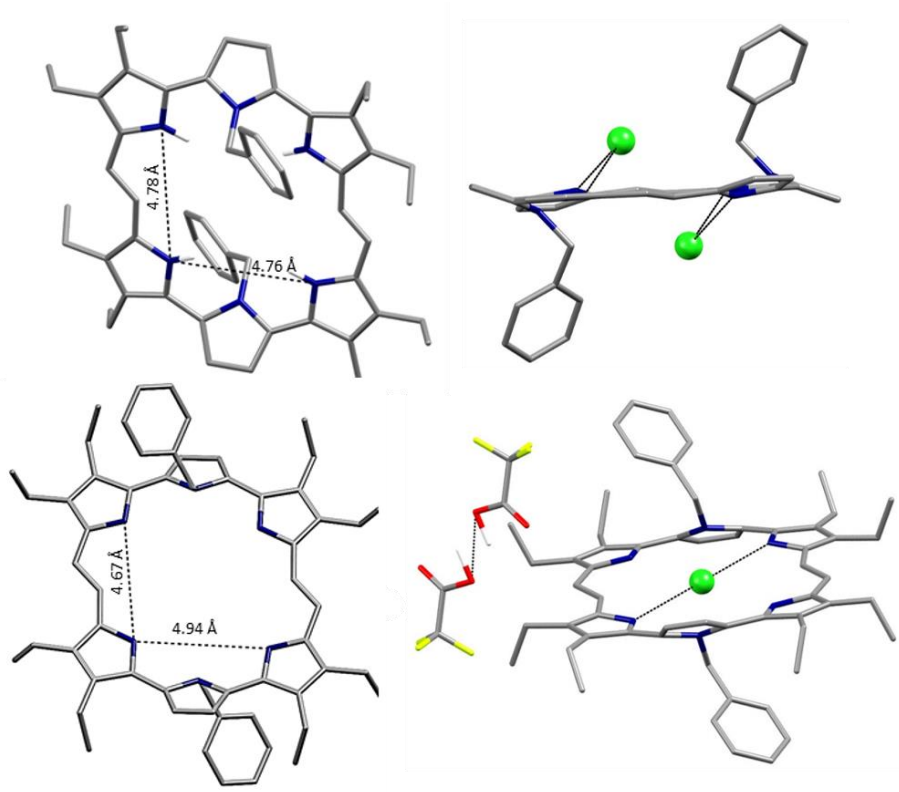

Figure 3.21 Molecular structures of dichloride salt of **3.42** top view (top-left), side view (top-right) and perspective view (bottom) of monochloride salt of **3.42**. All at 50% probability level. All hydrogens in the structures and ethyl groups in side views were omitted for clarity. Grey = Carbon, blue = Nitrogen, yellowish green = Fluorine, green = chloride and red = Oxygen.

the core almost planar but making the central pyrrole deviate with an angle of 26.6° w.r.t. the mean plane of the other two pyrroles of the terpyrrolic moiety. Both the chloride ions are situated on the opposite sides of mean macrocyclic plane with a distance of 1.65 Å. Interestingly the monochloride salt displays chloride ion sitting at the center of mean macrocyclic plane leading to a parallelogram type of core, with shorter and longer N-N distances of 4.67 and 4.94 Å respectively while the other TFA counter ion remains outside the plane in the form of an open hydrogen bridged dimeric trifluoroacetate ions i.e. $[(CF_3COO)_2H]^-$ and retaining all the features of dichloride salt.

3.3.6 DFT studies

We have carried out quantum mechanical calculations using Gaussian 09 program provided by CMSD facility of University of Hyderabad.[19] All calculations were carried out by density functional theory (DFT) with Becke's three-parameter hybrid exchange functional and the Lee-Yang-Parr correlation functional (B3LYP) parameter. The cc-

pVDZ and 6-31G basis sets were used for all the calculations and the molecular orbitals were visualized using Gauss view 5. The calculations performed for the normal and inverted isomers of bronzaphyrins **3.38** and **3.18** (Table 3 and 4) clearly showed that the inverted isomer possesses minimum energy in case of bronzaphyrin **3.38**, but maximum energy in case of bronzaphyrin **3.18**. The computational studies also revealed that the peak arising in the negative (shielded) region of ^{1}H NMR spectrum to be the β-protons of thiophene ring and the NH protons are much more deshielded (Figure 3.22).

Table 3 Comparative stabilities of the two different conformers of **3.38** after structure optimization.

Conformer	**Top view**	**Side view**	**Total Energy difference (in eV)**
Normal	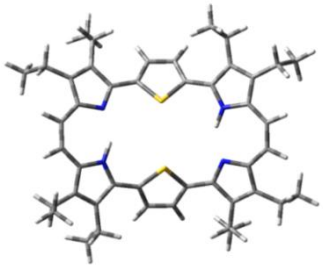		**0.14**
Inverted	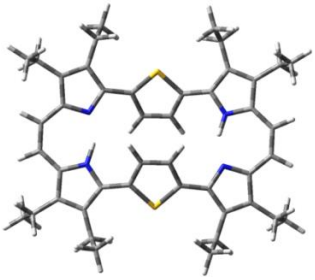	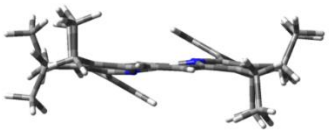	**0**

Table 4 Comparative stabilities of the two different conformers of **3.18** after structure optimization.

Conformer	Top view	Side view	Total Energy difference (in eV)
Normal	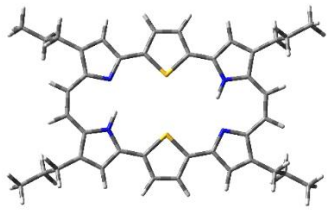		**0**
Inverted	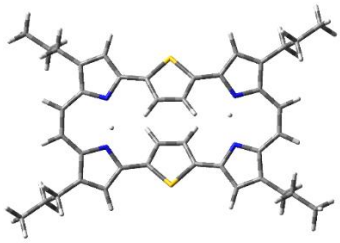	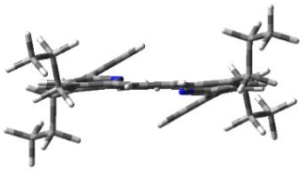	**0.42**

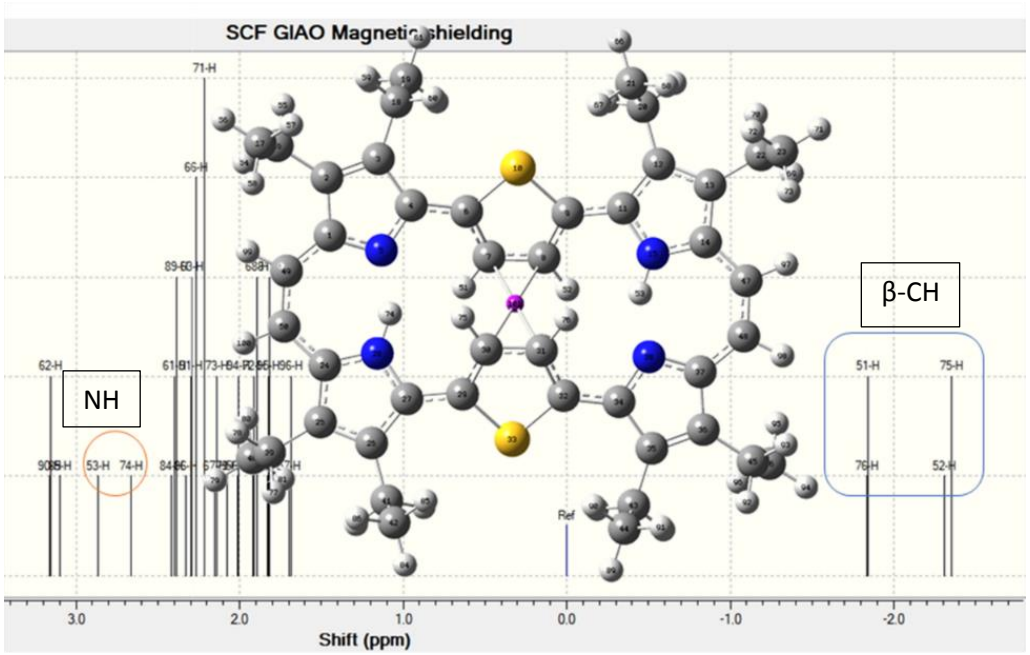

Figure 3.22 Theoretical ^{1}H NMR spectrum of **3.38** indicating NH and *β*-CH of thiophene.

Similarly, DFT analysis revealed while the dicisoid isomer is the most stable isomer of the freebase of **3.42**; upon protonation, the ditransoid isomer becomes the most stable form (Table 5 and 6).

Table 5 Comparative stabilities of the two different conformers of **3.42** after structure optimization.

Conformer	**Top view**	**Side view**	**Total energy difference (in eV)**
Cis	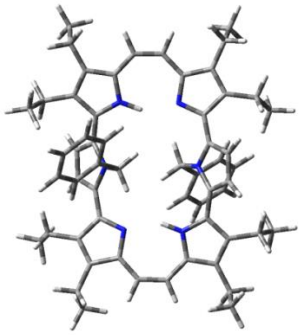	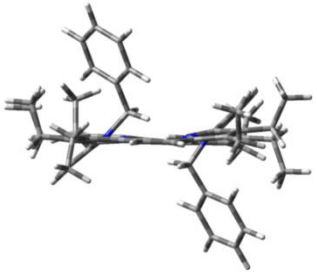	**0**
Trans	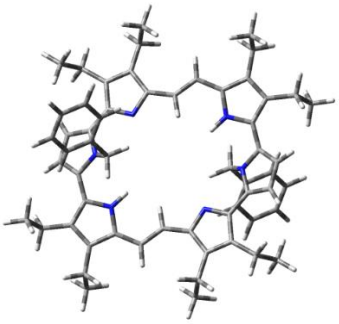	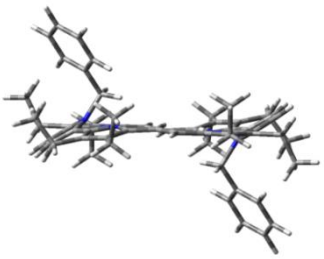	**0.77**

Table 6 Comparative stabilities of the two different conformers of **3.42.H_2^{2+}** after structure optimization.

Conformer	**Top view**	**Side view**	**Total energy difference (in eV)**
***Cis* with chlorides**	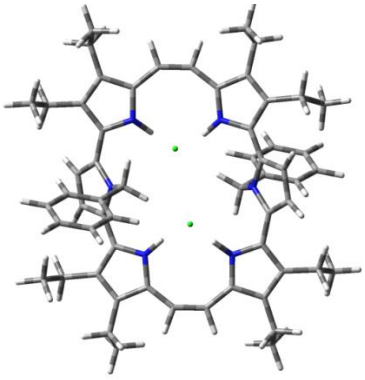	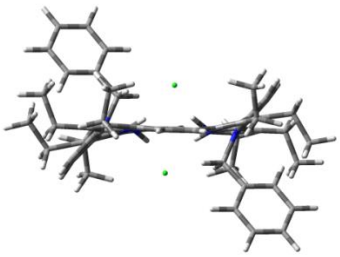	**1.0**

***Trans* with chlorides**	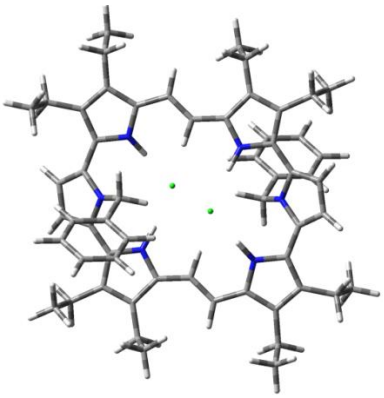	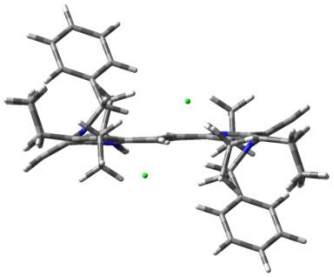	**0**

To obtain further insight, we have performed TD-DFT calculations and simulated the theoretical absorption spectra for both the bronzaphyrins **3.38** and **3.42**, and their corresponding protonated derivatives. The vertical electronic transitions and the steady state absorption spectra were found to be very similar (Figure 3.23 and 3.24), mainly involving the frontier orbitals: HOMO-1, HOMO, LUMO and LUMO+1. Energy level diagrams along with the delocalized π-electron densities of frontier orbitals are shown in Figures 3.25-3.28.

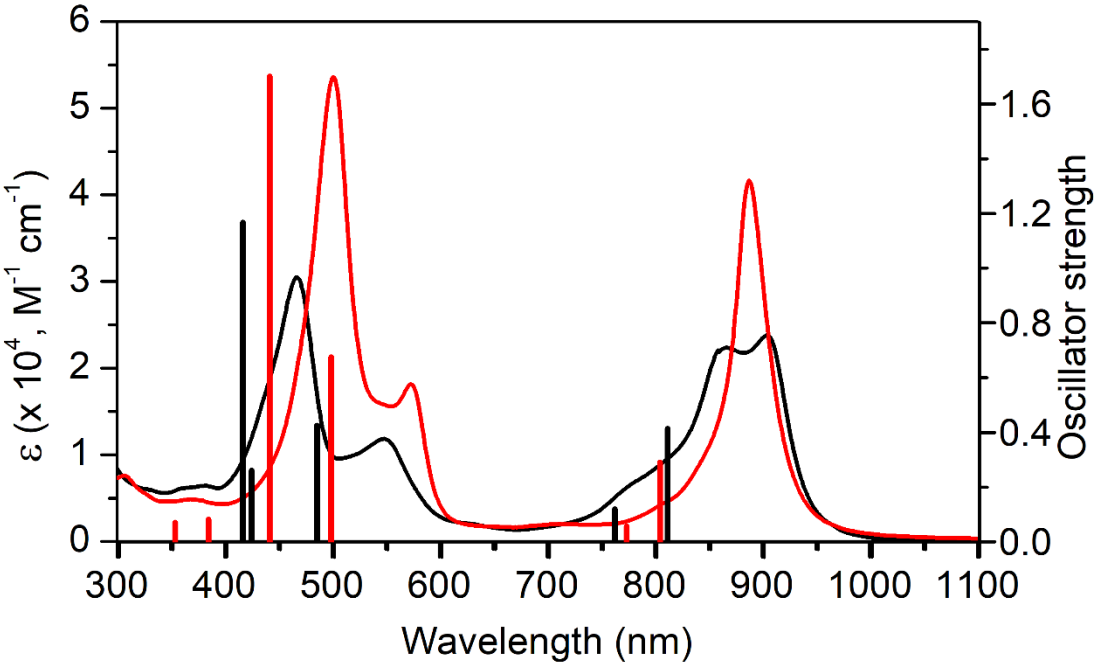

Figure 3.23 Theoretical (vertical bars) and experimental (continuous lines) UV-Vis-NIR absorption spectra of **3.38** (black) and **3.38.H$_2^{2+}$** (red) in chloroform.

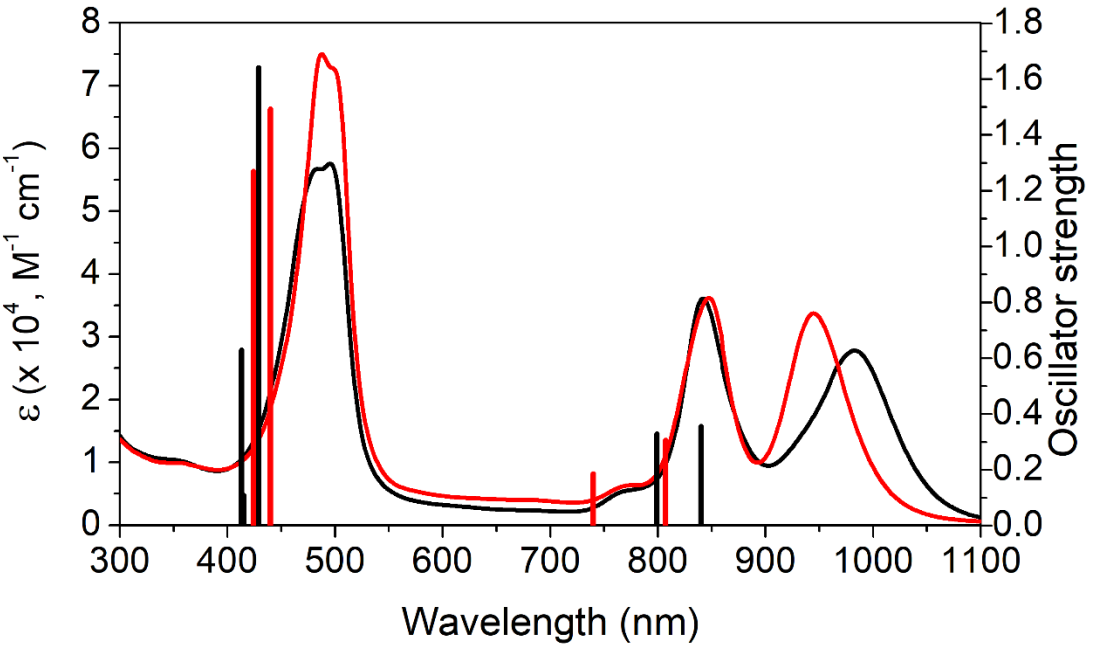

Figure 3.24 Theoretical (red vertical bars) and experimental (black continuous line) UV-Vis-NIR absorption spectra of **3.42** and **3.42.H**$_2^{2+}$ in chloroform.

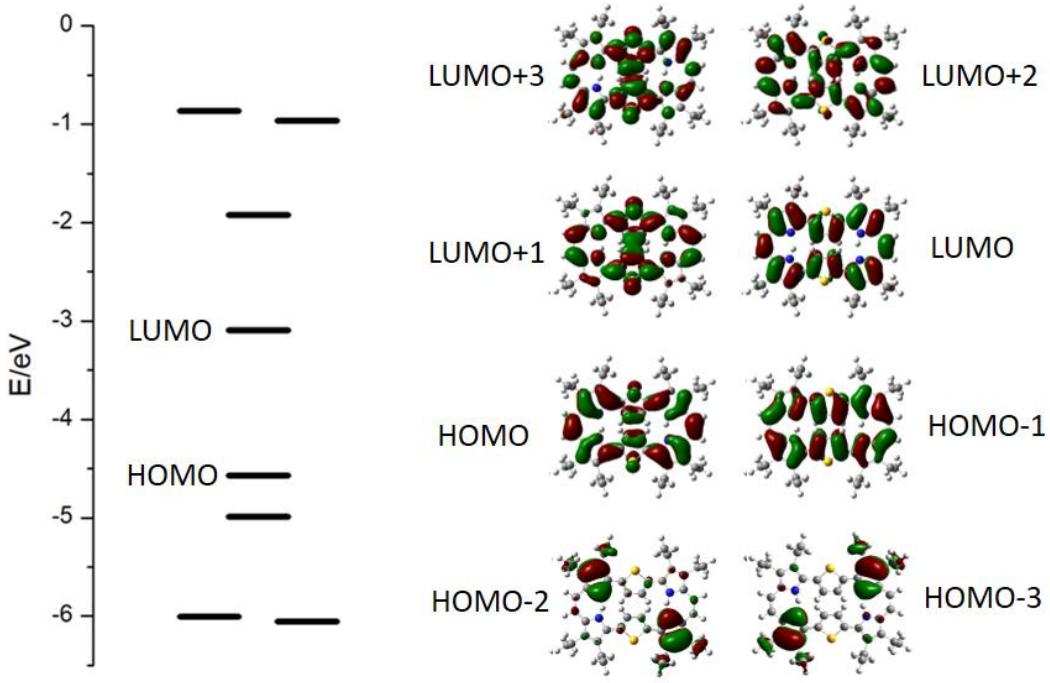

Figure 3.25 Delocalized electron densities of selected MOs of **3.38** with energy level diagram.

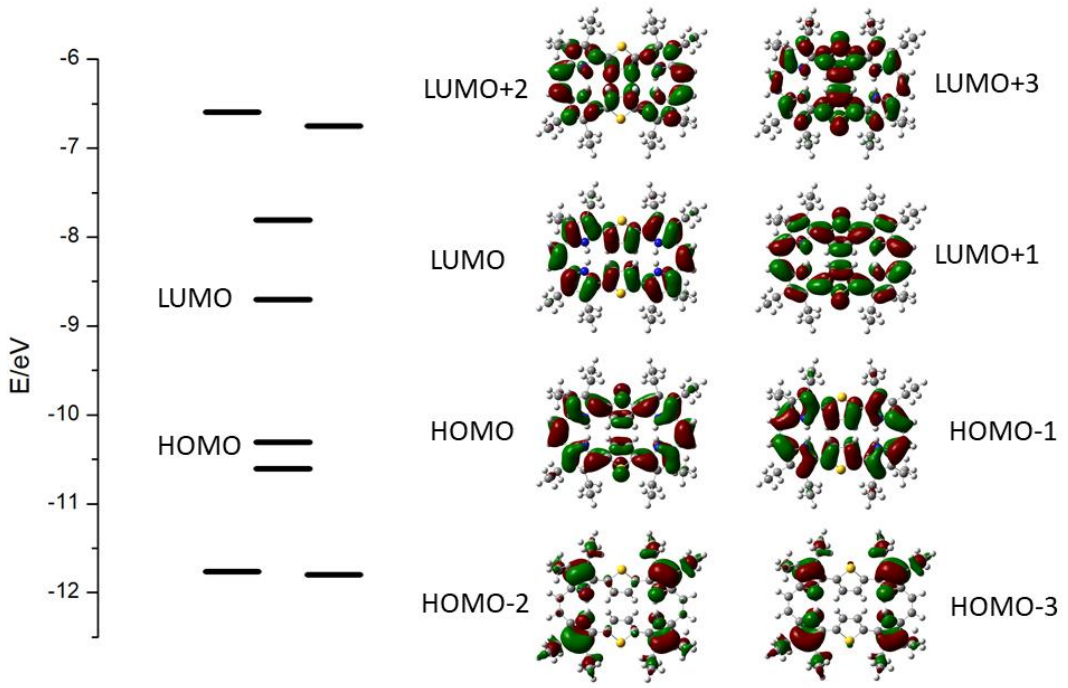

Figure 3.26 Delocalized electron densities of **s**elected MOs of **3.38.H_2^{2+}** with energy level diagram.

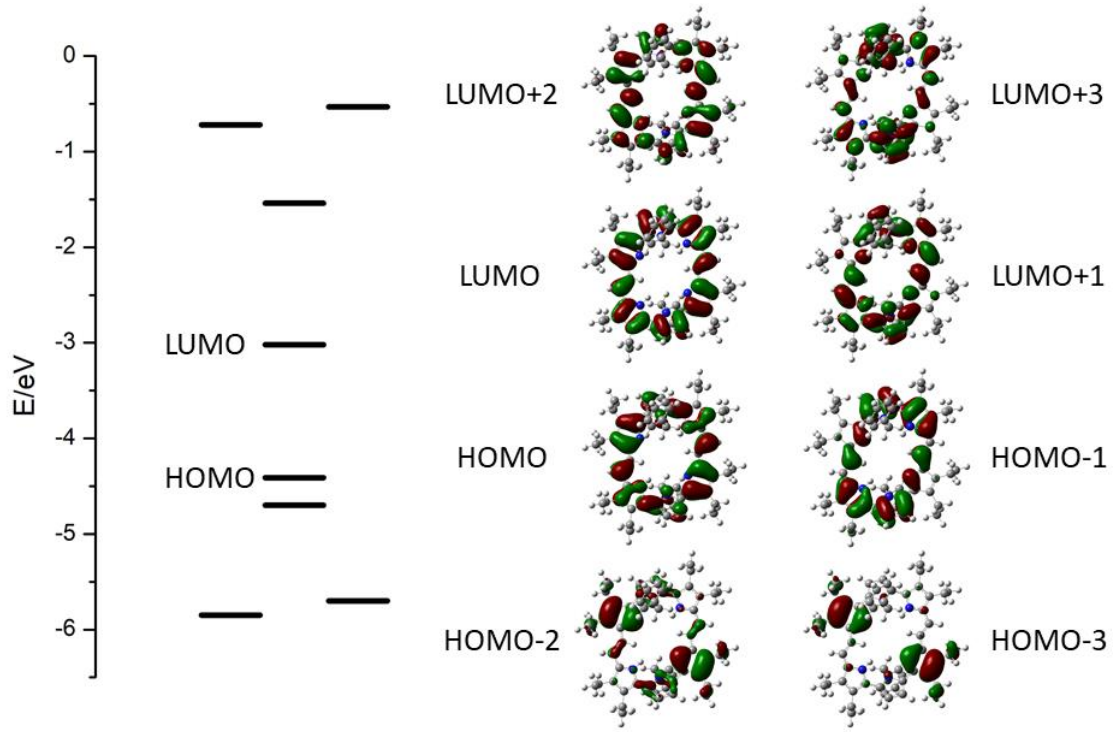

Figure 3.27 Delocalized electron densities of **s**elected MOs of **3.42** with energy level diagram.

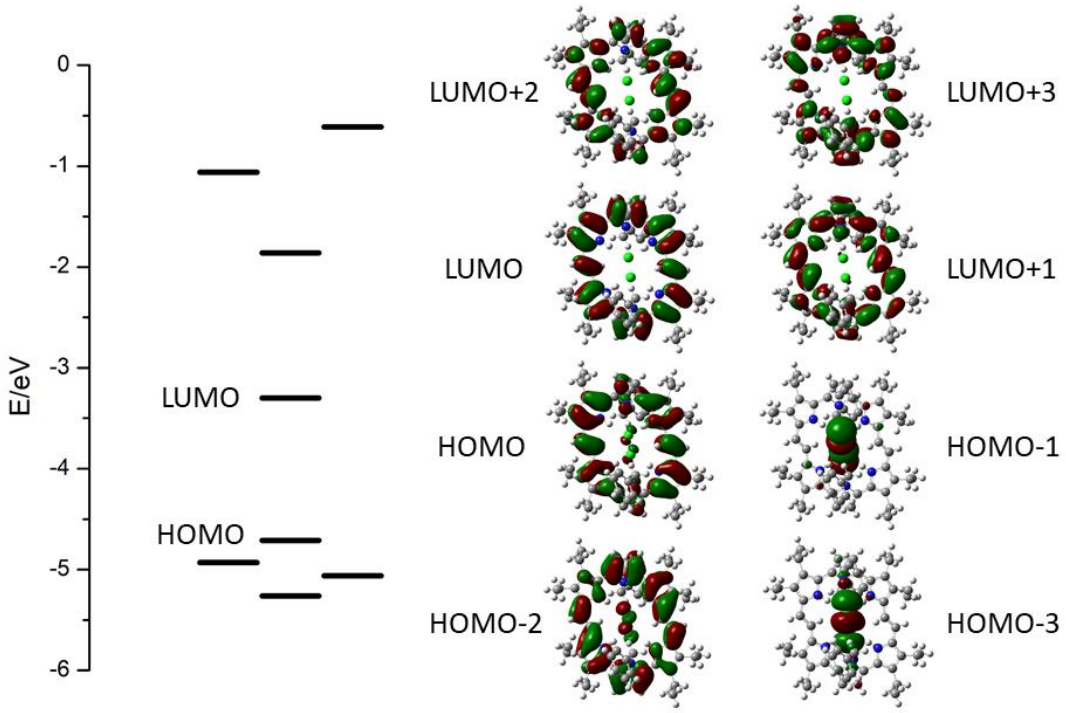

Figure 3.28 Delocalized electron densities of **s**elected MOs of **3.42.H$_2^{2+}$** with energy level diagram.

The NICS values were obtained with gauge independent atomic orbital (GIAO) method and HOMA (Harmonic Oscillator Model of Aromaticity) was calculated by using Ropt (C-C) = 1.388 Å and Ropt (C-N) = 1.334 Å. As expected, both bronzaphyrins, **3.38** and **3.42** are aromatic with a nucleus-independent chemical shift (NICS) values of -18.5 and -11.7 ppm at the center of the macrocycles, respectively (Figure 3.29 and 3.30).

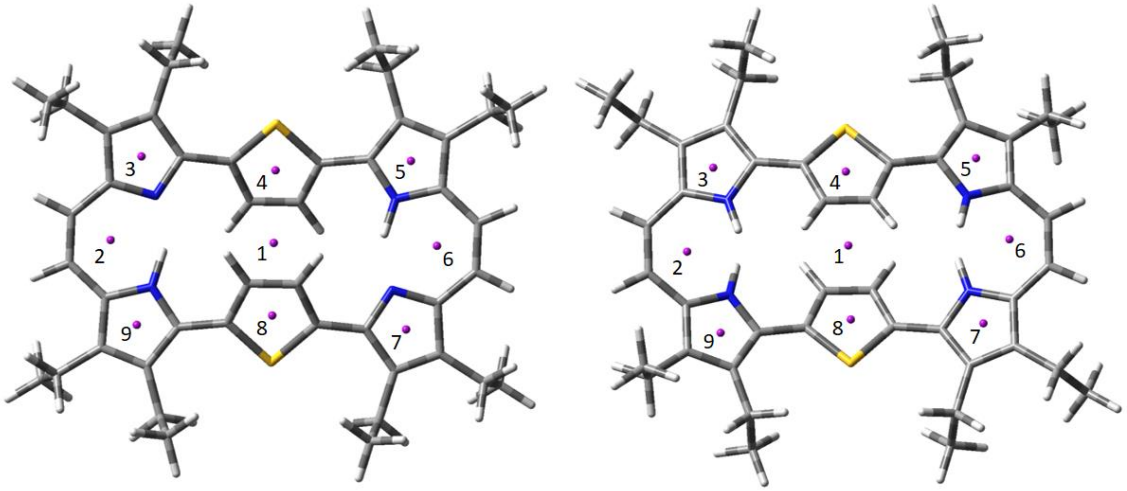

Figure 3.29 Selected positions for calculating NICS values of compounds **3.38** and **3.38.H$_2^{2+}$** 1-9 represent the ghost **Bq** atoms.

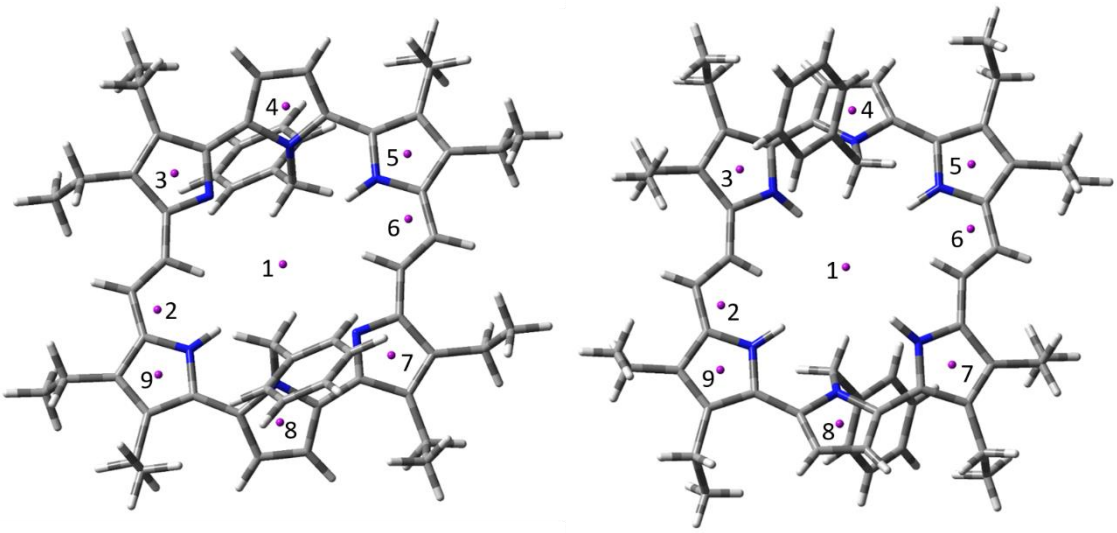

Figure 3.30 Selected positions for calculating NICS values of compounds **3.42** and **3.42.H$_2^{2+}$** 1-9 represent the ghost **Bq** atoms.

Table 7 NICS values of selected positions of compounds **3.38** and **3.38.H$_2^{2+}$; 3.42** and **3.42.H$_2^{2+}$**.

Bq atom no.	3.38	3.38.H$_2^{2+}$	3.42	3.42.H$_2^{2+}$
1	-18.5	-18.3	-11.7	-13.2
2	-16.2	-18.8	-31.5	-30.4
3	-2.4	-11.9	2.6	-11.4
4	-8.7	-9.3	-19.5	-16.4
5	-11.1	-12.9	-15.8	-11.7
6	-16.1	-18.8	-31.5	-30.4
7	-2.4	-11.9	2.6	-11.4
8	-8.3	-9.3	-19.5	-16.4
9	-10.7	-12.9	-15.8	-11.7

The extent of electron delocalization, indicated by harmonic oscillator model of aromaticity (HOMA) index, were found to be 0.75 and 0.62 for both bronzaphyrins **3.38** and **3.42**, respectively (Table 8).[20]

Table 8 Summary of **HOMA*** index values (* = calculated by considering the conjugation path of 26π e). **ΔRx** = Bond length alteration from the crystal structure.

Molecule	π-e	ΔR$_x$ (Å)	HOMA
3.38	26	0.106	0.75
3.38.H$_2^{2+}$	26	0.075	0.75
3.42	26	0.092	0.66
3.42.H$_2^{2+}$	26	0.128	0.623

3.3.7 Electrochemical studies

The electrochemical studies (CV and DPV, Figure 3.31) of dithiabronzaphyrin **3.38** exhibits two reversible oxidation peaks at +0.275 V and +0.565 V and one quasi reversible reduction peak of two overlapping one-electron reductions at -0.845 V (from DPV) similar to tetraalkyl analogue **3.18**,[7a] while bronzaphyrin **3.42** shows weak redox peaks of complicated shapes (Figure 3.32).

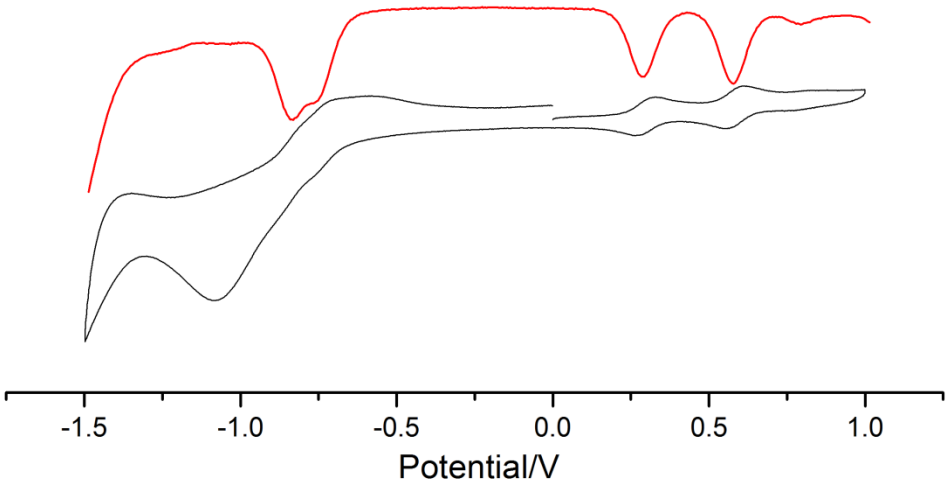

Figure 3.31 CV (below) and DPV (above) of bronzaphyrin **3.38** in dichloromethane measured at 298K.

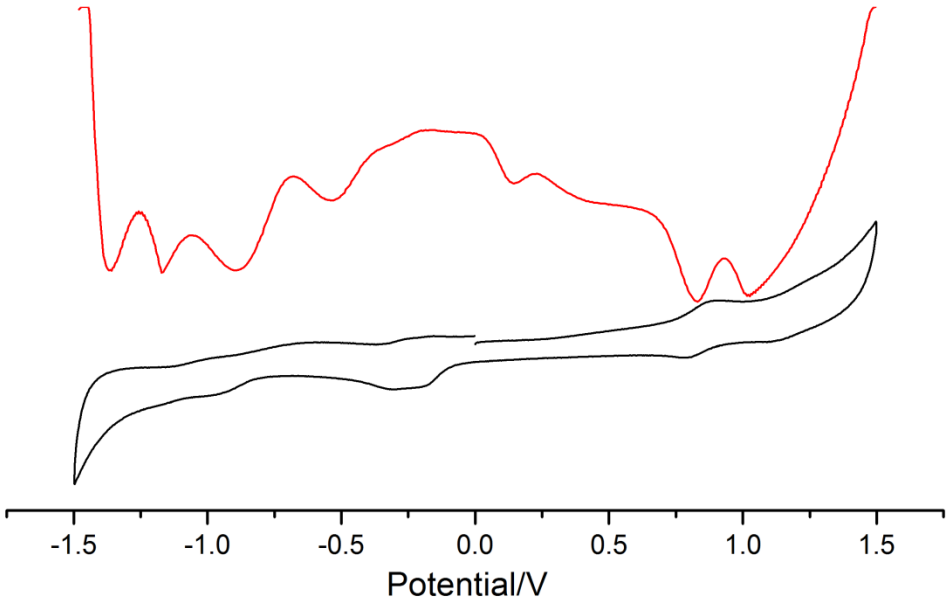

Figure 3.32 CV (below) and DPV (above) of bronzaphyrin **3.42** in dichloromethane measured at 298K.

3.4 Conclusion

In conclusion, we have shown an efficient approach towards the synthesis of several butadiyne bridged bipyrrole derivatives, without N-protection and also endowed with useful functional groups at their α-positions, along with their acetylene bridged counterparts. The protocol could be easily scaled up thereby making these bipyrrole derivatives to be used as simple building blocks in synthesizing acetylene incorporated, novel π-extended porphyrinoids, either by using directly or with minimal synthetic manipulation. We have also successfully demonstrated the utility of these bipyrrole derivatives in an efficient way towards the synthesis of terpyrroles and utilizing them further, showcased a simple approach towards synthesis of bronzaphyrins. We could unequivocally elucidate the crystal structures of the two bronzaphyrins, which has been done for the first time for this class of macrocycle, showed intriguing structural diversities. The dithiabronzaphyrin **3.38** displays inversion of thiophene rings, which remains stable even at higher temperature and upon protonation. The latter phenomenon revealed the macrocycle binding to four open hydrogen bridged dimeric TFA ions, $[(CF_3COO)_2H]^-$ in a unique anion coordination mode to form a stacked network, having no precedence in expanded porphyrin chemistry. Further, the all-azabronzaphyrin **3.42** exhibits hitherto unseen ditransoid structure in its diprotonated state and is found to be more stabilized in presence of anions. This class of hexaphyrins due to their intense absorption in the NIR region are unique among the ones endowed with meso-bridges. Further, by suitable manipulation on the periphery of the two terpyrroles, the photophysical and possibly structural attributes of bronzaphyrins can be altered. This creates a great scope towards fine tuning their properties, in order to develop new materials for NIR imaging and optoelectronics.[21]

3.5 Experimental details

The synthetic details regarding iodopyrrole derivatives was discussed in the materials and methods section.

General procedure for the synthesis of dipyrrolyl ethynes 3.34a-e:

To an oven dried two necked round bottom flask $PdCl_2(PPh_3)_2$ (42 mg, 0.06 mmol), CuI (19 mg, 0.1 mmol) and iodopyrrole derivative (1 mmol) were added and flushed with N_2. Nitrogen purged acetonitrile (5 mL) and DBU (0.9 mL, 6 mmol) were added and the

reaction mixture was kept for freeze-pump thaw cycle for 3 times. To this reaction mixture TMSA (71 µL, 0.5 mmol) and water (7 µL, 40 mol%) were added and stirred in dark for 24 h at room temperature. After completion of the reaction, the product was partitioned between ethyl acetate and dil. HCl. The organic layer was washed with brine and dried over anhyd sodium sulfate. Evaporation of solvent under reduced pressure gave crude product, which was purified by silica gel column chromatography to yield the titled compounds.

3.34a: Eluent:10% EtOAc + 90% hexane, Yield: 146 mg, 71%; off-white solid; mp 180-181 °C; FTIR data (in cm^{-1}): 3291, 2963, 2199, 1660; ^{1}H NMR (400 MHz, $CDCl_3$ δ in ppm): 8.87 (s, 2H), 4.33 (q, J = 7.6 Hz, 4H), 2.75 (q, J = 7.6 Hz, 4H), 2.56 (q, J = 7.6 Hz, 4H), 1.37 (t, J = 7.6 Hz, 6H), 1.17 (m, 12H); ^{13}C NMR (100 MHz, $CDCl_3$ δ in ppm): 160.7, 132.6, 132.5, 119.4, 114.1, 85.1, 60.2, 18.2, 18.1, 15.7, 14.5; HRMS m/z calcd. for $[M+H]^+$ $C_{24}H_{33}N_2O_4$:413.2440, found 413.2442.

3.34b: Eluent:10% EtOAc + 90% hexane, Yield: 174 mg, 65%; light brown solid and all data matched with previously reported compound.[1b]

3.34c: Eluent:15% EtOAc + 85% hexane, Yield: 138 mg, 58%; yellow solid; mp 196-197 °C; FTIR data (in cm^{-1}): 3300, 2966, 1593, 1414; ^{1}H NMR (400 MHz, $CDCl_3$ δ in ppm): 8.83 (s, 2H), 7.69 (d, J = 6.8 Hz, 4H), 7.55 (t, J = 7.2 Hz, 2H), 7.48 (t, J = 7.2 Hz, 4H), 2.58 (m, 8H), 1.22 (t, J = 7.6 Hz, 6H), 1.05 (t, J = 7.6 Hz, 6H); ^{13}C NMR (100 MHz, $CDCl_3$ δ in ppm): 185.8, 139.6, 134.0, 133.5, 131.5, 128.5, 128.3, 128.1, 115.8, 86.1, 18.4, 18.1, 15.7, 15.5; HRMS m/z calcd. for $[M+H]^+$ $C_{32}H_{33}N_2O_2$:477.2542, found 477.2546.

3.34d: Eluent:15-30% EtOAc in hexane, Yield: 92 mg, 52%; brown solid; mp 233-234 °C; FTIR data (in cm^{-1}): 3237, 2962, 1610, 1427; ^{1}H NMR (400 MHz, DMSO-d_6 δ in ppm): 11.93 (s, 2H), 2.69 (q, J = 7.6 Hz, 4H), 2.51 (q, J = 7.6 Hz, 4H), 2.40 (s, 6H), 1.09 (m, 12H); ^{13}C NMR (100 MHz, DMSO-d_6 δ in ppm): 187.8, 132.2, 131.7, 129.1, 114.7, 85.7, 28.1, 18.4, 17.8, 16.4, 16.0; HRMS m/z calcd. for $[M+H]^+$ $C_{22}H_{29}N_2O_2$:353.2229, found 353.2232.

3.34e: Eluent:15-30% EtOAc in hexane, Yield: 141 mg, 44%; yellow solid and all data matched with previously reported compound.[1a]

General procedure for the synthesis of dipyrrolyl butadiynes 3.35a-e:

To an oven dried two necked round bottom flask $PdCl_2(PPh_3)_2$ (42 mg, 0.06 mmol), CuI (19 mg, 0.1 mmol) and iodopyrrole derivative (1 mmol) were added and flushed with N2 gas. Nitrogen purged THF (5 mL) and DBU (0.9 mL, 6 mmol) were added and the reaction mixture was kept for freeze-pump thaw cycle for 3 times. To this reaction mixture TMSA (170 µL, 1.2 mmol) was added and stirred in dark for 16 h. Water (18 µL) was added and again stirred in dark for 24 h at room temperature under aerobic condition. After completion of the reaction product was partitioned between ethyl acetate and dilute HCl. The organic layer was washed with brine and dried over anhyd sodium sulfate. Evaporation of solvent under reduced pressure provided crude product, which was purified by silica gel column chromatography using 20-40% EtOAc in hexane to yield the desired compounds.

3.35a: Yield: 156 mg, 72%; yellow solid; mp 208-209 °C; FTIR data (in cm^{-1}): 3273, 2967, 2129, 1666; ^{1}H NMR (400 MHz, $CDCl_3$ δ in ppm): 9.02 (s, 2H), 4.34 (q, J = 7.2 Hz, 4H), 2.73 (q, J = 7.2 Hz, 4H), 2.56 (q, J = 7.2 Hz, 4H), 1.37 (t, J = 7.2 Hz, 6H), 1.16 (m, 12H); ^{13}C NMR (100 MHz, $CDCl_3$ δ in ppm): 160.4, 135.1, 132.4, 120.3, 113.1, 79.0, 74.9, 60.4, 18.2, 15.8, 15.6, 14.4; HRMS m/z calcd. for $[M+Na]^+$ $C_{26}H_{32}NaN_2O_4$:459.2260, found 459.2260.

3.35b: Yield: 188 mg, 67%; yellow solid; mp 175-176 °C; FTIR data (in cm^{-1}): 3288, 2959, 2131, 1666; ^{1}H NMR (400 MHz, $CDCl_3$ δ in ppm): 9.08 (s, 2H), 7.38 (m, 10H), 5.31 (s, 4H), 2.72 (q, J = 7.6 Hz, 4H), 2.53 (q, J = 7.6 Hz, 4H), 1.14 (m, 12H); ^{13}C NMR (100 MHz, $CDCl_3$ δ in ppm): 160.1, 135.9, 135.2, 133.0, 128.6, 128.3, 119.9, 113.4, 79.0, 74.8, 66.3, 18.2, 18.1, 15.7, 15.7; HRMS m/z calcd. for $[M+H]^+$ $C_{36}H_{37}N_2O_4$:561.2753, found 561.2754.

3.35c: Yield: 153 mg, 61%; yellow solid; mp 210-212 °C; FTIR data (in cm^{-1}): 3233, 2966, 1595; ^{1}H NMR (400 MHz, $CDCl_3$ δ in ppm): 8.89 (s, 2H), 7.68 (d, J = 7.2 Hz, 4H), 7.56 (t, J = 6.8 Hz, 2H), 7.48 (t, J = 7.2 Hz, 4H), 2.58 (q, J = 7.6 Hz, 8H), 1.21 (t, J = 7.6 Hz, 6H), 1.05 (t, J = 7.6 Hz, 6H); ^{13}C NMR (100 MHz, $CDCl_3$ δ in ppm): 185.7, 139.3, 136.0, 133.8, 131.7, 128.8, 128.6, 128.2, 114.7, 79.7, 75.2, 18.4, 18.1, 15.6; HRMS m/z calcd. for $[M+H]^+$ $C_{34}H_{33}N_2O_2$:501.2542, found 501.2545.

3.35d: Yield: 102 mg, 54%; yellow solid; mp 266-268 °C; FTIR data (in cm^{-1}): 3269, 2972, 1620; ^{1}H NMR (400 MHz, DMSO-d_6 δ in ppm): 12.15 (s, 2H), 2.67 (q, J = 7.2 Hz, 4H), 2.48 (q, J = 7.2 Hz, 4H), 2.39 (s, 6H), 1.11 (t, J = 7.2 Hz, 6H), 1.05 (t, J = 7.2 Hz, 6H); ^{13}C NMR (100 MHz, DMSO-d_6 δ in ppm): 188.0, 134.7, 131.5, 129.9, 112.9, 78.7, 76.4, 28.1, 18.3, 17.8, 16.3, 15.9; HRMS m/z calcd. for $[M+H]^+$ $C_{24}H_{29}N_2O_2$:377.2229, found 377.2230.

3.35e: Yield: 54 mg, 31%; yellow solid and all data matched with previously reported compound.[1c]

Synthesis of thiophene substituted terpyrrole diacid 3.36:

Butadiyne bridged bipyrrole **3.35a** (436 mg, 1 mmol) and Na_2S (1.2 g, 5 mmol) were dissolved in THF/2-methoxyethanol and heated at 70°C for 4 h. The solution thus obtained, poured in excess water and treated with HCl solution, yielding the desired product as precipitate (370 mg, 90%).

Melting point: 195-197°C; FTIR data: 3442, 2962, 1655, 1458 cm^{-1}; ^{1}H NMR (500 MHz, MeOH-d_4): δ in ppm 7.27 (s, 2H, *β*-CH thiophene), 2.80 (q, 4H, *J* = 7.5 Hz, CH_2 alkyl), 2.69 (q, 4H, *J* = 7.5 Hz, CH_2 alkyl), 1.18 (m, 12H, CH_3 alkyl); ^{13}C NMR not recorded due to lack of solubility; HRMS m/z calcd. for $(M+H)^+$ $C_{22}H_{27}N_2O_4S$:415.1692, found 415.1689.

Synthesis of thiophene substituted terpyrrole dialdehyde 3.37:

The diacid derivative **3.36 (**100 mg, 0.24 mmol) was dissolved in TFA (1 mL) under nitrogen atmosphere while maintaining the reaction flask at 0°C and stirred for further 15 min. Then triethylorthoformate (500 μL, 3 mmol) was added and stirred for 3h at rt. The reaction mixture was quenched using 1N NaOH solution and extracted with dichloromethane. After complete evaporation of the solvent, the crude product was purified by column chromatography in 20% EtOAc + 80% hexane to obtain the dialdehyde **3.37** in 38% yield.

Melting point: 248-250°C; FTIR data: 3248, 2961, 1653, 1456 cm^{-1}; ^{1}H NMR (400 MHz, $CDCl_3$): δ in ppm 9.63 (s, 2H, -CHO), 9.34 (s, 2H, NH), 7.28 (s, 2H, *β*-CH thiophene), 2.74 (m, 8H, CH_2 alkyl), 1.29 (t, 6H, *J*=7.6Hz, CH_3 alkyl), 1.22 (t, 6H, *J*=7.6Hz, CH_3 alkyl); ^{13}C NMR (100 MHz, $CDCl_3$): δ in ppm 176.94, 138.85, 133.45, 130.07, 128.55,

125.60, 125.54, 17.70, 17.59, 17.00, 15.50; HRMS m/z calcd. for $(M+H)^+$ $C_{22}H_{27}N_2O_2S$:383.1793, found 383.1793.

Synthesis of dithiabronzaphyrin 3.38:

To a three-neck round bottom flask fitted with a dropping funnel and a reflux condenser, activated zinc dust (654 mg, 10 mmol) was added followed by THF (50 mL). Keeping the flask in an ice bath, $TiCl_4$ (550 μL, 5 mmol) was added and subsequently, the reaction mixture was refluxed for 4h. Then thiophene substituted terpyrrole dialdehyde **3.37** (96 mg, 0.25 mmol) along with pyridine (1 mL) in THF (50 mL) was added slowly and the reflux continued for another 18 h. The reaction mixture was quenched using 10% K_2CO_3 solution, filtered and the aqueous layer was extracted with chloroform/ethyl acetate. After complete evaporation of solvent, the solid thus obtained was dissolved again in chloroform/dichloromethane, stirred for 1h to open air and was purified by column chromatography using 50% hexane in dichloromethane to obtain the desired pure macrocycle **3.38** (20 mg, 24%).

Melting point: >300°C; FTIR data: 2957, 2926, 1459, 1423 cm^{-1}; UV-Vis ($CHCl_3$): λ in nm (ε) 467 (4.48), 548 (4.07), 867 (4.35), 904 (4.38); ($CHCl_3$/TFA): λ in nm (ε) 501 (4.73), 574 (4.26), 888 (4.62); Fluorescence ($CHCl_3$, λ_{ex} = 490 nm with slit widths of 14 nm) λ_{max}: 959 nm; ^{1}H NMR (400 MHz, $CDCl_3$): δ in ppm 8.85 (s, 4H, meso CH), 6.50 (s, 2H, NH), 3.92 (q, 8H, *J* = 7.6 Hz, CH_2 alkyl), 3.67 (q, 8H, *J* = 7.6 Hz, CH_2 alkyl), 1.87 (t, 12H, *J* = 7.6 Hz, CH_3 alkyl), 1.72 (t, 12H, *J* = 7.6 Hz, CH_3 alkyl); ^{13}C NMR not recorded due to lack of solubility; HRMS m/z calcd. for $(M+H)^+$ $C_{44}H_{51}N_4S_2$:699.3555, found 699.3555.

Synthesis of N-benzyl derived terpyrrole diester 3.39:

Butadiyne bridged bipyrrole **3.35a** (436 mg, 1 mmol) was dissolved in mesitylene (10 mL), to which benzyl amine (2.7 mL, 25 mmol) and cuprous chloride (198 mg, 2 mmol) were added and heated at 140°C until complete consumption of starting material. The reaction mixture was parted between ethyl acetate and hydrochloric acid and the organic layer was ultimately washed with brine. After evaporating the solvent under reduced pressure, the crude product was purified by column chromatography using 15% EtOAc/hexane mixture to obtain the N-benzyl derived terpyrrole diester **3.39** as thick yellow gel (337 mg, 62%).

FTIR data: 3292, 2967, 1665 cm^{-1}; ^{1}H NMR (400 MHz, $CDCl_3$): δ in ppm 8.43 (s, 2H, NH), 7.26 (m, 3H, CH phenyl), 6.78 (m, 2H, CH phenyl), 6.38 (s, 2H, *β*-CH pyrrole), 4.97 (s, 2H, CH_2 benzyl), 4.20 (q, 4H, *J* = 7.2Hz, CH_2 ester), 2.75 (q, 4H, *J* = 7.6Hz, CH_2 alkyl), 2.41 (q, 4H, *J* = 7.6Hz, CH_2 alkyl), 1.26 (t, 3H, *J* = 7.6Hz, CH_3 ester), 1.21 (t, 3H, *J* = 7.6Hz, CH_3 alkyl), 1.06 (t, 3H, *J* = 7.6Hz, CH_3 alkyl); ^{13}C NMR (100 MHz, $CDCl_3$): δ in ppm 160.93, 138.86, 133.46, 129.05, 127.65, 126.74, 126.12, 125.61, 124.10, 118.28, 111.59, 59.67, 49.09, 18.37, 17.59, 16.12, 15.70, 14.43; HRMS m/z calcd. for $(M+H)^+$ $C_{33}H_{42}N_3O_4$:544.3175, found 544.3175.

Synthesis of N-benzyl derived terpyrrole dialdehyde 3.40:

The terpyrrole diester **3.39** (543 mg, 1 mmol) along with NaOH (400 mg, 10 mmol) was taken in an oven dried round bottom flask and dry ethylene glycol (10 mL) was added to it and refluxed for 2 h under nitrogen atmosphere. Nitrogen bubbled water was added and the mixture was then extracted with DCM. The organic layer was evaporated and the crude compound was used as it is.

^{1}H NMR (400 MHz, $CDCl_3$): δ in ppm 7.39 (s, 2H, NH), 7.22 (m, 3H, CH phenyl), 6.76 (d, 2H, *J* = 6.8Hz CH phenyl), 6.39 (s, 2H, *α*-CH pyrrole), 6.30 (s, 2H, *β*-CH pyrrole), 4.90 (s, 2H, CH_2 benzyl), 2.45 (m, 8H, CH_2 alkyl), 1.20 (t, 6H, *J* = 7.6Hz, CH_3 alkyl), 1.05 (t, 6H, *J* = 7.6Hz, CH_3 alkyl); ^{13}C NMR (100 MHz, $CDCl_3$): δ in ppm 140.23, 128.84, 127.21, 126.57, 125.71, 125.13, 124.34, 120.07, 114.17, 110.63, 48.42, 18.62, 17.98, 15.73, 14.36.

To a three neck round bottom flask fitted with a dropping funnel and a reflux condenser DMF (96 μL, 1.25 mmol) was added. The flask was immersed in an ice bath and $POCl_3$ (116 μL, 1.25 mmol) was added slowly through syringe. An exothermic reaction occurred with the formation of $POCl_3$-DMF complex. The ice bath was removed and the mixture was stirred for another 15 min at room temperature. 1,2-Dichloroethane (5 mL) was added and the ice bath was replaced. When the internal temperature has been lowered to 5 °C, the crude N-benzylterpyrrole (200 mg, 0.5 mmol) dissolved in 1,2-dichloroethane (15 mL) was added slowly to cooled mixture. After the addition was complete, the ice bath was replaced with heating mantle. The mixture was refluxed for 2h and then cooled to 25-30 °C and a saturated solution of sodium acetate (580 mg) was added slowly to the reaction mixture. The reaction mixture was again refluxed for 2h. After the completion of reaction, the content was extracted thrice with dichloromethane.

The combined organic layers were washed with saturated aqueous sodium carbonate solution and dried over anhydrous sodium carbonate. The crude product was purified by column chromatography in 20% EtOAc + 80% hexane. Evaporation of the eluent resulted in the desired product **3.40** as yellow solid (193 mg, 69%).

Melting point: 252-254°C; FTIR data: 3292, 2957, 2869, 1634 cm^{-1}; ^{1}H NMR (400 MHz, $CDCl_3$): δ in ppm 9.59 (s, 2H, -CHO), 8.82 (s, 2H, NH), 7.15 (m, 3H, CH phenyl), 6.59 (d, 2H, *J* = 4.4Hz, CH phenyl), 6.41 (s, 2H, *β*-CH pyrrole), 4.99 (s, 2H, CH_2 benzyl), 2.75 (q, 4H, *J* = 7.6Hz, CH_2 alkyl), 2.41 (q, 4H, *J* = 7.6Hz, CH_2 alkyl), 1.25 (t, 3H, *J* = 7.6Hz, CH_3 alkyl), 1.03 (t, 3H, *J* = 7.6Hz, CH_3 alkyl); ^{13}C NMR (100 MHz, $CDCl_3$): δ in ppm HRMS m/z calcd. for $(M+Na)^+$ $C_{29}H_{33}NaN_3O_2$:478.2470, found 478.2471.

Synthesis of all-azabronzaphyrin 3.42:

To a three-neck round bottom flask fitted with a dropping funnel and a reflux condenser, activated zinc dust (520 mg, 8 mmol) was added followed by THF. Keeping the flask in an ice bath, $TiCl_4$ (440 μL, 4 mmol) was added and subsequently, the reaction mixture was refluxed for 4h. Then N-benzyl derived terpyrrole dialdehyde **3.40** (91 mg, 0.2 mmol) along with pyridine (1 mL) in THF was added slowly and the reflux continued for another 18h. The reaction mixture was quenched using 10% K_2CO_3 solution, filtered and the aqueous layer was extracted with ethyl acetate. The combined organic solvent was evaporated and the crude product was purified immediately without any delay using 10% EtOAc in hexane to obtain the macrocycle **3.41**.

^{1}H NMR (400 MHz, $CDCl_3$): δ in ppm 7.923 (s, 4H, NH), 6.97 (t, 2H, *J* = 7.2Hz, CH phenyl), 6.81 (t, 4H, *J* = 7.6Hz, CH phenyl), 6.58 (d, 4H, *J* = 7.6Hz, CH phenyl), 6.11 (d, 8H, *J* = 4.8Hz, meso CH and *β*-CH pyrrole), 4.46 (s, 4H, CH_2 benzyl), 2.53 (q, 8H, *J* = 7.6Hz, CH_2 alkyl), 2.33 (q, 4H, *J* = 7.2Hz, CH_2 alkyl), 2.16 (q, 4H, *J* = 7.2Hz, CH_2 alkyl), 1.16 (t, 12H, *J* = 7.6Hz, CH_3 alkyl), 1.01 (t, 12H, *J* = 7.6Hz, CH_3 alkyl); ^{13}C NMR (100 MHz, $CDCl_3$): δ in ppm 137.99, 127.86, 127.25, 127.15, 126.61, 126.50, 125.93, 120.72, 111.84, 111.44, 48.32, 18.14, 17.90, 16.37, 15.61.

The compound **3.41** from the previous step was dissolved in chloroform and treated with dil. $HClO_4$ or dil. HCl to obtain the corresponding bronzaphyrin **3.42** as dichloride or monochloride salts. The product was subsequently purified by column chromatography

using 10% MeOH/DCM to obtain the desired pure macrocycle **3.42** (3 mg, 4% dichloride salt and 2.3 mg, 3% monochloride salt).

Melting point: >300°C; FTIR data: 2961, 2924, 2853, 1455 cm^{-1}; UV-Vis ($CHCl_3$): λ in nm (ε) 483 (4.75), 495 (4.76), 842 (4.56), 982 (4.44); ($CHCl_3$/TFA): λ in nm (ε) 488 (4.88), 847 (4.56), 944 (4.53); Fluorescence ($CHCl_3$, λ_{ex} = 490 nm with slit widths of 14 nm) λ_{max}: 1022 nm; ^{1}H NMR (400 MHz, $CDCl_3$): δ in ppm 11.90 (d, 2H, *J* = 1.8Hz, meso CH), 9.44 (s, 4H, *β*-CH), 6.31 (m, 2H, CH phenyl), 5.97 (m, 4H, CH phenyl), 4.82 (m, 4H, CH_2 alkyl), 4.63 (m, 12H, CH_2 alkyl), 3.31 (m, 4H, CH phenyl), 2.48 (m, 6H, CH_3 alkyl), 2.35 (m, 6H, CH_3 alkyl), 2.20 (m, 12H, CH_3 alkyl), -2 to -7 (10H, comprising CH_2 benzyl, 4H; NH, 4H; meso CH, 2H); HRMS: m/z calcd. for $(M+H)^+$ $C_{58}H_{65}N_6$:845.5271, found 845.5270.

3.6 Crystallographic data and structure refinement information

Crystal data and structure refinement for 3.34a

CCDC No.	1500785	
Identification code	MA	
Empirical formula	C24 H32 N2 O4	
Formula weight	412.51	
Temperature	293(2) K	
Wavelength	0.71073 Å	
Crystal system	Monoclinic	
Space group	C 2/c	
Unit cell dimensions	*a* = 13.470(3) Å	*α* = 90°.
	b = 15.343(3) Å	*β* = 113.48(3)°.
	c = 12.671(3) Å	*γ* = 90°.
Volume	2401.9(10) $Å^3$	
Z	4	
Density (calculated)	1.141 g/cm^3	
Absorption coefficient	0.077 mm^{-1}	
F(000)	888	
Crystal size	0.21 x 0.12 x 0.08 mm^3	
Theta range for data collection	2.116 to 26.013°.	
Index ranges	$-16 \leq h \leq 16, -18 \leq k \leq 18, -15 \leq l \leq 15$	
Reflections collected	9605	
Independent reflections	2375 [R(int) = 0.0264]	

Completeness to theta = 25.242°	100.0%
Absorption correction	Semi-empirical from equivalents
Refinement method	Full-matrix least-squares on F^2
Data / restraints / parameters	2375 / 0 / 143
Goodness-of-fit on F^2	1.029
Final R indices [I>2sigma(I)]	R1 = 0.0618, wR2 = 0.1724
R indices (all data)	R1 = 0.0740, wR2 = 0.1844
Largest diff. peak and hole	0.202 and -0.230 e.Å^{-3}

Crystal data and structure refinement for 3.35a

CCDC No.	1500784	
Identification code	DA	
Empirical formula	C26 H32 N2 O4	
Formula weight	436.53	
Temperature	298(2) K	
Wavelength	0.71073 Å	
Crystal system	Triclinic	
Space group	P -1	
Unit cell dimensions	a = 7.0237(14) Å	α = 115.430(2)°.
	b = 9.437(2) Å	β = 97.730(3)°.
	c = 10.321(2) Å	γ = 97.951(3)°.
Volume	597.3(2) Å^3	
Z	1	
Density (calculated)	1.214 g/cm^3	
Absorption coefficient	0.082 mm^{-1}	
F(000)	234	
Crystal size	0.20 x 0.18 x 0.16 mm^3	
Theta range for data collection	2.238 to 25.093°.	
Index ranges	$-8 \leq h \leq 8$, $-11 \leq k \leq 11$, $-12 \leq l \leq 12$	
Reflections collected	5762	
Independent reflections	2106 [R(int) = 0.0218]	
Completeness to theta = 25.093°	99.3%	
Absorption correction	Semi-empirical from equivalents	
Refinement method	Full-matrix least-squares on F^2	
Data / restraints / parameters	2106 / 0 / 153	
Goodness-of-fit on F^2	1.060	
Final R indices [I>2sigma(I)]	R1 = 0.0445, wR2 = 0.1214	

R indices (all data)	R1 = 0.0495, wR2 = 0.1268
Extinction coefficient	0.031(8)
Largest diff. peak and hole	0.255 and -0.172 e.Å^{-3}

Crystal data and structure refinement for 3.38

CCDC No.	1500782	
Identification code	BrzSS	
Empirical formula	C44 H50 N4 S2	
Formula weight	699.00	
Temperature	298(2) K	
Wavelength	1.54184 Å	
Crystal system	Triclinic	
Space group	*P* -1	
Unit cell dimensions	*a* = 8.7071(7) Å	*α*= 98.972(5)°.
	b = 9.6083(5) Å	*β*= 106.931(7)°.
	c = 12.2192(8) Å	*γ* = 103.162(6)°.
Volume	924.76(12) Å^3	
Z	1	
Density (calculated)	1.255 g/cm^3	
Absorption coefficient	1.581 mm^{-1}	
F(000)	374	
Crystal size	0.18 x 0.16 x 0.14 mm^3	
Theta range for data collection	3.894 to 70.066°.	
Index ranges	-10 ≤ h ≤ 9, -8 ≤ k ≤ 11, -14 ≤ l ≤ 14	
Reflections collected	5814	
Independent reflections	3487 [R(int) = 0.0325]	
Completeness to theta = 67.684°	99.8%	
Absorption correction	Semi-empirical from equivalents	
Max. and min. transmission	1.00000 and 0.83196	
Refinement method	Full-matrix least-squares on F^2	
Data / restraints / parameters	3487 / 0 / 230	
Goodness-of-fit on F^2	1.043	
Final R indices [I>2sigma(I)]	R1 = 0.0489, wR2 = 0.1242	
R indices (all data)	R1 = 0.0616, wR2 = 0.1370	
Largest diff. peak and hole	0.419 and -0.307 e.Å^{-3}	

Crystal data and structure refinement for 3.38.H_2^{2+}

CCDC No.	1869467	
Identification code	BrzSStfa	
Empirical formula	C52 H54 F12 N4 O8 S2	
Formula weight	1155.11	
Temperature	100(2) K	
Wavelength	0.71073 Å	
Crystal system	Monoclinic	
Space group	P $2_{1/c}$	
Unit cell dimensions	a = 12.4875(4) Å	α = 90°.
	b = 12.9069(4) Å	β = 98.0780(10)°.
	c = 16.8517(6) Å	γ = 90°.
Volume	2689.12(15) $Å^3$	
Z	2	
Density (calculated)	1.427 g/cm^3	
Absorption coefficient	0.197 mm^{-1}	
F(000)	1196	
Crystal size	0.16 x 0.14 x 0.10 mm^3	
Theta range for data collection	2.281 to 27.558°.	
Index ranges	$-16 \leq h \leq 16$, $-16 \leq k \leq 16$, $-21 \leq l \leq 21$	
Reflections collected	69513	
Independent reflections	6206 [R(int) = 0.0526]	
Completeness to theta = 25.242°	99.9%	
Absorption correction	Semi-empirical from equivalents	
Max. and min. transmission	0.7456 and 0.6669	
Refinement method	Full-matrix least-squares on F^2	
Data / restraints / parameters	6206 / 0 / 368	
Goodness-of-fit on F^2	0.992	
Final R indices [I>2sigma(I)]	R1 = 0.0605, wR2 = 0.1541	
R indices (all data)	R1 = 0.0751, wR2 = 0.1648	
Extinction coefficient	n/a	
Largest diff. peak and hole	1.892 and -1.039 e.$Å^{-3}$	

Crystal data and structure refinement for 3.40

CCDC No.	1500783
Identification code	BnTPAld

Empirical formula	C29 H33 N3 O2	
Formula weight	455.58	
Temperature	298(2) K	
Wavelength	0.71073 Å	
Crystal system	Triclinic	
Space group	P -1	
Unit cell dimensions	a = 8.6512(8) Å	α = 65.8790(10)°.
	b = 11.6599(10) Å	β = 79.2940(10)°.
	c = 14.1342(12) Å	γ = 85.0230(10)°.
Volume	1278.51(19) $Å^3$	
Z	2	
Density (calculated)	1.183 g/cm^3	
Absorption coefficient	0.075 mm^{-1}	
F(000)	488	
Crystal size	0.28 x 0.24 x 0.20 mm^3	
Theta range for data collection	1.601 to 26.029°.	
Index ranges	$-10 \leq h \leq 10$, $-14 \leq k \leq 14$, $-17 \leq l \leq 17$	
Reflections collected	13377	
Independent reflections	5012 [R(int) = 0.0318]	
Completeness to theta = 25.242°	99.7%	
Refinement method	Full-matrix least-squares on F^2	
Data / restraints / parameters	5012 / 0 / 327	
Goodness-of-fit on F^2	1.040	
Final R indices [I>2sigma(I)]	R1 = 0.0524, wR2 = 0.1262	
R indices (all data)	R1 = 0.0675, wR2 = 0.1363	
Largest diff. peak and hole	0.167 and -0.164 e.$Å^{-3}$	

Crystal data and structure refinement for 3.42.H_2^{2+}

CCDC No.	1500781	
Identification code	BrzNBn	
Empirical formula	C62 H70 Cl10 N6	
Formula weight	1253.74	
Temperature	100(2) K	
Wavelength	0.71073 Å	
Crystal system	Monoclinic	
Space group	P $2_{1/c}$	
Unit cell dimensions	a = 8.2756(7) Å	α= 90°.

	b = 14.7669(14) Å	β= 95.693(3)°.
	c = 24.817(2) Å	γ = 90°.
Volume	3017.8(5) $Å^3$	
Z	2	
Density (calculated)	1.380 g/cm^3	
Absorption coefficient	0.507 mm^{-1}	
F(000)	1308	
Crystal size	0.2 x 0.14 x 0.12 mm^3	
Theta range for data collection	2.473 to 25.682°.	
Index ranges	$-10 \leq h \leq 9$, $-18 \leq k \leq 18$, $-30 \leq l \leq 30$	
Reflections collected	89421	
Independent reflections	5704 [R(int) = 0.1023]	
Completeness to theta = 25.242°	99.9 %	
Absorption correction	Semi-empirical from equivalents	
Max. and min. transmission	0.941 and 0.918	
Refinement method	Full-matrix least-squares on F^2	
Data / restraints / parameters	5704 / 0 / 360	
Goodness-of-fit on F^2	1.239	
Final R indices [I>2sigma(I)]	R1 = 0.0803, wR2 = 0.1910	
R indices (all data)	R1 = 0.0952, wR2 = 0.1966	
Largest diff. peak and hole	0.858 and -0.546 $e.Å^{-3}$	

3.7 References

1. (a) Jux, N.; Koch, P.; Schmickler, H.; Lex, J.; E. Vogel, *Angew. Chem., Int. Ed. Engl.* **1990**, *29*, 1385. (b) Vogel, E.; Bröring, M.; Fink, J.; Rosen, D.; Schmickler, H.; Lex, J.; Chan, K. W. K.; Wu, Y.-D.; Plattner, D. A.; Nendel, M.; Houk, K. N. *Angew. Chem., Int. Ed. Engl.* **1995**, *34*, 2511. (c) Mártire, D. O.; Jux, N.; Aramendía, P. F.; Negri, R. M.; Lex, J.; Braslavsky, S. E.; Schaffner, K.; Vogel, E. *J. Am. Chem. Soc.* **1992**, *114*, 9969. (d) Berman, A.; Levanon, H. *Chem. Phys. Lett.* **1993**, *211*, 549. (e) Rana, A.; Lee, S.; Kim, D.; Panda, P. K. *Chem. Eur. J.* **2015**, *21*, 12129.
2. Sondheimer, F.; Gaoni, Y. *J. Am. Chem. Soc.* **1960**, *82*, 5765; Sondheimer, F.; Gaoni, Y.; Jackman, L. M.; Bailey, N. A.; Mason, R. *ibid.* **1962**, *84*, 4595.
3. Cho, D. H.; Lee, J. H.; Kim, B. H. *J. Org. Chem.* **1999**, *64*, 8048.
4. (a) Sakida, T.; Yamaguchi, S.; Shinokubo, H. *Angew. Chem. Int. Ed.* **2011**, *50*, 2280. (b) Umetani, M.; Tanaka, T.; Kim, T.; Kim, D.; Osuka, A. *Angew. Chem., Int. Ed.* **2016**, *55*, 8095. (c) Weghorn, S. J.; Lynch, V.; Sessler, J. L. *Tetrahedron Lett.* 1995, 36, 4713. (d) Maeda, C.; Yoneda, T.; Aratani, N.; Yoon, M.-C.; Lim, J. M.; Kim, D.; Yoshioka, N.; Osuka, A. *Angew. Chem., Int. Ed.* **2011**, *50*, 5691. (e) Masuda, M.; Maeda, C. *Chem. Eur. J.* **2013**, *19*, 2971.
5. Sessler, J. L.; Weghorn, S. J.; Hiseada, Y.; Lynch, V. *Chem. Eur. J.* **1995**, *1*, 56.
6. (a) Weghorn, S. J.; Sessler, J. L.; Lynch, V.; Baumann, T. F.; Sibert, J. W. *Inorg. Chem.* **1996**, *35*, 1089. (b) Y. Ishimaru, N. Shimoyama, T. Fujihara, K. Watanabe, J. Setsune, *Chem. Asian J.* **2015**, *10*, 329.
7. (a) Johnson, M. R.; Miller, D. C.; Bush, K.; Becker, J. J.; Ibers, J. A. *J. Org. Chem.* **1992**, *57*, 4414. (b) Miller, D. C.; Johnson, M. R.; Ibers, J. A. *J. Org. Chem.* **1994**, *59*, 2877. (c) Johnson, M. R. *J. Org. Chem.* **1997**, *62*, 1168Z. (d) Hu, C. Scordilis-Kelley, M. P. Cava, *Tetrahedron Lett.* **1993**, *34*, 1879. (e) Hu, Z.; Atwood, J. L.; Cava, M. P. *J. Org. Chem.* **1994**, *59*, 8071. (f) Kozaki, M.; Parakka, J.; Cava, M. P. *J. Org. Chem.* 1996, **61**, 3657. (g) Ellinger, F.; Gieren, A.; Hübner, Th.; Lex, J.; Lucchesini, F.; Merz, A.; Neidlein, R.; Salbeck, J. *Monatsh. für Chemie* **1993**, *124*, 931.
8. (a) Robles-Machín, R.; López-Pérez, A.; González-Esguevillas, M.; Adrio, J.; Carretero, J. C. *Chem. Eur. J.* **2010**, *16*, 9864. (b) Merrill, B. A.; LeGoff, E. *J. Org. Chem.* **1990**, *55*, 2904. (c) Rapoport, H.; Castagnoli Jr., N.; Holden, K. G. *J. Org. Chem.* **1964**, *29*, 883.
9. (a) Gossauer, A. *Bull. Soc. Chim. Belg.* **1983**, *92*, 793. (b) Ishida, M.; Shin, J.-Y.; Lim, J. M.; Lee, B. S.; Yoon, M.-C.; Koide, T.; Sessler, J. L.; Osuka, A.; Kim, D. *J. Am. Chem. Soc.* **2011**, *133*, 15533. (c) Sung, Y. M.; Oh, J.; Naoda, K.; Lee, T.; Kim, W.; Lim, M.; Osuka A.; Kim, D. *Angew. Chem., Int. Ed. Engl.* **2016**, *55*, 11930. (d) Lim, J. M.; Ganesan, K.; Sung, Y. M.; Srinivasan, A.; Chandrashekar T. K.; Kim, D. *Chem. Commun.*, **2014**, *50*, 4358. (e) Hisamune, Y.; Nishimura, K.; Isakari, K.; Ishida, M.; Mori, S.; Karasawa, S.; Kato, T.; Lee, S.; kim D.; Furuta, H. *Angew. Chem., Int. Ed. Engl.* **2015**, *54*,

7323. (f) Vogel, A.; Dechert, S.; John, M.; Brückner C.; Meyer, F. *Chem. Eur. J.* 2016, **22**, 2307.

10. (a) Sessler, J. L.; Morishima T.; Lynch, V. *Angew. Chem., Int. Ed. Engl.* **1991**, *30*, 977. (b) Chandrashekar, T. K.; Prabhuraja, V.; Gokulnath, S.; Sabarinathan, R.; Srinivasan, A. *Chem. Commun.,* **2010**, *46*, 5915. (c) Kee, S.-Y.; Lim, J. M.; Kim, S.-J.; Yoo, J.; Park, J.-S.; Sarma, T.; Lynch, V. M.; Panda, P. K.; Sessler, J. L.; Kim, D.; Lee, C.- H. *Chem. Commun.*, **2011**, *47*, 6813. (d) Ishida, M.; Furuyama, T.; Lim, J. M.; Lee, S.; Zhang, Z.; Ghosh, S. K.; Lynch, V. M.; Lee, C.-H.; Kobayashi, N.; Kim, D.; Sessler, J. L. *Chem. Eur. J.* **2017**, *23*, 6682.
11. (a) Sessler, J. L.; Weghorn, S. J.; Morishima, T.; Rosingana, M.; Lynch V.; Lee, V. *J. Am. Chem. Soc.* **1992**, *114*, 8306. (b) Ishida M.; Kim, S.-J.; Preihs, C.; Ohkubo, K.; Lim, J. M.; Lee, B. S.; Park, J. S.; Lynch, V. M.; Roznyatovskiy, V. V.; Sarma, T.; Panda, P. K.; Lee, C. –H.; Fukuzumi, S.; Kim, D.; Sessler, J. L. *Nat. Chem.* **2013**, *5*, 15. (c) Fukuzumi, S.; Ohkubo, K.; Ishida, M.; Preihs, C.; Chen, B.; Borden, W. T.; Kim D.; Sessler, J. L. *J. Am. Chem. Soc.* 2015, **137**, 9780.
12. Kohler, T.; Seidel, D.; Lynch, V.; Arp, F. O.; Ou, Z.; Kadish, K. M.; Sessler, J. L. *J. Am. Chem. Soc.* 2003, **125**, 6872.
13. Mio, M. J.; Kopel, L. C.; Braun, J. B.; Gadzikwa, T. L.; Hull, K. L.; Brisbois, R. G.; Markworth, C. J.; Grieco, P. A. *Org. Lett.* **2002**, *4*, 3199.
14. a) Chalk, A. J. *Tetrahedron Lett.* **1972**, *33*, 3487. (b) Maeda, C.; Shinokubo, H.; Osuka, A. *Org. Lett.* **2010**, *12*, 1820. (c) O'Connor, M. J.; Haley, M. M. *Org. Lett.* **2008**, *10*, 3973. (d) Krömer, J.; Rios-Carreras, I.; Fuhrmann, G.; Musch, C.; Wunderlin, M.; Debaerdemaeker, T.; Mena-Osteritz, E.; Bäuerle, P. *Angew. Chem., Int. Ed.* **2000**, *39*, 3481. (e) Arnold, D. P.; Nitschinsk, L. J. *Tetrahedron* **1992**, *48*, 8781. (f) Jiang, H.; Zeng, W.; Li, Y.; Wu, W.; Huang, L.; Fu, W. *J. Org. Chem.* **2012**, *77*, 5179.
15. Clezy, P. S.; Fookes C. J. R.; Liepa, A. J. *Aust. J. Chem.* **1972**, *25*, 1979.
16. (a) Sarma, T.; Panda, P. K.; Anusha, P. T.; Rao, S. V. *Org. Lett.* **2011**, *13*, 188. (b) Oohora, K.; Ogawa, A.; Fukuda, T.; Onoda, A.; Hasegawa, J.; Hayashi, T. *Angew. Chem., Int. Ed. Engl.* **2015**, *54*, 6227. (c) Roznyatovskiy, V.; Lynch, V. M.; Sessler, J. L. *Org. Lett.* **2010**, *12*, 4424; (d) Waluk, J. *Chem. Rev.* **2017**, *117*, 2447.
17. (a) Rachlewicz, K.; Sprutta, N.; Latos-Grażyński, L.; Chmielewski, P. J.; Szterenberg, L. *J. Chem. Soc., Perkin Trans. 2* **1998**, 959. (b) Shetti, V. S.; Kee, S.-Y.; Lee, C. H. *Chem. Asian J.* **2014**, *9*, 734. (c) Shimizu, S.; Taniguchi, R.; Osuka, A. *Angew. Chem., Int. Ed.* **2005**, *44*, 2225.
18. (a) Macdonald, A. L.; Speakman, J. C. *J. Chem. Soc. Perkin Trans. 2* **1972**, 825. (b) Gómez-Lor, B.; Hennrich, G.; Alonso, B.; Monge, A.; Gutierrez-Puebla, E.; Echavarren, A. M. *Angew. Chem. Int. Ed.* **2006**, *45*, 4491.
19. Gaussian 09, Revision C.01, Frisch, M. J.; Trucks, G. W.; Schlegel, H. B.; Scuseria, G. E.; Robb, M. A.; Cheeseman, J. R.; Scalmani, G.; Barone, V.;

Mennucci, B.; Petersson, G. A.; Nakatsuji, H.; Caricato, M.; Li, X.; Hratchian, H. P.; Izmaylov, A. F.; Bloino, J.; Zheng, G.; Sonnenberg, J. L.; Hada, M.; Ehara, M.; Toyota, K.; Fukuda, R.; Hasegawa, J.; Ishida, M.; Nakajima, T.; Honda, Y.; Kitao, O.; Nakai, H.; Vreven, T.; Montgomery Jr., J. A.; Peralta, J. E.; Ogliaro, F.; Bearpark, M.; Heyd, J. J.; Brothers, E.; Kudin, K. N.; Staroverov, V. N.; Keith, T.; Kobayashi, R.; Normand, J.; Raghavachari, K.; Rendell, A.; Burant, J. C.; Iyengar, S. S.; Tomasi, J.; Cossi, M.; Rega, N.; Millam, J. M.; Klene, M.; Knox, J. E.; Cross, J. B.; Bakken, V.; Adamo, C.; Jaramillo, J.; Gomperts, R.; Stratmann, R. E.; Yazyev, O.; Austin, A. J.; Cammi, R.; Pomelli, C.; Ochterski, J. W.; Martin, R. L.; Morokuma, K.; Zakrzewski, V. G.; Voth, G. A.; Salvador, P.; Dannenberg, J. J.; Dapprich, S.; Daniels, A. D.; Farkas, O.; Foresman, J. B.; Ortiz, J. V.; Cioslowski, J.; Fox, D. J. *Gaussian, Inc.,* Wallingford CT, 2010.

20. (a) Chen, Z.; Wannere, C. S.; Corminboeuf, C.; Puchta, R.; Schleyer, P. v. R.; *Chem. Rev.* **2005**, *105*, 3842. (b) Krygowski, T. M.; Cryan'ski, M. *Chem. Rev.* **2001**, *101*, 1385.
21. Pansare, V. J.; Hejazi, S.; Faenza, W. J.; Prud'homme, R. K. *Chem. Mater.* **2012**, *24*, 812.

3.8 ^{1}H NMR, ^{13}C NMR, IR and HRMS spectra

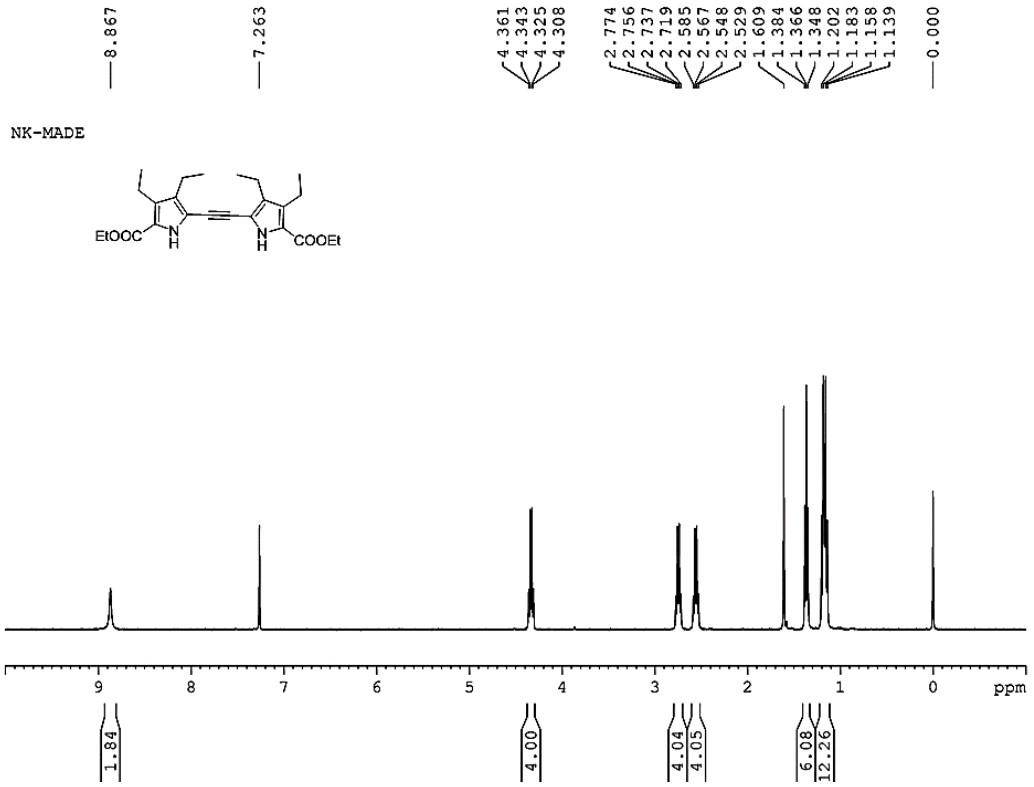

Figure 3.33 ^{1}H NMR spectrum of **3.34a** in $CDCl_3$.

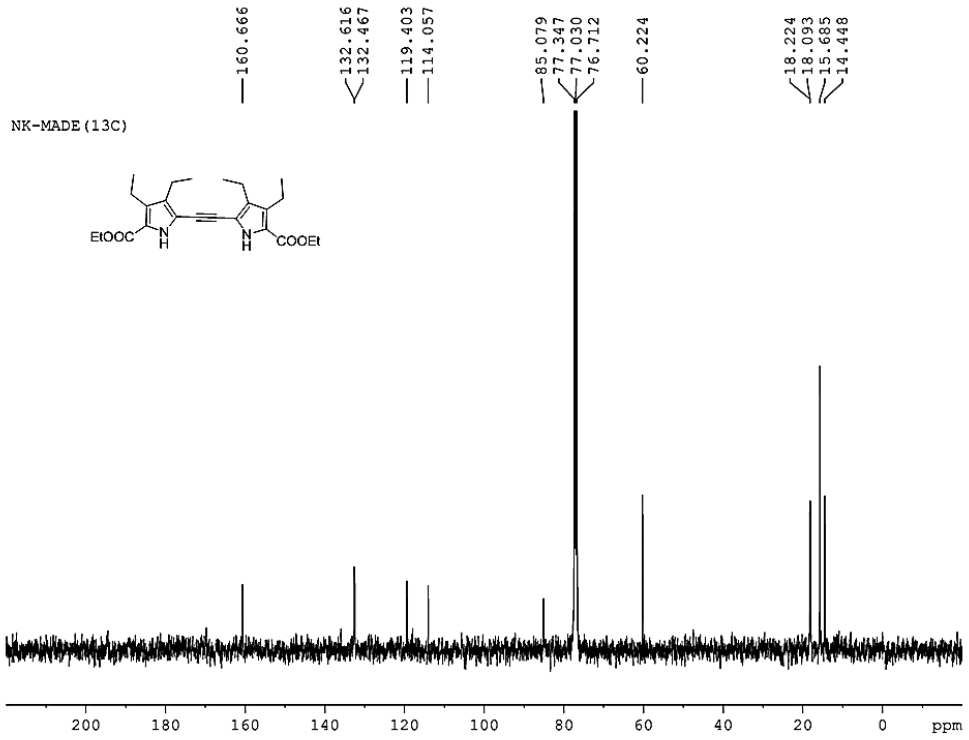

Figure 3.34 ^{13}C NMR spectrum of **3.34a** in $CDCl_3$.

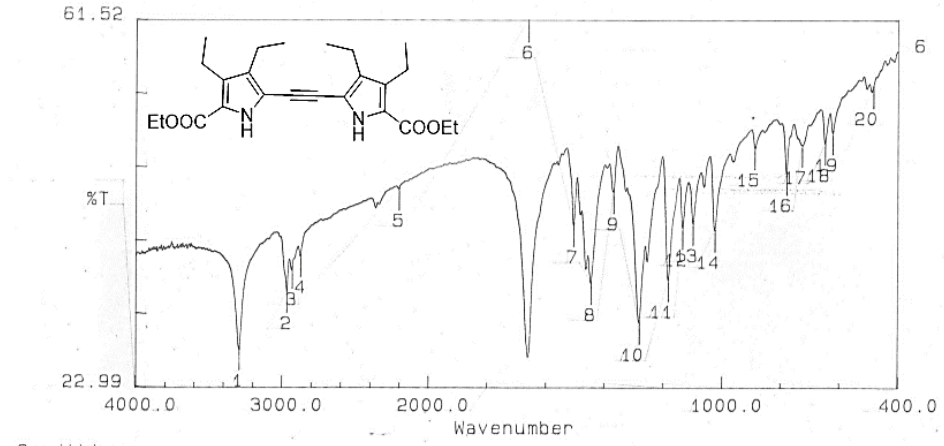

Condition
upper 61.52 lower 22.98 depth 2.00

Peak table

1:	3290.86 (27.1)	2:	2962.93 (33.1)	3:	2926.28 (35.6)	4:	2868.41 (36.9)
5:	2199.05 (43.9)	6:	1660.86 (26.2)	7:	1504.61 (40.1)	8:	1444.81 (34.0)
9:	1367.65 (43.5)	10:	1278.92 (29.8)	11:	1180.54 (34.3)	12:	1132.32 (39.8)
13:	1097.60 (40.3)	14:	1024.29 (39.6)	15:	887.34 (48.2)	16:	777.38 (45.5)
17:	725.30 (48.5)	18:	646.21 (48.7)	19:	621.13 (49.8)	20:	484.18 (54.6)

Figure 3.35 IR spectrum of **3.34a**.

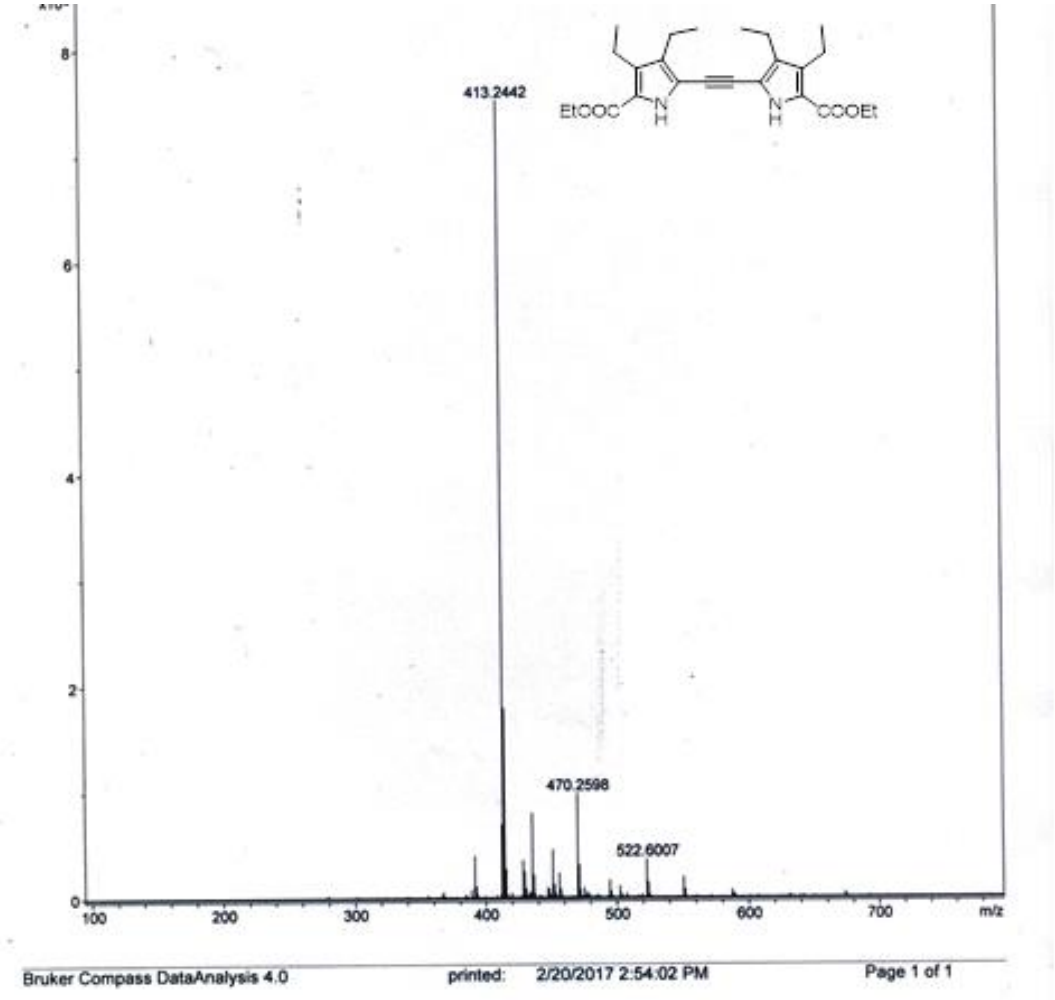

Figure 3.36 HRMS spectrum of **3.34a** for $[M+H]^+$ $C_{24}H_{33}N_2O_4$:413.2440, found 413.2442.

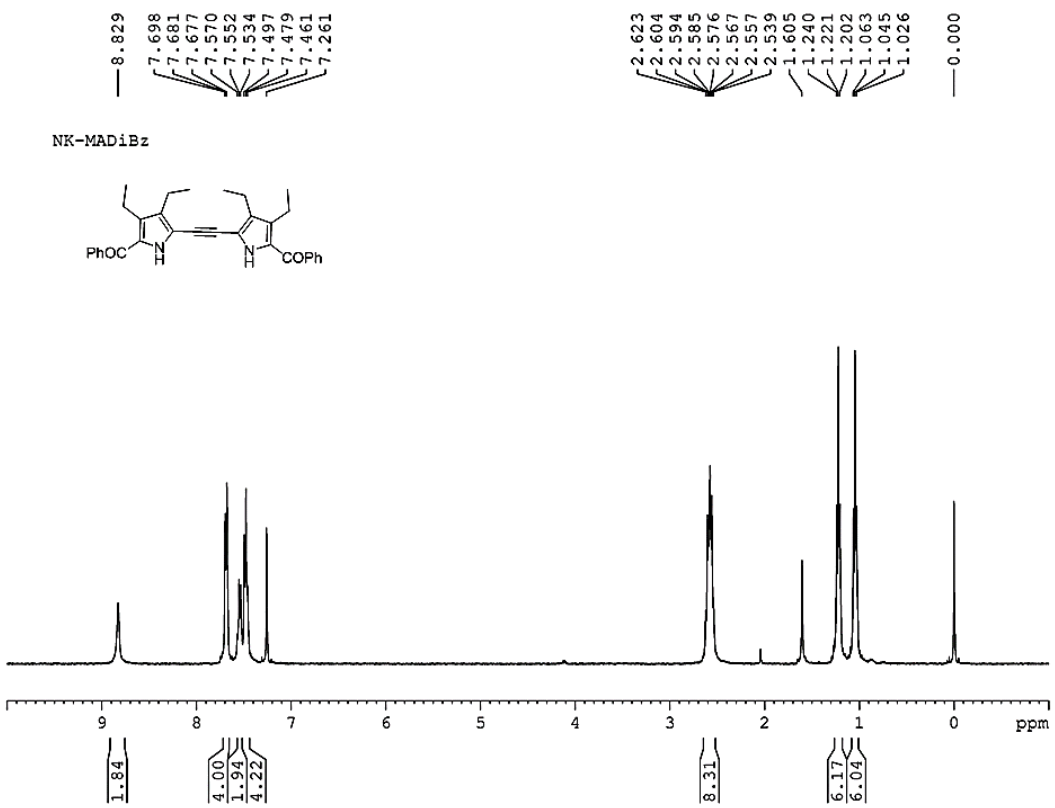

Figure 3.37 ^{1}H NMR spectrum of **3.34c** in $CDCl_3$.

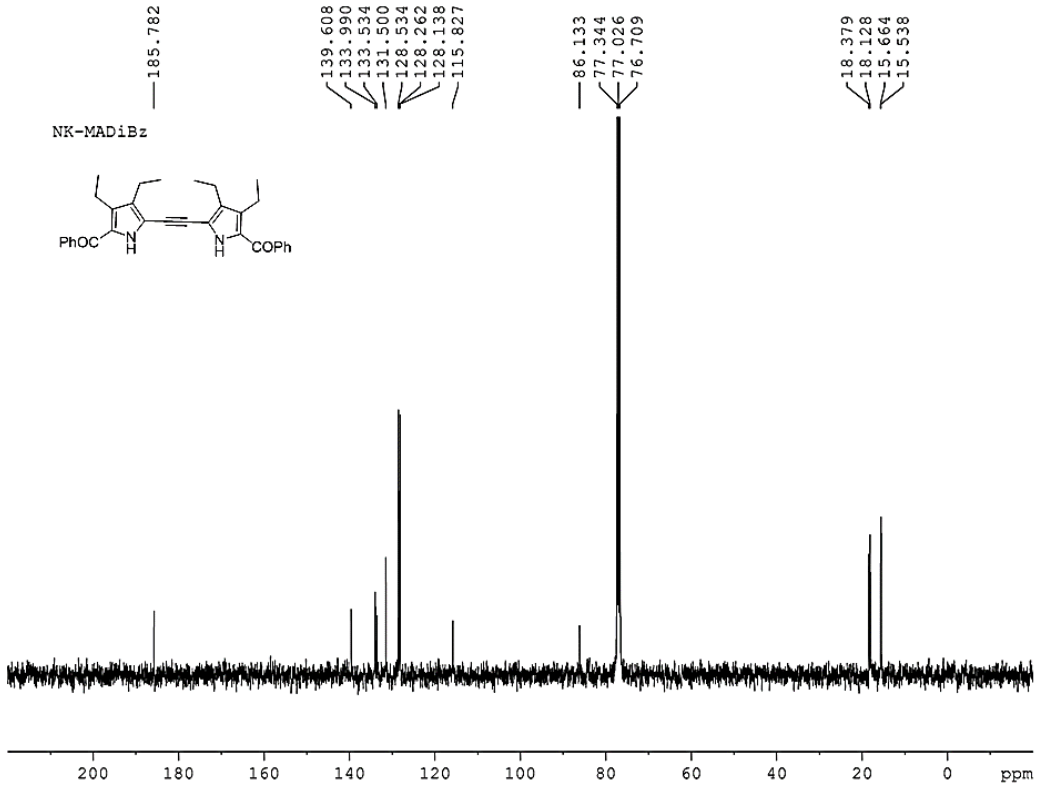

Figure 3.38 ^{13}C NMR spectrum of **3.34c** in $CDCl_3$.

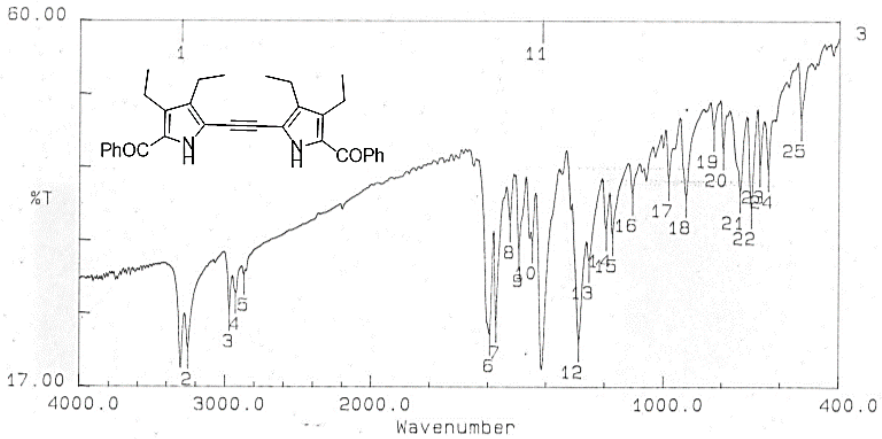

Condition
upper 60.00 lower 17.00 depth 2.00

Peak table

1:	3300.50 (19.2)	2:	3252.28 (21.6)	3:	2966.79 (26.1)	4:	2926.28 (28.1)
5:	2866.48 (30.3)	6:	1593.35 (23.3)	7:	1572.13 (24.8)	8:	1523.90 (36.6)
9:	1493.04 (33.3)	10:	1446.74 (34.2)	11:	1413.95 (19.1)	12:	1286.64 (22.6)
13:	1251.91 (31.9)	14:	1194.04 (35.7)	15:	1172.83 (35.0)	16:	1105.31 (39.8)
17:	981.86 (41.5)	18:	922.06 (39.6)	19:	827.54 (47.3)	20:	794.74 (45.1)
21:	736.87 (40.1)	22:	698.29 (38.3)	23:	669.36 (43.2)	24:	640.42 (42.6)
25:	528.54 (48.6)						

Figure 3.39 IR spectrum of **3.34c**.

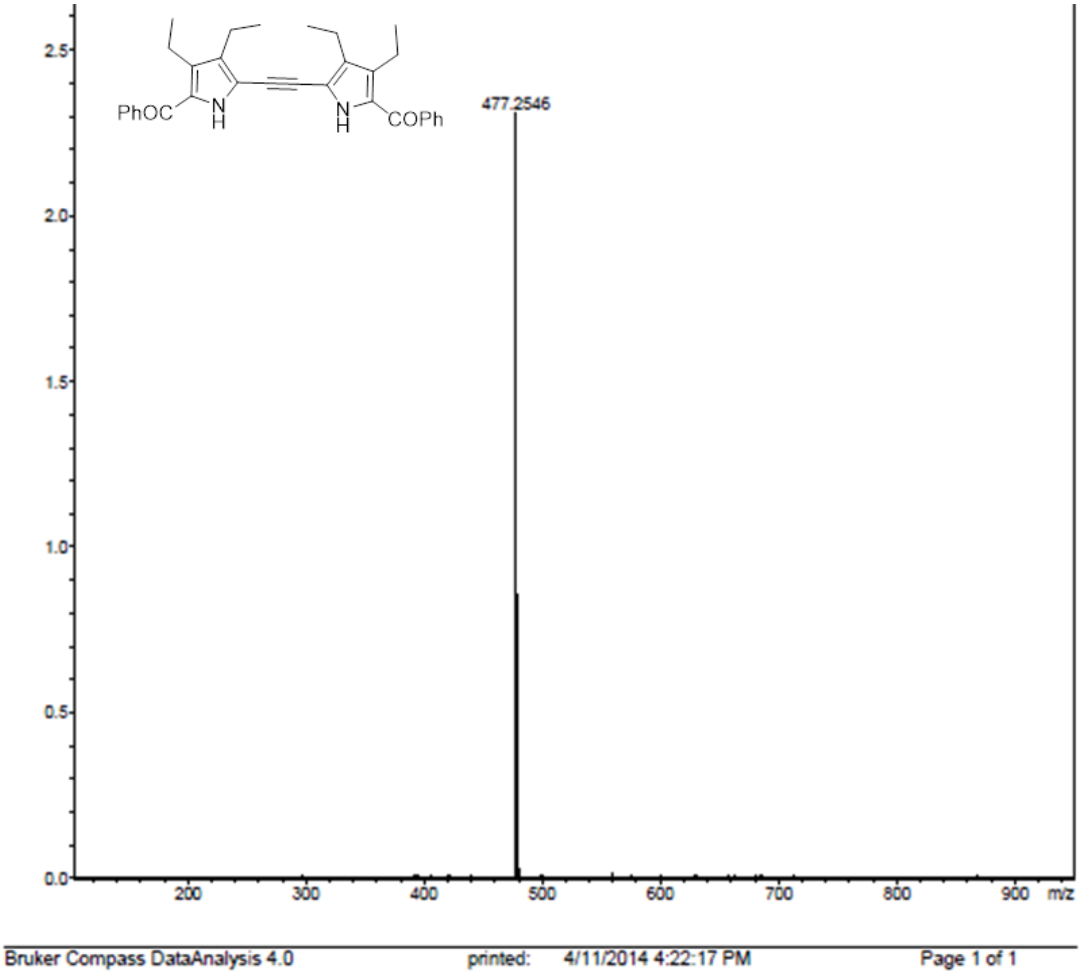

Figure 3.40 HRMS spectrum of **3.34c** $[M+H]^+$ $C_{32}H_{33}N_2O_2$:477.2542, found 477.2546.

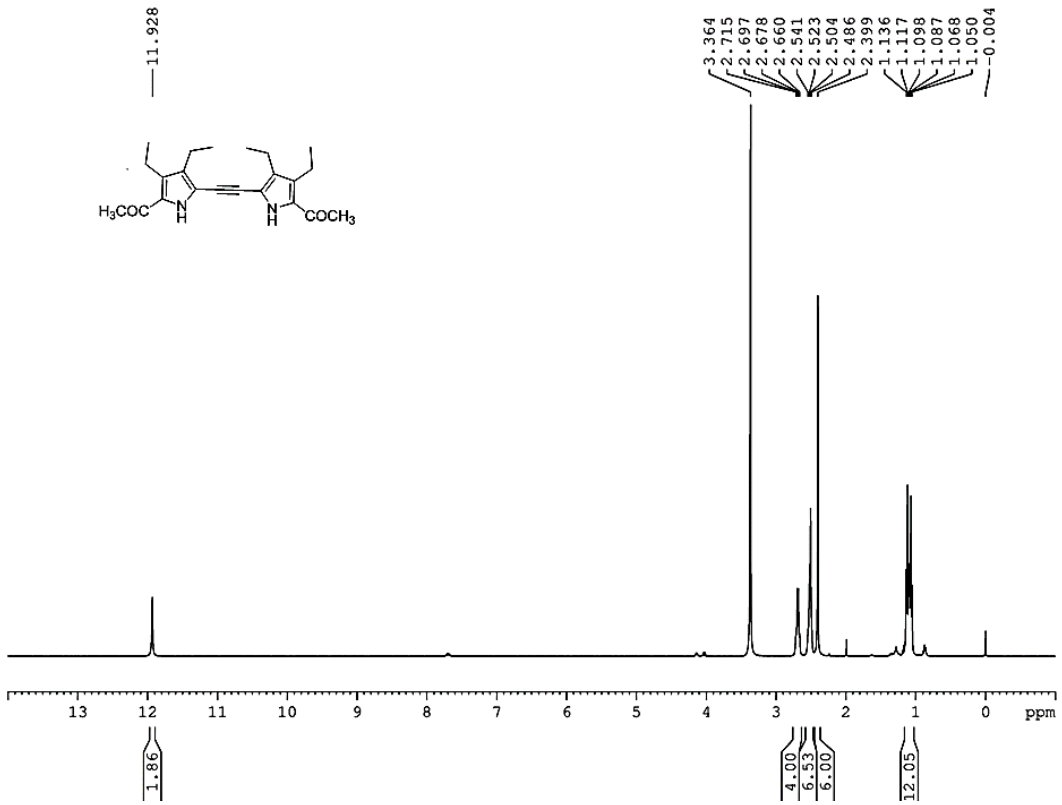

Figure 3.41 ^{1}H NMR spectrum of **3.34d** in DMSO-d_6.

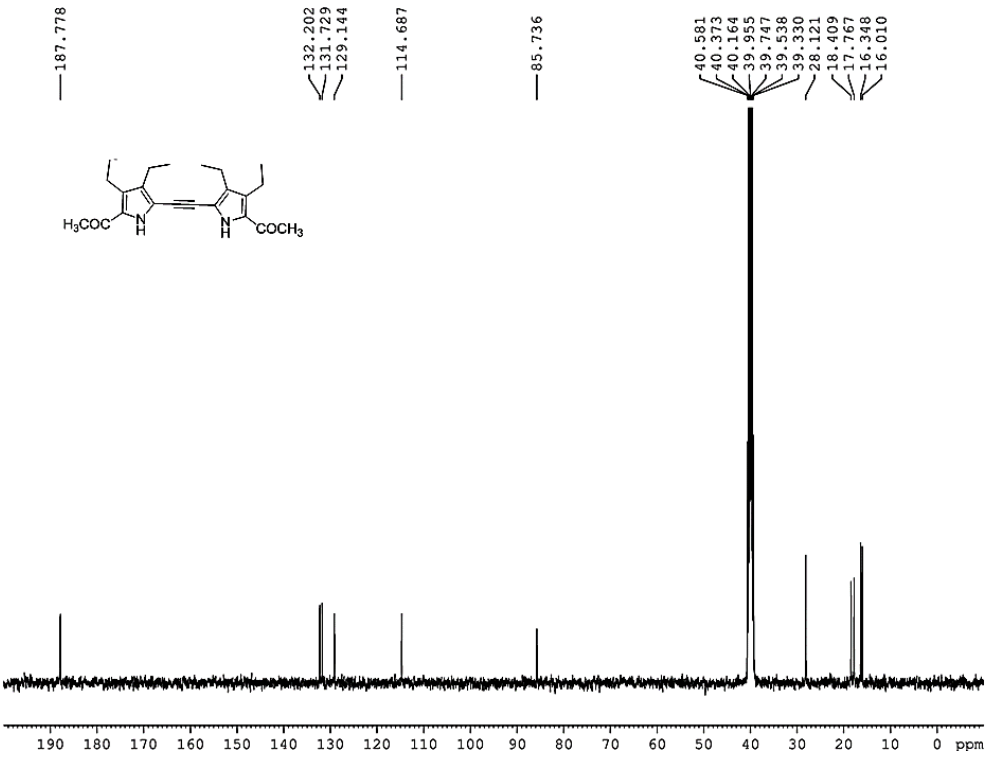

Figure 3.42 ^{13}C NMR spectrum of **3.34d** in DMSO-d_6.

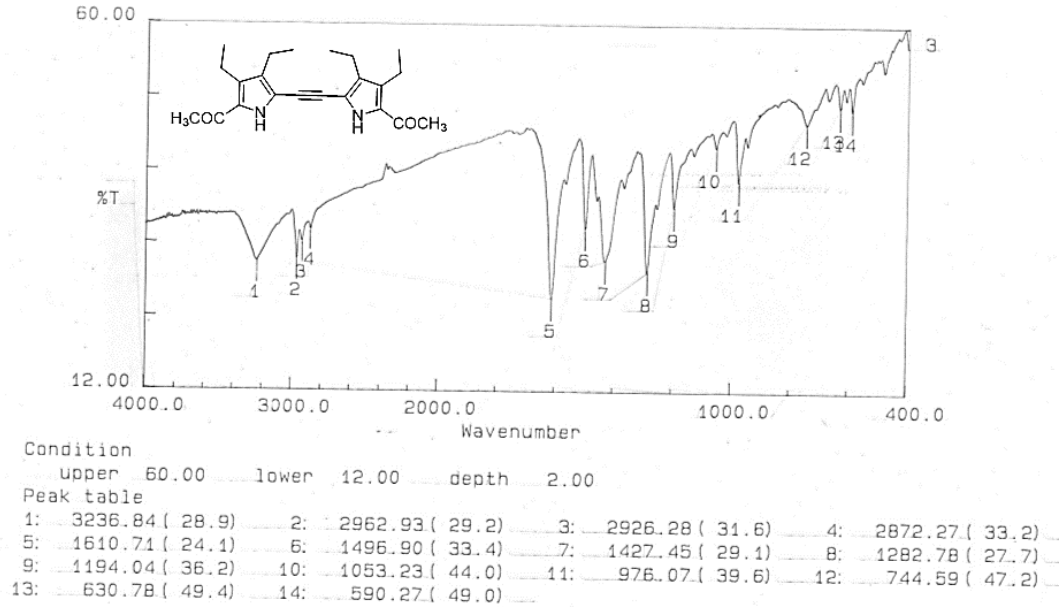

Figure 3.43 IR spectrum of **3.34d**.

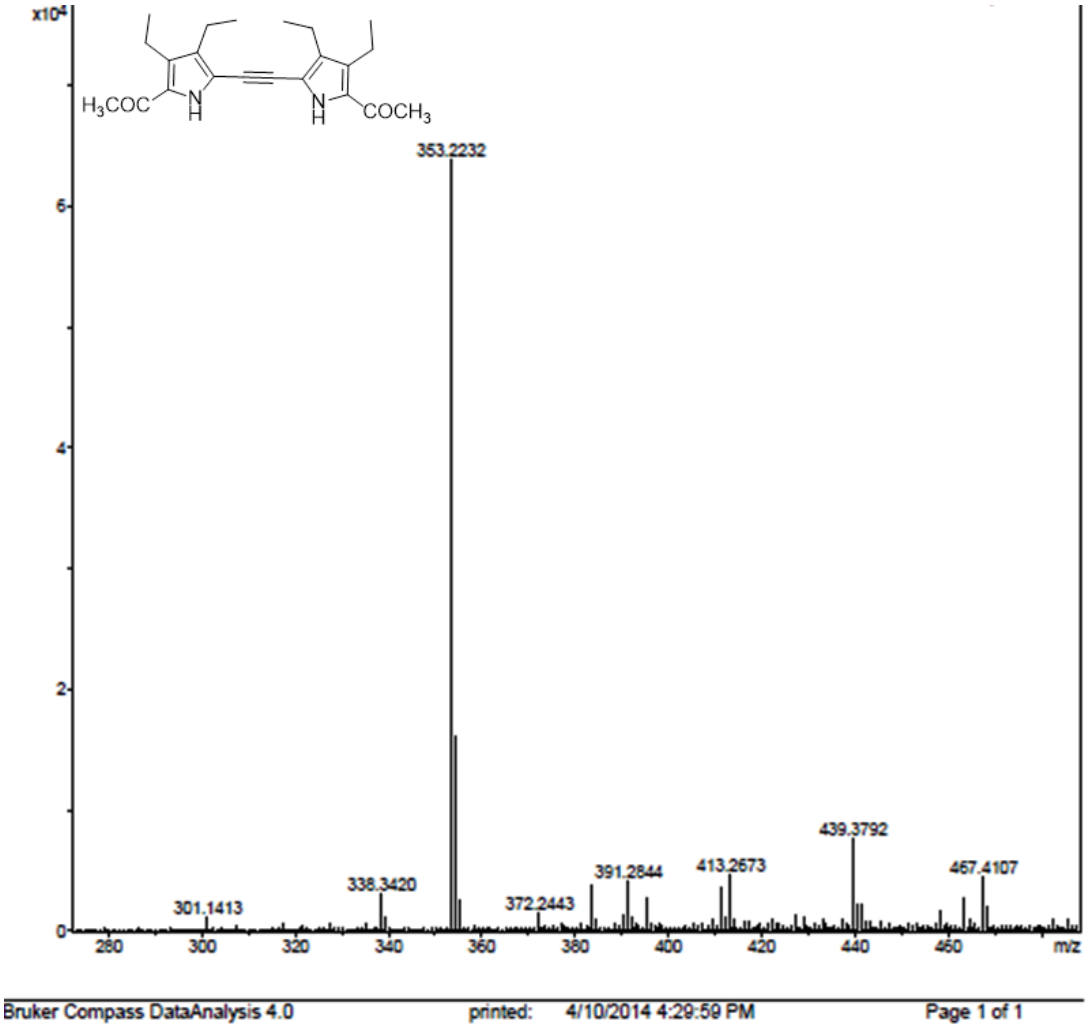

Figure 3.44 HRMS spectrum of **3.34d** $[M+H]^+$ $C_{22}H_{29}N_2O_2$:353.2229, found 353.2232.

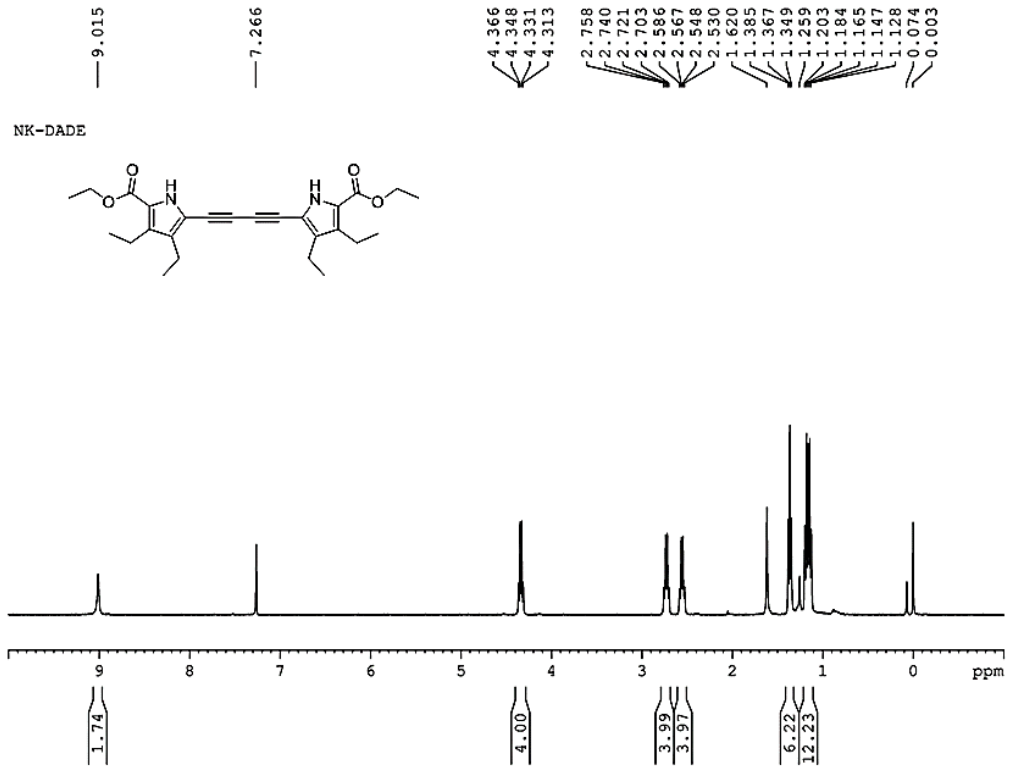

Figure 3.45 ^{1}H NMR spectrum of **3.35a** in $CDCl_3$.

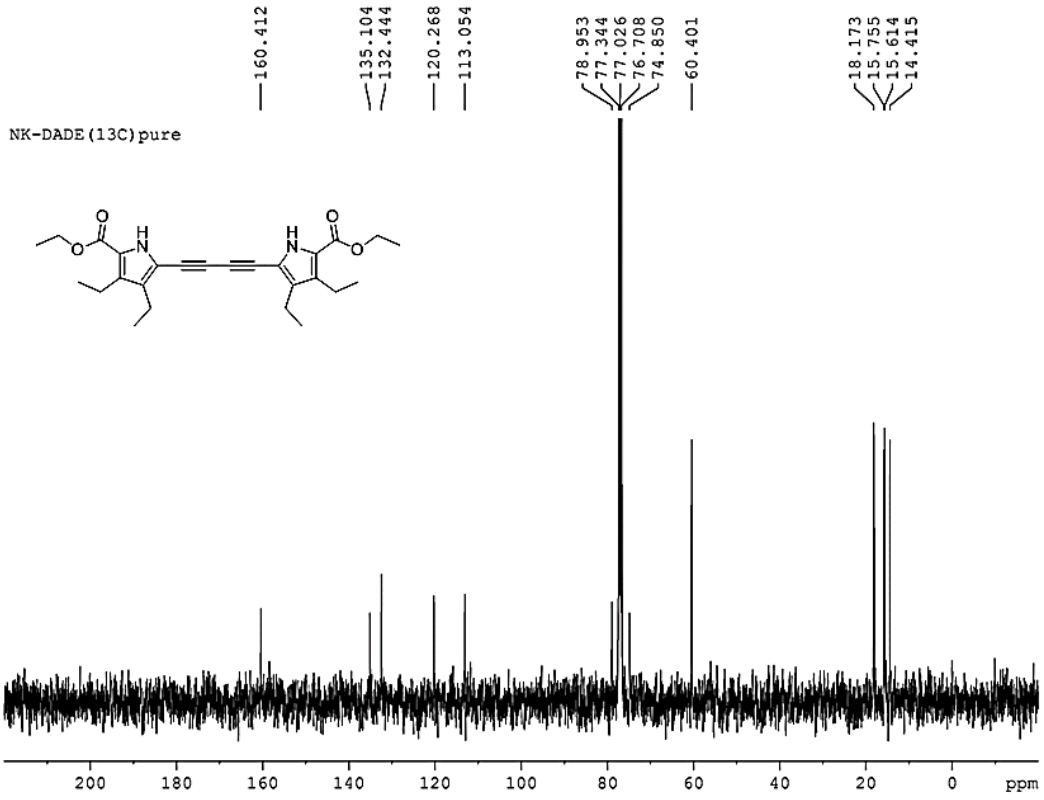

Figure 3.46 ^{13}C NMR spectrum of **3.35a** in $CDCl_3$.

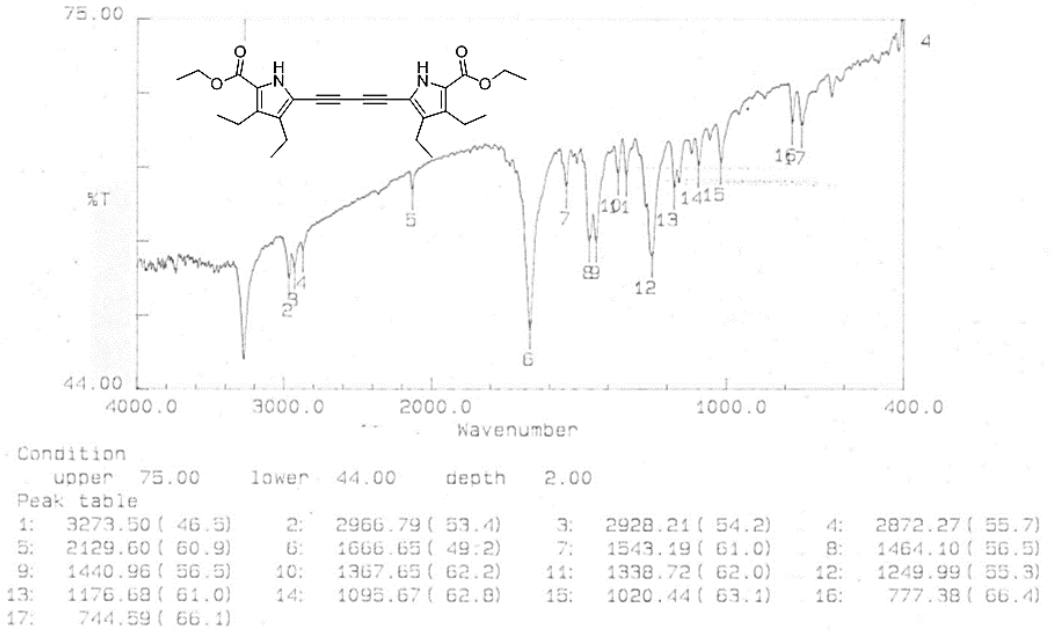

Figure 3.47 IR spectrum of **3.35a**.

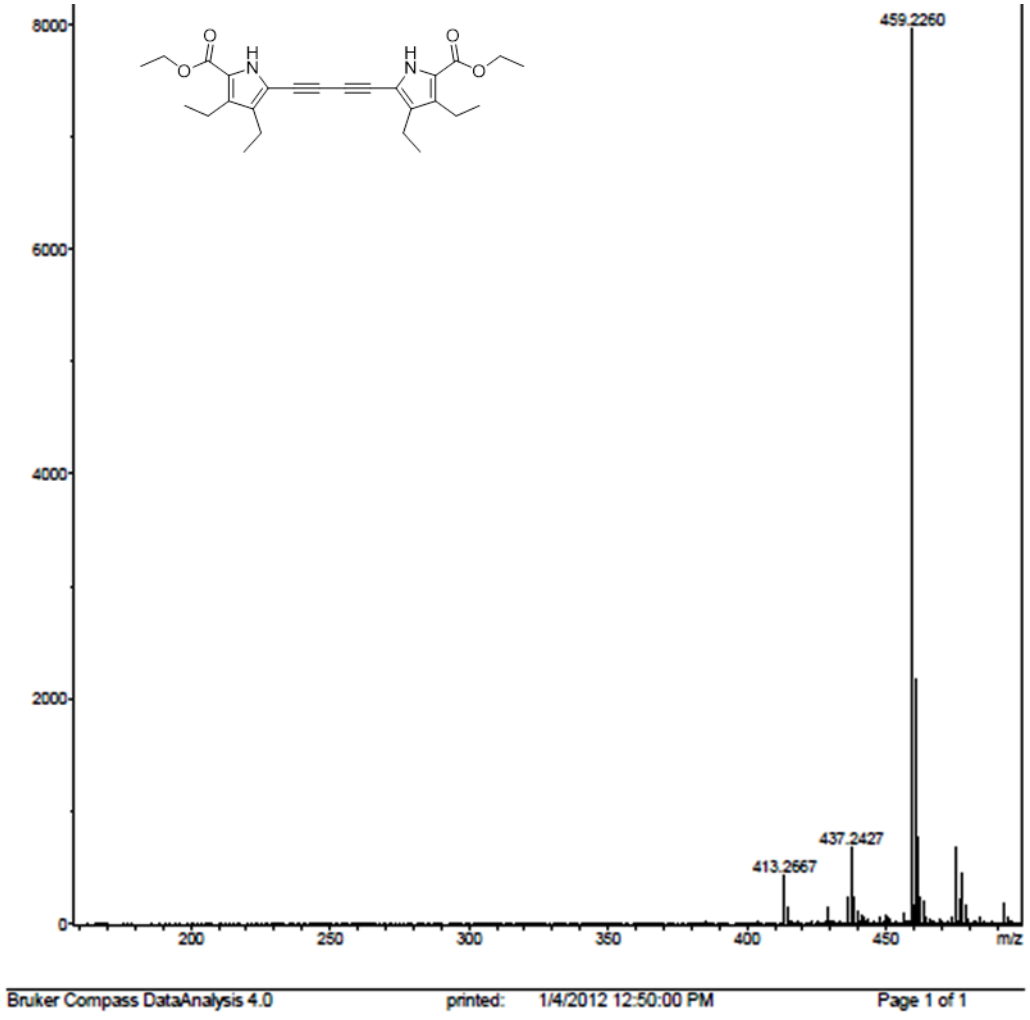

Figure 3.48 HRMS spectrum of **3.35a** $[M+Na]^+$ $C_{26}H_{32}NaN_2O_4$:459.2260, found 459.2260.

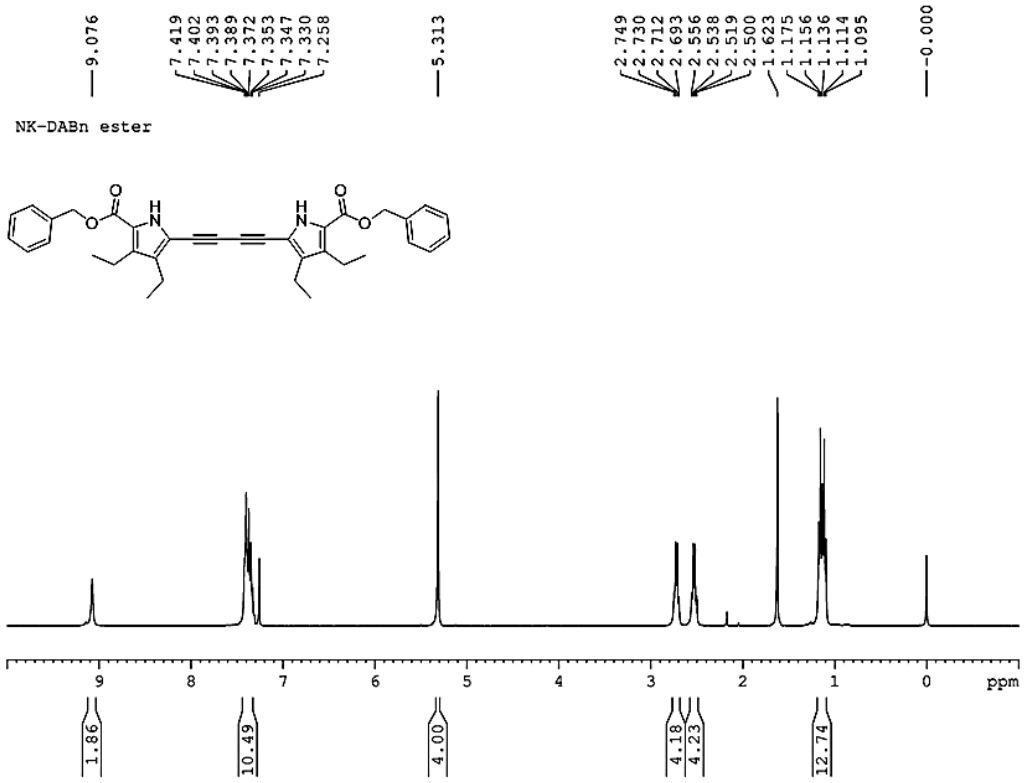

Figure 3.49 ^{1}H NMR spectrum of **3.35b** in $CDCl_3$.

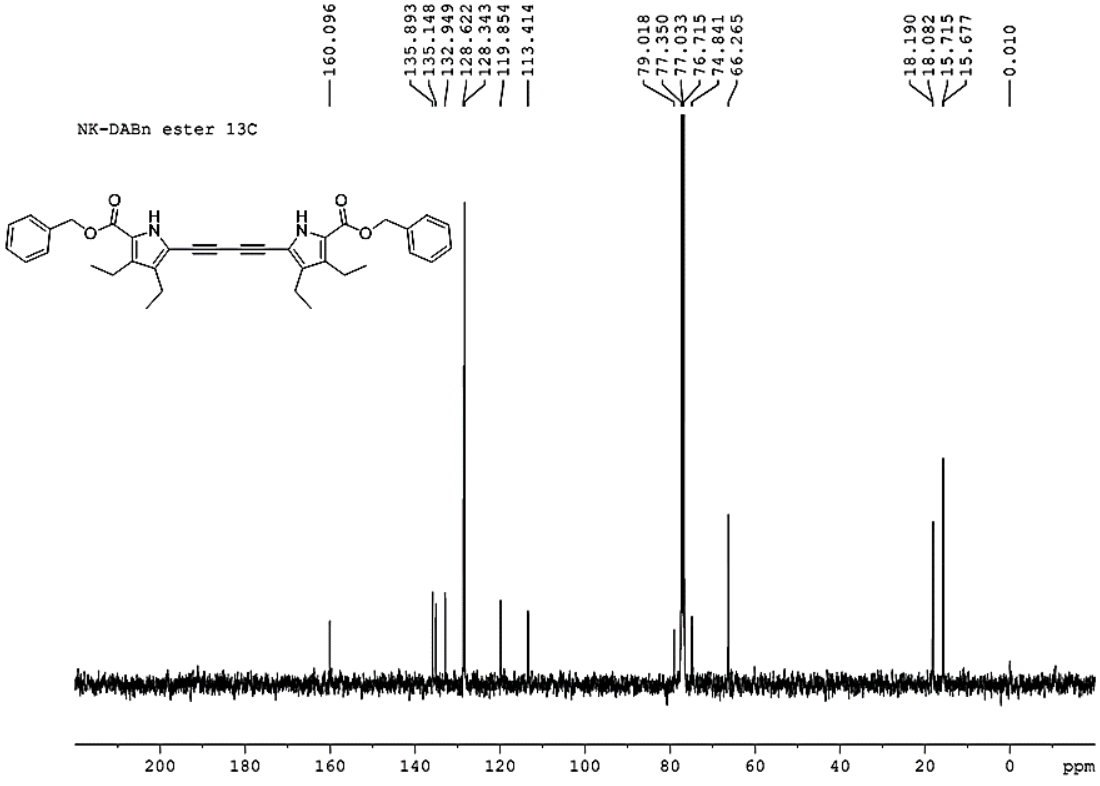

Figure 3.50 ^{13}C NMR spectrum of **3.35b** in $CDCl_3$.

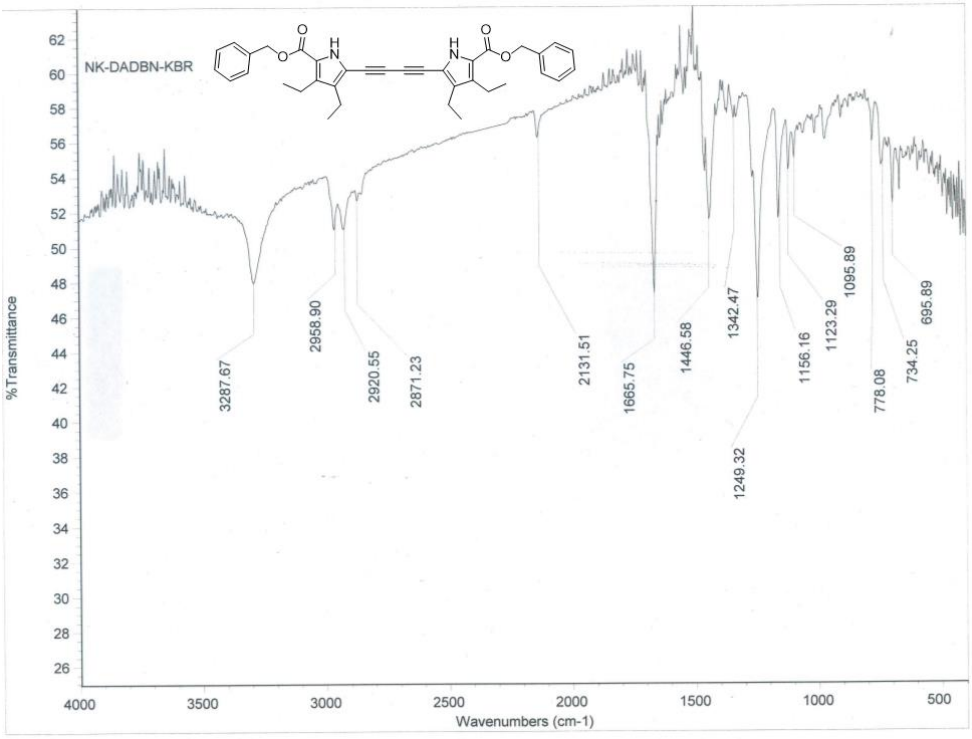

Figure 3.51 IR spectrum of **3.35b**.

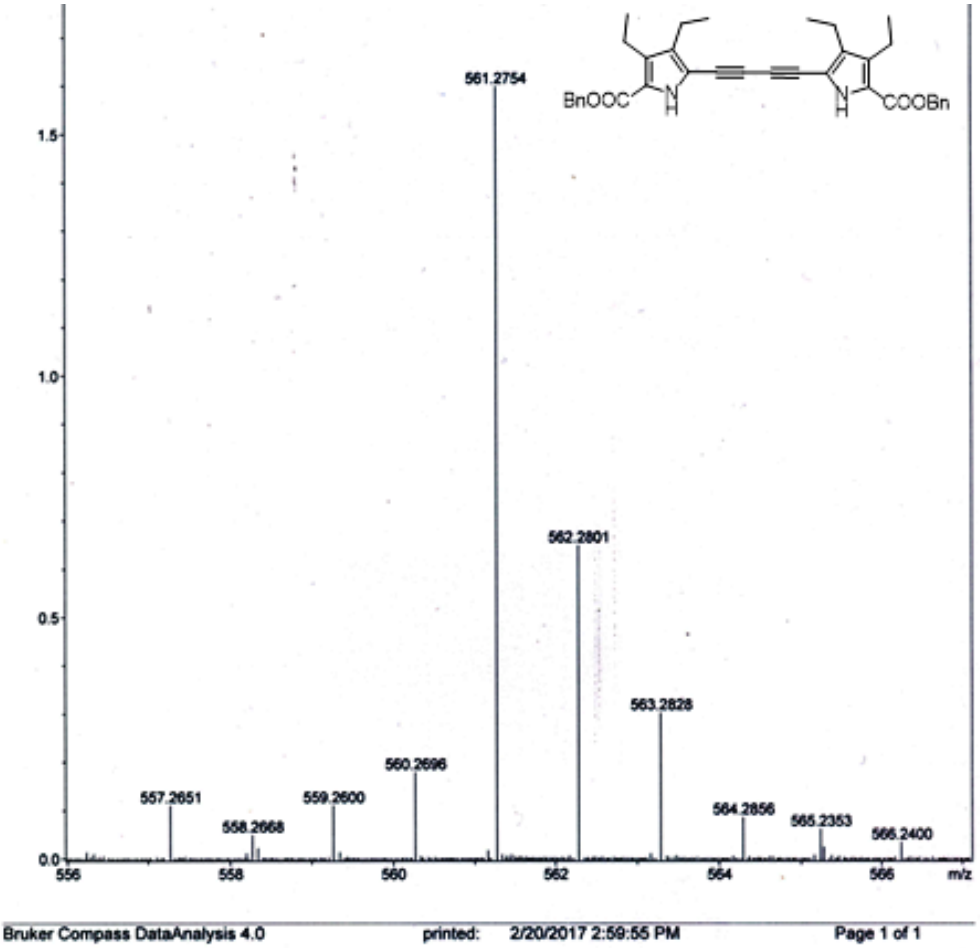

Figure 3.52 HRMS spectrum of **3.35b** $[M+H]^+$ $C_{36}H_{37}N_2O_4$:561.2753, found 561.2754.

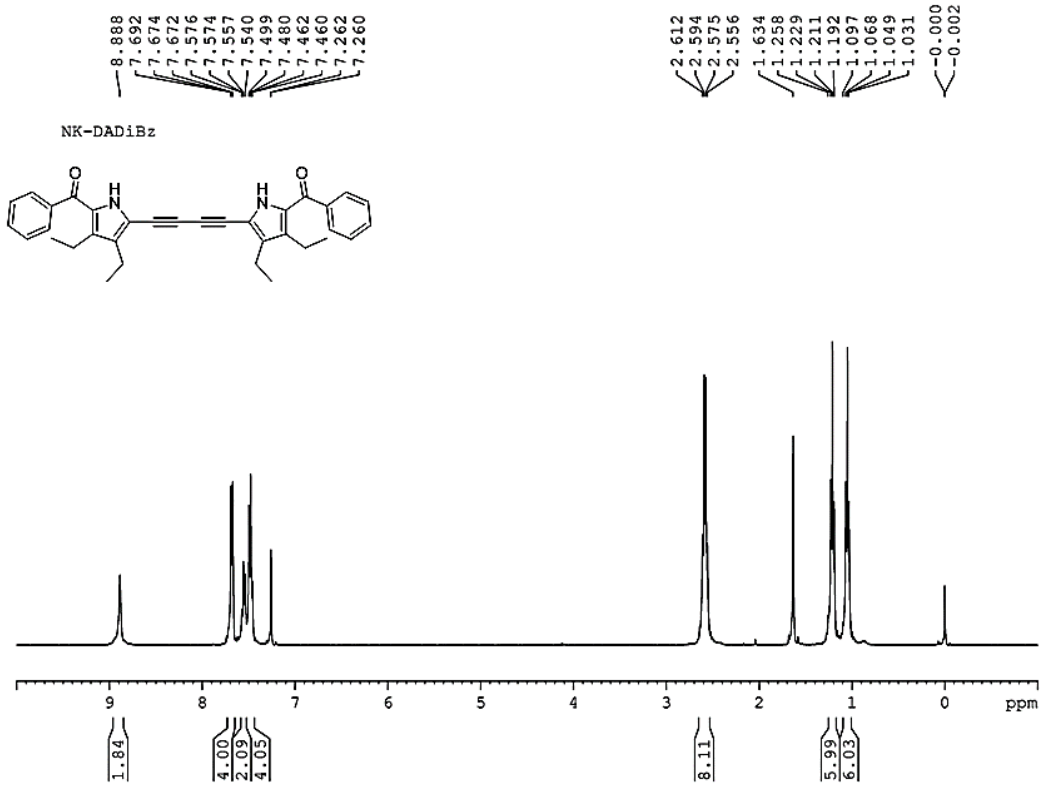

Figure 3.53 ^{1}H NMR spectrum of **3.35c** in $CDCl_3$.

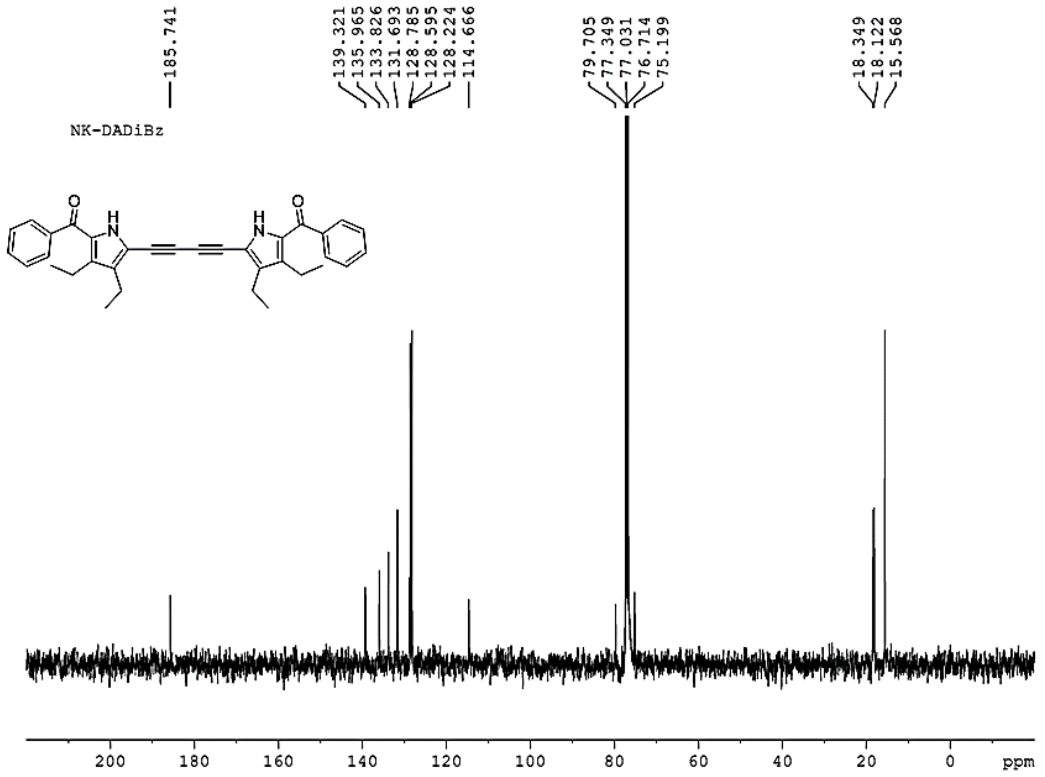

Figure 3.54 ^{13}C NMR spectrum of **3.35c** in $CDCl_3$.

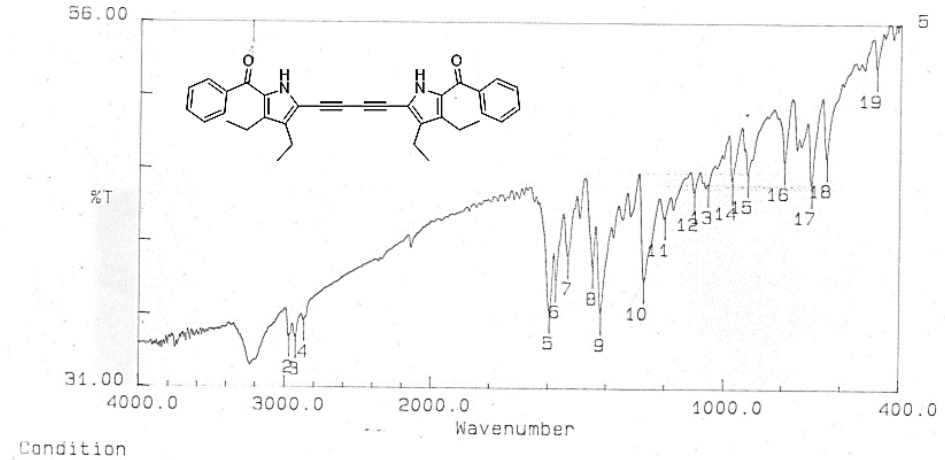

Condition
upper 56.00 lower 31.00 depth 2.00

Peak table

1:	3232.99 (32.5)	2:	2966.79 (34.6)	3:	2924.35 (34.5)	4:	2866.48 (35.7)
5:	1595.27 (36.3)	6:	1574.06 (38.5)	7:	1531.62 (40.0)	8:	1446.74 (39.4)
9:	1417.81 (36.2)	10:	1271.20 (38.4)	11:	1199.83 (42.7)	12:	1101.45 (44.5)
13:	1055.16 (45.0)	14:	972.21 (45.3)	15:	918.20 (45.7)	16:	792.81 (46.6)
17:	700.22 (45.0)	18:	648.14 (46.8)	19:	480.32 (53.0)		

Figure 3.55 IR spectrum of **3.35c**.

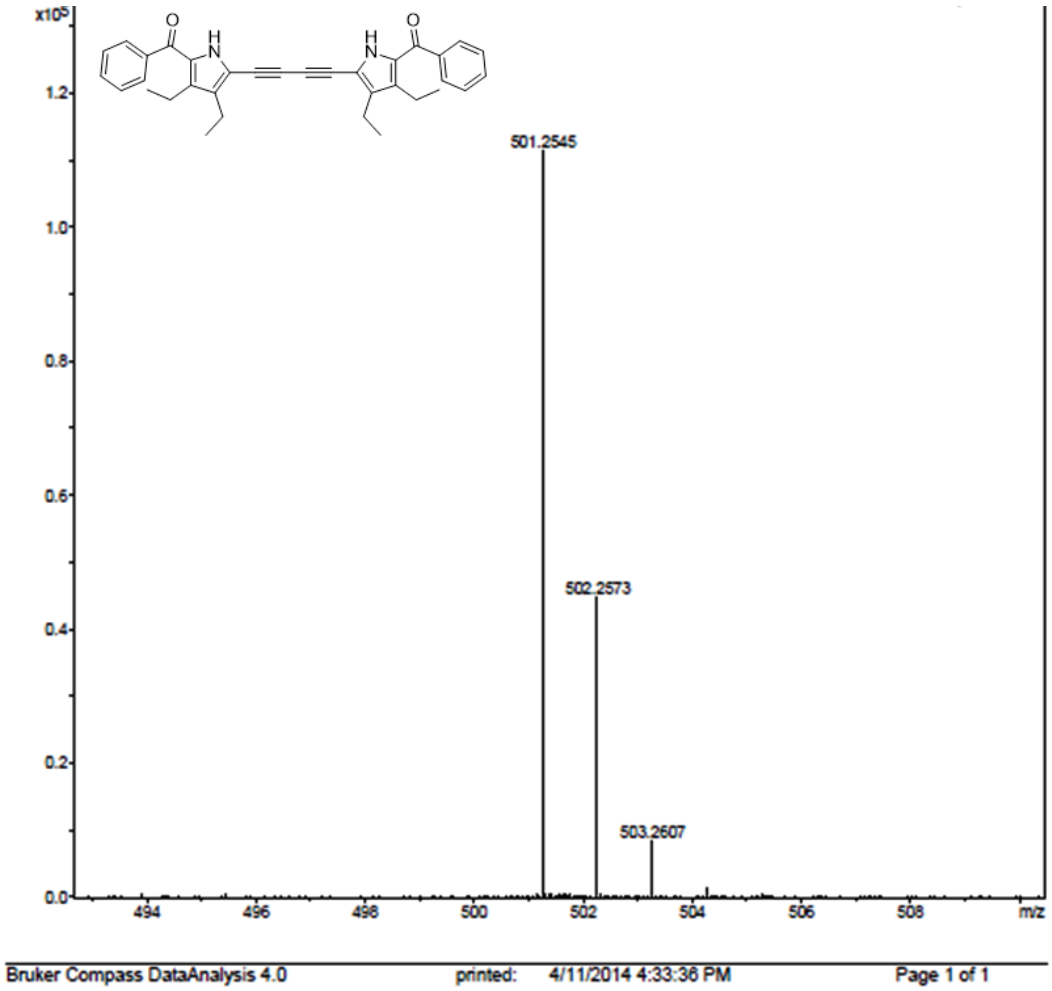

Figure 3.56 HRMS spectrum of **3.35c** $[M+H]^+$ $C_{34}H_{33}N_2O_2$:501.2542, found 501.2545.

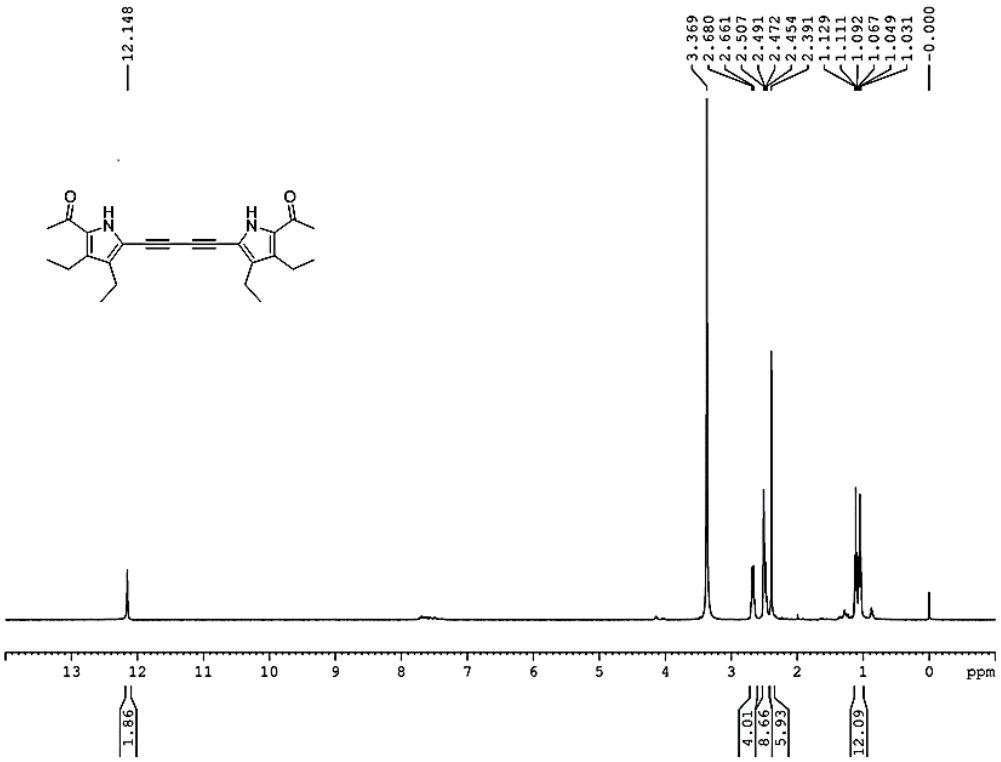

Figure 3.57 ^{1}H NMR spectrum of **3.35d** in DMSO-*d*6.

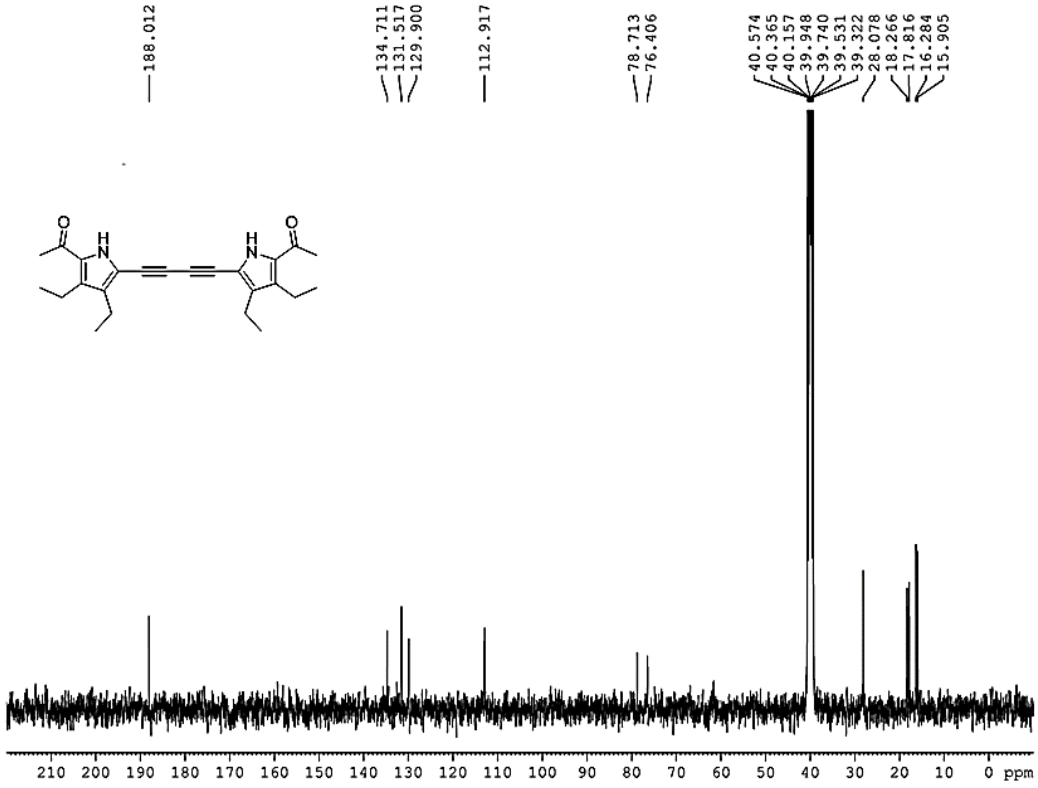

Figure 3.58 ^{13}C NMR spectrum of **3.35d** in DMSO-*d*6.

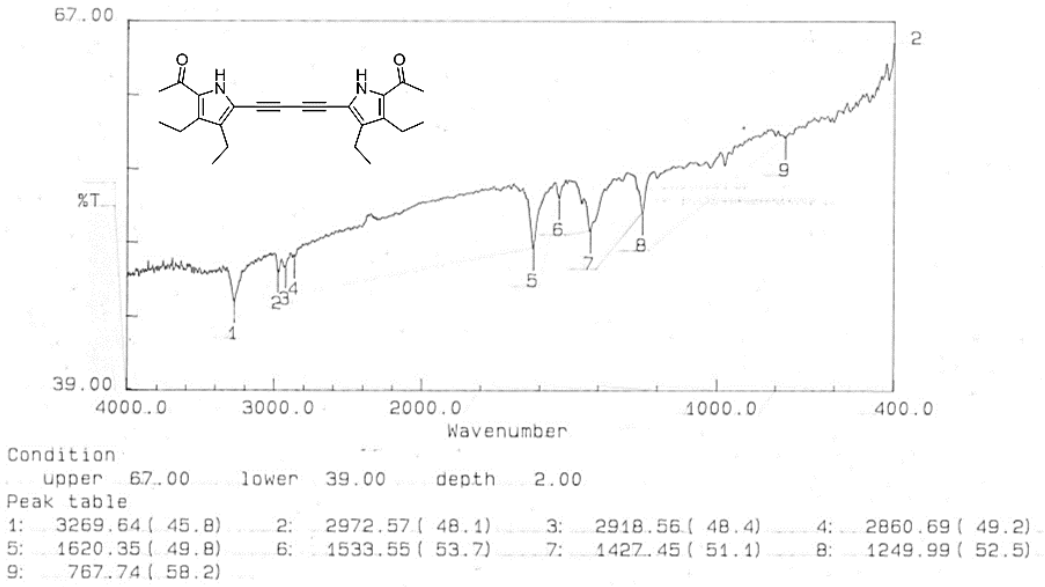

Figure 3.59 IR spectrum of **3.35d.**

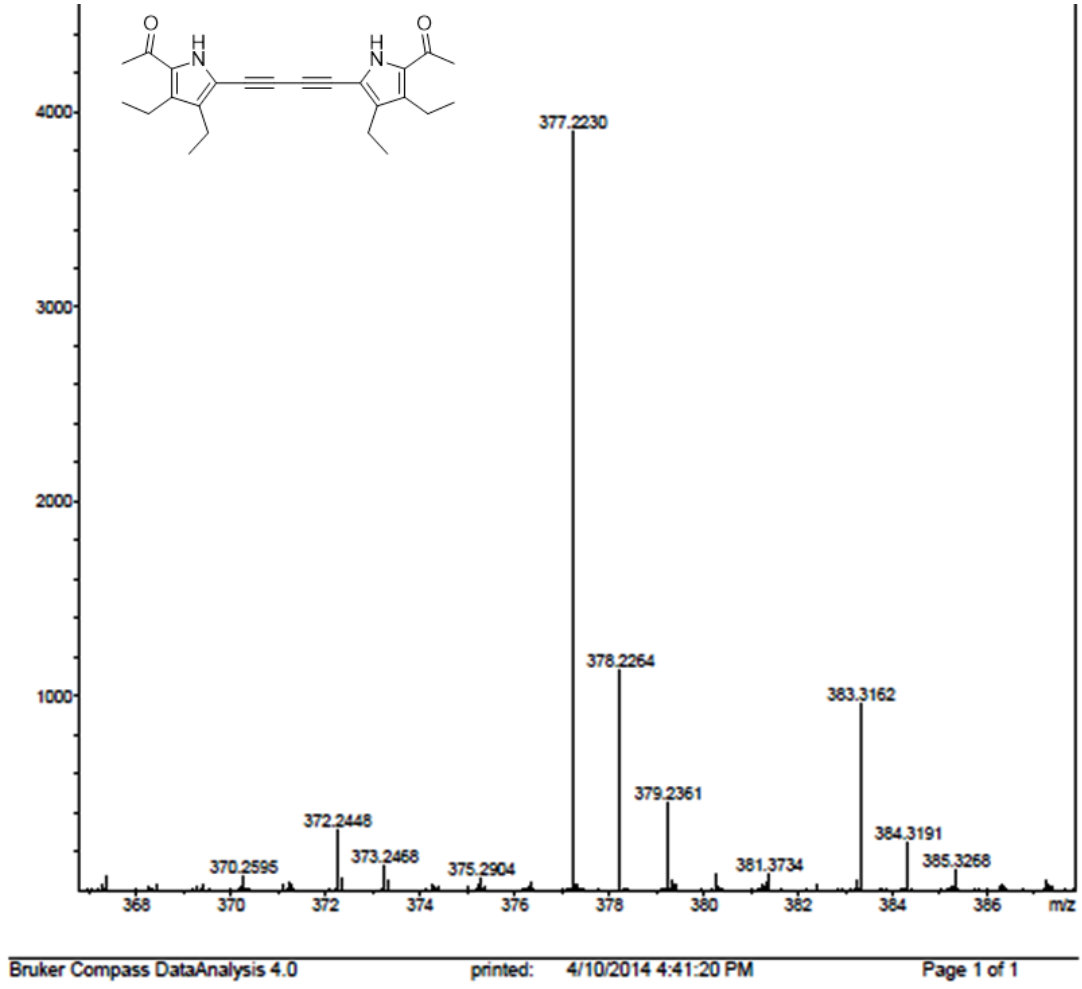

Figure 3.60 HRMS spectrum of **3.35d** $[M+H]^+$ $C_{24}H_{29}N_2O_2$:377.2229, found 377.2230.

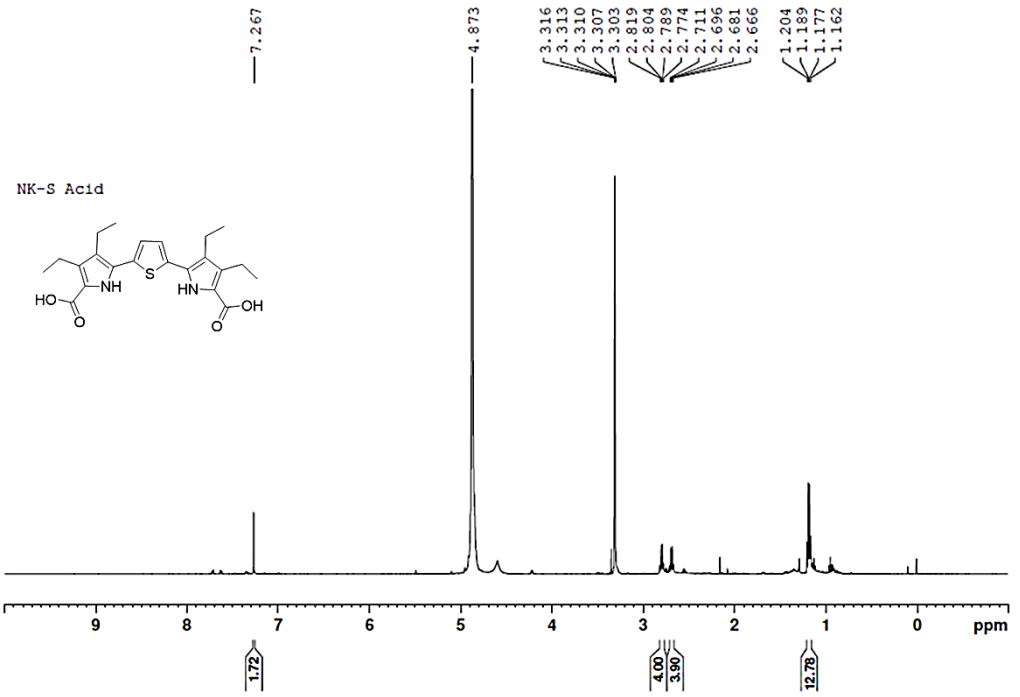

Figure 3.61 ^{1}H NMR spectrum of **3.36** in Methanol-d_4.

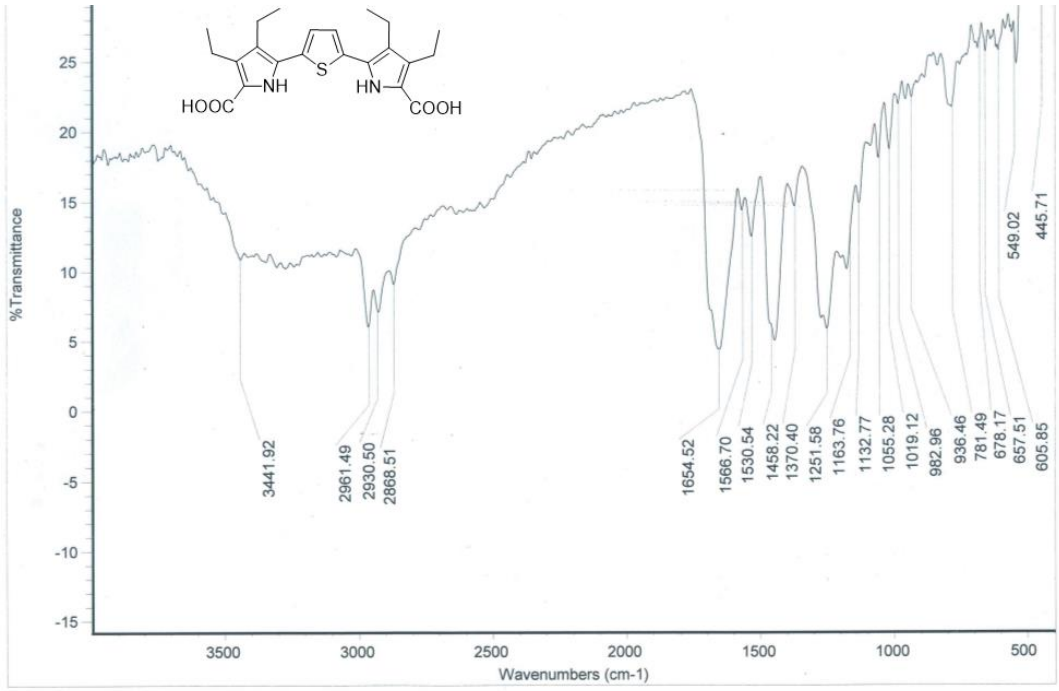

Figure 3.62 IR spectrum of **3.36**.

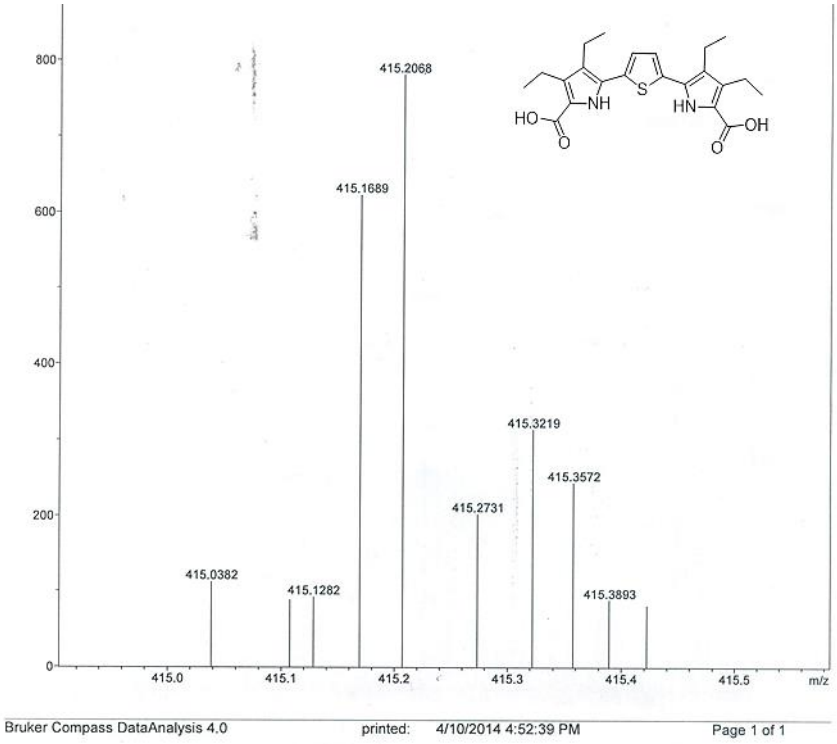

Figure 3.63 HRMS spectrum of **3.36** $(M+H)^+$: Calculated for $C_{22}H_{27}N_2O_4S$: 415.1692; found: 415.1689.

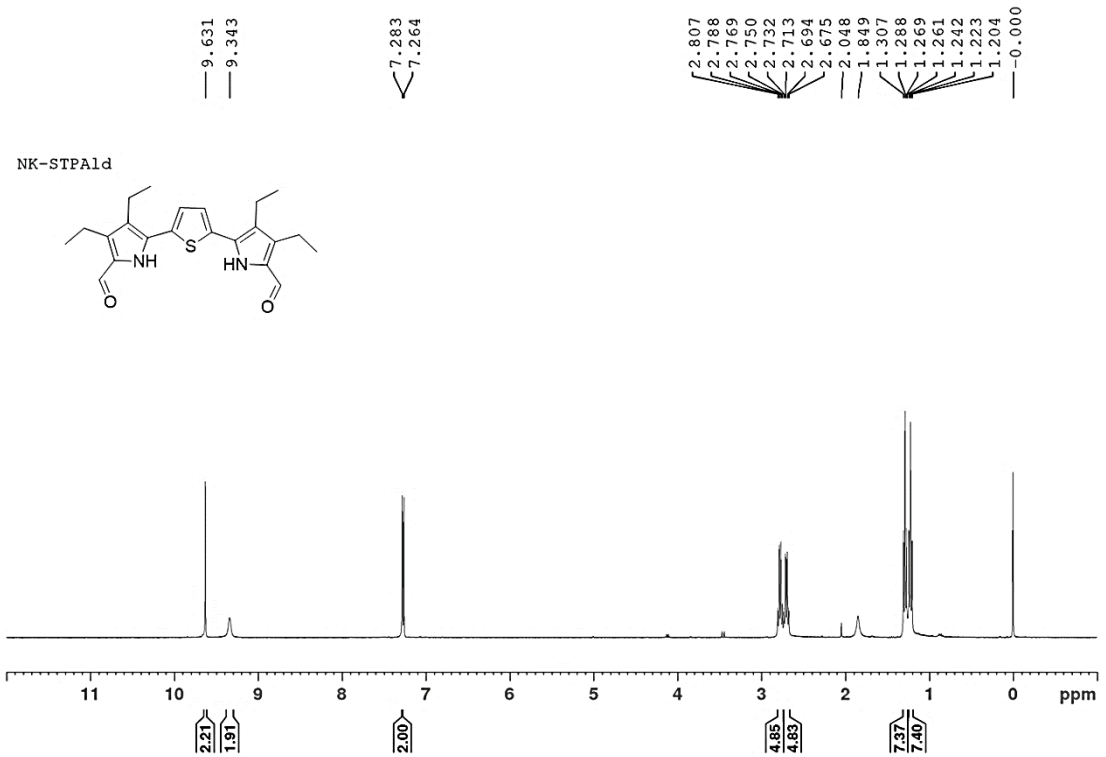

Figure 3.64 ^{1}H NMR spectrum of **3.37** in $CDCl_3$.

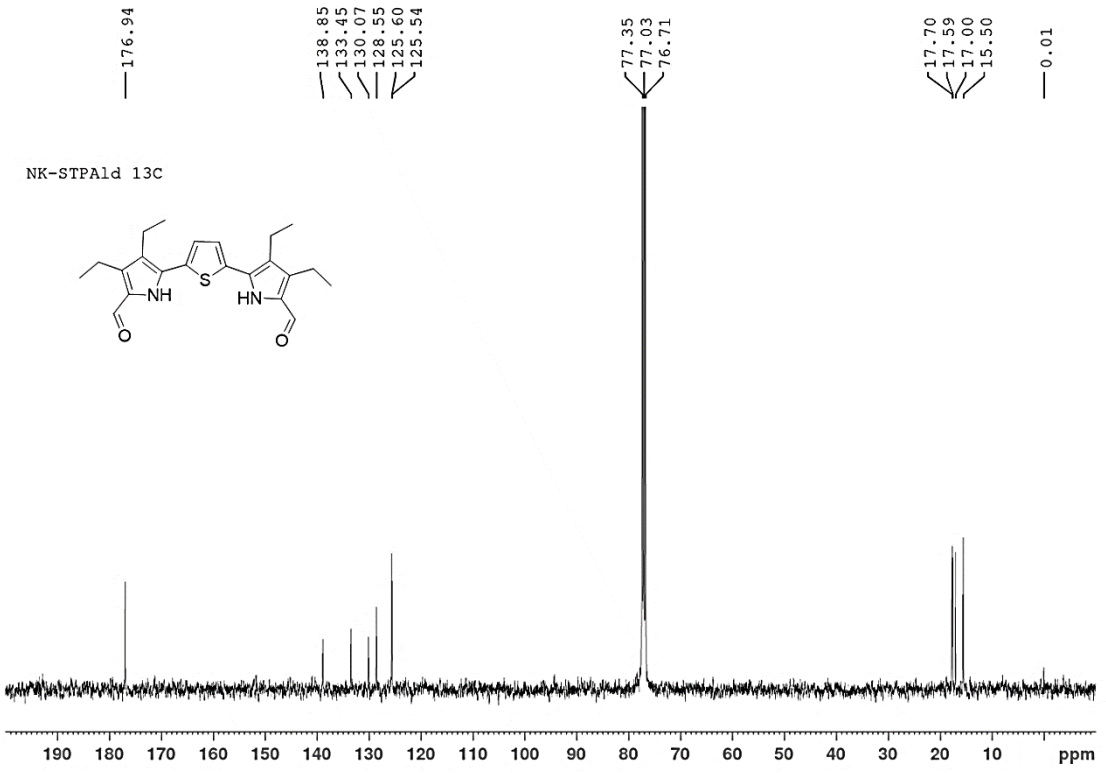

Figure 3.65 ^{13}C NMR spectrum of **3.37** in $CDCl_3$.

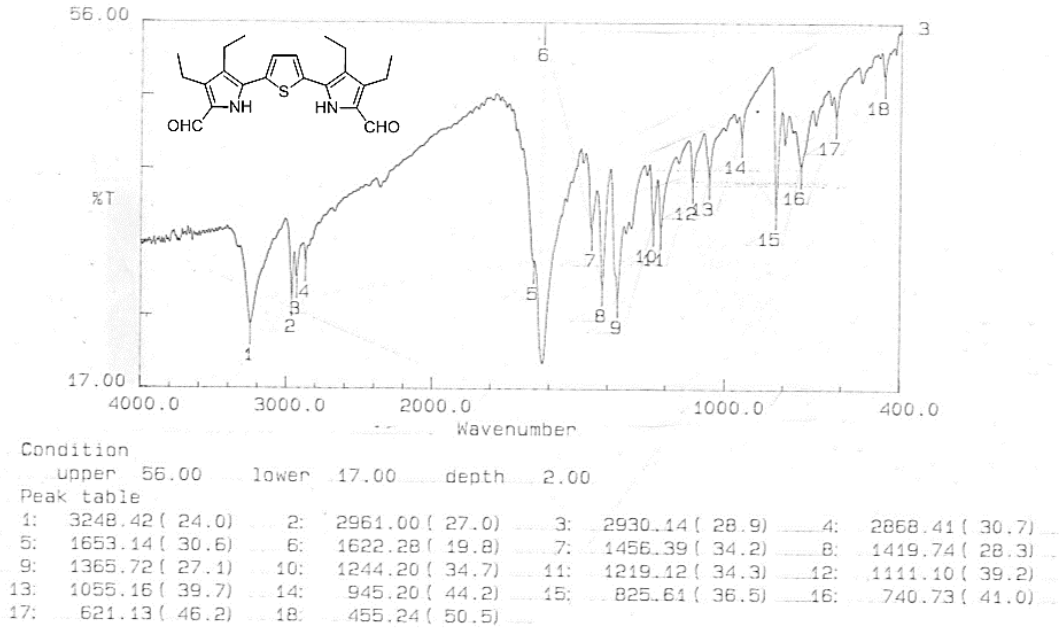

Figure 3.66 IR spectrum of **3.37**.

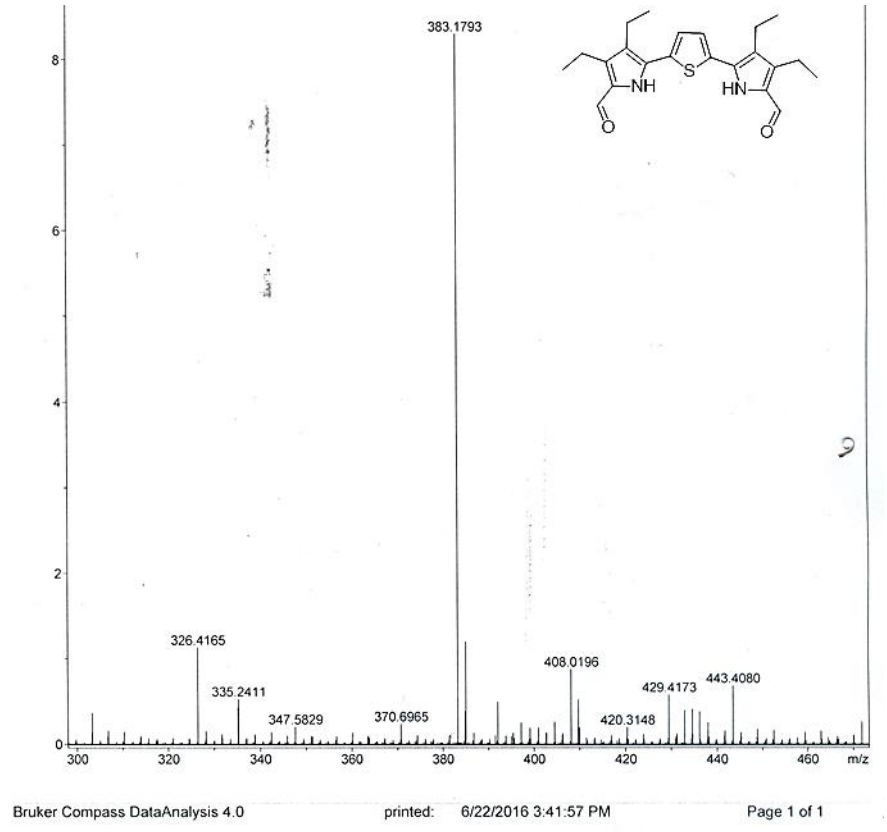

Figure 3.67 HRMS spectrum of **3.37** $(M+H)^+$; Calculated for $C_{22}H_{27}N_2O_2S$: 383.1793; found: 383.1793.

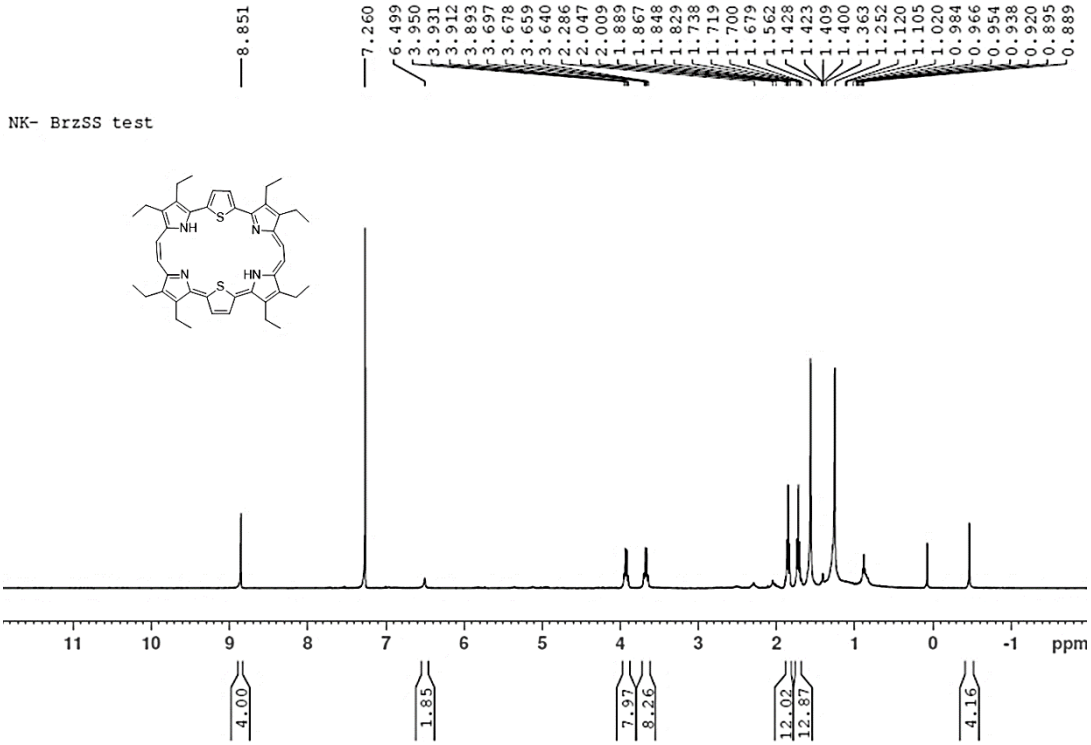

Figure 3.68 ^{1}H NMR spectrum of **3.38** in $CDCl_3$.

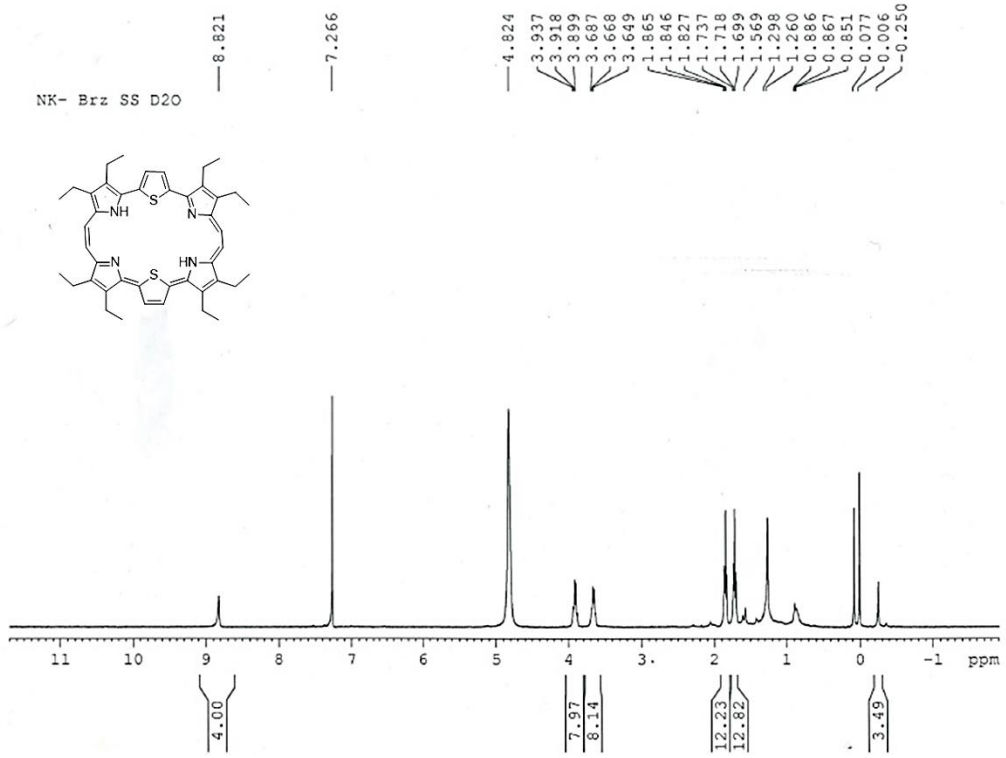

Figure 3.69 ^{1}H NMR spectrum of **3.38** in $CDCl_3$ + D_2O.

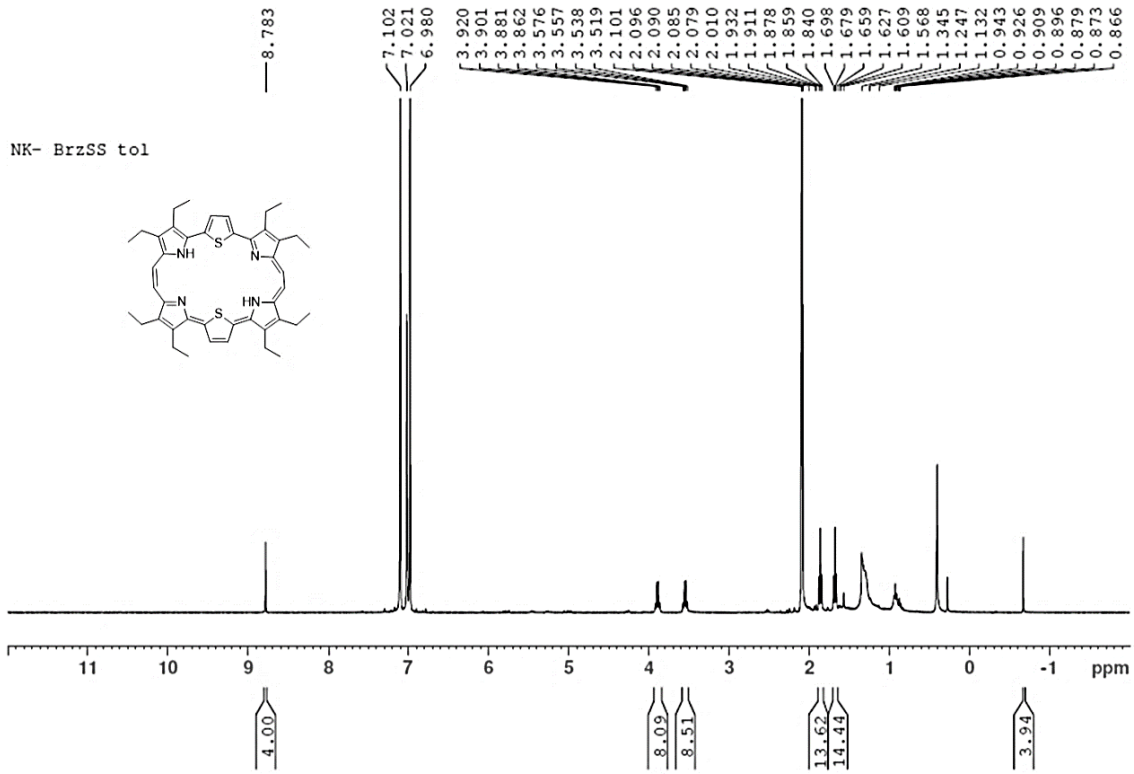

Figure 3.70 ^{1}H NMR spectrum of **3.38** at rt in toluene-d_8.

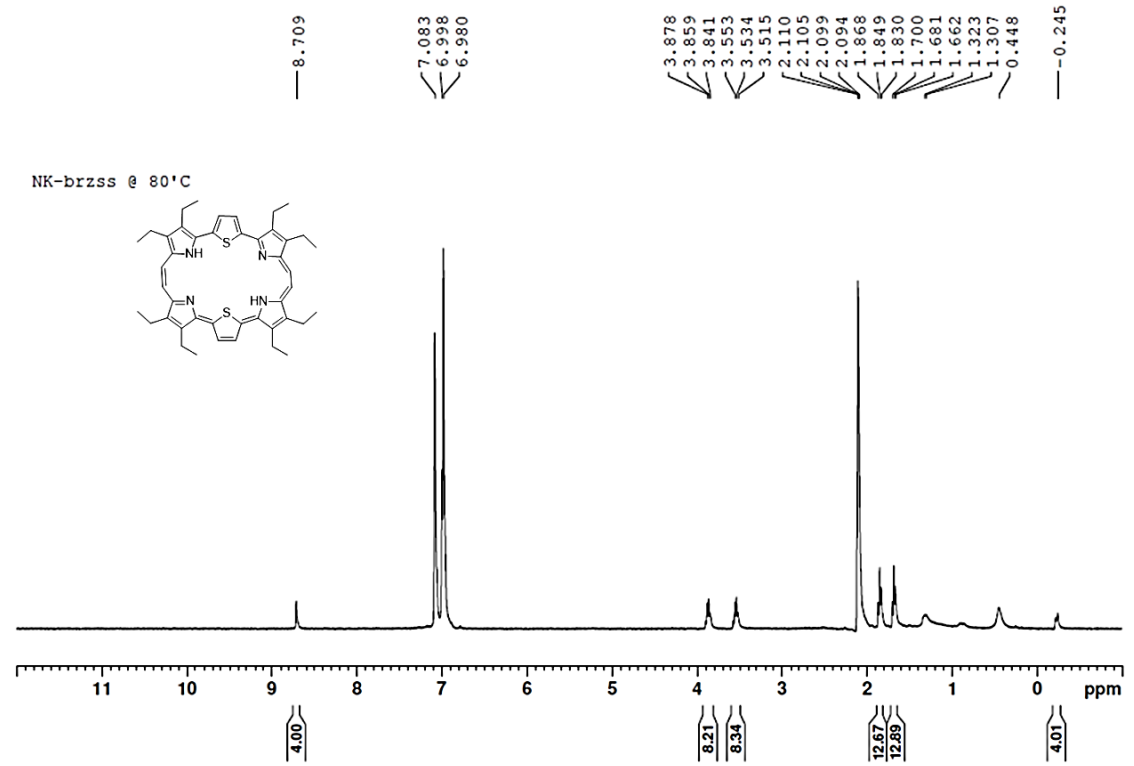

Figure 3.71 ^{1}H NMR spectrum of **3.38** at 80°C in toluene-d_8.

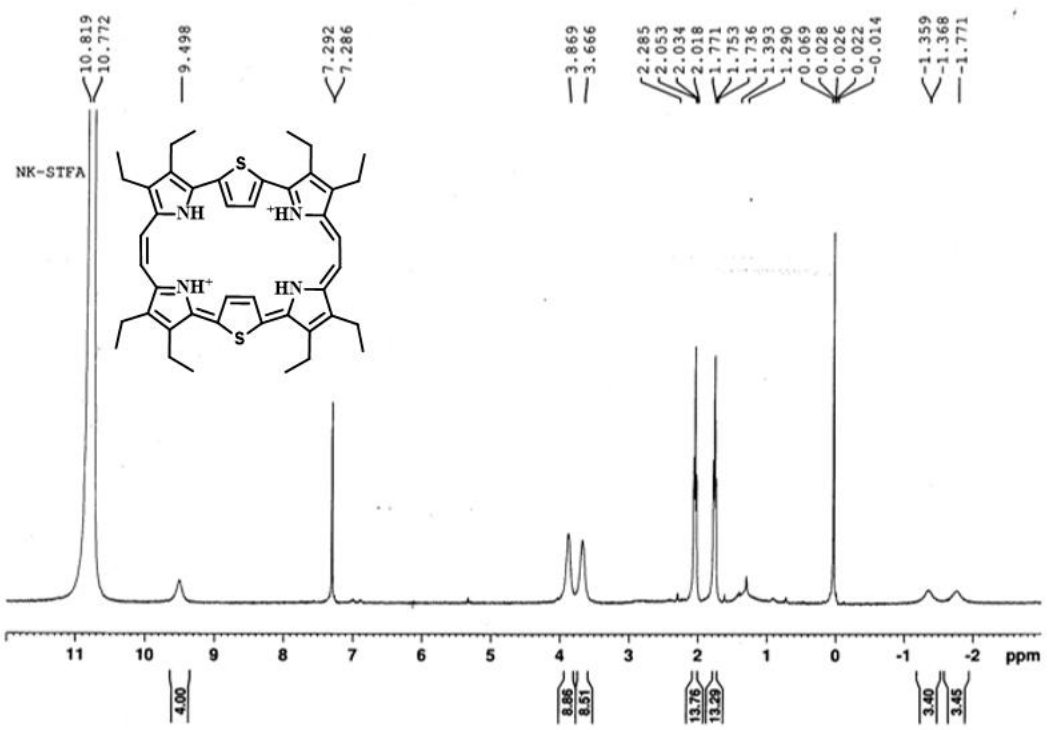

Figure 3.72 ^{1}H NMR spectrum of **3.38** in $CDCl_3$ + TFA.

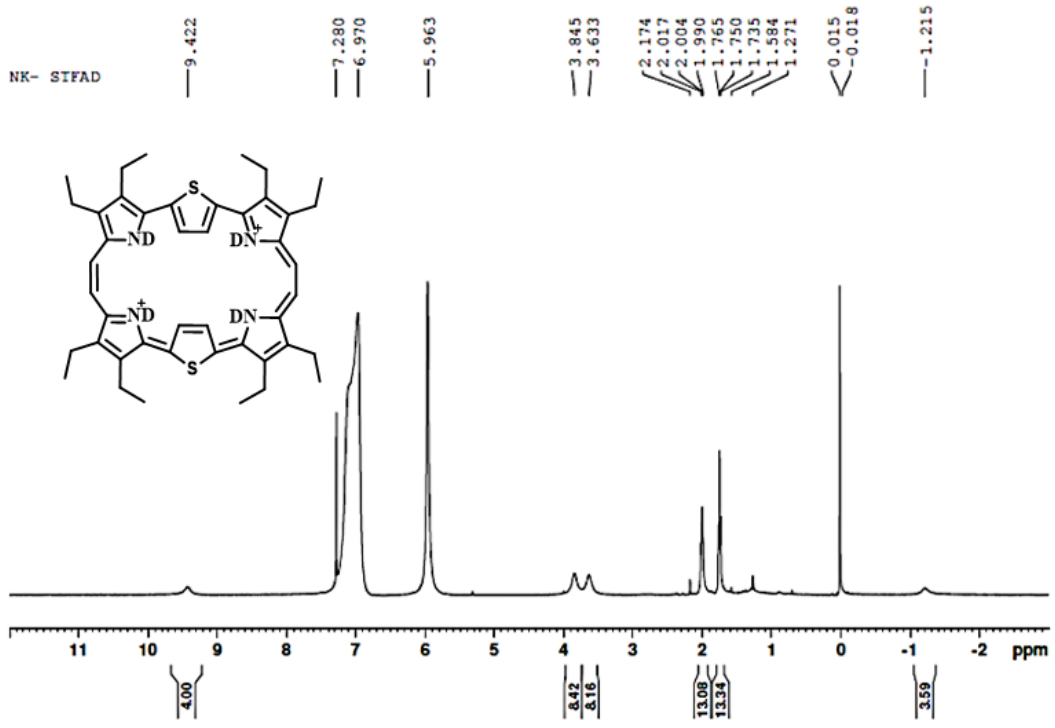

Figure 3.73 ^{1}H NMR spectrum of **3.38** in $CDCl_3$ +TFA + D_2O.

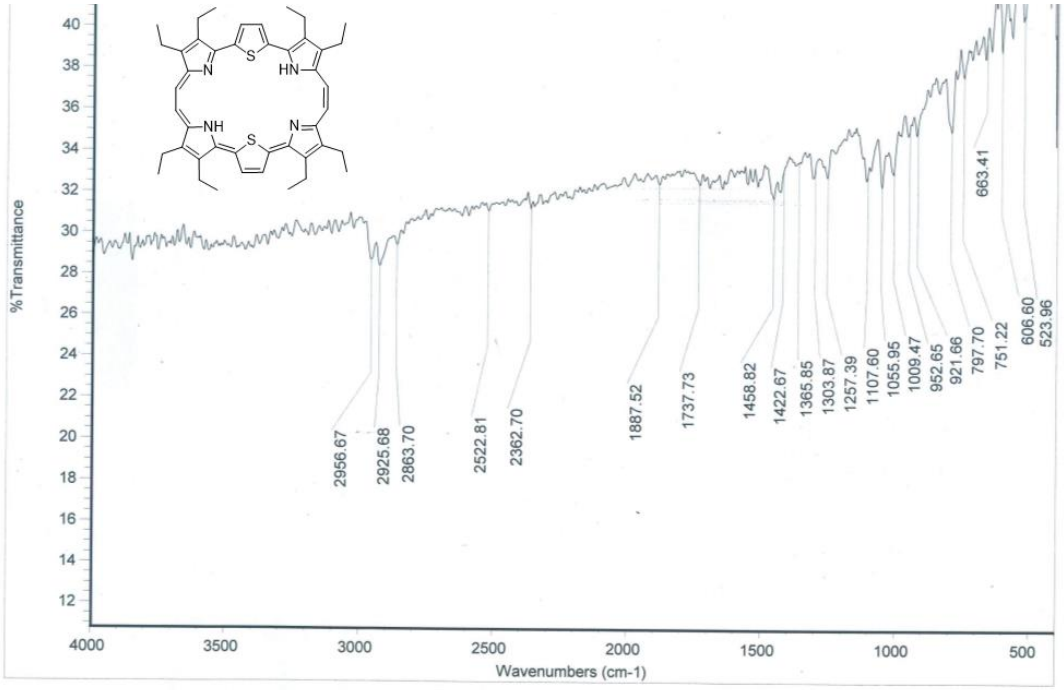

Figure 3.74 IR spectrum of **3.38**.

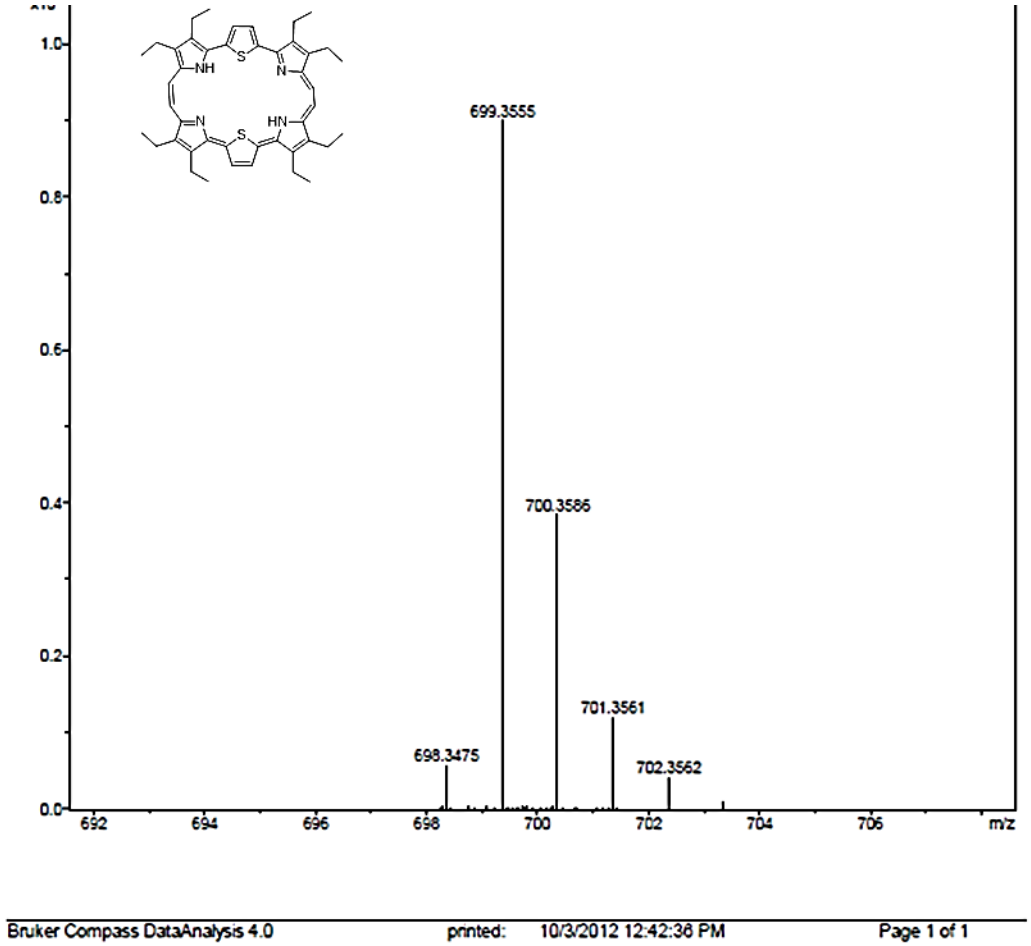

Figure 3.75 HRMS spectrum of **3.38** $(M+H)^+$; Calculated for $C_{44}H_{51}N_4S_2$: 699.3555; found: 699.3555.

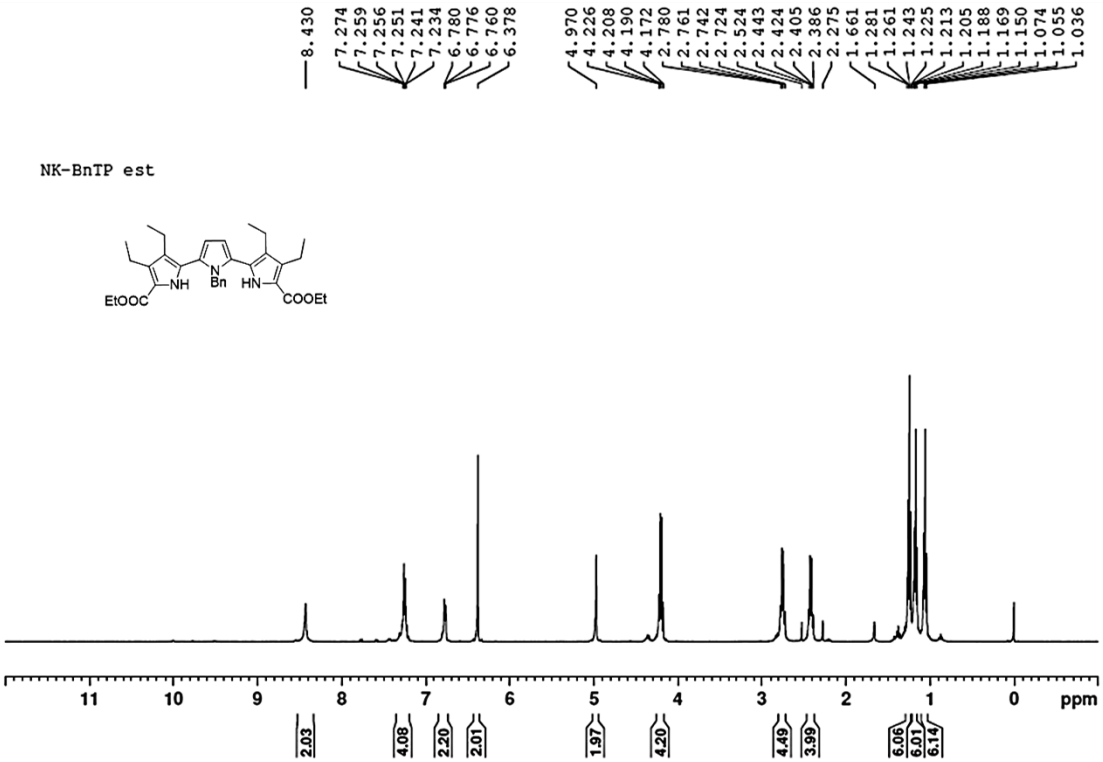

Figure 3.76 ^{1}H NMR spectrum of **3.39** in $CDCl_3$.

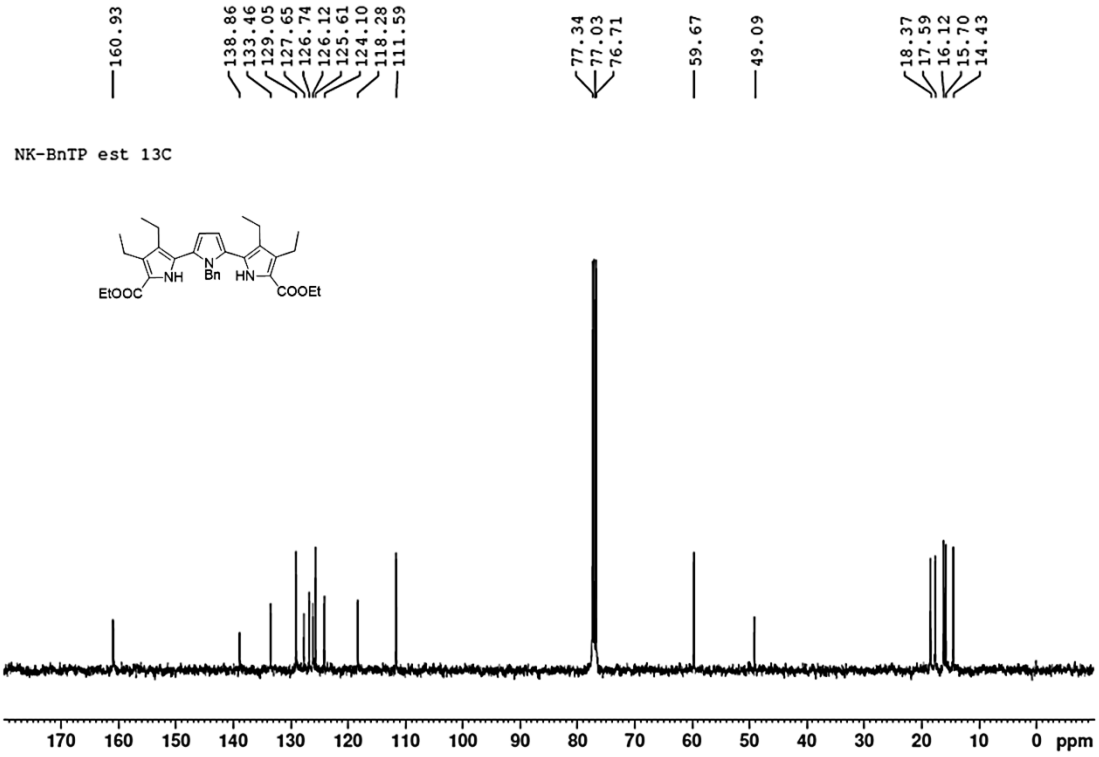

Figure 3.77 ^{13}C NMR spectrum of **3.39** in $CDCl_3$.

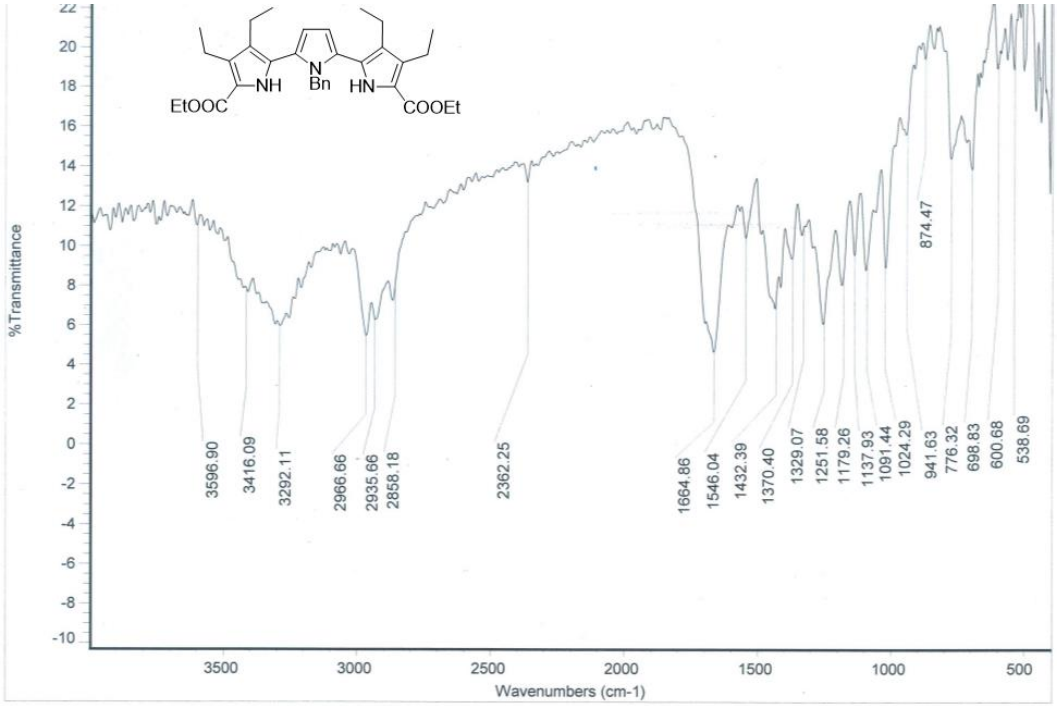

Figure 3.78 IR spectrum of **3.39**.

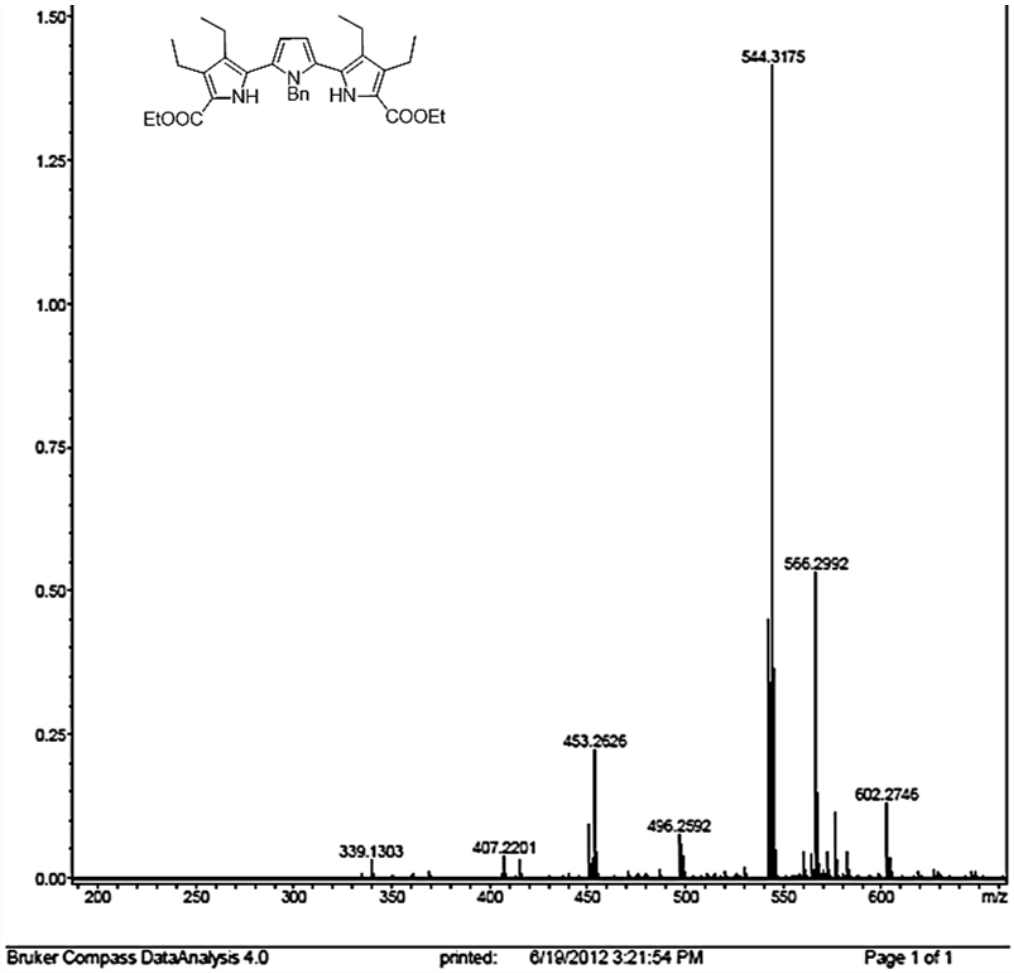

Figure 3.79 HRMS spectrum of **3.39** $(M+H)^+$ $C_{33}H_{42}N_3O_4$:544.3175 found 544.3175.

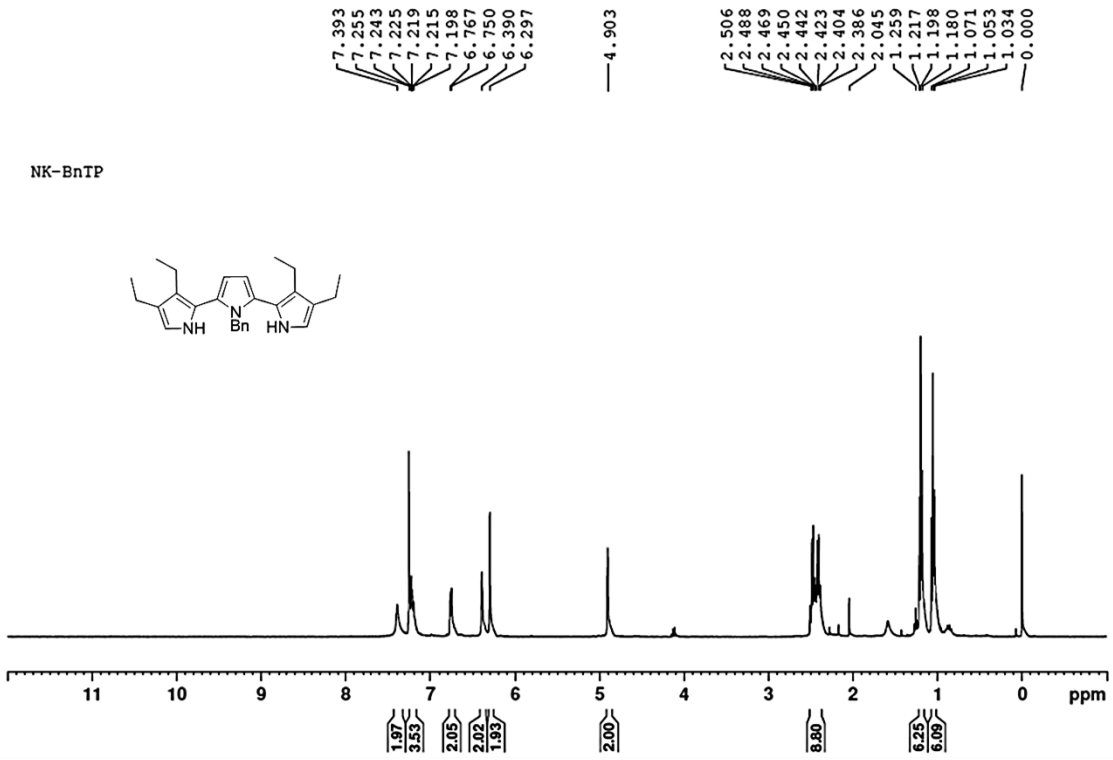

Figure 3.80 ^{1}H NMR spectrum of crude N-benzyl terpyrrole in $CDCl_3$.

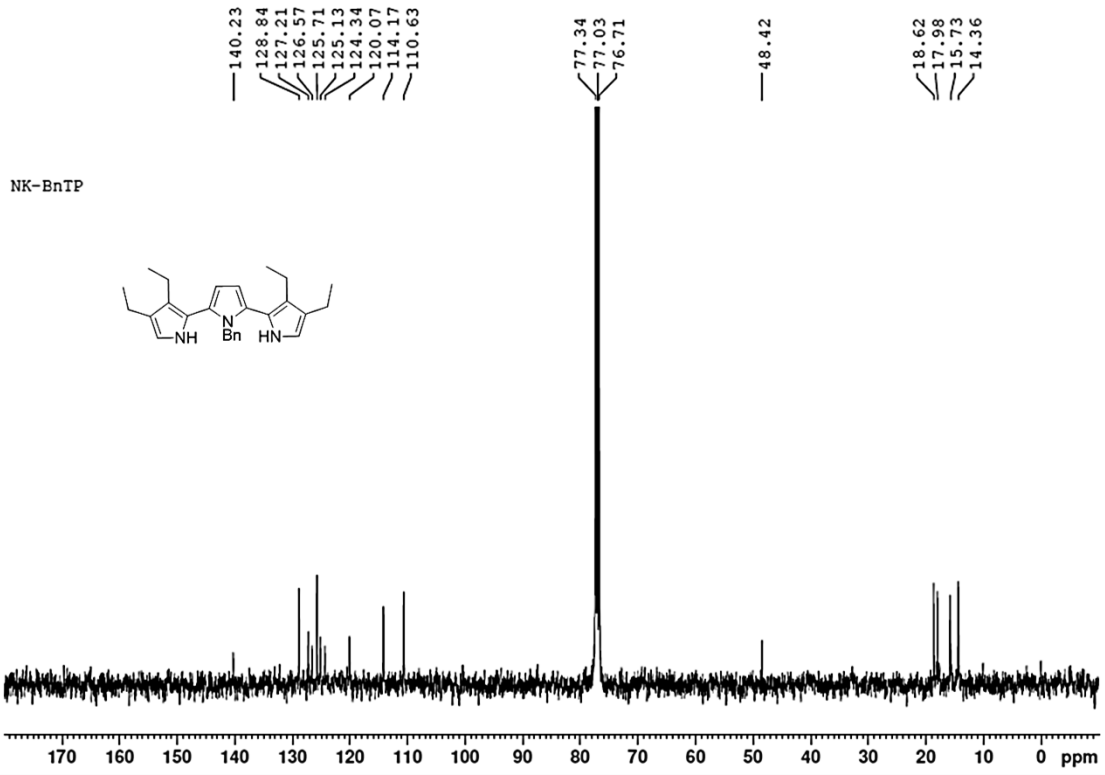

Figure 3.81 ^{13}C NMR spectrum of crude N-benzyl terpyrrole in $CDCl_3$.

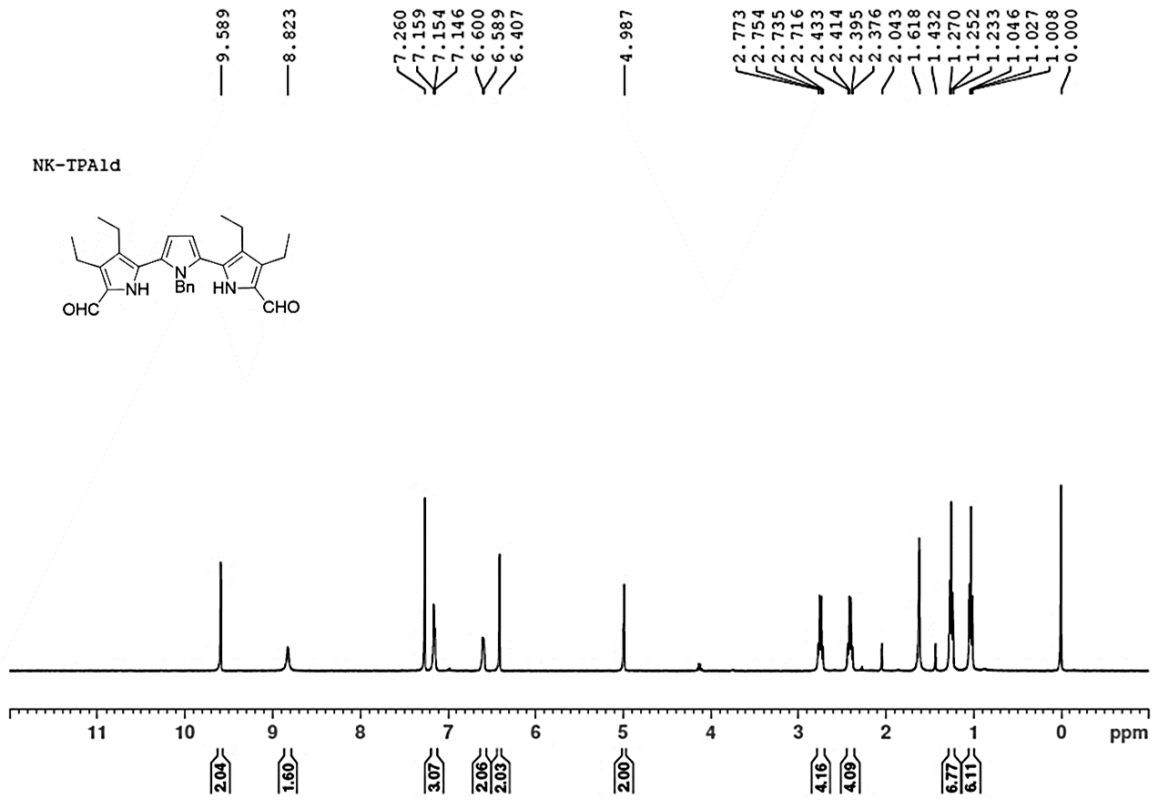

Figure 3.82 ^{1}H NMR spectrum of **3.40** in $CDCl_3$.

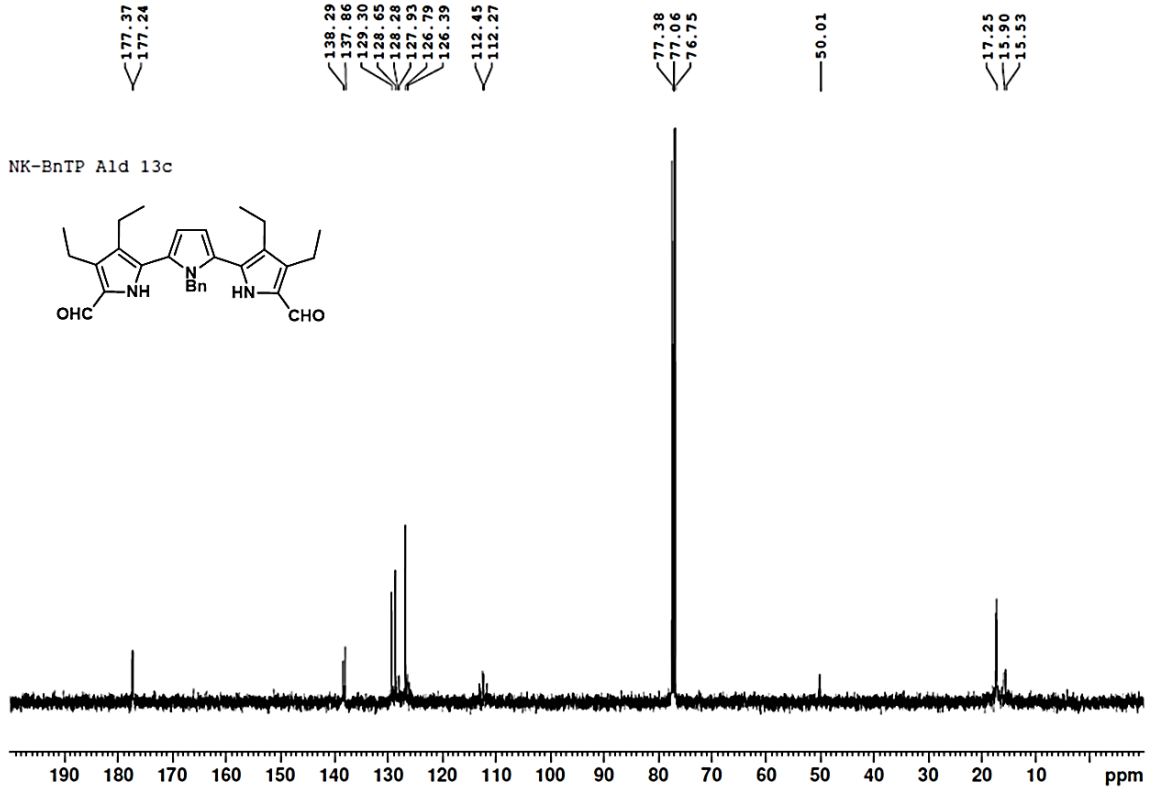

Figure 3.83 ^{13}C NMR spectrum of **3.40** in $CDCl_3$.

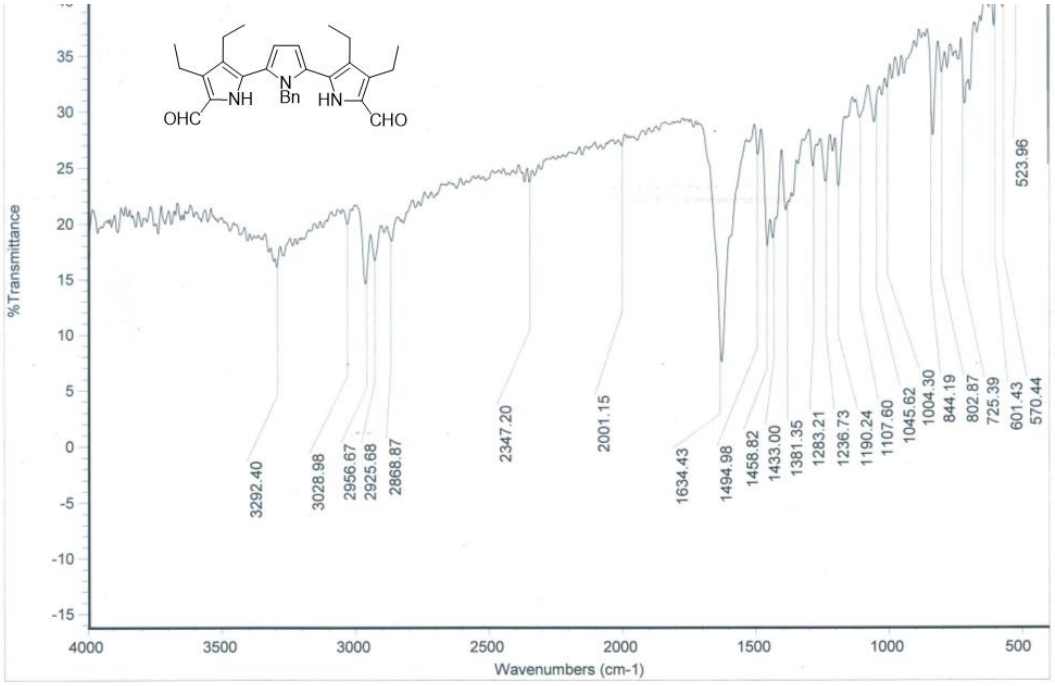

Figure 3.84 IR spectrum of **3.40**.

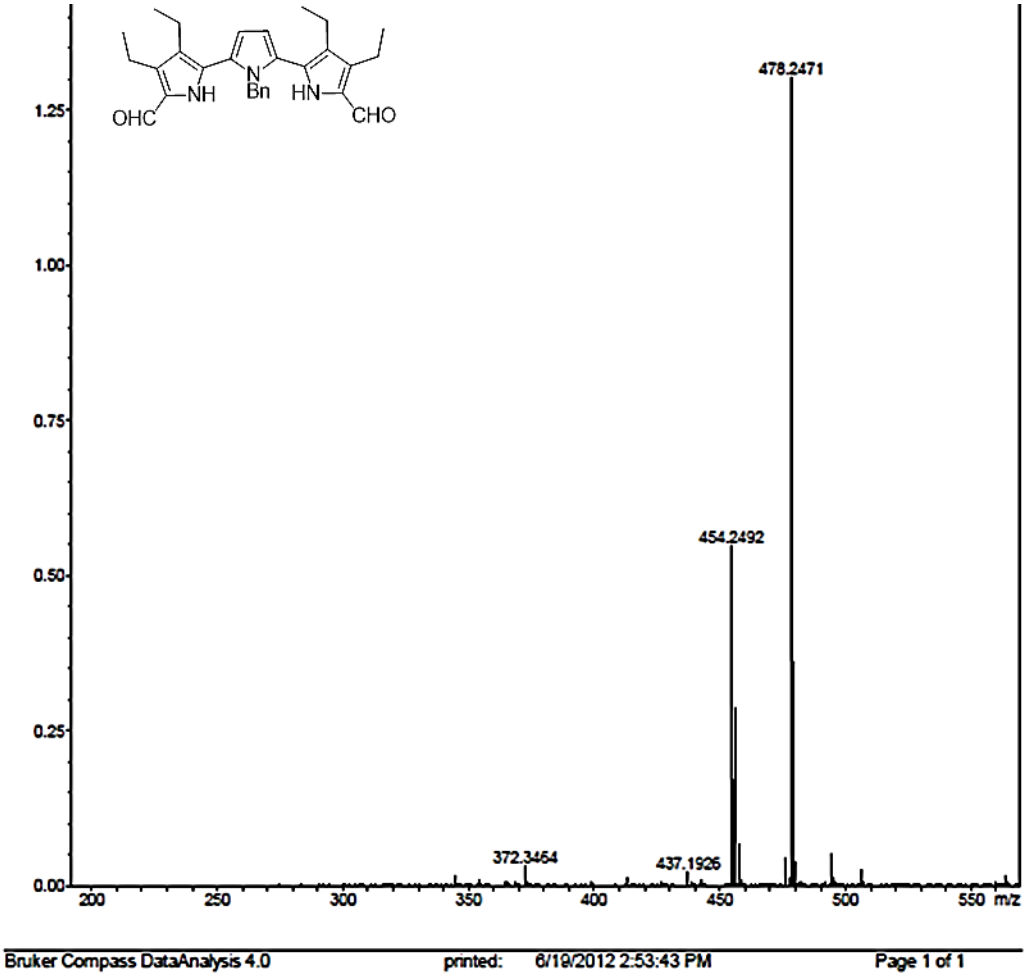

Figure 3.85 HRMS spectrum of **3.40** $(M+Na)^+$ $C_{29}H_{33}NaN_3O_2$:478.2470 found 478.2471.

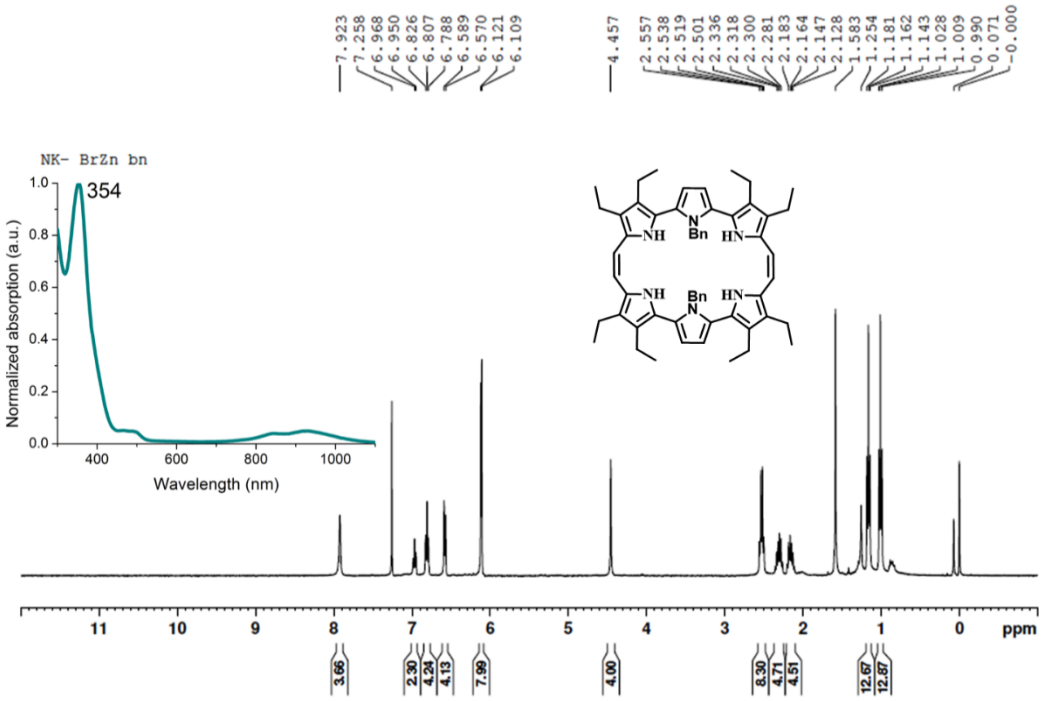

Figure 3.86 ^{1}H NMR spectrum of **3.41** in $CDCl_3$ (in set: absorption spectrum in chloroform).

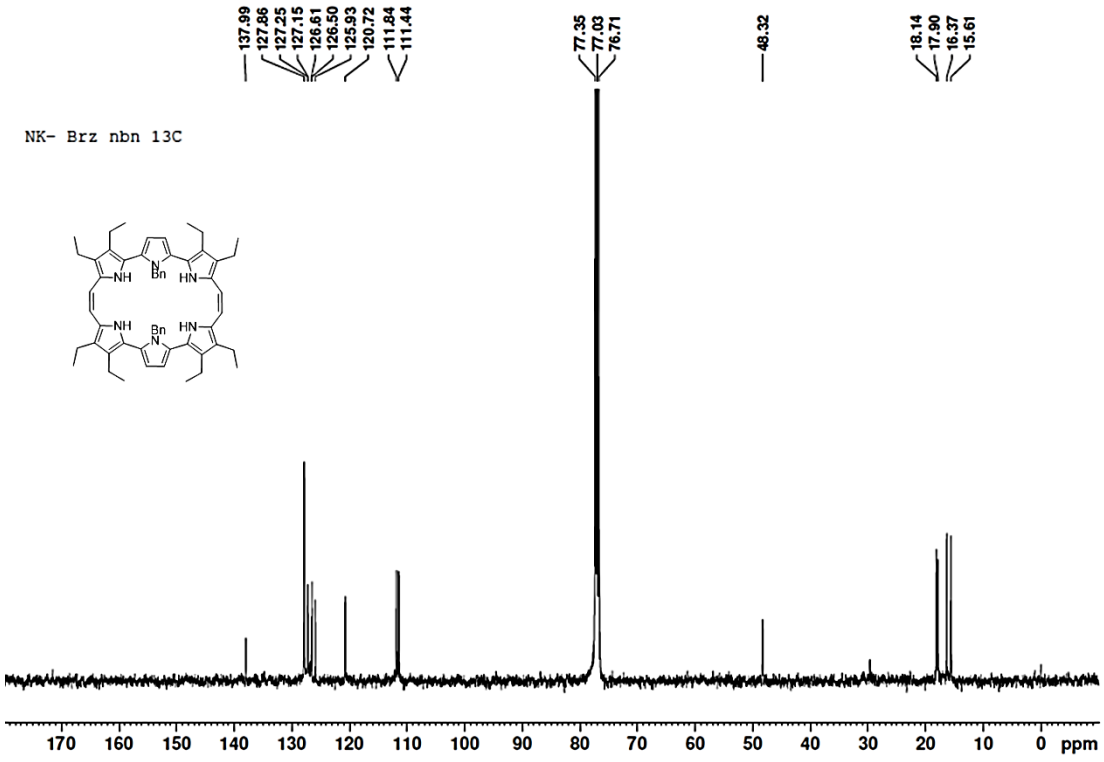

Figure 3.87 ^{13}C NMR spectrum of **3.41** in $CDCl_3$.

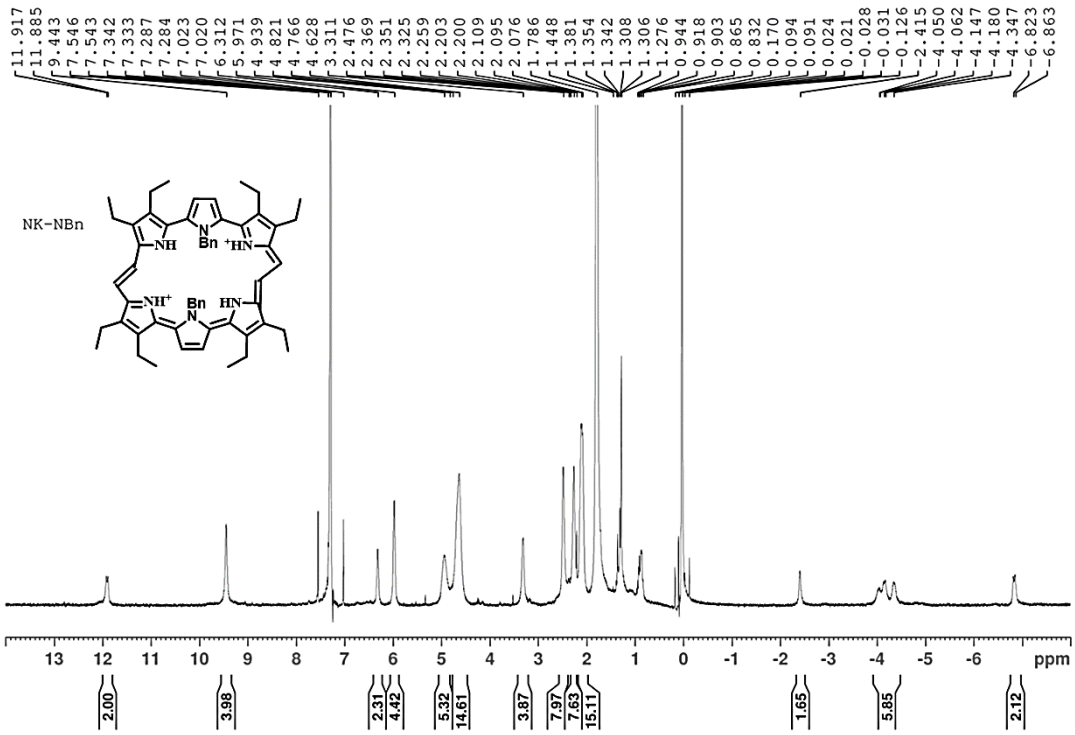

Figure 3.88 ^{1}H NMR spectrum of **3.42.H$_2^{2+}$** (monochloride salt) in $CDCl_3$.

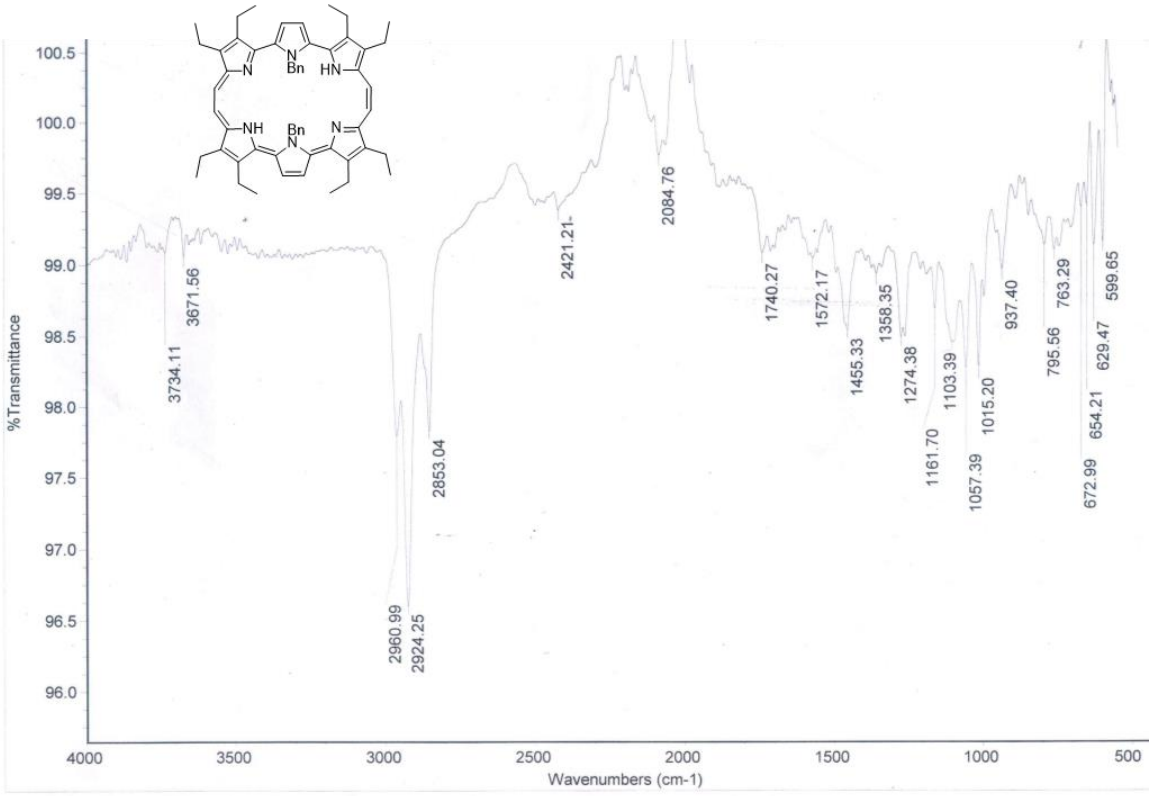

Figure 3.89 IR spectrum of **3.42.H$_2^{2+}$**.

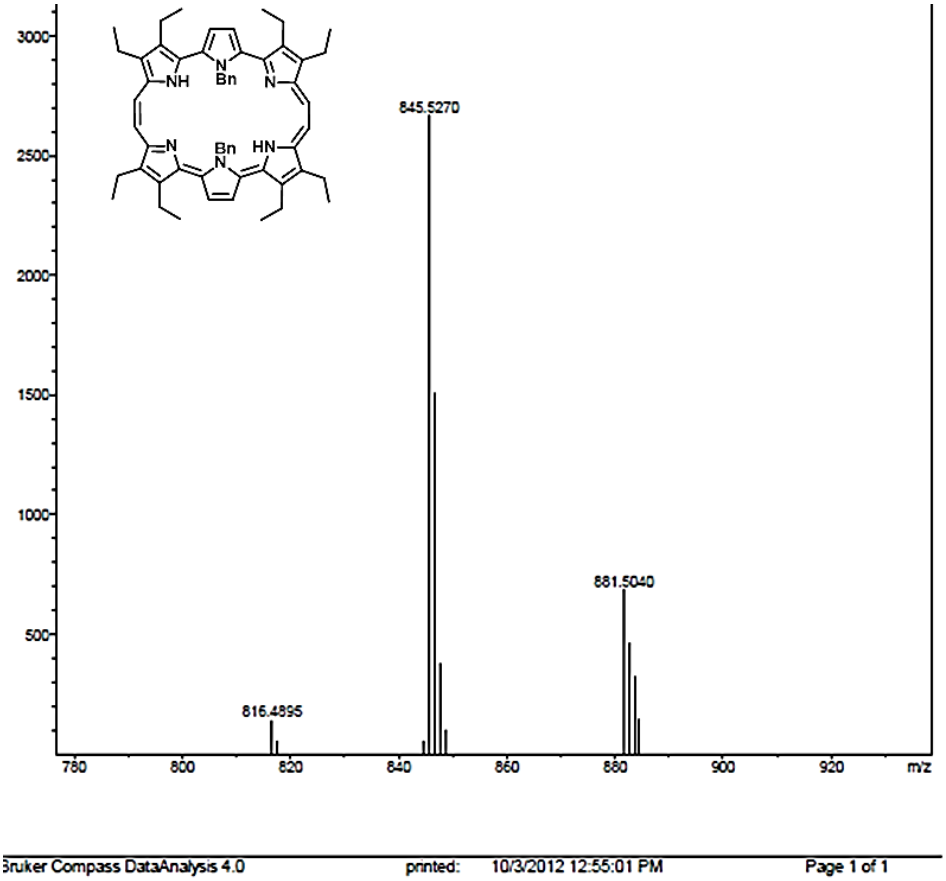

Figure 3.90 HRMS spectrum of **3.42** $(M+H)^+$ $C_{58}H_{65}N_6$:845.5271 found 845.5270.

3.9 Computational studies

Optimization coordinates of normal and inverted conformers for the two bronzaphyrins **3.38** and **3.18**:

Table 9 Coordinates of the optimized structure of normal isomer of **3.38**.

Atom Label	Symbol	X	Y	Z	Atom Label	Symbol	X	Y	Z
1	C	1.356197	2.762181	0.514457	51	H	1.300718	4.526094	1.818073
2	C	0.743953	3.815149	1.215675	52	H	-1.26264	4.569608	1.631579
3	C	-0.64383	3.84066	1.114261	53	H	-2.81063	0.488568	-0.22663
4	C	-1.18384	2.802045	0.339086	54	H	-1.23657	-4.47201	1.946468
5	S	0.115593	1.760395	-0.24581	55	H	1.320506	-4.5297	1.685238
6	C	2.740405	2.527579	0.277097	56	H	2.817412	-0.49958	-0.29184
7	C	-2.5481	2.651589	-0.04227	57	H	6.409315	1.081259	-1.31083
8	N	3.207044	1.356196	-0.2325	58	H	-6.42599	-1.09745	-1.13118
9	C	4.528067	1.568491	-0.51044	59	H	6.325005	-1.17587	-1.60772
10	C	4.921256	2.933294	-0.16958	60	H	-6.34621	1.154036	-1.47035
11	C	3.803485	3.536833	0.362199	61	H	5.667983	-4.81066	-1.68841
12	C	-3.49668	3.7044	-0.28903	62	H	6.374209	-3.26587	-2.12653
13	C	-4.65032	3.107406	-0.79294	63	H	7.856879	-4.48181	-0.52

14	C	-4.43476	1.691004	-0.8068	64	H	7.249431	-2.98795	0.244397
15	N	-3.14738	1.461606	-0.37908	65	H	6.538806	-4.55641	0.679846
16	C	-1.32581	-2.74824	0.592132	66	H	4.276208	-5.69703	-0.23181
17	C	-0.69549	-3.78064	1.307861	67	H	2.89958	-5.44909	0.814184
18	C	0.688747	-3.81155	1.167959	68	H	2.278847	-6.89185	-1.12753
19	C	1.208215	-2.79891	0.347493	69	H	1.370555	-5.36152	-1.22933
20	S	-0.10585	-1.77265	-0.23194	70	H	2.788953	-5.62048	-2.27001
21	C	-2.7159	-2.51848	0.384795	71	H	-2.71992	-5.38426	0.728972
22	C	2.56258	-2.65988	-0.07686	72	H	-4.45845	-5.54373	0.56283
23	N	-3.19504	-1.35796	-0.13711	73	H	-3.73323	-6.10346	2.891993
24	C	-4.52291	-1.57447	-0.37654	74	H	-4.81954	-4.68992	2.892795
25	C	-4.90721	-2.93165	0.001768	75	H	-3.07723	-4.45891	3.107825
26	C	-3.77603	-3.52495	0.5174	76	H	-6.7309	-3.22395	-1.08923
27	C	3.509583	-3.71443	-0.32369	77	H	-6.19997	-4.62638	-0.17441
28	C	4.6525	-3.12077	-0.85668	78	H	-8.23294	-3.61322	0.865957
29	C	4.434173	-1.70504	-0.88413	79	H	-6.85319	-3.48509	1.98911
30	N	3.153695	-1.47341	-0.43831	80	H	-7.38326	-2.05845	1.074659
31	C	5.448703	0.6376	-1.03822	81	H	6.716312	3.204967	-1.31248
32	C	-5.45682	-0.6513	-0.89518	82	H	6.209366	4.623822	-0.40962
33	C	5.404231	-0.73952	-1.21438	83	H	8.268293	3.628424	0.595709
34	C	-5.41507	0.722319	-1.09685	84	H	6.918123	3.521761	1.756438
35	C	5.916955	-3.81493	-1.28716	85	H	7.424207	2.078264	0.854831
36	C	6.950781	-3.96948	-0.15707	86	H	2.756927	5.403412	0.561987
37	C	3.294419	-5.20069	-0.18284	87	H	4.491557	5.553894	0.354997
38	C	2.378509	-5.8024	-1.26355	88	H	3.8205	6.158519	2.689034
39	C	-3.6751	-4.93258	1.040514	89	H	4.901736	4.741029	2.691207
40	C	-3.83197	-5.05401	2.568014	90	H	3.163835	4.520688	2.949349
41	C	-6.28232	-3.52803	-0.12763	91	H	-2.22289	5.43151	-0.24418
42	C	-7.24354	-3.1497	1.014824	92	H	-3.81697	5.716546	-0.9232
43	C	6.292666	3.526479	-0.34522	93	H	-3.60424	6.815378	1.313615
44	C	7.28304	3.168316	0.778683	94	H	-4.86653	5.557044	1.361537
45	C	3.717215	4.954279	0.861013	95	H	-3.28221	5.240065	2.085412
46	C	3.908358	5.102988	2.382148	96	H	-5.96745	4.793952	-0.79353
47	C	-3.28796	5.185834	-0.11467	97	H	-6.78626	3.249561	-0.95372
48	C	-3.78563	5.73079	1.236429	98	H	-6.85719	4.506229	-3.11481
49	C	-5.89164	3.807631	-1.27742	99	H	-5.89596	3.01794	-3.32359
50	C	-5.93375	3.989631	-2.80567	100	H	-5.07531	4.584113	-3.15823

Table 10 Coordinates of the optimized structure of inverted isomer of **3.38**.

Atom Label	Symbol	X	Y	Z	Atom Label	Symbol	X	Y	Z
1	C	-4.66343	1.719688	-0.10102	51	H	-1.2897	0.408667	-1.61547
2	C	-4.74255	3.174233	0.012838	52	H	1.321214	0.356135	-1.62151
3	C	-3.44596	3.646788	-0.10111	53	H	3.154255	0.256522	-0.15183

4	C	-2.61754	2.471416	-0.32163	54	H	-6.82063	3.55409	-0.35667
5	N	-3.37054	1.341501	-0.29996	55	H	-5.84976	5.001564	-0.13382
6	C	-1.22026	2.319988	-0.58176	56	H	-7.34879	4.627315	1.837612
7	C	-0.66034	1.185557	-1.18745	57	H	-5.64107	4.500073	2.340336
8	C	0.729091	1.16099	-1.18886	58	H	-6.61078	3.027989	2.122291
9	C	1.326346	2.280522	-0.58958	59	H	-3.73899	5.698605	0.422975
10	S	0.073422	3.413127	-0.06546	60	H	-2.06333	5.181241	0.49674
11	C	2.725498	2.400978	-0.34158	61	H	-2.41856	6.706734	-1.44971
12	C	3.619737	3.513297	-0.19611	62	H	-1.97433	5.085679	-2.04199
13	C	4.912914	2.985173	-0.08916	63	H	-3.67026	5.616893	-2.10744
14	C	4.799239	1.551307	-0.13639	64	H	4.022297	5.555318	-0.6903
15	N	3.474602	1.256093	-0.29566	65	H	2.330866	5.091229	-0.849
16	C	-5.99482	3.975697	0.242244	66	H	2.637466	6.609099	1.106621
17	C	-6.42516	4.03674	1.719641	67	H	2.117076	5.005589	1.683825
18	C	-2.98851	5.081122	-0.09689	68	H	3.820656	5.489509	1.831852
19	C	-2.74846	5.656152	-1.50471	69	H	6.976763	3.277932	-0.58002
20	C	3.222774	4.964633	-0.21256	70	H	6.068551	4.766807	-0.34488
21	C	2.933171	5.549885	1.181727	71	H	7.66692	4.396243	1.543
22	C	6.202095	3.746804	0.051006	72	H	5.991991	4.337004	2.153267
23	C	6.720595	3.832594	1.498618	73	H	6.90027	2.829459	1.917188
24	C	-4.79645	-1.54855	0.007641	74	H	-3.15193	-0.25617	0.042599
25	C	-4.90804	-2.98252	-0.05109	75	H	-1.31532	-0.35054	1.497307
26	C	-3.61727	-3.51033	0.062984	76	H	1.294486	-0.4025	1.482768
27	C	-2.72432	-2.40001	0.231424	77	H	-6.08767	-4.7503	0.213548
28	N	-3.47415	-1.25452	0.188884	78	H	-6.99805	-3.25167	0.33438
29	C	-1.3244	-2.27981	0.473941	79	H	-7.56365	-4.45001	-1.78681
30	C	-0.72482	-1.15763	1.06657	80	H	-6.76625	-2.90019	-2.16962
31	C	0.66428	-1.18169	1.060422	81	H	-5.8523	-4.41871	-2.29075
32	C	1.222826	-2.31877	0.457675	82	H	-4.00766	-5.55591	-0.41302
33	S	-0.07232	-3.41587	-0.04749	83	H	-2.30606	-5.12782	-0.46559
34	C	2.618837	-2.47067	0.19358	84	H	-2.77741	-6.58027	1.511879
35	C	3.445698	-3.64499	-0.0371	85	H	-2.25622	-4.96919	2.067586
36	C	4.741978	-3.17234	-0.15549	86	H	-3.97924	-5.40882	2.11886
37	C	4.664133	-1.71839	-0.03428	87	H	3.736221	-5.69366	-0.57447
38	N	3.373256	-1.34095	0.174752	88	H	2.060191	-5.17616	-0.63659
39	C	-6.19095	-3.74744	-0.23128	89	H	2.426976	-6.71331	1.299229
40	C	-6.61912	-3.8877	-1.7037	90	H	1.983766	-5.09625	1.902915
41	C	-3.23521	-4.96626	0.106227	91	H	3.68069	-5.62573	1.956855
42	C	-3.05136	-5.51284	1.533385	92	H	5.849612	-5.00042	-0.02204
43	C	2.988367	-5.07934	-0.04713	93	H	6.822428	-3.554	0.198684
44	C	2.755919	-5.66266	1.358554	94	H	7.335237	-4.62107	-2.00238
45	C	5.992439	-3.97344	-0.39594	95	H	6.596522	-3.02039	-2.27726
46	C	6.412844	-4.03021	-1.87639	96	H	5.624283	-4.49107	-2.49326
47	C	5.824507	0.574567	-0.07405	97	H	6.83393	0.991942	-0.03584

48	C	5.762214	-0.81951	-0.0969	98	H	6.737973	-1.31048	-0.15125
49	C	-5.76111	0.821073	-0.0467	99	H	-6.73791	1.311104	-0.00347
50	C	-5.82131	-0.57355	-0.07	100	H	-6.82933	-0.99261	-0.12406

Table 11 Coordinates of the optimized structure of normal isomer of **3.18**.

Atom Label	Symbol	X	Y	Z	Atom Label	Symbol	X	Y	Z
1	C	-1.24259	2.935193	-0.09702	45	H	-6.60216	1.26313	0.464867
2	C	-0.65175	4.202233	-0.27435	46	H	6.637746	-1.22559	-0.04757
3	C	0.733117	4.185656	-0.29766	47	H	-6.65402	-0.99549	0.729914
4	C	1.295646	2.902205	-0.14345	48	H	6.702024	1.046986	-0.0693
5	S	0.013384	1.708656	0.034943	49	H	-6.08112	-4.63269	1.35577
6	C	-2.63375	2.67715	-0.0152	50	H	-6.87793	-3.07143	1.536808
7	C	2.687085	2.638714	-0.12539	51	H	-7.12268	-2.9141	-0.97503
8	N	-3.22449	1.466606	0.170776	52	H	-6.32461	-4.47693	-1.14343
9	C	-4.57177	1.720135	0.216994	53	H	6.935499	-3.31915	0.532888
10	C	-4.84656	3.150987	0.044613	54	H	6.101148	-4.84964	0.277614
11	C	4.937199	3.032039	-0.12795	55	H	6.028882	-4.41492	-2.19387
12	C	4.694721	1.615724	-0.06512	56	H	6.849758	-2.87333	-1.95926
13	N	3.327468	1.423714	-0.05801	57	H	-6.85868	3.410348	0.765268
14	C	1.260903	-2.92403	0.169649	58	H	-6.06014	4.891682	0.244067
15	C	0.664241	-4.19962	0.22157	59	H	-6.2201	4.151875	-2.15004
16	C	-0.71701	-4.17762	0.32425	60	H	-7.00877	2.658013	-1.64821
17	C	-1.27094	-2.88157	0.354487	61	H	6.170197	4.714082	-0.56026
18	S	0.014883	-1.68299	0.251297	62	H	6.99125	3.166048	-0.74769
19	C	2.65176	-2.6658	0.081992	63	H	6.976452	2.866208	1.76462
20	C	-2.65687	-2.60946	0.461192	64	H	6.165966	4.422152	1.936565
21	N	3.249246	-1.44483	0.047015	65	C	8.234814	4.570881	1.294609
22	C	4.596246	-1.69805	-0.00974	66	H	8.157084	5.584086	0.864332
23	C	4.862852	-3.14067	-0.0195	67	H	8.641734	4.671339	2.313443
24	C	-4.8961	-2.98594	0.709312	68	H	8.973706	4.013992	0.693223
25	C	-4.65586	-1.57428	0.575643	69	C	-8.24334	4.42646	-1.41072
26	N	-3.29475	-1.39159	0.433904	70	H	-8.14362	5.500929	-1.1797
27	C	-5.61548	0.795742	0.42315	71	H	-8.71931	4.341151	-2.40085
28	C	5.648825	-0.76118	-0.03574	72	H	-8.9366	3.99404	-0.66878
29	C	-5.65264	-0.58488	0.582585	73	C	-8.317	-4.59066	-0.28827
30	C	5.693331	0.628386	-0.05007	74	H	-8.82564	-4.74273	-1.25363
31	C	-6.23144	-3.65801	0.860968	75	H	-8.19048	-5.58074	0.182152
32	C	-6.97207	-3.88553	-0.47251	76	H	-8.99334	-4.00388	0.356732
33	C	6.198083	-3.82368	-0.11686	77	C	8.11521	-4.6034	-1.62211
34	C	6.760983	-3.89535	-1.55116	78	H	8.04681	-5.63934	-1.24801
35	C	-6.1886	3.825282	-0.00887	79	H	8.492881	-4.64662	-2.65634
36	C	-6.88563	3.722155	-1.38098	80	H	8.873181	-4.08319	-1.01146

37	C	6.276386	3.71323	-0.10844	81	C	3.700833	3.643692	-0.17072
38	C	6.878236	3.864468	1.303582	82	H	3.517194	4.713579	-0.22026
39	H	-1.24057	5.110866	-0.38317	83	C	3.634572	-3.73383	0.039113
40	H	1.339421	5.079603	-0.43212	84	C	-3.62214	3.737357	-0.10023
41	H	2.936899	0.46173	-0.02299	85	C	-3.66537	-3.60588	0.632635
42	H	1.246443	-5.11817	0.18324	86	H	-3.48077	-4.6742	0.706381
43	H	-1.32771	-5.07761	0.369324	87	H	-3.42176	4.796886	-0.24397
44	H	-2.90665	-0.43463	0.320923	88	H	3.429034	-4.80193	0.056364

Table 12 Coordinates of the optimized structure of inverted isomer of **3.18**.

Atom Label	Symbol	X	Y	Z	Atom Label	Symbol	X	Y	Z
1	S	0.104145	3.382268	0.047595	45	C	1.13009	-2.29107	-0.69141
2	N	-3.31728	1.34439	0.622456	46	C	-3.63271	-3.45792	0.183501
3	N	3.501338	1.217217	-0.08225	47	C	-1.39346	-2.24068	-0.44445
4	C	4.904406	2.952087	-0.44735	48	C	-4.79834	-1.51447	0.400647
5	C	-3.36719	3.634239	0.443797	49	C	2.542518	-2.45817	-0.57224
6	C	4.61723	-1.74566	-0.55506	50	C	0.52376	-1.14916	-1.23271
7	C	5.800377	0.534044	-0.61577	51	C	-2.76052	-2.35889	-0.05962
8	H	6.798743	0.946785	-0.78145	52	C	5.916401	-4.05125	-0.35888
9	C	-4.67889	3.205334	0.456727	53	H	5.680145	-5.07498	-0.696
10	C	0.858791	1.119169	1.095002	54	H	6.688857	-3.6727	-1.05261
11	C	-1.1301	2.291053	0.691302	55	C	-5.72785	0.860616	0.609949
12	C	3.63273	3.45795	-0.18348	56	H	-6.69676	1.3626	0.686056
13	C	1.39347	2.240722	0.444476	57	C	6.5152	-4.12059	1.061252
14	C	4.798359	1.514489	-0.40052	58	H	5.746634	-4.50897	1.75235
15	C	-2.54252	2.458137	0.572109	59	H	6.746184	-3.09803	1.407853
16	C	-0.52376	1.149177	1.232664	60	C	-6.15977	-3.74573	0.672829
17	C	2.760535	2.358936	0.059682	61	H	-5.89133	-4.72607	1.102171
18	C	-5.9164	4.051238	0.358846	62	H	-6.79149	-3.24483	1.427213
19	H	-5.68012	5.074978	0.695915	63	C	-6.99104	-3.97173	-0.60675
20	H	-6.68882	3.672715	1.052631	64	H	-6.35993	-4.48032	-1.35652
21	C	5.727851	-0.86062	-0.60986	65	H	-7.25387	-2.99287	-1.04514
22	H	6.696755	-1.3626	-0.68594	66	H	-1.49	-0.31203	-1.46335
23	C	-6.51529	4.120527	-1.06126	67	H	1.112675	-0.37404	-1.7178
24	H	-5.74676	4.508885	-1.75241	68	H	-3.16053	-0.22124	0.22609
25	H	-6.74629	3.097953	-1.40781	69	H	3.355099	4.508416	-0.11837
26	C	6.159802	3.745728	-0.6728	70	H	-3.01629	4.664759	0.402431
27	H	5.891358	4.726046	-1.10218	71	H	-3.35508	-4.50838	0.118322
28	H	6.791514	3.244787	-1.42716	72	H	3.016296	-4.66479	-0.40263
29	C	6.991072	3.971784	0.60677	73	C	-8.26025	-4.78669	-0.35221
30	H	6.359964	4.480411	1.356517	74	H	-8.83332	-4.93751	-1.28102
31	H	7.253897	2.99294	1.045206	75	H	-8.02193	-5.78258	0.058769
32	H	1.490014	0.312108	1.463447	76	H	-8.92356	-4.28227	0.37119

33	H	-1.11268	0.374059	1.717763	77	C	7.770856	-4.99145	1.132214
34	H	3.160573	0.221242	-0.22576	78	H	8.175919	-5.03062	2.156155
35	S	-0.10415	-3.38228	-0.04769	79	H	7.558574	-6.0274	0.816874
36	N	3.317278	-1.34442	-0.62257	80	H	8.56656	-4.60382	0.472979
37	N	-3.50131	-1.21718	0.082447	81	C	8.260287	4.786719	0.352197
38	C	-4.90438	-2.95207	0.447415	82	H	8.021971	5.7826	-0.05883
39	C	3.367192	-3.63427	-0.44396	83	H	8.833353	4.937577	1.280993
40	C	-4.61723	1.745639	0.55504	84	H	8.923594	4.282265	-0.37118
41	C	-5.80037	-0.53405	0.615911	85	C	-7.77095	4.991387	-1.13217
42	H	-6.79873	-0.94679	0.78159	86	H	-7.55865	6.027343	-0.81688
43	C	4.678886	-3.20535	-0.45681	87	H	-8.17607	5.030516	-2.15609
44	C	-0.85879	-1.11912	-1.09496	88	H	-8.56661	4.603779	-0.47288

Optimization coordinates of *cis* and *trans* conformers for the two bronzaphyrins **3.42** and **3.42.H_2^{2+}**:

Table 13 Coordinates of the optimized structure of *cis* isomer of **3.42**.

Atom Label	Symbol	X	Y	Z	Atom Label	Symbol	X	Y	Z
1	C	-0.58594	3.040823	0.989418	65	H	-3.51492	-4.60749	-1.51156
2	C	-0.01542	3.812873	2.024576	66	H	-4.36866	-6.09287	0.295412
3	C	1.333403	3.511981	2.102525	67	H	-3.34078	-4.8119	0.994943
4	C	1.630291	2.552202	1.111284	68	H	-5.10814	-4.69902	1.128181
5	C	-1.97443	3.114714	0.619712	69	H	0.989017	-5.60005	-0.96653
6	C	2.953778	2.05172	0.880373	70	H	2.480202	-6.31863	-0.37829
7	N	-2.77703	2.067196	0.288952	71	H	2.004611	-7.00451	-2.73665
8	C	-4.04617	2.594805	0.19706	72	H	3.54067	-6.1116	-2.63434
9	C	-4.02843	4.036925	0.391379	73	H	2.098621	-5.3079	-3.27417
10	C	-2.72227	4.373755	0.675006	74	H	5.61487	-4.7032	0.748426
11	C	4.15245	2.825656	1.03266	75	H	4.665959	-5.91101	-0.10596
12	C	5.230537	1.948698	0.915679	76	H	6.837687	-5.53544	-1.26567
13	C	4.700745	0.642827	0.68905	77	H	5.503544	-5.0097	-2.32665
14	N	3.327489	0.751481	0.62633	78	H	6.473026	-3.80149	-1.46387
15	C	0.476191	-2.8503	-0.91195	79	H	-6.09217	4.508466	0.755638
16	C	-0.10654	-3.52981	-2.00131	80	H	-5.01375	5.888965	0.82339
17	C	-1.46459	-3.24727	-2.01863	81	H	-6.44404	5.98603	-1.2264
18	C	-1.74772	-2.39004	-0.9383	82	H	-4.73028	5.815302	-1.69202
19	C	1.861007	-2.95917	-0.53921	83	H	-5.81209	4.408621	-1.77027
20	C	-3.06998	-1.94402	-0.60281	84	H	-1.63995	5.883834	1.797538
21	N	2.645544	-1.96244	-0.04641	85	H	-3.06524	6.453978	0.956829
22	C	3.89799	-2.52056	0.092652	86	H	-1.03182	7.334635	-0.14086
23	C	3.885079	-3.92915	-0.262	87	H	-1.85599	6.217699	-1.26137
24	C	2.602818	-4.21039	-0.68718	88	H	-0.39499	5.691921	-0.38646
25	C	-4.25117	-2.74836	-0.69416	89	H	3.401968	4.775489	1.591738

26	C	-5.3392	-1.91939	-0.41475	90	H	5.144036	4.588607	1.736234
27	C	-4.82943	-0.60846	-0.17487	91	H	4.554267	6.065636	-0.19572
28	N	-3.45315	-0.67279	-0.24547	92	H	5.332005	4.579681	-0.80439
29	C	-5.26781	1.895991	0.083641	93	H	3.569192	4.76444	-0.91945
30	C	5.106281	-1.86849	0.420106	94	H	6.852932	3.323404	0.675253
31	C	-5.60609	0.555483	-0.02666	95	H	7.281872	1.65077	0.356355
32	C	5.455883	-0.54362	0.633752	96	H	8.308572	2.433227	2.501545
33	C	-6.79322	-2.30918	-0.41118	97	H	7.131407	1.136671	2.84212
34	C	-7.47366	-2.14943	-1.78339	98	H	6.697249	2.829789	3.156383
35	C	-4.3311	-4.24378	-0.87466	99	N	0.433556	2.240909	0.464951
36	C	-4.28511	-5.00608	0.462567	100	N	-0.54167	-2.11717	-0.29306
37	C	2.081946	-5.56982	-1.08628	101	C	-0.43953	-1.52842	1.053289
38	C	2.450352	-6.02147	-2.51115	102	H	-0.91835	-0.53979	1.04947
39	C	5.049834	-4.88007	-0.18316	103	H	0.632103	-1.37698	1.236448
40	C	6.021382	-4.80248	-1.37688	104	C	0.328996	1.467954	-0.78367
41	C	-5.21134	4.959072	0.266622	105	H	0.708922	0.451758	-0.61328
42	C	-5.57166	5.312609	-1.18781	106	H	-0.74531	1.382824	-0.99361
43	C	-2.20135	5.778169	0.85656	107	C	1.052779	2.083475	-1.96869
44	C	-1.32025	6.282231	-0.30001	108	C	0.697275	3.353704	-2.44899
45	C	4.277277	4.327838	1.106305	109	C	2.06046	1.366609	-2.62768
46	C	4.443894	4.971953	-0.28311	110	C	1.34306	3.897745	-3.56115
47	C	6.691568	2.293141	1.03025	111	H	-0.09361	3.919258	-1.95173
48	C	7.239693	2.165869	2.463839	112	C	2.704293	1.908841	-3.74492
49	H	-0.57772	4.443479	2.704049	113	H	2.34791	0.378251	-2.26037
50	H	2.035224	3.858713	2.854062	114	C	2.349412	3.175882	-4.21318
51	H	2.747246	-0.09158	0.469365	115	H	1.055023	4.886843	-3.92526
52	H	0.446465	-4.09514	-2.74281	116	H	3.489132	1.337864	-4.24639
53	H	-2.18356	-3.54287	-2.77651	117	H	2.853013	3.601081	-5.08449
54	H	-2.88496	0.186907	-0.13434	118	C	-1.04503	-2.385	2.151791
55	H	-6.13823	2.554464	0.125865	119	C	-2.11271	-1.90089	2.918993
56	H	5.958794	-2.54961	0.465807	120	C	-0.52253	-3.65609	2.44044
57	H	-6.68008	0.358673	-0.04975	121	C	-2.65111	-2.66946	3.956289
58	H	6.521473	-0.37836	0.805657	122	H	-2.53018	-0.91514	2.699142
59	H	-6.88903	-3.35653	-0.08258	123	C	-1.06276	-4.42619	3.472355
60	H	-7.3395	-1.71205	0.337415	124	H	0.316202	-4.0418	1.856042
61	H	-8.53272	-2.4519	-1.73512	125	C	-2.12866	-3.93448	4.234663
62	H	-7.43182	-1.10396	-2.12882	126	H	-3.48399	-2.27734	4.544526
63	H	-6.97657	-2.76878	-2.54754	127	H	-0.64495	-5.41242	3.688367
64	H	-5.26559	-4.49191	-1.40469	128	H	-2.5482	-4.53673	5.04389

Table 14 Coordinates of the optimized structure of *trans* isomer of **3.42**.

Atom Label	Symbol	X	Y	Z	Atom Label	Symbol	X	Y	Z
1	C	-4.47124	0.488088	0.870892	65	H	3.363937	6.923913	0.113282
2	C	-5.31681	-0.06219	1.858312	66	H	1.640601	6.790103	0.433208
3	C	-5.1884	-1.46093	1.823364	67	H	2.056644	8.346175	-1.48143
4	C	-4.26834	-1.78285	0.807264	68	H	1.158795	6.914367	-2.0544
5	C	-3.37125	-2.89213	0.633879	69	H	2.899756	7.055442	-2.37934
6	C	-3.89771	1.794795	0.698316	70	H	5.570672	4.31992	-1.69175
7	C	-3.43674	-4.31209	0.721994	71	H	5.02836	5.87177	-1.07858
8	C	-2.15132	-4.81847	0.429494	72	H	6.93709	5.007356	0.284423
9	C	-1.28751	-3.70757	0.172931	73	H	5.471272	5.103154	1.29607
10	N	-2.0802	-2.5845	0.297327	74	H	6.022803	3.52829	0.675253
11	N	-2.67301	1.8516	0.13993	75	H	6.143774	-2.60178	-2.68672
12	C	-2.24657	3.144694	0.241558	76	H	6.141303	-4.29276	-2.22733
13	C	-3.281	3.974633	0.854414	77	H	8.033767	-3.08528	-1.12577
14	C	-4.32681	3.116784	1.154673	78	H	6.895237	-3.69448	0.105852
15	C	4.198973	-0.58787	-1.09128	79	H	6.891785	-1.9717	-0.32689
16	C	5.227393	0.016592	-1.85155	80	H	4.965	-5.92531	-1.26883
17	C	5.093093	1.401739	-1.76206	81	H	3.386913	-6.26728	-0.57371
18	C	3.976154	1.679436	-0.94572	82	H	3.56502	-7.26625	-2.85739
19	C	3.267305	2.905489	-0.75155	83	H	2.316216	-5.99149	-2.86379
20	C	3.794706	-1.95769	-1.00748	84	H	3.917023	-5.66297	-3.55872
21	C	3.661459	4.274857	-0.7077	85	H	-2.6279	-6.89701	0.264807
22	C	2.507314	5.038963	-0.44128	86	H	-1.11564	-6.43547	-0.51255
23	C	1.39441	4.150693	-0.35103	87	H	-0.66599	-7.78275	1.541976
24	N	1.907583	2.883888	-0.53114	88	H	-0.03468	-6.13017	1.766407
25	N	2.545076	-2.26522	-0.59403	89	H	-1.55852	-6.60749	2.543609
26	C	2.422518	-3.61552	-0.67729	90	H	-4.71804	-6.00538	0.421607
27	C	3.668519	-4.22034	-1.13996	91	H	-5.56206	-4.49299	0.752134
28	C	4.54191	-3.1731	-1.36782	92	H	-5.75322	-6.03013	2.704623
29	C	1.181295	-4.25381	-0.38139	93	H	-4.79563	-4.60083	3.175991
30	C	2.420559	6.535139	-0.30389	94	H	-3.97963	-6.14095	2.837042
31	C	2.116621	7.25549	-1.62999	95	H	-4.0047	5.764141	1.783676
32	C	5.068247	4.798278	-0.83502	96	H	-2.25704	5.70867	1.587484
33	C	5.924176	4.596859	0.427921	97	H	-3.25517	7.367698	0.007416
34	C	5.969699	-3.27851	-1.83213	98	H	-2.53689	6.028166	-0.92615
35	C	7.007879	-2.98858	-0.73292	99	H	-4.29657	6.104325	-0.70271
36	C	3.892374	-5.69056	-1.36813	100	H	-6.40425	2.741134	1.506378
37	C	3.394372	-6.18312	-2.73956	101	H	-5.97482	4.446745	1.494572
38	C	-1.73469	-6.2627	0.385065	102	H	-6.52707	3.6873	3.818128
39	C	-0.95355	-6.72223	1.630021	103	H	-4.82227	4.204685	3.726792
40	C	-4.68322	-5.09311	1.041244	104	H	-5.21745	2.476918	3.755736
41	C	-4.8103	-5.48879	2.523136	105	H	-0.29095	5.401659	0.139098

42	C	-3.20922	5.4587	1.084882	106	H	-0.50111	2.363803	-0.44549
43	C	-3.32991	6.288363	-0.20638	107	H	0.293972	-2.39966	-0.24527
44	C	-5.62895	3.454536	1.831354	108	H	3.66136	-2.04313	1.989016
45	C	-5.54678	3.455181	3.369376	109	H	5.313448	-2.34897	3.82334
46	C	0.012818	4.381085	-0.09838	110	H	6.437712	-0.36612	4.837586
47	C	-0.89352	3.334231	-0.12394	111	H	5.88491	1.923405	4.012455
48	C	0.068937	-3.4671	-0.14486	112	H	4.23262	2.222359	2.185873
49	N	-3.91023	-0.5857	0.17816	113	H	2.168029	-0.57512	0.766547
50	N	3.460896	0.452765	-0.50644	114	H	2.235669	1.187926	1.035011
51	C	3.844676	0.1071	1.951101	115	C	-3.58809	-0.52406	-1.27309
52	C	4.155665	-1.17491	2.42903	116	H	-2.78124	0.202298	-1.40565
53	C	5.084186	-1.34403	3.460701	117	H	-3.22889	-1.51854	-1.56106
54	C	5.713848	-0.23369	4.029943	118	C	-4.78643	-0.15029	-2.12599
55	C	5.405414	1.048914	3.56599	119	C	-5.8245	-1.06854	-2.34834
56	C	4.475988	1.216141	2.536067	120	C	-4.86797	1.117476	-2.7187
57	C	2.830633	0.291486	0.835666	121	C	-6.92185	-0.72553	-3.14084
58	H	-5.85685	0.506972	2.610025	122	H	-5.77088	-2.06236	-1.896
59	H	-5.59001	-2.16103	2.552371	123	C	-5.96379	1.461891	-3.51644
60	H	-1.72257	-1.63668	0.306808	124	H	-4.06564	1.838434	-2.54749
61	H	5.932204	-0.51322	-2.48468	125	C	-6.99417	0.542351	-3.72817
62	H	5.659706	2.139787	-2.32343	126	H	-7.72121	-1.45191	-3.30667
63	H	1.344898	2.055558	-0.66179	127	H	-6.01202	2.453628	-3.97259
64	H	1.135145	-5.34505	-0.37819	128	H	-7.8507	0.810157	-4.35141

Table 15 Coordinates of the optimized structure of *cis* isomer of **3.42** with dichloride.

Atom Label	Symbol	X	Y	Z	Atom Label	Symbol	X	Y	Z
1	Cl	-0.19992	1.441881	2.122809	67	C	3.653923	-0.5398	-1.21145
2	N	-1.19562	-3.0818	0.211475	68	C	3.612025	-1.94486	-0.93432
3	N	-2.4414	2.544607	0.562629	69	N	2.963778	0.419169	-0.48164
4	C	-3.66935	0.523451	1.177049	70	C	0.877162	4.406798	-0.15417
5	C	-3.62222	1.927438	0.899072	71	C	2.419564	2.883007	-0.79548
6	N	-2.96076	-0.43872	0.470466	72	C	3.798049	1.415346	-2.32712
7	C	-0.87618	-4.42364	0.179647	73	H	3.92323	2.134544	-3.12934
8	C	-2.4218	-2.90086	0.820685	74	C	-1.6528	4.932266	0.507577
9	C	-3.85555	-1.42792	2.292228	75	C	3.035756	1.633541	-1.15055
10	H	-4.01793	-2.14309	3.089959	76	C	2.006529	5.117549	-0.6921
11	C	1.648319	-4.9466	-0.51117	77	C	5.128053	0.897289	1.520115
12	C	-3.05278	-1.65247	1.142534	78	H	5.459486	0.422168	0.593865
13	C	-1.98765	-5.13541	0.756875	79	C	5.35001	4.690902	-0.48066
14	C	-5.10756	-0.86746	-1.55616	80	H	6.339708	4.960128	-0.88518
15	H	-5.43895	-0.39333	-0.62963	81	H	5.454754	3.758515	0.095757
16	C	-5.43718	-4.36668	0.784619	82	H	5.041934	5.481164	0.222908
17	H	-6.39103	-4.65676	1.255058	83	C	4.014256	-4.17182	-0.86069

18	H	-5.52285	-3.32213	0.449202	84	C	-0.2957	5.106038	0.235207
19	H	-5.29347	-4.99035	-0.11228	85	H	-0.06063	6.172622	0.253212
20	C	-4.0237	4.154588	0.817326	86	C	2.129048	6.610984	-0.84145
21	C	0.294137	-5.12057	-0.21892	87	H	1.672977	7.11888	0.024331
22	C	-2.08802	-6.6287	0.924528	88	H	3.194853	6.885917	-0.81125
23	H	-1.6267	-7.13783	0.06268	89	C	3.760869	0.936792	1.836809
24	H	-3.14953	-6.92042	0.896789	90	C	4.325206	4.525119	-1.61858
25	C	-3.73836	-0.93133	-1.86031	91	H	4.697356	3.764521	-2.31439
26	C	-4.27014	-4.54792	1.771232	92	H	4.267781	5.460427	-2.19846
27	H	-4.47121	-3.96911	2.683119	93	C	4.191252	0.084927	-2.35659
28	H	-4.24038	-5.59727	2.101427	94	H	4.683296	-0.43226	-3.1755
29	C	-4.24507	-0.09803	2.306231	95	C	2.618434	-3.92464	-0.60527
30	H	-4.76344	0.421086	3.107385	96	C	4.627429	-2.93501	-1.08429
31	C	-2.624	3.908017	0.585358	97	C	3.358538	1.569261	3.02306
32	C	-4.64024	2.917789	1.031627	98	H	2.293364	1.622775	3.261103
33	C	-3.33832	-1.56127	-3.04879	99	C	4.683278	-5.51882	-0.85605
34	H	-2.27253	-1.63401	-3.27822	100	H	4.095717	-6.22792	-1.4653
35	C	-4.69261	5.501634	0.800307	101	H	5.65961	-5.43427	-1.35891
36	H	-4.11724	6.210385	1.421548	102	C	2.947408	4.180457	-1.10775
37	H	-5.6787	5.417037	1.283729	103	C	6.086198	-2.67144	-1.34755
38	C	-2.92533	-4.20028	1.180648	104	H	6.469101	-3.42238	-2.0596
39	C	-6.10389	2.656926	1.269988	105	H	6.198207	-1.69528	-1.84265
40	H	-6.49501	3.403695	1.982045	106	C	1.505699	7.154935	-2.13997
41	H	-6.2275	1.677556	1.755679	107	H	1.632138	8.247807	-2.20788
42	C	-1.45456	-7.15049	2.226742	108	H	0.428335	6.930712	-2.18935
43	H	-1.56093	-8.24486	2.303853	109	H	1.977579	6.700787	-3.02623
44	H	-0.38141	-6.90611	2.273105	110	C	4.88793	-6.11562	0.548668
45	H	-1.93424	-6.69753	3.109417	111	H	5.393642	-7.09295	0.48688
46	C	-4.86873	6.099252	-0.60788	112	H	3.926147	-6.2614	1.065263
47	H	-5.37522	7.076764	-0.55605	113	H	5.502219	-5.45226	1.178046
48	H	-3.89652	6.244679	-1.10459	114	C	6.074508	1.469551	2.375027
49	H	-5.4702	5.436239	-1.24984	115	H	7.134913	1.430333	2.113179
50	C	-6.05754	-1.41296	-2.42446	116	C	5.66729	2.087745	3.561824
51	H	-7.11913	-1.35512	-2.17109	117	H	6.407151	2.533376	4.231153
52	C	-5.65231	-2.02838	-3.61307	118	C	2.707699	0.273064	0.962603
53	H	-6.39477	-2.45314	-4.29303	119	H	1.708353	0.65231	1.210304
54	C	-2.6802	-0.2961	-0.96983	120	H	2.674618	-0.8054	1.164029
55	H	-1.68715	-0.69716	-1.20701	121	C	4.307585	2.135742	3.880215
56	H	-2.61753	0.781612	-1.16815	122	H	3.977368	2.62557	4.799578
57	C	-4.29091	-2.10068	-3.91941	123	C	6.958418	-2.68466	-0.07919
58	H	-3.9619	-2.58847	-4.84031	124	H	8.00934	-2.46279	-0.32671
59	C	-6.95699	2.683447	-0.01118	125	H	6.929024	-3.66666	0.418826
60	H	-8.01198	2.462225	0.218984	126	H	6.611767	-1.93312	0.647936
61	H	-6.91807	3.669589	-0.50022	127	H	1.537722	-2.12722	-0.92701

62	H	-6.60146	1.937454	-0.73965	128	H	0.665605	2.352702	0.346155
63	H	-1.54617	2.105682	0.916046	129	Cl	0.184859	-1.52892	-2.16335
64	H	-0.69174	-2.38372	-0.36948	130	H	-2.1252	5.899155	0.699497
65	N	1.182241	3.061612	-0.20923	131	H	2.11798	-5.91471	-0.70397
66	N	2.437128	-2.56033	-0.57814	132	H	0.064382	-6.18822	-0.2209

Table 16 Coordinates of the optimized structure of *trans* isomer of **3.42** with dichloride.

Atom Label	Symbol	X	Y	Z	Atom Label	Symbol	X	Y	Z
1	Cl	-0.63392	-0.11217	1.856629	67	N	-1.72653	2.038315	-2.5464
2	N	1.726534	-2.03832	2.546402	68	N	2.298075	1.99673	0.029296
3	N	-2.29808	-1.99673	-0.0293	69	C	1.730709	3.833865	-1.3926
4	C	-1.73071	-3.83387	1.392598	70	C	2.609788	3.236869	-0.43155
5	C	-2.60979	-3.23687	0.431547	71	N	0.392197	3.465683	-1.40639
6	N	-0.3922	-3.46568	1.406388	72	C	-2.96639	1.644257	-2.98874
7	C	2.966391	-1.64426	2.988744	73	C	-1.42018	3.285794	-3.02328
8	C	1.420175	-3.28579	3.023277	74	C	0.795141	4.617349	-3.31029
9	C	-0.79514	-4.61735	3.310285	75	H	0.681659	5.005593	-4.31908
10	H	-0.68166	-5.00559	4.31908	76	C	-2.93323	-0.32772	-1.57199
11	C	2.933225	0.327723	1.571989	77	H	-2.029	0.109152	-1.14233
12	H	2.029003	-0.10915	1.142326	78	C	-0.18102	3.871297	-2.60805
13	C	0.181021	-3.8713	2.608052	79	C	-3.47672	2.70496	-3.80877
14	C	3.47672	-2.70496	3.808771	80	C	-0.21757	5.546734	0.70819
15	C	0.217569	-5.54673	-0.70819	81	H	-0.31084	5.924944	-0.31336
16	H	0.310836	-5.92494	0.313363	82	C	-3.18499	6.159217	-3.51056
17	C	3.184987	-6.15922	3.510556	83	H	-3.25887	7.135522	-4.01678
18	H	3.25887	-7.13552	4.016781	84	H	-2.52441	6.277082	-2.63684
19	H	2.524414	-6.27708	2.636837	85	H	-4.18642	5.891336	-3.13657
20	H	4.186424	-5.89134	3.136567	86	C	4.141208	2.657113	1.156891
21	C	-4.14121	-2.65711	-1.15689	87	C	-3.54712	0.417701	-2.56502
22	C	3.547122	-0.4177	2.565016	88	H	-4.47686	0.100765	-3.03989
23	H	4.476862	-0.10077	3.039891	89	C	-4.8144	2.699613	-4.49719
24	C	4.814397	-2.69961	4.497187	90	H	-5.55058	2.174366	-3.866
25	H	5.550578	-2.17437	3.866002	91	H	-5.18577	3.732609	-4.59464
26	H	5.185767	-3.73261	4.594636	92	C	-0.20144	4.162205	0.940941
27	C	0.201444	-4.16221	-0.94094	93	C	-2.64431	5.083315	-4.46987
28	C	2.644307	-5.08332	4.469872	94	H	-1.66497	5.407785	-4.85773
29	H	1.664969	-5.40779	4.857733	95	H	-3.3069	5.010574	-5.3474
30	H	3.306902	-5.01057	5.3474	96	C	1.972917	4.594184	-2.55989
31	C	-1.97292	-4.59418	2.55989	97	H	2.944344	4.96613	-2.87521
32	H	-2.94434	-4.96613	2.875209	98	C	3.188426	1.591756	0.996084
33	C	-3.18843	-1.59176	-0.99608	99	C	3.791269	3.673119	0.257254
34	C	-3.79127	-3.67312	-0.25725	100	C	-0.08437	3.692997	2.25691
35	C	0.084371	-3.693	-2.25691	101	H	-0.08947	2.615121	2.44237

36	H	0.089467	-2.61512	-2.44237	102	C	5.265963	2.674573	2.154709
37	C	-5.26596	-2.67457	-2.15471	103	H	5.783132	1.699317	2.139083
38	H	-5.78313	-1.69932	-2.13908	104	H	6.016468	3.418098	1.841619
39	H	-6.01647	-3.4181	-1.84162	105	C	-2.51363	3.726016	-3.83254
40	C	2.513631	-3.72602	3.832541	106	C	4.454367	5.013127	0.085971
41	C	-4.45437	-5.01313	-0.08597	107	H	5.541937	4.898839	0.230236
42	H	-5.54194	-4.89884	-0.23024	108	H	4.322573	5.35477	-0.95313
43	H	-4.32257	-5.35477	0.953134	109	C	-4.77674	2.041506	-5.88877
44	C	4.776736	-2.04151	5.888773	110	H	-5.77468	2.053972	-6.3567
45	H	5.774677	-2.05397	6.356704	111	H	-4.44163	0.993727	-5.82431
46	H	4.441628	-0.99373	5.82431	112	H	-4.07821	2.569138	-6.55816
47	H	4.078208	-2.56914	6.558162	113	C	4.815847	2.987074	3.5939
48	C	-4.81585	-2.98707	-3.5939	114	H	5.677158	2.981681	4.281828
49	H	-5.67716	-2.98168	-4.28183	115	H	4.084502	2.247289	3.955814
50	H	-4.0845	-2.24729	-3.95581	116	H	4.336302	3.976681	3.652701
51	H	-4.3363	-3.97668	-3.6527	117	C	-0.11314	6.446888	1.771091
52	C	0.11314	-6.44689	-1.77109	118	H	-0.12883	7.522153	1.575934
53	H	0.128825	-7.52215	-1.57593	119	C	0.004339	5.97336	3.082968
54	C	-0.00434	-5.97336	-3.08297	120	H	0.082778	6.677312	3.915084
55	H	-0.08278	-6.67731	-3.91508	121	C	-0.40332	3.164279	-0.18457
56	C	0.403315	-3.16428	0.184574	122	H	-1.45269	3.197524	-0.49745
57	H	1.452692	-3.19752	0.497445	123	H	-0.21835	2.141554	0.164235
58	H	0.218346	-2.14155	-0.16424	124	C	0.015824	4.596723	3.320738
59	C	-0.01582	-4.59672	-3.32074	125	H	0.102577	4.217768	4.341974
60	H	-0.10258	-4.21777	-4.34197	126	C	3.925516	6.099907	1.038887
61	C	-3.92552	-6.09991	-1.03889	127	H	4.434505	7.060039	0.853239
62	H	-4.43451	-7.06004	-0.85324	128	H	4.094808	5.823246	2.091608
63	H	-4.09481	-5.82325	-2.09161	129	H	2.842894	6.250296	0.90808
64	H	-2.84289	-6.2503	-0.90808	130	H	1.661661	1.341146	-0.4849
65	H	-1.66166	-1.34115	0.484904	131	H	-0.97288	1.378591	-2.22651
66	H	0.972877	-1.37859	2.226506	132	Cl	0.63392	0.11217	-1.85663

Table 17 Selected transitions, oscillator strength, symmetry calculated (H = HOMO, L = LUMO) from DFT analysis for bronzaphyrin **3.38**.

S. No.	Wavelength (nm)	Oscillator strength	Symmetry	Major contributors
1	810.401	0.4128	Singlet-A	H-1->L+1 (11%), H->L (85%)
2	761.100	0.1204	Singlet-A	H-1->L (73%), H->L+1 (20%)
3	483.780	0.425	Singlet-A	H-3->L (37%), H-1->L (18%), H->L+1 (44%)
4	423.4403	0.2607	Singlet-A	H-5->L (63%), H-1->L+1 (25%)
5	414.687	1.1666	Singlet-A	H-6->L (11%), H-5->L (18%), H-1->L+1 (60%)

Table 18 Selected transitions, oscillator strength, symmetry calculated (H = HOMO, L = LUMO) from DFT analysis for bronzaphyrin **3.38.H_2^{2+}**.

S. No.	Wavelength (nm)	Oscillator strength	Symmetry	Major contributors
1	802.845	0.2895	Singlet-A	H-1->L+1 (20%), H->L (82%)
2	771.857	0.0569	Singlet-A	H-1->L (71%), H->L+1 (29%)
3	496.868	0.6741	Singlet-A	H-1->L (33%), H->L+1 (72%)
4	439.673	1.701	Singlet-A	H-1->L+1 (79%), H->L (23%)
5	383.019	0.082	Singlet-A	H-8->L (98%)
6	352.015	0.071	Singlet-A	H-3->L+1 (98%)

Table 19 Selected transitions, oscillator strength, symmetry calculated (H = HOMO, L = LUMO) from DFT for bronzaphyrin **3.42**.

S. No.	Wavelength (nm)	Oscillator strength	Symmetry	Major contributors
1	840.394	0.3557	Singlet-A	H-1->L (22%), H->L (72%)
2	799.428	0.3282	Singlet-A	H-1->L (63%), H->L (26%), H->L+1 (11%)
3	429.082	1.6405	Singlet-A	H-1->L (18%), H->L+1 (73%)
4	415.382	0.1088	Singlet-A	H-8->L (51%), H-1->L+1 (15%), H-12->L (11%), H-10->L (11%)
5	412.562	0.6284	Singlet-A	H-8->L (11%), H-1->L+1 (72%)

Table 19 Selected transitions, oscillator strength, symmetry calculated (H = HOMO, L = LUMO) from DFT for bronzaphyrin **3.42.H_2^{2+}**.

S. No.	Wavelength (nm)	Oscillator strength	Symmetry	Major contributors
1	807.078	0.306	Singlet-A	H-1->L+1 (13%), H->L (90%)
2	739.713	0.1864	Singlet-A	H-1->L (74%), H->L+1 (26%)
3	439.470	1.4927	Singlet-A	H-1->L (26%), H-1->L+1 (11%), H->L+1 (64%)
4	423.802	1.2712	Singlet-A	H-1->L+1 (74%), H->L (14%)

3.10 ORTEP diagrams

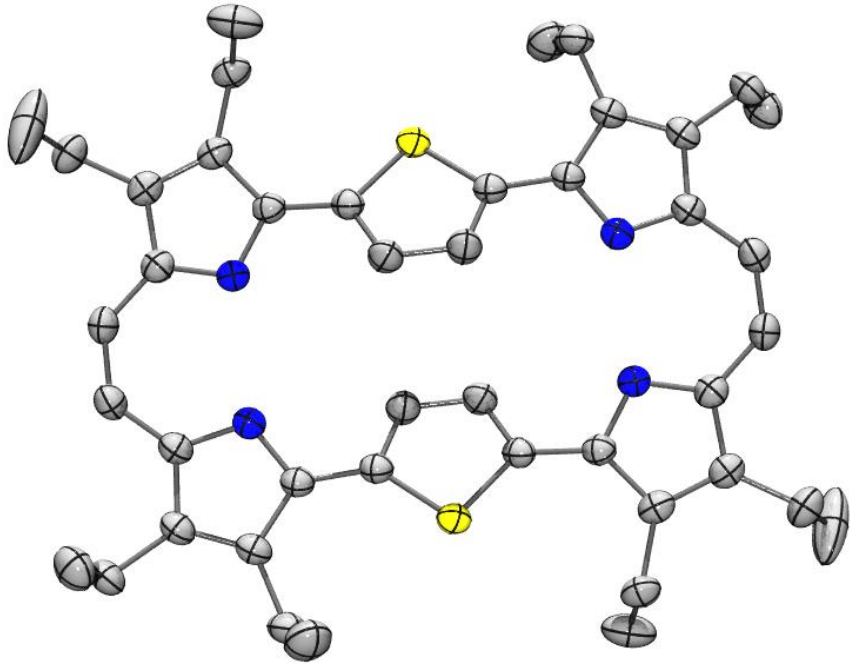

Figure 3.91 ORTEP-POVRAY diagram of **3.38** (top view). All hydrogens are excluded for clarity and thermal ellipsoids are scaled up to 50% probability level. Color code: grey = Carbon, blue = Nitrogen and yellow = Sulphur.

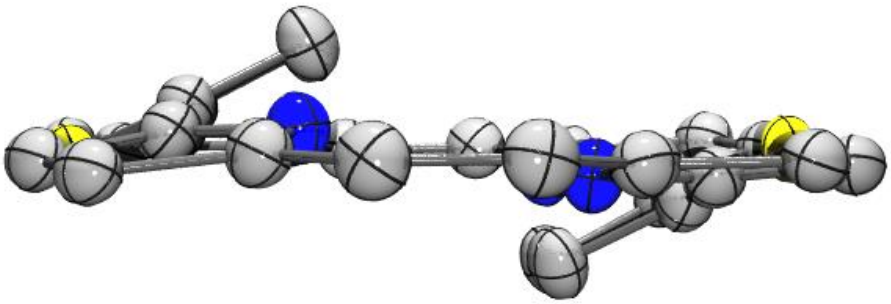

Figure 3.92 ORTEP-POVRAY diagram of **3.38** (side view). All hydrogens and ethyl groups are excluded for clarity and thermal ellipsoids are scaled up to 50% probability level. Color code: grey = Carbon, blue = Nitrogen and yellow = Sulphur.

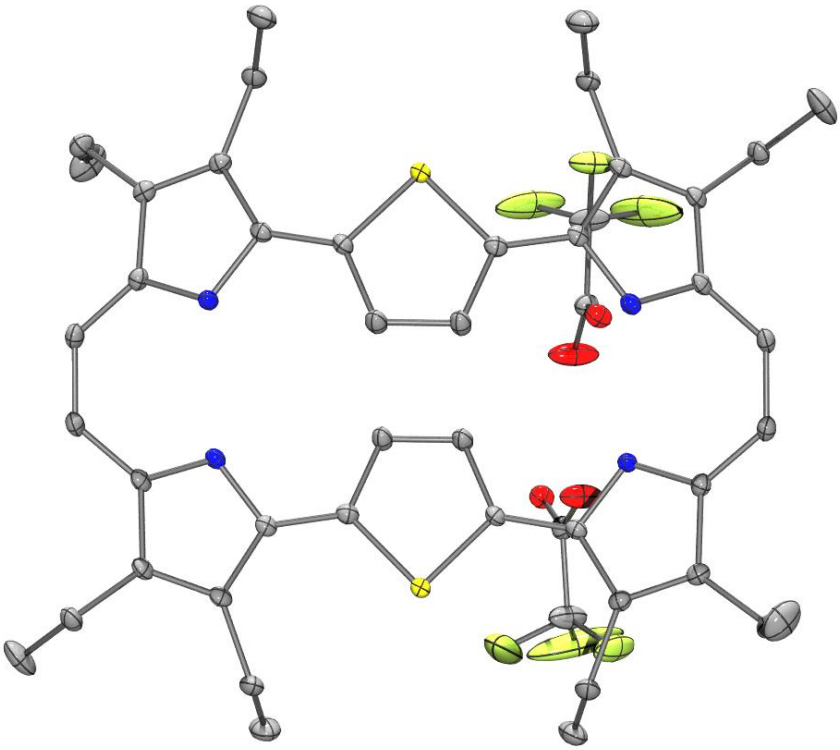

Figure 3.93 ORTEP-POVRAY diagram of **3.38.H$_2$**$^{2+}$ (top view). All hydrogens are excluded for clarity and thermal ellipsoids are scaled up to 50% probability level. Color code: grey = Carbon, blue = Nitrogen, yellowish green = Fluorine, red = Oxygen and yellow = Sulphur.

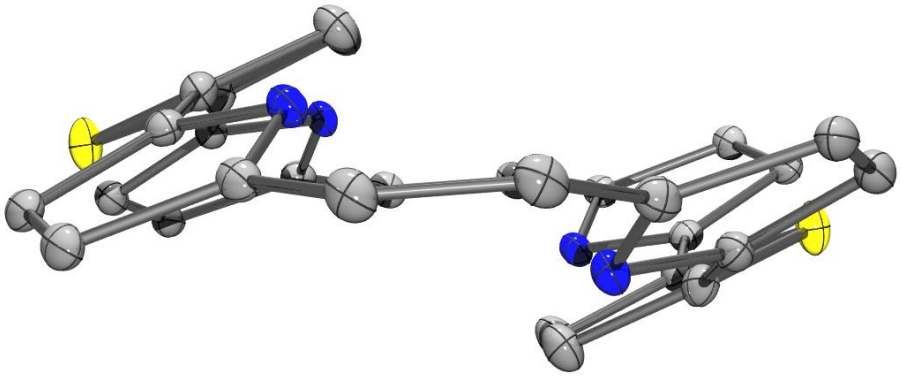

Figure 3.94 ORTEP-POVRAY diagram of **3.38.H$_2$**$^{2+}$ (side view). All hydrogens, TFA and ethyl groups are excluded for clarity and thermal ellipsoids are scaled upto 50% probability level. Color code: grey = Carbon, blue = Nitrogen and yellow = Sulphur.

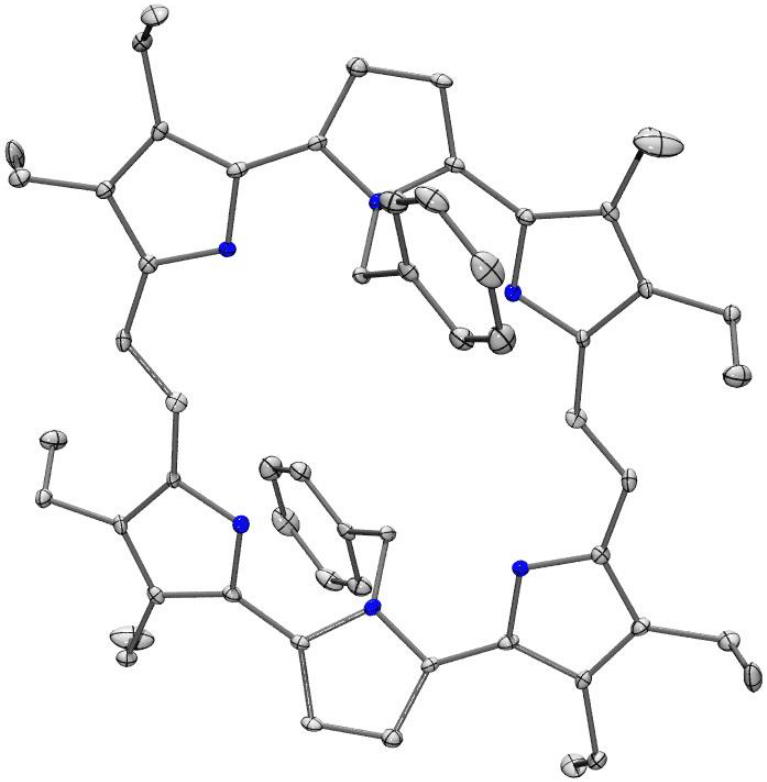

Figure 3.95 ORTEP-POVRAY diagram of **3.42**.$\mathbf{H_2}^{2+}$ All hydrogens and chloride ion are excluded for clarity and thermal ellipsoids are scaled up to 50% probability level. Color code: grey = Carbon, blue = Nitrogen.

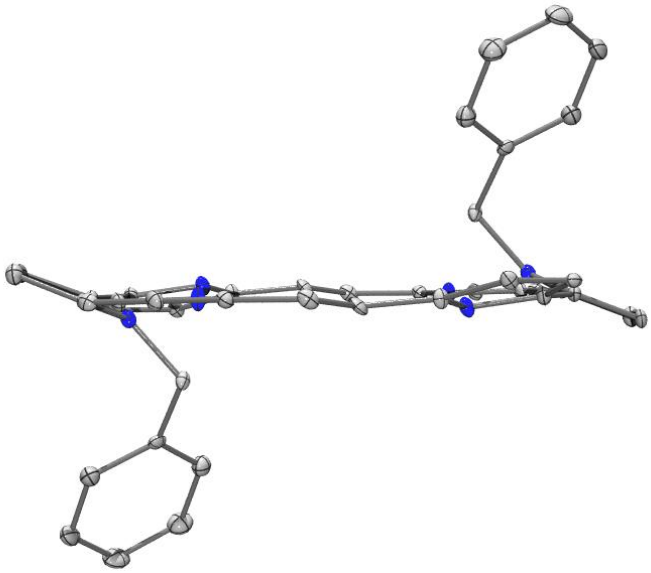

Figure 3.96 ORTEP-POVRAY diagram of **3.42**.$\mathbf{H_2}^{2+}$ All hydrogens, chloride ion and ethyl groups are excluded for clarity. Thermal ellipsoids are scaled up to 50% probability level. Color code: grey = Carbon, blue = Nitrogen.

CHAPTER 4

Tetrathiabronzaphyrin

4.1 Introduction

Synthetic procedures for obtaining terpyrrole were very limited, though it forms a major constituent in different expanded porphyrins such as orangarin,[1] amethyrin[2] and bronzaphyrin.[3] The first synthetic report can be traced back to 1964, where Rapoport et al. utilized acid catalysis, followed by dehydrogenation to yield α-carboethoxy substituted terpyrrole **4.6**, which was further deprotected to give α-free terpyrrole **4.7** as shown in Scheme 4.1.[4] The ester protection group was imminent to prevent the oxidative degradation, that generally happens with α-free pyrrolic compounds, and could be deprot-

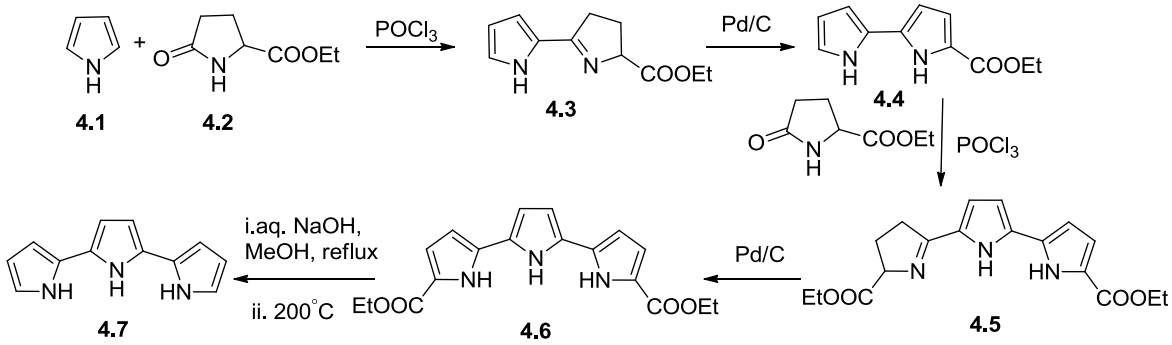

Scheme 4.1 Synthesis of terpyrrole by Rapoport et al.

ected when and where required. The above synthesis involves multiple steps with very minimal overall yield, hence LeGeoff and coworkers developed an alternative strategy, by making the central pyrrolic ring as the key step through transformation of the corresponding the 1,4-diketo compound **4.9** using Paal-Knorr approach (Scheme 4.2).[5]

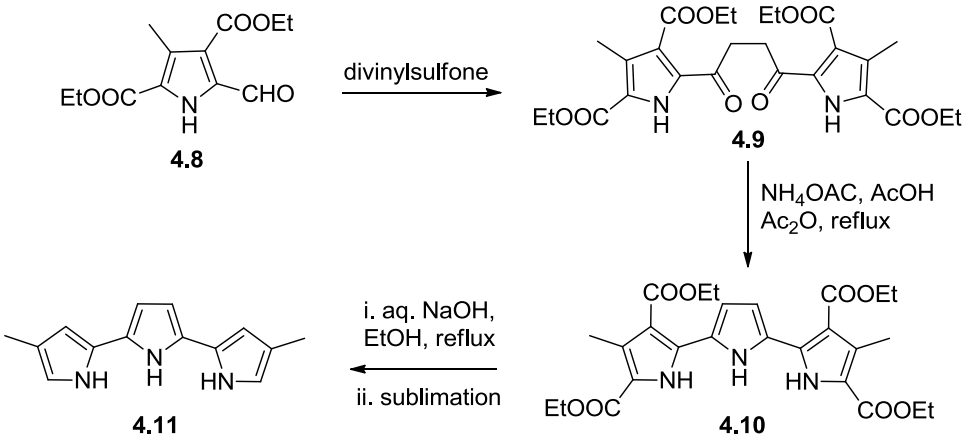

Scheme 4.2 Synthesis of terpyrrole reported by LeGeoff and coworkers.

This approach was later extended by Sessler's group in synthesizing hexaalkyl substituted terpyrrole **4.15**, as good resourceful materials, as they can provide sufficient electron density at α-positions, thereby facilitating electrophilic attack and the full β-substitution

creates a helical effect, due to steric strain, that led to macrocyclization rather than polymerization, in moderate yields as shown in Scheme 4.3.[1]

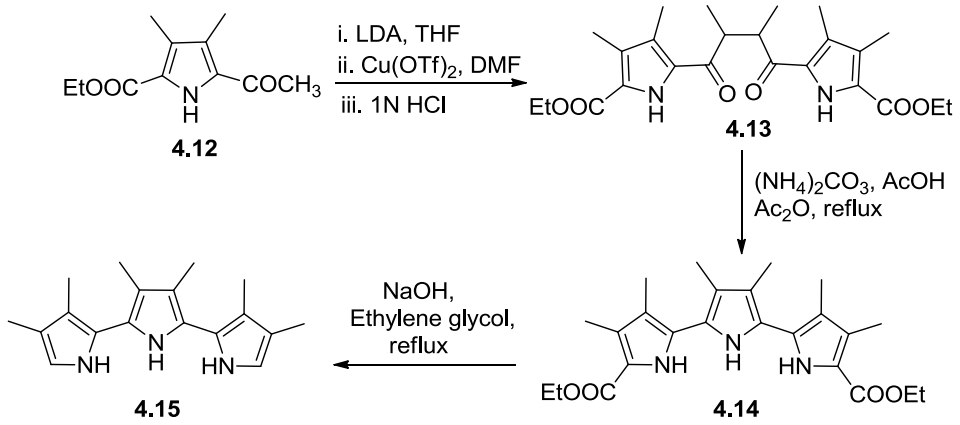

Scheme 4.3 Synthesis of hexaalkylterpyrrole **4.15**.

Further, Carretero and coworkers developed metal catalyzed 1,3-dipolar cycloaddition reactions of bis(azomethine ylide) substituted pyrrole/thiophene with trans-1,2-bis(phenylsulfonyl)ethylene to yield terpyrrole derivative **4.18** in a good yield (Scheme 4.4).[6] However, it needs another step for deprotecting the benzyl group to get N-unprotected terpyrrole.

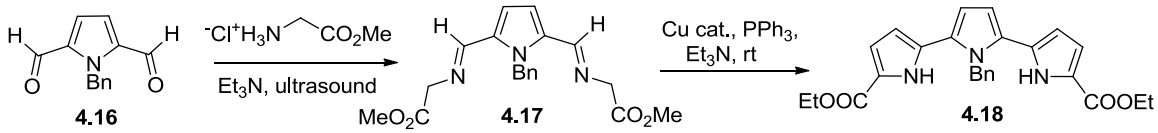

Scheme 4.4 Synthesis of N-benzyl substituted terpyrrole using 1,3-dipolar cycloaddition.

Though the above syntheses of terpyrroles look elegant in nature, they suffer from a poor to moderate yields with large number of steps. Furthermore, the terpyrroles has to be protected or capped at α-positions to stabilize the molecules. Hence there is a scope to develop terpyrroles with much less laborious methods and with good yields. In the meanwhile, Setsune and coworkers highlighted the versatility of the Suzuki-Miyaura cross- coupling reaction in synthesizing bispyrrolyl arenes in good yields as shown in Scheme 4.5.[7]

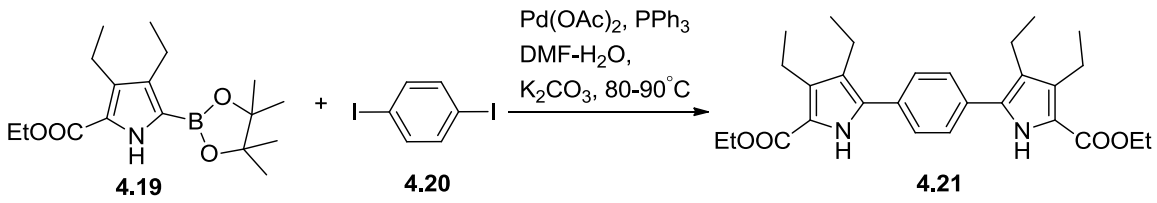

Scheme 4.5 Synthesis of one of the derivatives of bispyrrolylarenes.

Recently Sessler's group demonstrated this approach in the preparation of cyclo[m]pyridine[n]pyrroles for *e.g.* **4.24**, which display fascinating properties such as expanded conjugation on protonation, dynamic twisting and as sensors for organic solvents and anions (Scheme 4.6).[8]

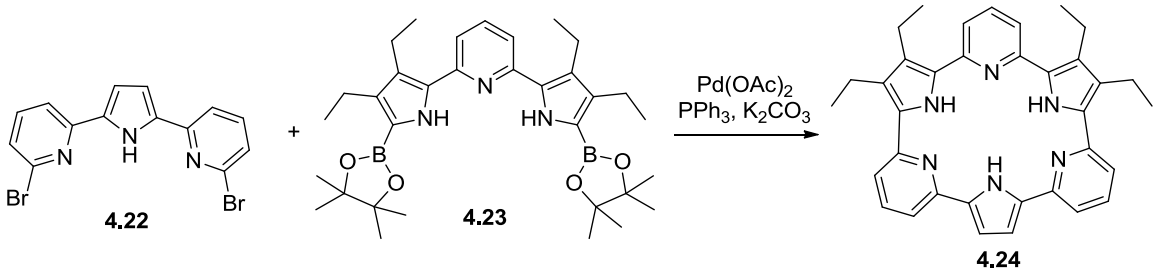

Scheme 4.6 Synthesis of cyclo[m]pyridine[n]pyrroles through Suzuki coupling.

So having seen the importance of this efficient single step approach, we wanted to utilize it in synthesizing terpyrrole and further demonstrate its utility in novel bronzaphyrin synthesis.

4.2 Research goal

As explained above, we wish to utilize the Suzuki protocol in synthesizing stable α-free terpyrrole without any protection, so that it can be employed in further course of reactions with ease. As shown in the Scheme 4.7 below, we opted for an N-unprotected dithiaterpyrrole derivative purely for exploring the ability of the resultant bronzaphyrin towards aromatization, once the macrocycle has been synthesized. We anticipate Cava and coworkers have failed because of their N-protected approach, which hindered the aromatization. In addition, introduction of ester groups with long alkyl chains of isopentyl groups at the β-positions of central pyrrole ring not only stabilizes the α-free terpyrrole but also enhances its solubility along with that of the bronzaphyrin macrocycle. We have also envisioned that the presence of strong electron withdrawing ester groups on the periphery of the macrocycle may stabilize the 28π nonaromatic reduced bronzaphyrin species, as it was easily oxidized in previous cases.[3a-c] In addition, we wanted to assess

the stability, photophysical and structural aspects of both the reduced and oxidized bronzaphyrins.

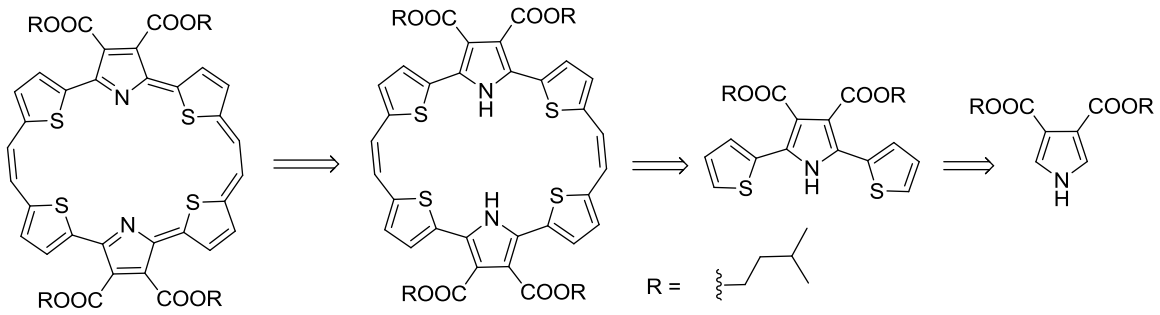

Scheme 4.7 Retrosynthetic approach of tetrathiabronzaphyrin.

4.3 Results and discussion

4.3.1 Synthesis of bronzaphyrin

As emphasized, to enhance the solubility we have opted in synthesizing diisopentylfumarate **4.27** from the corresponding starting materials of isopentanol **4.25** and fumaric acid **4.26** in presence of catalytic conc. H_2SO_4 as shown in Scheme 4.8, in more than 90% yield.

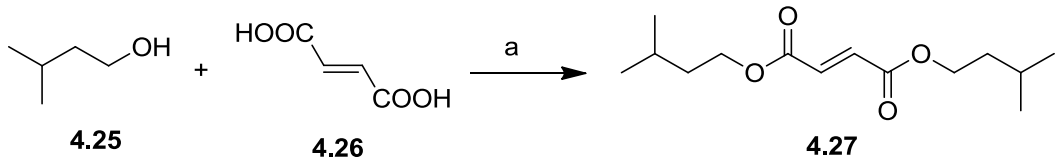

Scheme 4.8 Synthesis of diisopentylfumarate. a) conc. H_2SO_4, reflux, 12 h.

The fumarate ester **4.27** thus obtained was treated with TOSMIC in presence of NaH at 0°C to yield diisopentyl-pyrrole-3,4dicarboxylate **4.28** in 62% yield (Scheme 4.9).

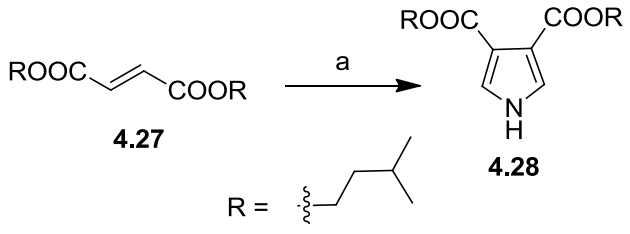

Scheme 4.9 Synthesis of diisopentyl-pyrrole-3,4dicarboxylate. a) NaH, TOSMIC, dry THF, 0°C.

The pyrrole ester **4.28** was then converted to its diiodo derivative **4.29** under reflux in methanol using periodic acid/iodine as the iodinating agent to give 94% yield (Scheme 4.10). All reactions involving other reagents gave lesser yields.

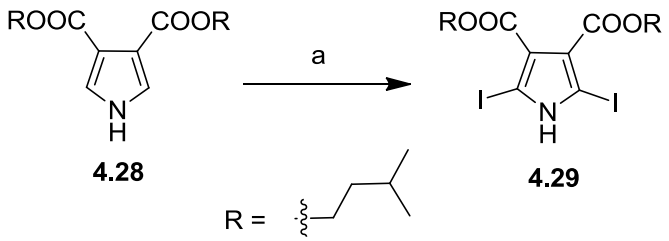

Scheme 4.10 Synthesis of diiodo derivativeof pyrrole ester **4.29**. a) H_5IO_6, I_2, methanol, reflux.

The diiodo derivative **4.29** was then subjected to Suzuki protocol conditions in presence of borylthiophene **4.30** to obtain α-free dithiaterpyrrole **4.31** in a good yield of 54% as shown in Scheme 4.11.

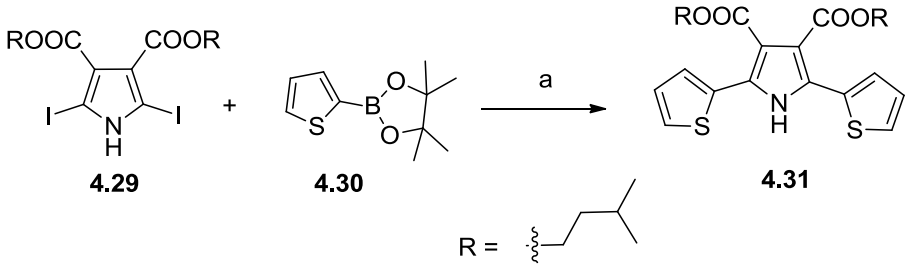

Scheme 4.11 Synthesis of dithiaterpyrrole **4.31**. a) $Pd(OAc)_2$, PPh_3, K_2CO_3, DMF-H_2O, 85°C.

The terpyrrole **4.31** was further formylated under Vilsmeier-Haack conditions to give the corresponding dialdehyde derivative **4.32** in a good yield of 85% (Scheme 4.12). Due to the presence of two isopentyl groups the terpyrrole dialdehyde 4.32 is highly soluble in organic solvents.

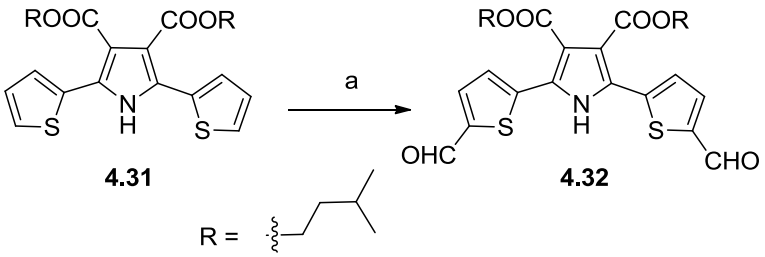

Scheme 4.12 Synthesis of terpyrrole dialdehyde **4.32**. a) DMF, $POCl_3$, DCE, reflux, and then aq. NaOAc, reflux.

Having the terpyrrole dialdehyde **4.32** in hand, we subjected it to McMurry coupling following Ibers's conditions to give the reduced tetrathiabronzaphyrin **4.33** as a bright orange colour spot in 18% yield as shown in Scheme 4.13.

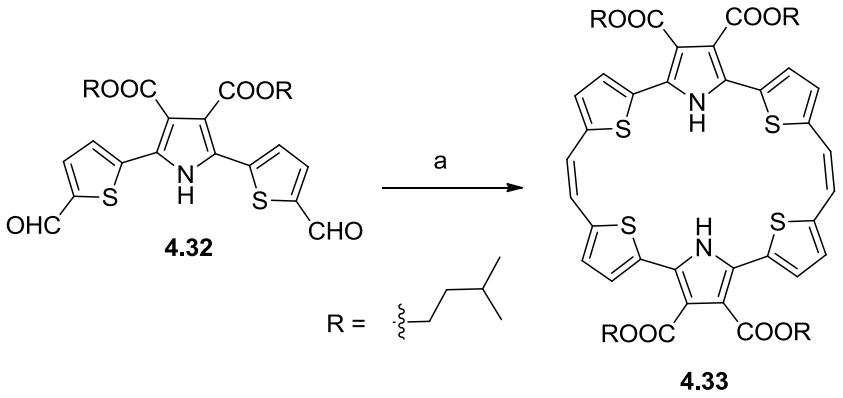

Scheme 4.13 Synthesis of reduced tetrathiabronzaphyrin **4.33**. a) Zn, $TiCl_4$, THF, pyridine, reflux, 16 h.

The reduced system **4.33** thus obtained was dissolved in DCM/chloroform and fortunately, oxidation with MnO_2 led to the corresponding oxidized macrocycle **4.34** as the first aromatic tetrathiabronzaphyrin in almost quantitative yield (Scheme 4.14).

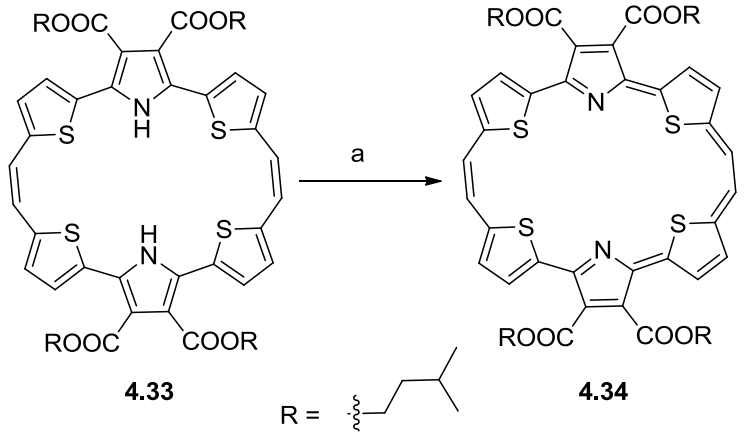

Scheme 4.14 Synthesis of oxidized tetrathiabronzaphyrin **4.34**. a) MnO_2, DCM/chloroform, rt.

4.3.2 ^{1}H NMR studies

As expected the reduced bronzaphyrin **4.33** showed a characteristic NMR spectrum corresponding to a nonaromatic species with two protons resonating at 9.5 ppm and were assigned to be NH protons from a D_2O exchange study (Figure 4.1). The meso and two sets of β-protons were found to resonate as three broad singlets between 6.5 and 7.5 ppm. After the D_2O exchange, the β-protons got resolved and resonated as doublets at 7 and 7.4 ppm, respectively and the meso protons were found to resonate as a singlet at 6.6 ppm. In oxidized bronzaphyrin **4.34**, due to the diamagnetic ring current effect, the meso and β-protons are much more deshielded and resonate as broad singlets at 10.8 and 11.4 ppm, respectively (Figure 4.2). Even the alkoxy protons were deshielded further and resonated

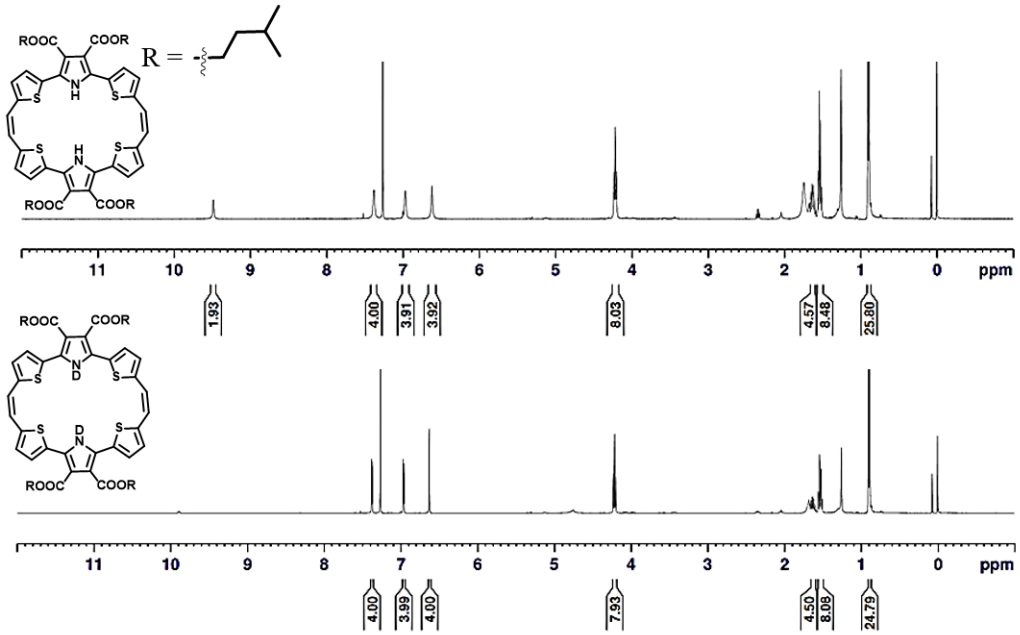

Figure 4.1 ^{1}H NMR spectrum of **4.33** in $CDCl_3$ (top) and $CDCl_3$ + D_2O (bottom).

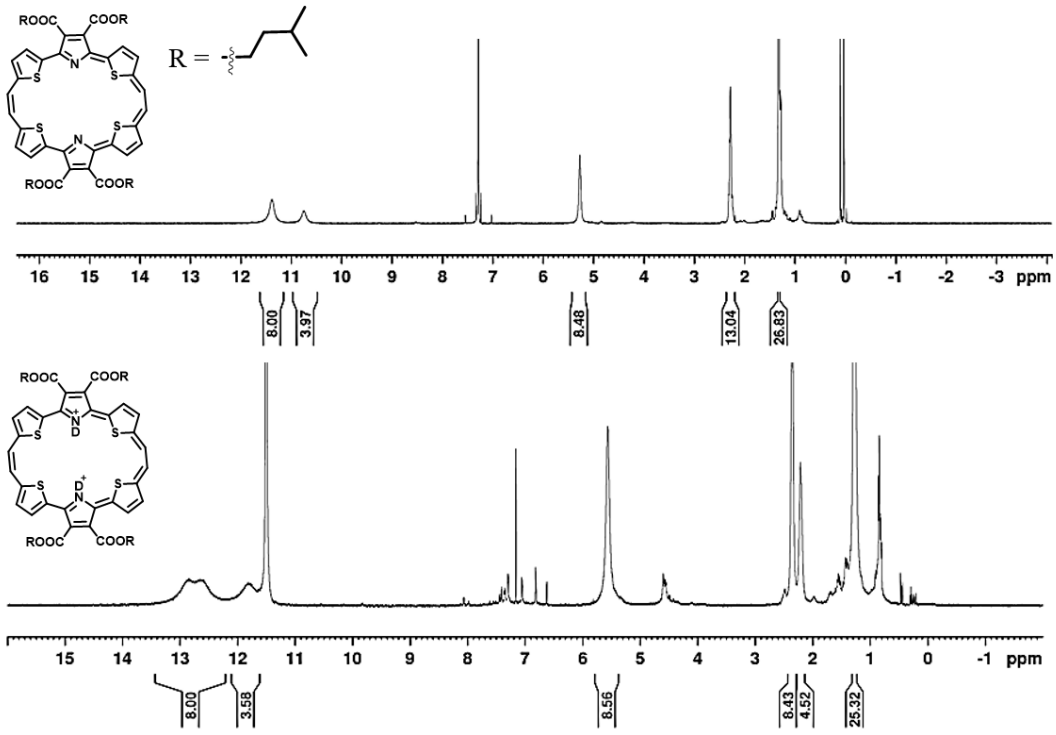

Figure 4.2 ^{1}H NMR spectrum of **4.34** in $CDCl_3$ (top) and TFA-*d* (bottom).

as a broad singlet at 5.3 ppm. However, ^{1}H NMR of tetrathiabronzaphyrin salt, could be achieved as a fully protonated species only when recorded in presence of TFA-*d*. The spectrum is similar to that of freebase with meso-protons resonating as singlet and β-protons as a doublet and deshielded to 11.8 and 12.8 ppm, respectively. However, the

compound looked gradually decomposing, which can be seen as small impurity signals being generated.

4.3.3 UV-Vis-NIR and fluorescence studies

UV-Vis-NIR absorption spectra of both the reduced and oxidized bronzaphyrins **4.33** and **4.34** clearly exhibit the characteristic difference between nonaromatic and aromatic species. While the nonaromatic reduced bronzaphyrin **4.33** displayed blue shifted absorption band with a peak maximum at 345 nm (ε = 1.24 X 10^5), due to lack of conjugation and the oxidized species **4.34**, due to its characteristic aromatic nature display an intense Soret band at 499 nm (ε = 1.75 X 10^5) and much bathochromically shifted low energy Q bands at 812 and 991 nm separated by a shoulder at 882 nm, when compared to the dithiabronzaphyrins **3.18** and **3.38** (Figure 4.3).[3a] The high molar extinction coefficie-

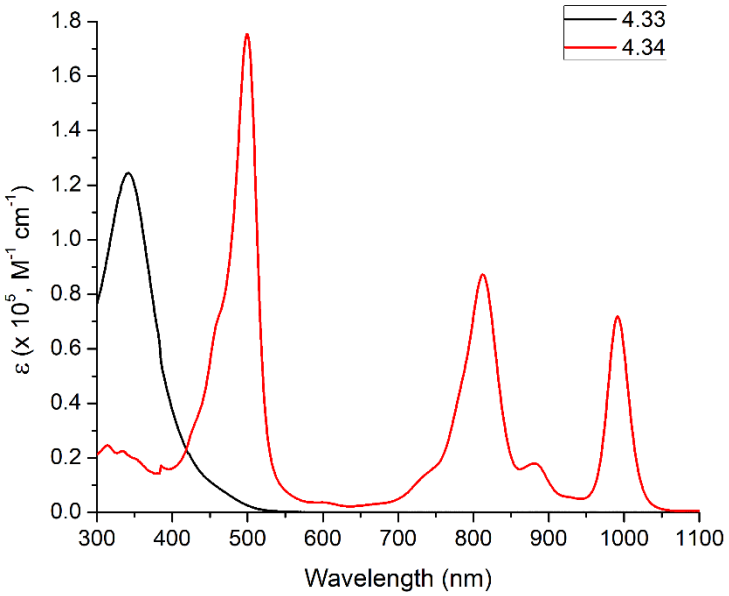

Figure 4.3 UV-Vis-NIR absorption spectra of bronzaphyrins **4.33** and **4.34** measured in chloroform.

nt of bronzaphyrin **4.34** compared to dithiabronzaphyrin **3.38** may be ascribed to its nearly planar structure and is comparable with the previously reported bronzaphyrin **3.18** (ε = 1.9 x 10^5). As protonation often leads to interesting photophysical properties, we performed protonation study for **4.34** in presence of HCl (added as methanolic solution). Surprisingly, it led to a blue shifted less intense Soret band at 415 nm and a much red shifted lowest energy band at 1077 nm at initial stages of protonation (Figure 4.4).

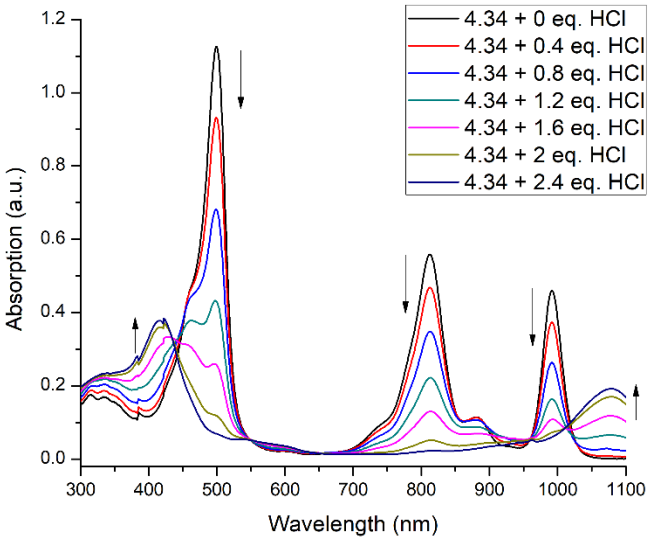

Figure 4.4 Acidometric titration spectra of **4.34** in chloroform up to 2.4 eq. of HCl.

Further, addition of HCl up to 20 eq. led to a complete transformation generating a single blue shifted absorption band indicating the formation of a nonaromatic species as shown in Figure 4.5. This result may probably ascribed to the proton coupled reduction reaction, which was recently observed in case of an extended rosarian derivative.[9]

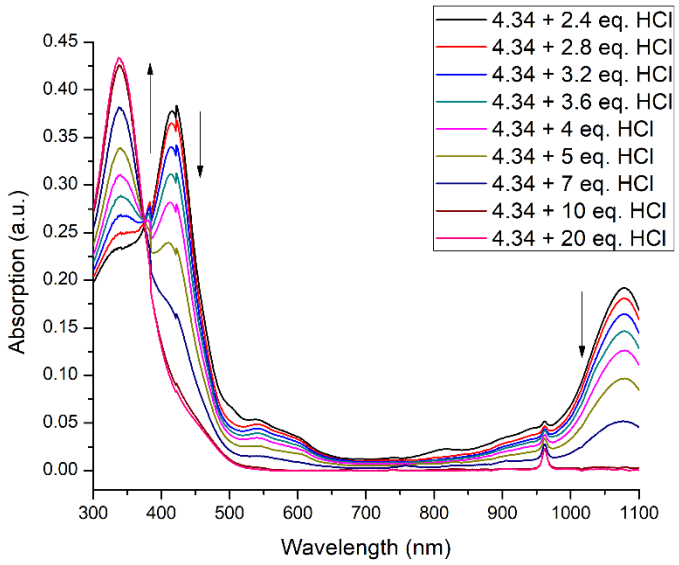

Figure 4.5 Acidometric titration spectra of **4.34** in chloroform from 2.4 eq. to 20 eq. of HCl.

In this scenario, the 26π-aromatic **4.34** may be reducing to 28π-nonaromatic species via a 27π-radical species, and this presumption was supported by the initial studies done using EPR spectroscopy, which clearly showed formation of the radical (Figure 4.6).

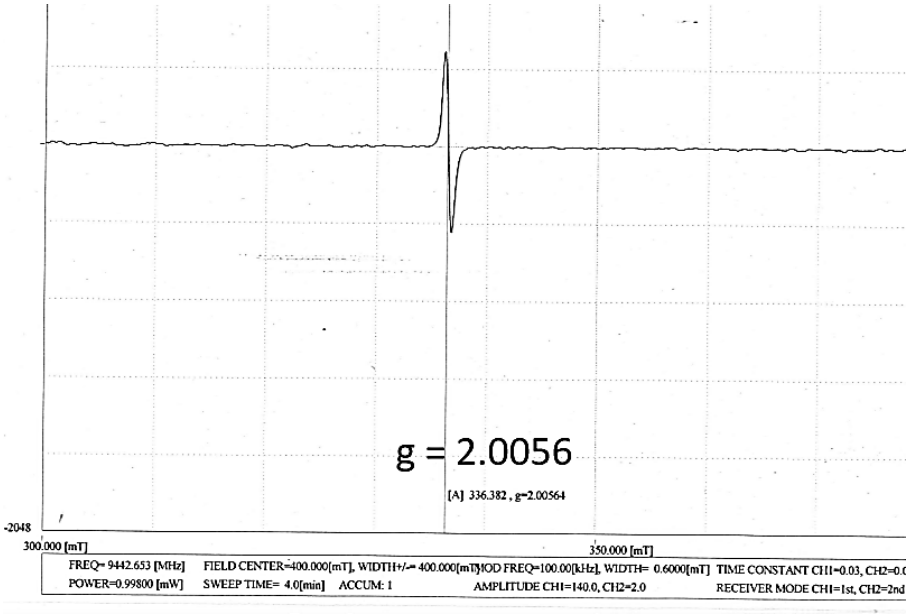

Figure 4.6 EPR spectrum of 27π-radical species.

Quenching with triethylamine led to the generation of freebase at the initial stages of protonation but becomes irreversible at later stages once upon formation of nonaromatic species (Figure 4.7).

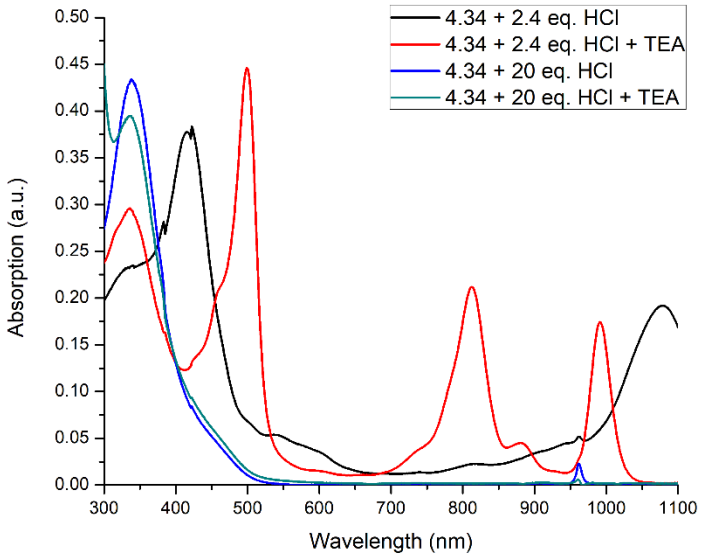

Figure 4.7 Reactivities of **4.34** in chloroform with HCl and TEA.

Similarly, by using the reducing agents such as sodium dithionate and potassium superoxide the nonaromatic species **4.33** can be generated, which can be further converted back to **4.34** by oxidizing with MnO_2 as shown in Figure 4.8.

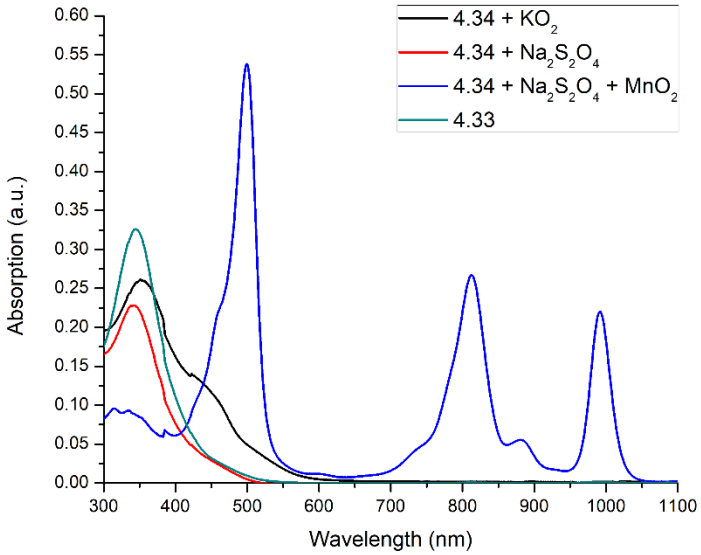

Figure 4.8 Reactivities of **4.34** in chloroform with different reducing agents and its comparision with **4.33**.

Finally, we could able to obtain the protonated species of **4.34** using large excess of TFA and $HClO_4$. Surprisingly, there is very little hypsochromic shift of around 5 nm in case of Soret band, whereas, the lowest energy bands are much more blue shifted (Figure 4.9).

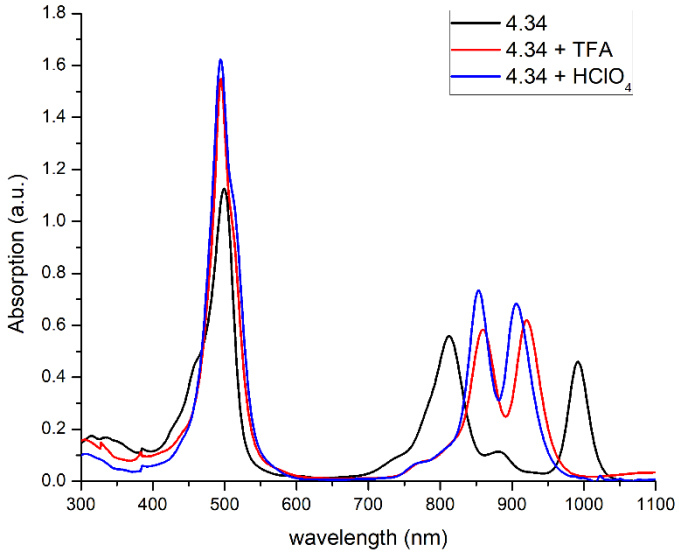

Figure 4.9 UV-Vis-NIR absorption spectra of protonation of bronzaphyrin **4.34** with different acids measured in chloroform.

Both the reduced **4.33** and oxidized **4.34** bronzaphyrins display good emission peaks. While the reduced bronzaphyrin **4.33** exhibit a three shouldered band having a peak maximum at 438 nm and the corresponding oxidized bronzaphyrin **4.34** display a sharp NIR emission with a peak maximum at 1007 nm (Figure 4.10).

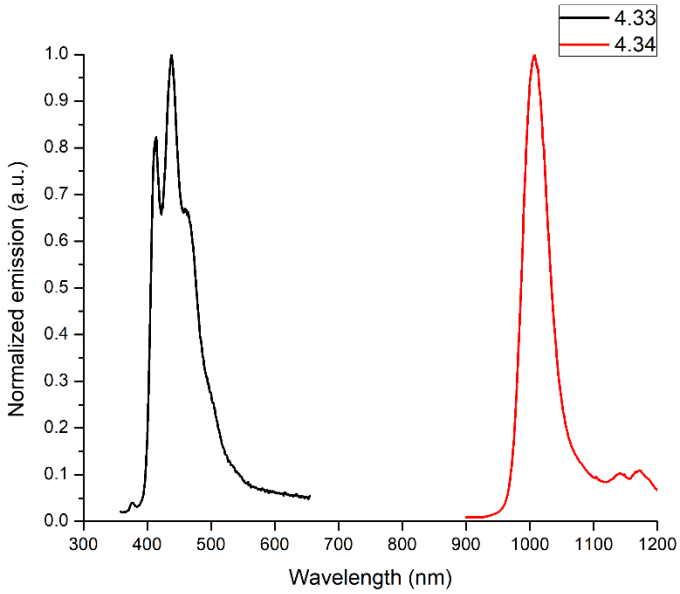

Figure 4.10 Emission spectra of bronzaphyrins **4.33** and **4.34** in chloroform with peak maxima at 438 and 1007 nm (λ_{ex} = 320 nm, slit widths of 4 nm for **4.33** and λ_{ex} = 490 nm, slit widths of 14 nm for **4.34**).

4.3.4 X-ray crystal structure analysis

So far, after several attempts, we could able to grow diffraction grade crystals of only the reduced bronzaphyrin **4.33** from the slow evaporation of its chloroform solution. The crystal structure displays three different conformations in a single asymmetric unit, probably owing to hydrophobic interactions which has forced the long isopentyloxy groups to take different orientations (Figure 4.11 and 4.12). Due to these effects, the core of the macrocycle undergoes alterations in all of the conformations leading to different distances between the atoms as shown in Figure 4.14 and different dihedral angles between the C-C bridging units, listed in Table 4.1. The central pyrrole ring flips out of the mean macrocyclic plane making an angle of 21° and 26.8° in two conformations while the third conformation is more unsymmetrically distorted, leading to two different dihedral angles of 6.4° and 27.4° (Figure 4.13). This may be attributed to the relatively flexible core of the nonaromatic macrocycle.

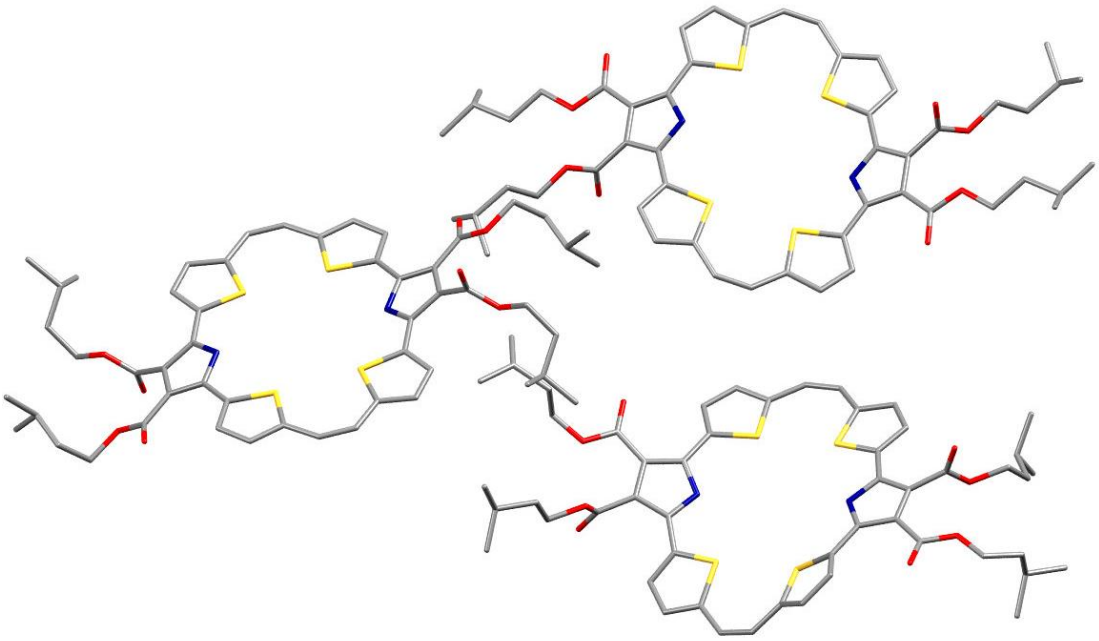

Figure 4.11 Perspective views of different conformations of the reduced bronzaphyrin **4.33** in a single asymmetric unit. All at 50% probability level. All hydrogens in the structures were omitted for clarity. Grey = Carbon, blue = Nitrogen, red = Oxygen and yellow = Sulphur.

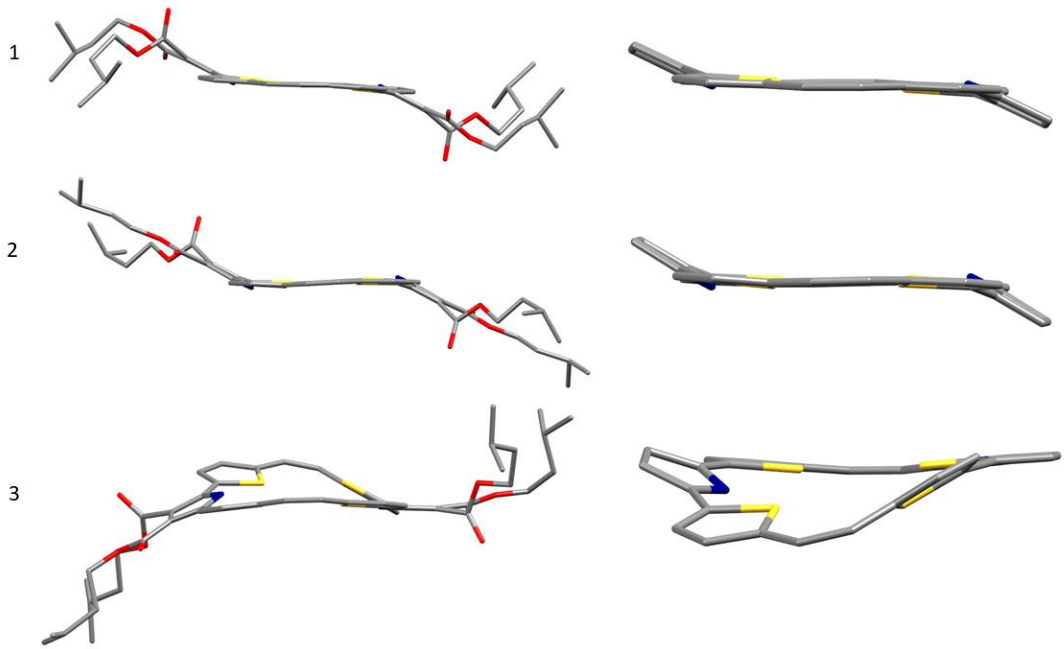

Figure 4.12 Side views of different conformations with ester (left) and without ester (right) of the reduced bronzaphyrin **4.33**. All at 50% probability level. All hydrogens and ester groups (right picture) in the structures were omitted for clarity. Grey = Carbon, blue = Nitrogen, red = Oxygen and yellow = Sulphur.

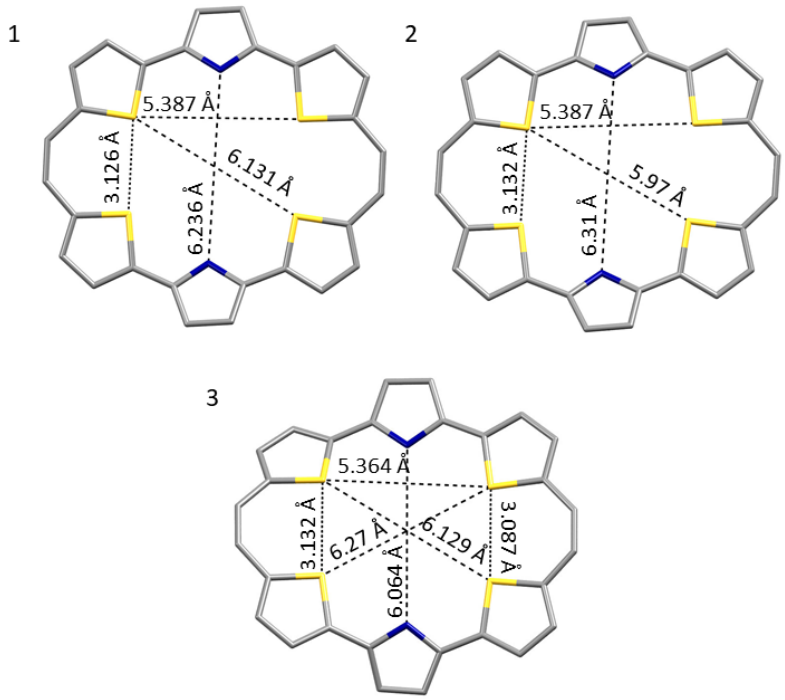

Figure 4.13 Top views of different conformations with different bond distances in a single asymmetric unit of the reduced bronzaphyrin **4.33**. All at 50% probability level. All hydrogens and ester groups in the structures were omitted for clarity. Grey = Carbon, blue = Nitrogen and yellow = Sulphur.

Table 4.1 Dihedral angles of bridging C-C units in different conformations of reduced bronzaphyrin **4.33**.

	Conformation 1	Conformation 2	Conformation 3
Dihedral angles	-177.8° and -177.1°	-175.9° and -173.5°	153.5°, -168.5°, -174.1° and 172.8°

The packing diagram revealed that the macrocycles form a close π-π stacking with interplanar distance ranging from 3.7 to 4 Å leading to layered network as shown in Figure 4.14.

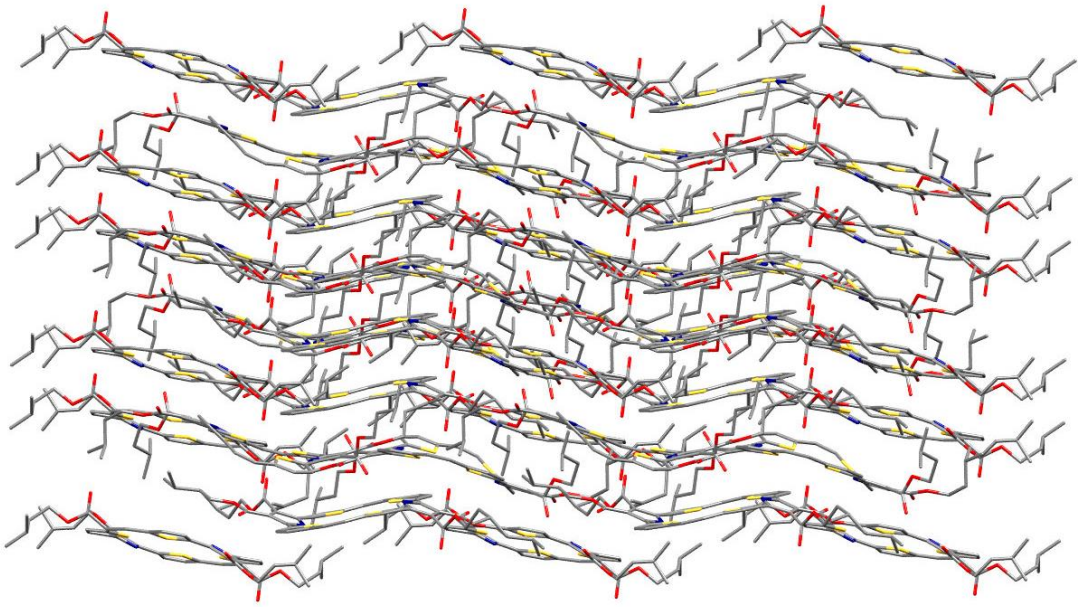

Figure 4.14 Crystal packing diagram showing layered network of **4.33**. All hydrogens in the structures were omitted for clarity. Grey = Carbon, blue = Nitrogen, yellow = Sulphur and red = Oxygen.

4.3.5 DFT studies

The quantum mechanical calculations has been done by our collaborator Prof. Dongho Kim from South Korea. All calculations were carried out by Gaussian 09-density functional theory (DFT) with Becke's three-parameter hybrid exchange functional and the Lee-Yang-Parr correlation functional (B3LYP) parameter.[10] The 6-31G basis sets were used for all

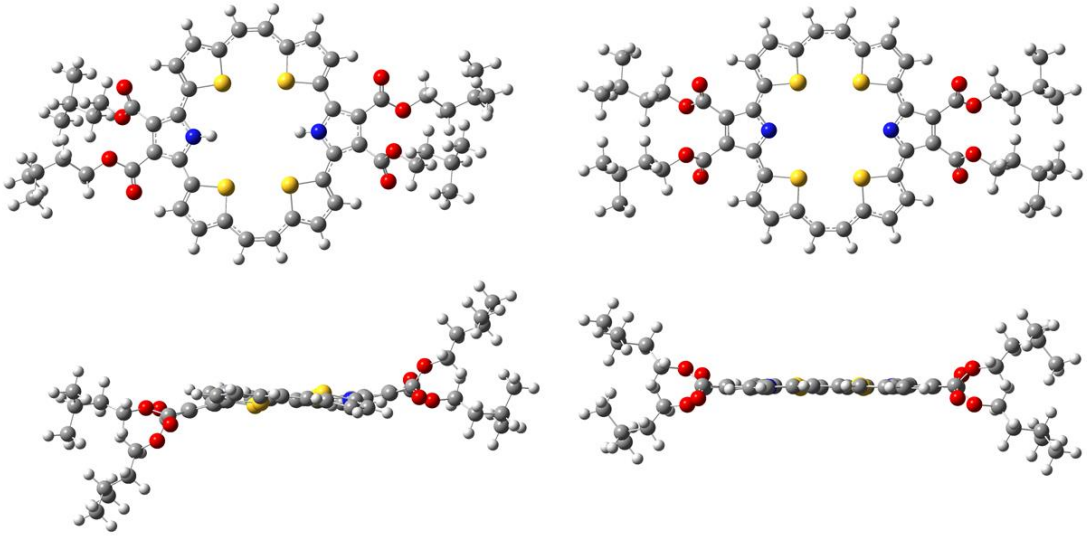

Figure 4.15 Optimized structures (top and side views) of reduced bronzaphyrin **4.33** (left) and oxidized bronzaphyrin **4.34** (right).

the calculations and the molecular orbitals were visualized using Gauss view 5. The optimized calculations done for both the compounds further confirmed the deviation of pyrrole rings from the mean macrocyclic plane in case of reduced bronzaphyrin **4.33** and showed a nearly planar structure for the oxidized bronzaphyrin **4.34** (Figure 4.15).

To gain further insight, TD-DFT calculations have been performed and the theoretical absorption spectra for both the bronzaphyrins **4.33** and **4.34** were obtained. The vertical electronic transitions and the steady state absorption spectra were found to be very similar (Figure 4.16), mainly involving the frontier orbitals: HOMO-1, HOMO, LUMO and

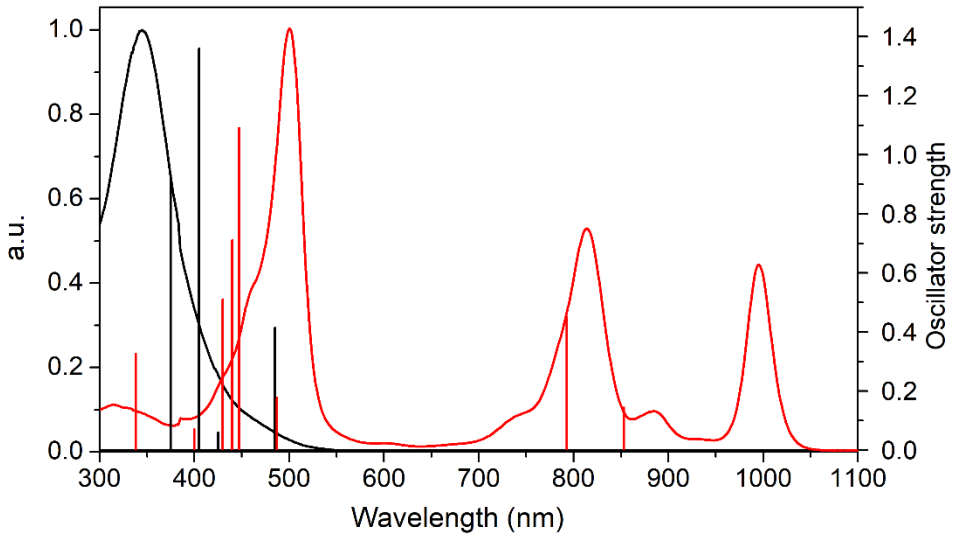

Figure 4.16 Theoretical (red vertical bars) and experimental (black continuous line) UV-Vis-NIR absorption spectra of **4.33** and **4.34** measured in chloroform.

LUMO+1. Energy level diagrams along with the delocalized π-electron densities of frontier orbitals are shown in Figures 4.17 and 4.18. As expected, the HOMO-LUMO energy difference reduced upon oxidation of **4.33** (2.33 eV) to **4.34** (1.55 eV), which is clearly reflected in the absorption bands in the NIR region for the latter.

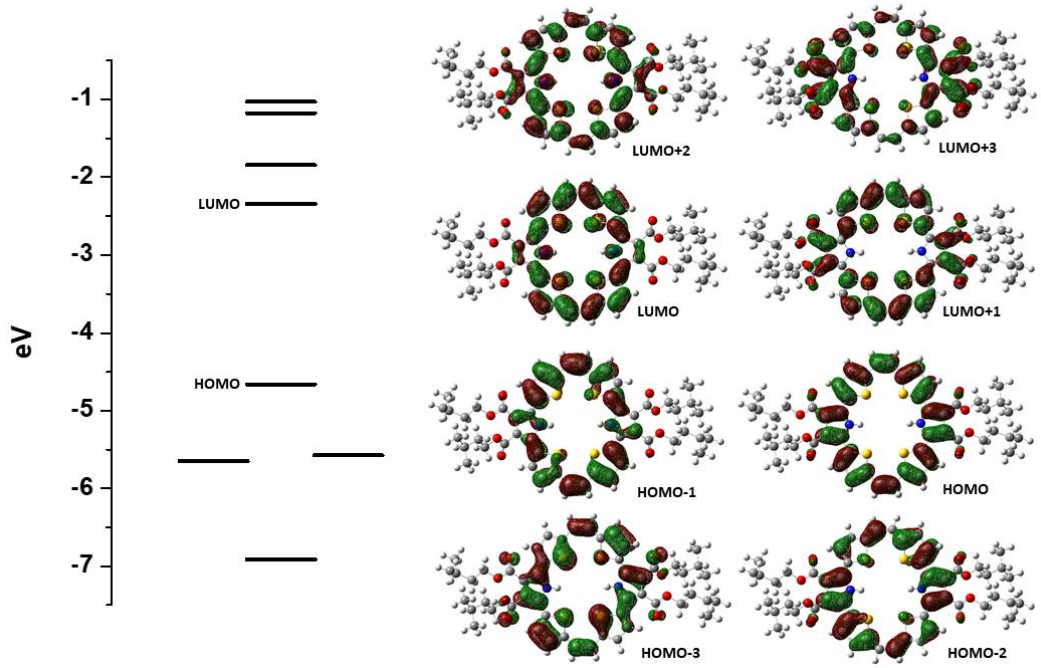

Figure 4.17 Delocalized electron densities of **s**elected MOs of **4.33** with energy level diagram.

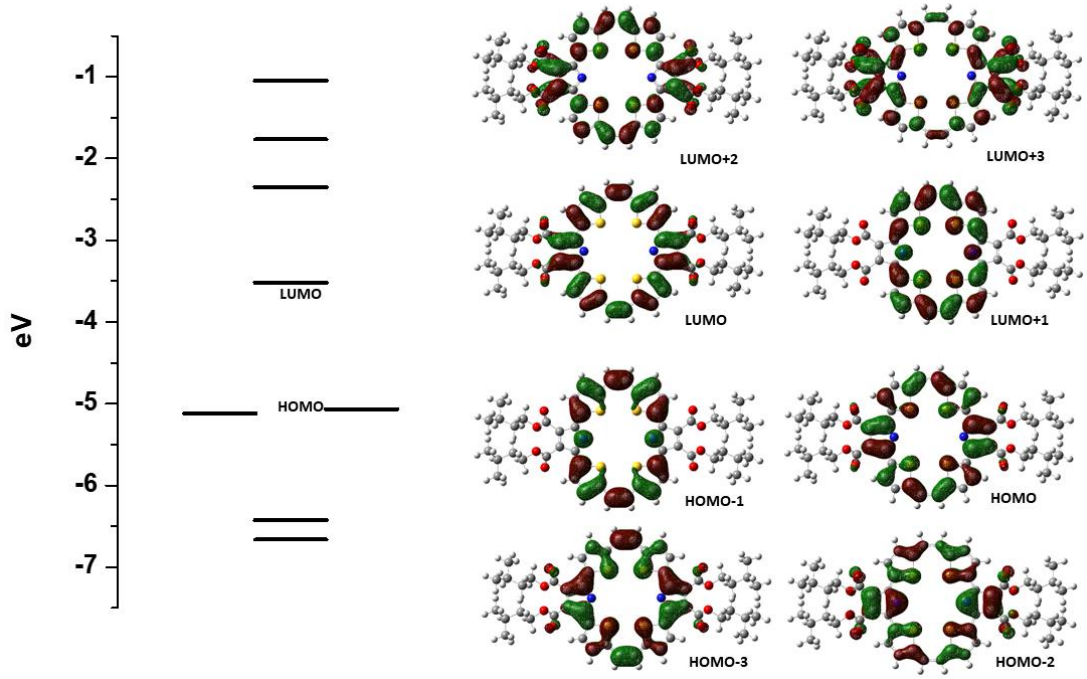

Figure 4.18 Delocalized electron densities of **s**elected MOs of **4.34** with energy level diagram.

The NICS (nucleus-independent chemical shift) values were obtained with gauge independent atomic orbital (GIAO) method and HOMA (Harmonic Oscillator Model of Aromaticity) was calculated by using Ropt (C-C) = 1.388 Å and Ropt (C-N) = 1.334 Å. As expected, reduced bronzaphyrins, **4.33** displayed a weak antiaromatic nature with a

NICS value of + 3.86 and oxidized bronzaphyrin **4.34** was aromatic with a NICS value of -12.6 ppm at the centre of the macrocycles, respectively (Figure 4.19).

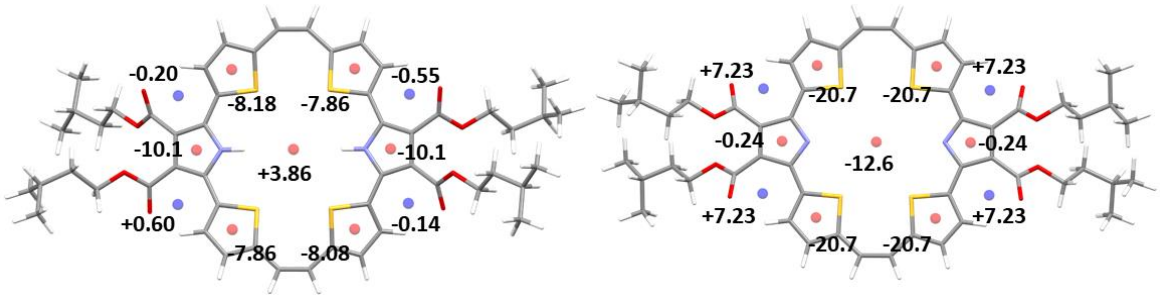

Figure 4.19 Selected positions for calculating NICS values of compounds **4.33** and **4.34**, dots in the macrocycle represent the ghost **Bq** atoms.

The extent of electron delocalization, indicated by harmonic oscillator model of aromaticity (HOMA) index, were found to be 0.43 and 0.85 for both bronzaphyrins **4.33** and **4.34**, respectively (Table 2).[11]

Table 2 Summary of **HOMA*** index values (* = calculated by considering the conjugation path of 26π e). **ΔRx** = Bond length alteration from the crystal structure.

Molecule	π-e	ΔR_x (Å)	HOMA
4.33	26	0.384	0.43
4.34	26	0.058	0.85

4.4 Conclusion

In summary, we have synthesized highly stable α-free terpyrrole endowed with β-ester groups by means of Suzuki protocol, which was further utilized in bronzaphyrin synthesis. Long isopentyl groups have been incorporated in ester moieties for increasing the solubility. The presence of strong electron withdrawing ester groups at the periphery, led us to isolate and characterize the reduced bronzaphyrin **4.33**, which was later easily oxidized using MnO_2 to give the first 26π aromatic tetrathiabronzaphyrin **4.34**. As expected, due to lack of conjugation, reduced bronzaphyrin **4.33** displayed nonaromatic behavior confirmed by its blue shifted absorption band and characteristic ^{1}H NMR spectral pattern. Finally, the structure was unequivocally resolved by single crystal X-ray diffraction analysis. The crystal structure displayed three conformations in a single asymmetric unit due to hydrophobic interaction ascribed to the periphery ester groups. The oxidized bronzaphyrin **4.34** exhibited much red shifted absorption when compared to

dithiabronzaphyrins, tail reaching up to 1050 nm. Surprisingly, protonation study with HCl generated back the 28π-bronzaphyrin via a radical intermediate 27π-electron system. Though the intermediate can be converted back to freebase by quenching with triethylamine, the completely reduced species remained unaffected by trimethylamine. The 26π-aromatic bronzaphyrin **4.34** can be directly reduced to the corresponding reduced derivative **4.33** in presence of sodium dithionite or potassium superoxide and again reverted back to oxidized species employing MnO_2, indicating a redox switch between all the three states (Figure 4.20). The computational studies further support the nonaromatic and aromatic nature of both the bronzaphyrins **4.33** and **4.34**. Finally, scaffolds such as bronzaphyrin **4.34** due to its elegant photophysical properties and redox switching may find application in NIR imaging and smart optoelectronic materials.

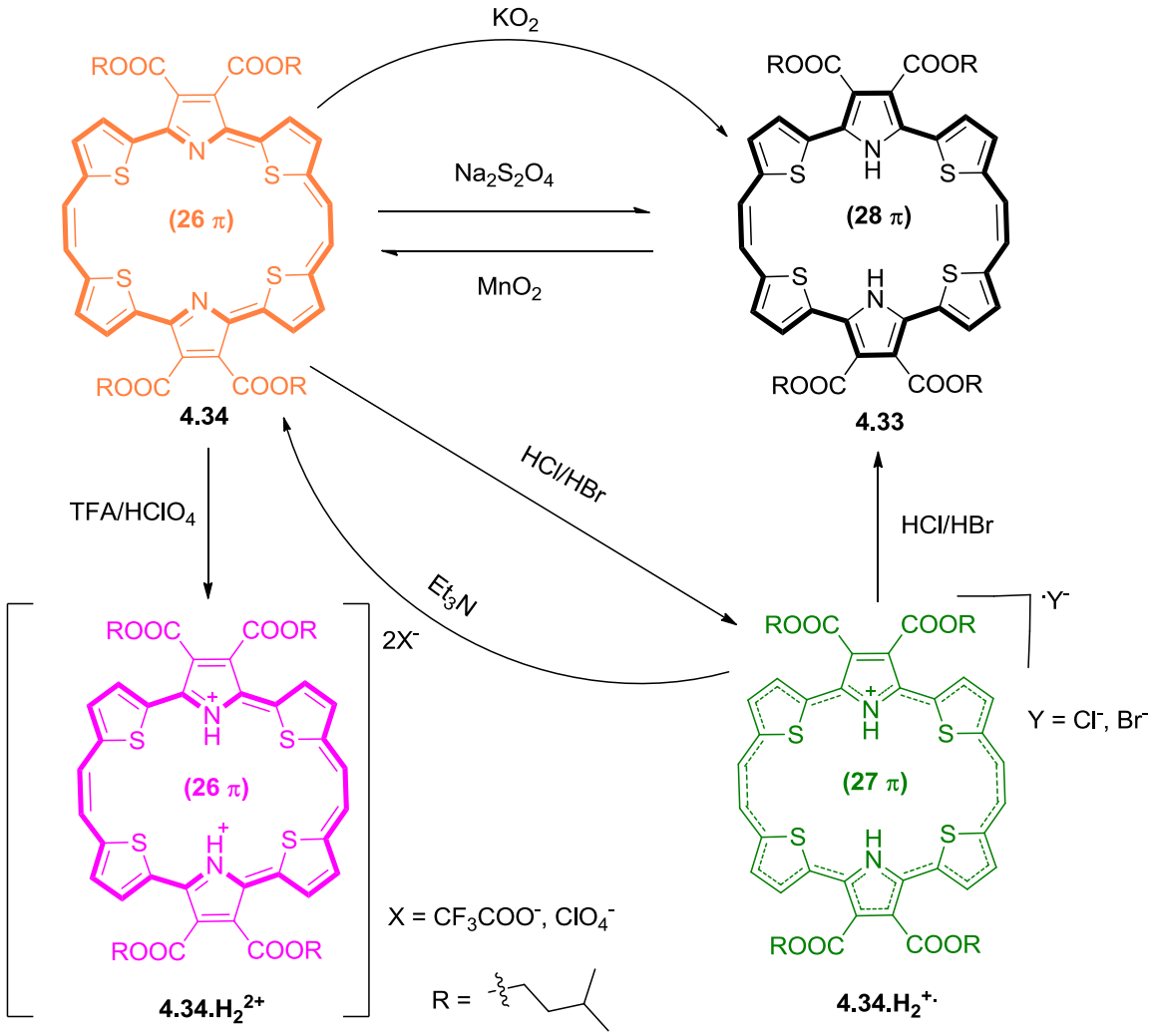

Figure 4.20 Redox switch between the three different states of **4.34**.

4.5 Experimental details

Synthesis of diisopentylfumarate 4.27

To the solution of isoamylalcohol **4.25** (18.75 mL, 17.3 mmol) and H_2SO_4 (2 mL), fumaric acid **4.26** (10 g, 8.62 mmol) was added and refluxed for 12 h under nitrogen atmosphere. Later, the reaction mixture was concentrated in vacuo. The residue was diluted with water and extracted with ethyl acetate (2 x 50 mL). The combined organic layer was washed with water (50 mL), brine and dried over anhyd sodium sulfate. Concentration of organic layer in vacuo followed by silica gel column chromatographic purification of the crude product using hexane: ethyl acetate (9:1) as eluent resulted diisopentylfumarate as clear liquid (20.2 g, 91%).

FTIR data: 3438, 3054, 1719 cm^{-1}; ^1H NMR (400 MHz, $CDCl_3$): δ in ppm 6.84 (s, 2H, CH), 4.23 (t, 4H, *J* = 5.6 Hz, CH_2 ester), 1.71 (m, 2H, CH alkyl), 1.58 (m, 4H, CH_2 alkyl), 0.94 (m, 12H, CH_3 alkyl); ^{13}C NMR (100 MHz, $CDCl_3$): δ in ppm 165.1, 133.6, 64.0, 37.2, 25.0, 22.4; HRMS m/z calcd. for $[M+Na]^+$ $C_{14}H_{24}O_4Na$: 279.1572, found 279.1567.

Synthesis of diisopentyl pyrrole-3,4-dicarboxylate 4.28

TOSMIC (3.6 g, 18.7 mmol) in dry THF (20 mL) was added dropwise to a mixture of **4.27** (4 g, 15.6 mmol) and NaH (1.12 g, 28.1 mmol) in dry THF (20 mL) at 0°C. After stirring for 2 h at 0° C, the reaction mixture was poured into ice-water and extracted with ethyl acetate (2 x 100 mL). The combined organic layer was washed with water (150 mL), brine and dried over anhyd sodium sulfate. Concentration of organic layer in vacuo followed by silica gel column chromatographic purification of the crude product using hexane: ethyl acetate (4:1) as eluent provided the desired product **4.28** as off-white solid (2.85 g, 62%).

Melting point: 148 °C; FTIR data: 3456, 2959, 1713, 1295 cm^{-1}; ^1H NMR (400 MHz, $CDCl_3$): δ in ppm 8.27 (s, 1H, NH), 7.34 (d, 2H, *J* = 4.0 Hz, CH), 4.27 (t, 4H, *J* = 4.0 Hz, CH_2 ester), 1.75 (m, 2H, CH alkyl), 1.71 (m, 4H, CH_2 alkyl), 0.95 (d, 12H, *J* = 4.0 Hz, CH_3 alkyl); ^{13}C NMR (100 MHz, $CDCl_3$): δ in ppm 163.8, 124.9, 116.6, 63.1, 37.5, 25.2, 22.6; HRMS m/z calcd. for $[M+Na]^+$ $C_{16}H_{25}NO_4Na$: 318.1681, found 318.1683.

Synthesis of diisopentyl 2,5-diiodo-pyrrole-3,4-dicarboxylate 4.29

Periodic acid (0.3 g, 1.36 mmol) was taken in dry methanol (40 mL) under nitrogen atmosphere and stirred for 15 min. Then iodine (0.69 g, 2.7 mmol) was added and stirred

further for 15 min. Later compound **4.28** (1 g, 3.4 mmol) was added to the reaction mixture and refluxed until TLC analysis confirmed the complete conversion of **4.28**. Methanol was removed in a rotary evaporator and the crude product was dissolved in DCM (100 mL) and washed with saturated sodium thiosulfate solution. Finally the organic layer was concentrated and purified by column chromatography by using hexane: ethyl acetate (5:1) as eluent to give the desired product **4.29** as gel (1.75 g, 94%).

FTIR data: 3216, 2952, 1698, 1190 cm^{-1}; ^{1}H NMR (400 MHz, $CDCl_3$): δ in ppm 8.75 (s, 1H, NH), 7.34 (m, 4H, CH), 7.05 (m, 2H, CH), 4.22 (q, 4H, *J* = 6.8 Hz, CH_2 ester), 1.67 (m, 2H, CH alkyl), 1.57 (m, 4H, CH_2 alkyl), 0.95 (m, 12H, CH_3 alkyl); ^{13}C NMR (100 MHz, $CDCl_3$): δ in ppm 164.7, 131.4, 128.0, 127.4, 126.6, 114.9, 63.7, 37.2, 24.9, 22.4; HRMS m/z calcd. for $[M+Na]^+$ $C_{16}H_{23}I_2NO_4Na$: 569.9614, found 569.9614.

Synthesis of thiophene substituted terpyrrole 4.31

Diiodopyrrole derivative **4.29** (1.33 g, 2.43 mmol), borylthiophene **4.30** (1.33 g, 6.32 mmol), $Pd(OAc)_2$ (55 mg, 0.24 mmol) and PPh_3 (130 mg, 0.48 mmol) were taken in a (preheated and cooled under nitrogen) two necked round bottom flask under nitrogen atmosphere and kept for 0.5 h under vacuum. To the reaction mixture, degassed DMF (100 mL) and aq. K_2CO_3 solution (3.36 g, 24.3 mmol in 33 mL water) were added under nitrogen and stirred for 18 h at 85 °C. After completion of reaction and cooling, the solvent was evaporated under reduced pressure in rotary evaporator and the residue was dissolved in chloroform and organic layer was separated from water-chloroform mixture through separating funnel. The combined organic layer was passed through anhyd sodium sulfate and evaporated to dryness under reduced pressure. Crude product was purified by silica gel column using hexane: ethyl acetate (5:1) as eluent to give the desired product **4.31** as gel (0.6 g, 54%).

FTIR data: 3270, 2956, 1694, 1442 cm^{-1}; ^{1}H NMR (400 MHz, $CDCl_3$): δ in ppm 8.75 (s, 1H, NH), 7.34 (m, 4H, CH), 7.05 (m, 2H, CH), 4.22 (q, 4H, *J* = 6.8 Hz, CH_2 ester), 1.67 (m, 2H, CH alkyl), 1.57 (m, 4H, CH_2 alkyl), 0.95 (m, 12H, CH_3 alkyl); ^{13}C NMR (100 MHz, $CDCl_3$): δ in ppm 164.7, 131.4, 128.0, 127.4, 126.6, 114.9, 63.7, 37.2, 24.9, 22.4; HRMS m/z calcd. for $[M+Na]^+$ $C_{24}H_{29}NO_4S_2Na$: 482.1435, found 482.1441.

Synthesis of thiophene substituted terpyrrole dialdehyde 4.32

To a three neck round bottom flask fitted with a dropping funnel and a reflux condenser, DMF (500 μL, 6.14 mmol) was added. The flask was immersed in an ice bath and $POCl_3$

(570 μL, 6.14 mmol) was added slowly through syringe. An exothermic reaction occurred with the formation of $POCl_3$-DMF complex. The ice bath was removed and the mixture was stirred for another 15 min at room temperature. 1,2-Dichloroethane (5 mL) was added and the ice bath was replaced. When the internal temperature has been lowered to 5°C, the terpyrrole **4.31** (0.28 g, 0.614 mmol) dissolved in 1,2-dichloroethane (15 mL) was added slowly to cooled reaction mixture. After the addition was complete, the ice bath was replaced with heating mantle. The mixture was refluxed for 2 h and then cooled to 25-30°C and a saturated solution of sodium acetate (2.52 g) was added slowly to the reaction mixture. The reaction mixture was again refluxed for 2 h. After the completion of reaction, the content was extracted thrice with dichloromethane. The combined organic layers were washed with saturated aqueous sodium carbonate solution and dried over anhyd sodium carbonate. The crude product was purified by column chromatography using hexane: ethyl acetate (4:1) as eluent to give the desired dialdehyde **4.32** as yellow solid (0.27 g, 85%).

Melting point: 76 °C; FTIR data: 3200, 2955, 2871, 1724, 1644 cm^{-1}; ^1H NMR (400 MHz, $CDCl_3$): δ in ppm 9.89 (s, 2H, -CHO) 9.67 (s, 1H, NH), 7.74 (d, 2H, *J* = 3.2 Hz, CH), 7.58 (m, 2H, CH), 4.29 (t, 4H, *J* = 5.6 Hz, CH_2 ester), 1.67 (m, 2H, CH alkyl), 1.59 (m, 4H, CH_2 alkyl), 0.91 (m, 12H, CH_3 alkyl); ^{13}C NMR (100 MHz, $CDCl_3$): δ in ppm 182.9, 164.1, 143.5, 140.5, 136.7, 128.4, 127.7, 117.5, 64.3, 37.2, 25.0, 22.5; HRMS m/z calcd. for $[M+Na]^+$ $C_{26}H_{29}NO_6S_2Na$: 538.1334, found 538.1334.

Synthesis of reduced tetrathiabronzaphyrin 4.33:

To a three-neck round bottom flask fitted with a dropping funnel and a reflux condenser, activated zinc dust (507 mg, 7.76 mmol) was added followed by THF (50 mL). Keeping the flask in an ice bath, $TiCl_4$ (425 μL, 3.88 mmol) was added and subsequently, the reaction mixture was refluxed for 4 h. Then thiophene substituted terpyrrole dialdehyde **4.32** (100 mg, 0.194 mmol) along with pyridine (1 mL) in THF (50 mL) was added slowly and the refluxing was continued for another 18 h. The reaction mixture was quenched using 10% K_2CO_3 solution, filtered and the aqueous layer was extracted with ethyl acetate. After complete evaporation of solvent, the solid thus obtained was purified by column chromatography using hexane: ethyl acetate (4:1) as eluent to give the desired product **4.33** as bright orange solid (17 mg, 18%).

Melting point: >300°C; FTIR data: 3279, 2957, 2925, 1713 cm^{-1}; UV-Vis ($CHCl_3$): λ in nm (ε) 345 (5.09); Fluorescence ($CHCl_3$, λ_{ex} = 320 nm with slit width of 4 nm) λ_{max}: 438 nm; ^{1}H NMR (400 MHz, $CDCl_3$): δ in ppm 9.49 (s, 2H, NH), 7.38 (s, 4H, CH), 6.97 (s, 4H, CH), 6.62 (s, 4H, meso CH), 4.22 (t, 8H, *J* = 6.8 Hz, CH_2 ester), 1.65 (m, 4H, CH alkyl), 1.54 (t, 8H, *J* = 6.8 Hz, CH_2 alkyl), 0.89 (t, 24H, *J* = 6.0 Hz, CH_3 alkyl); ^{13}C NMR not recorded due to lack of solubility; HRMS m/z calcd. for $[M+Na]^+$ $C_{52}H_{58}N_2O_8S_4Na$: 989.2974, found 989.2973.

The compound **4.33** (10 mg, 10.3 μmol) was dissolved in chloroform and oxidized with MnO_2 (50 mg) to obtain the corresponding 26π-aromatic bronzaphyrin **4.34**. The suspension was subsequently passed through celite pad to obtain the desired pure macrocycle in almost quantitative yield as green colored solid.

Melting point: >300°C; FTIR data: 2956, 2926, 1716 cm^{-1}; UV-Vis ($CHCl_3$): λ in nm (ε) 499 (5.24), 812 (4.94), 882 (4.26), 991 (4.86); Fluorescence ($CHCl_3$, λ_{ex} = 490 nm with slit width of 14 nm) λ_{max}: 1007 nm; ^{1}H NMR (400 MHz, $CDCl_3$): δ in ppm 11.24 (s, 8H, β-CH), 10.63 (s, 4H, meso CH), 5.26 (s, 8H, CH_2 ester), 2.27 (m, 12H, CH and CH_2 alkyl), 1.26 (m, 24H, CH_3 alkyl); ^{13}C NMR not recorded due to lack of solubility; HRMS m/z calcd. for $[M+H]^+$ $C_{52}H_{57}N_2O_8S_4$: 965.2998, found 965.2997.

4.6 Crystallographic data and structure refinement information

Crystal data and structure refinement for 4.33.

Identification code	MVNK_a	
Empirical formula	C_{52} H_{56} N_2 O_8 S_4	
Formula weight	965.22	
Temperature	100(2) K	
Wavelength	0.71073 Å	
Crystal system	Triclinic	
Space group	P -1	
Unit cell dimensions	*a* = 14.7385(6) Å	*α*= 77.434(2)°.
	b = 16.0079(7) Å	*β*= 78.101(2)°.
	c = 22.5400(10) Å	*γ* = 74.682(2)°.
Volume	4943.3(4) $Å^3$	
Z	4	
Density (calculated)	1.297 g/cm^3	
Absorption coefficient	0.248 mm^{-1}	
F(000)	2040	

Crystal size	0.16 x 0.14 x 0.10 mm^3
Theta range for data collection	2.182 to 27.950°.
Index ranges	$-19 \leq h \leq 19$, $-20 \leq k \leq 20$, $-29 \leq l \leq 29$
Reflections collected	218783
Independent reflections	23127 [R(int) = 0.3105]
Completeness to theta = 25.242°	99.9 %
Refinement method	Full-matrix least-squares on F^2
Data / restraints / parameters	23127 / 30 / 1221
Goodness-of-fit on F^2	0.994
Final R indices [I>2sigma(I)]	R1 = 0.0776, wR2 = 0.1313
R indices (all data)	R1 = 0.1854, wR2 = 0.1617
Extinction coefficient	n/a
Largest diff. peak and hole	1.307 and -0.858 $e.Å^{-3}$

4.7 References

1. Sessler, J. L.; Weghorn, S. J.; Hiseada, Y.; Lynch, V. *Chem. Eur. J.* **1995**, *1*, 56.
2. (a) Weghorn, S. J.; Sessler, J. L.; Lynch, V.; Baumann, T. F.; Sibert, J. W. *Inorg. Chem.* **1996**, *35*, 1089. (b) Y. Ishimaru, N. Shimoyama, T. Fujihara, K. Watanabe, J. Setsune, *Chem. Asian J.* **2015**, *10*, 329.
3. (a) Johnson, M. R.; Miller, D. C.; Bush, K.; Becker, J. J.; Ibers, J. A. *J. Org. Chem.* **1992**, *57*, 4414. (b) Miller, D. C.; Johnson, M. R.; Ibers, J. A. *J. Org. Chem.* **1994**, *59*, 2877. (c) Johnson, M. R. *J. Org. Chem.* **1997**, *62*, 1168Z. (d) Hu, C. Scordilis-Kelley, M. P. Cava, *Tetrahedron Lett.* **1993**, *34*, 1879. (e) Hu, Z.; Atwood, J. L.; Cava, M. P. *J. Org. Chem.* **1994**, *59*, 8071. (f) Kozaki, M.; Parakka, J.; Cava, M. P. *J. Org. Chem.* 1996, **61**, 3657. (g) Ellinger, F.; Gieren, A.; Hübner, Th.; Lex, J.; Lucchesini, F.; Merz, A.; Neidlein, R.; Salbeck, J. *Monatsh. für Chemie* **1993**, *124*, 931.
4. Rapoport, H.; Castagnoli, N., Jr.; Holden, K. G. *J. Org. Chem.* **1964**, *29*, 883.
5. Merrill, B. A.; LeGoff, E. *J. Org. Chem.* **1990**, *55*, 2904.
6. (a) Lopez-Perez, A.; Robles-Machin, R.; Adrio, J.; Carretero, J. C. *Angew. Chem., Int. Ed.* **2007**, *46*, 9261. (b) Robles-Machin, R.; Lopez-Perez, A.; Gonzalez-Esguevillas, M.; Adrio, J.; Carretero, J. C. *Chem. - Eur. J.* **2010**, *16*, 9864.
7. Setsune, J.; Toda, M.; Watanabe, K.; Panda, P. K.; Yoshida, T. *Tetrahedron Lett.* **2006**, *47*, 7541.
8. (a) Zhang, Z.; Lim, J. M.; Ishida, M.; Roznyatovskiy, V. V.; Lynch, V. M.; Gong, H.-Y.; Yang, X.; Kim, D.; Sessler, J. L. *J. Am. Chem. Soc.* **2012**, *134*, 4076. (b) Zhang, Z.; Cha, W.-Y.; Williams, N. J.; Rush, E. L.; Ishida, M.; Lynch, V. M.; Kim, D.; Sessler, J. L. *J. Am. Chem. Soc.* **2014**, *136*, 7591.
9. Ishida M.; Kim, S.-J.; Preihs, C.; Ohkubo, K.; Lim, J. M.; Lee, B. S.; Park, J. S.; Lynch, V. M.; Roznyatovskiy, V. V.; Sarma, T.; Panda, P. K.; Lee, C. –H.; Fukuzumi, S.; Kim, D.; Sessler, J. L. *Nat. Chem.* **2013**, *5*, 15.
10. Gaussian 09, Revision C.01, Frisch, M. J.; Trucks, G. W.; Schlegel, H. B.; Scuseria, G. E.; Robb, M. A.; Cheeseman, J. R.; Scalmani, G.; Barone, V.; Mennucci, B.; Petersson, G. A.; Nakatsuji, H.; Caricato, M.; Li, X.; Hratchian, H. P.; Izmaylov, A. F.; Bloino, J.; Zheng, G.; Sonnenberg, J. L.; Hada, M.; Ehara, M.; Toyota, K.; Fukuda, R.; Hasegawa, J.; Ishida, M.; Nakajima, T.; Honda, Y.; Kitao, O.; Nakai, H.; Vreven, T.; Montgomery Jr., J. A.; Peralta, J. E.; Ogliaro, F.; Bearpark, M.; Heyd, J. J.; Brothers, E.; Kudin, K. N.; Staroverov, V. N.; Keith, T.; Kobayashi, R.; Normand, J.; Raghavachari, K.; Rendell, A.; Burant, J. C.; Iyengar, S. S.; Tomasi, J.; Cossi, M.; Rega, N.; Millam, J. M.; Klene, M.; Knox, J. E.; Cross, J. B.; Bakken, V.; Adamo, C.; Jaramillo, J.; Gomperts, R.; Stratmann, R. E.; Yazyev, O.; Austin, A. J.; Cammi, R.; Pomelli, C.; Ochterski, J. W.; Martin, R. L.; Morokuma, K.; Zakrzewski, V. G.; Voth, G. A.; Salvador, P.; Dannenberg, J. J.; Dapprich, S.; Daniels, A. D.; Farkas, O.; Foresman, J. B.; Ortiz, J. V.; Cioslowski, J.; Fox, D. J. Gaussian, Inc., Wallingford CT, 2010.

11. (a) Chen, Z.; Wannere, C. S.; Corminboeuf, C.; Puchta, R.; Schleyer, P. v. R.; *Chem. Rev.* **2005**, *105*, 3842. (b) Krygowski, T. M.; Cryan′ski, M. *Chem. Rev.* **2001**, *101*, 1385.

4.8 ^{1}H NMR, ^{13}C NMR, IR and HRMS spectra

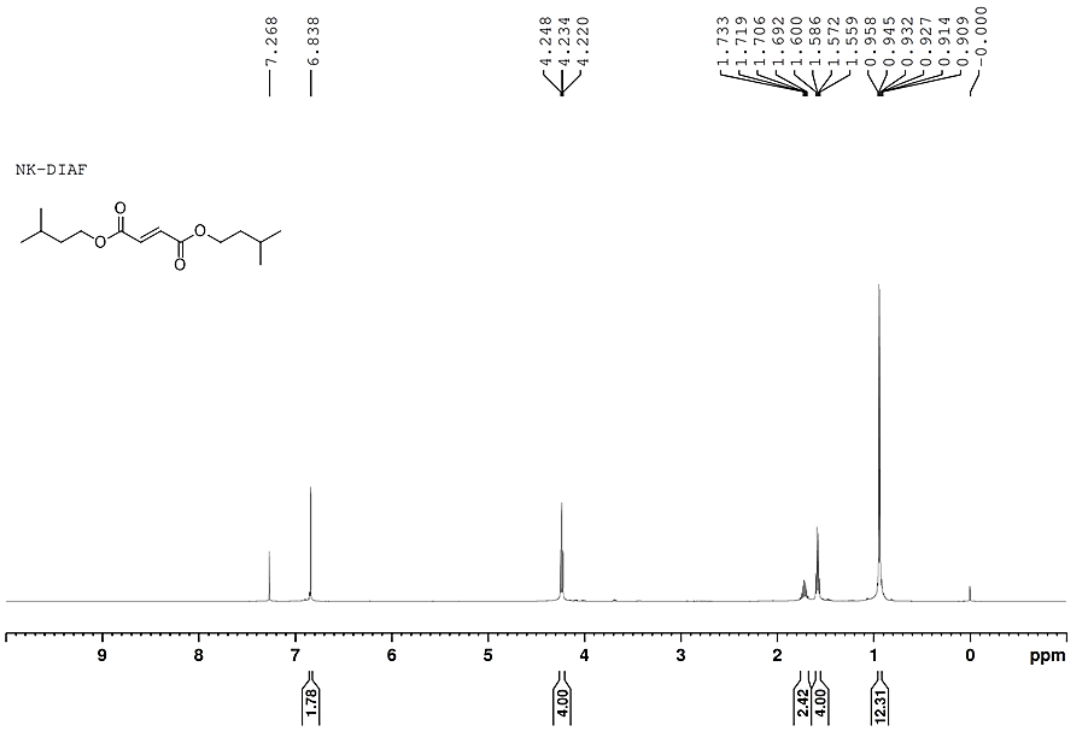

Figure 4.21 ^{1}H NMR spectrum of **4.27** in $CDCl_3$.

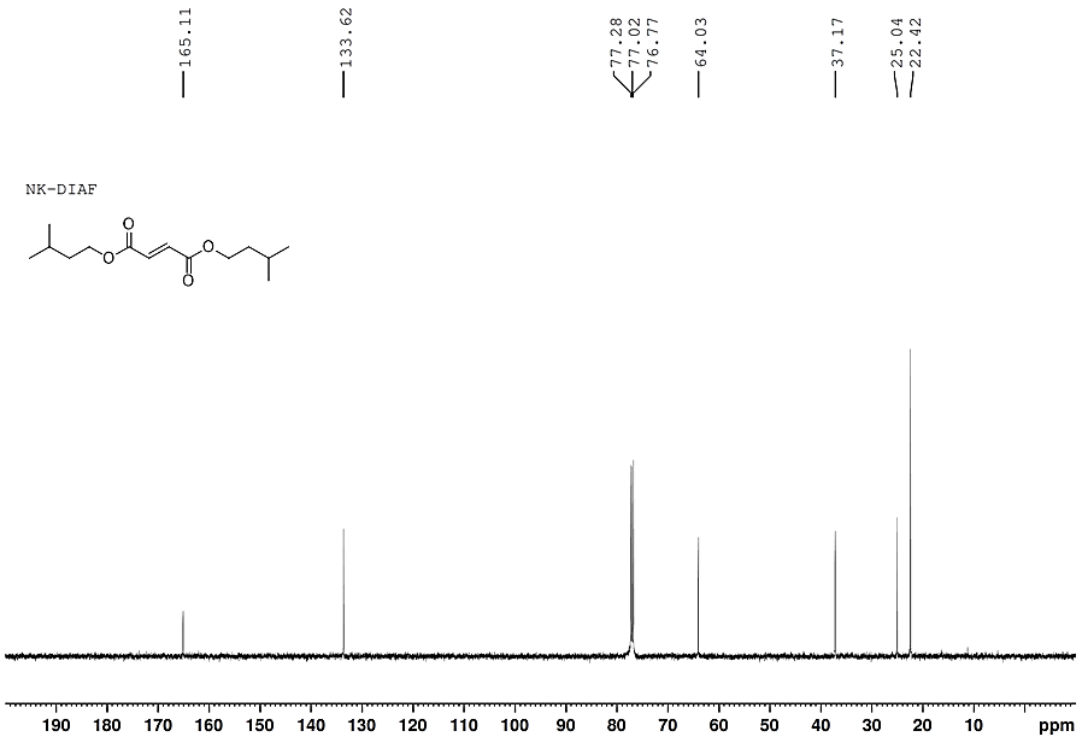

Figure 4.22 ^{13}C NMR spectrum of **4.27** in $CDCl_3$.

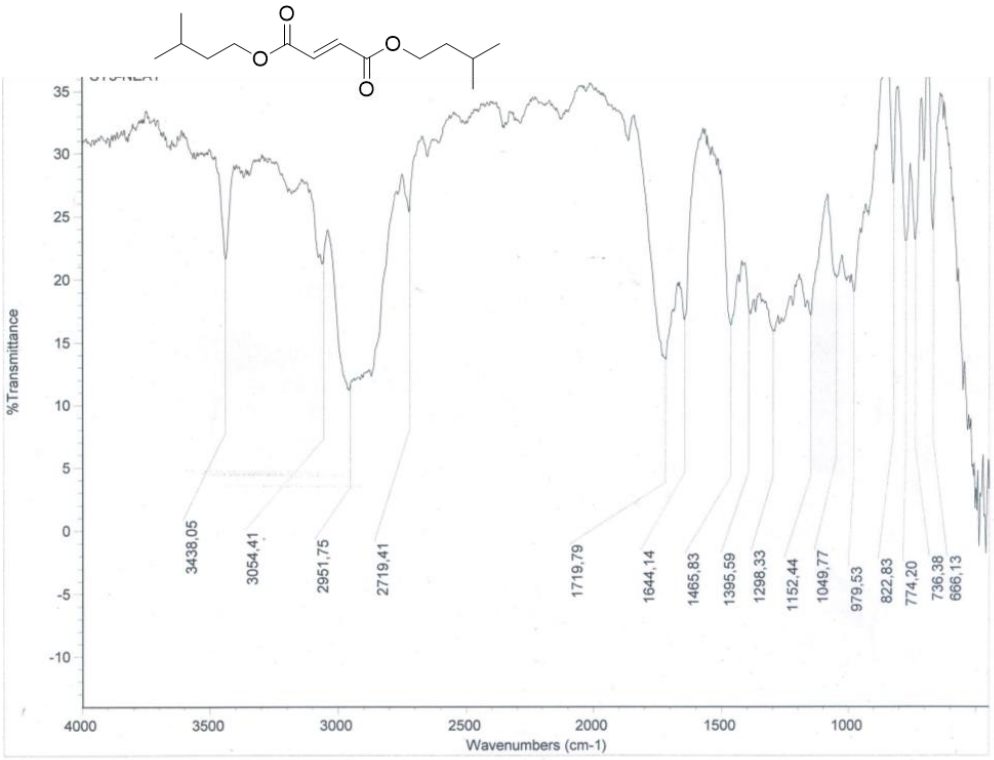

Figure 4.23 IR spectrum of **4.27**.

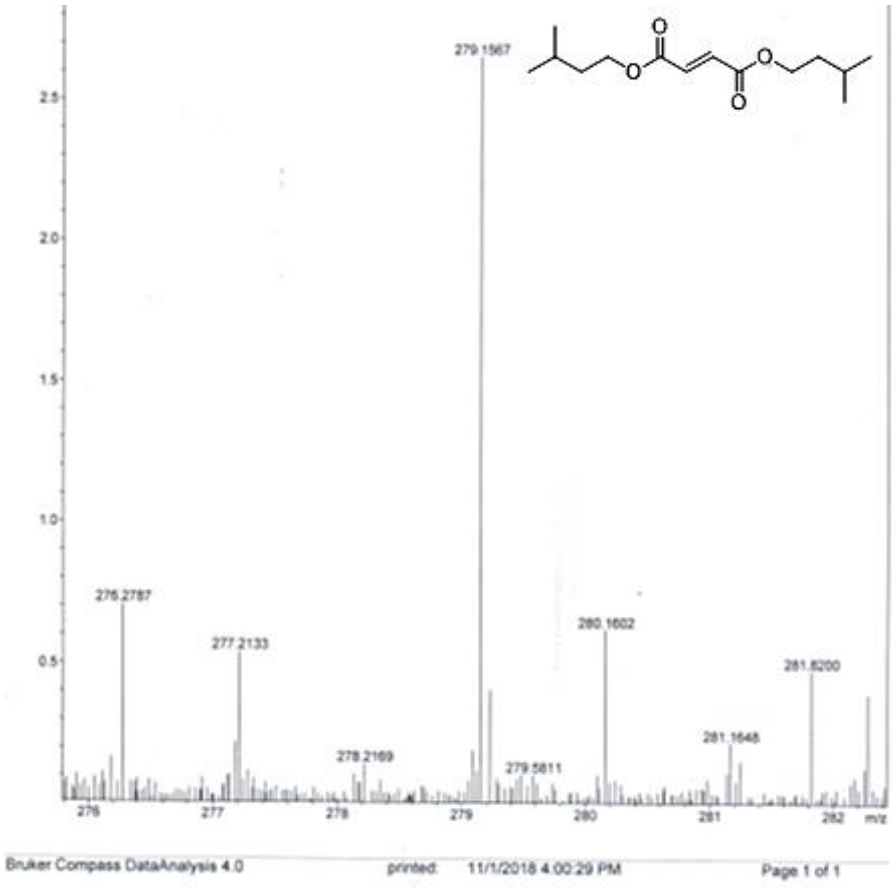

Figure 4.24 HRMS spectrum of **4.27** $[M+Na]^+$ $C_{14}H_{24}O_4Na$: 279.1572, found 279.1567.

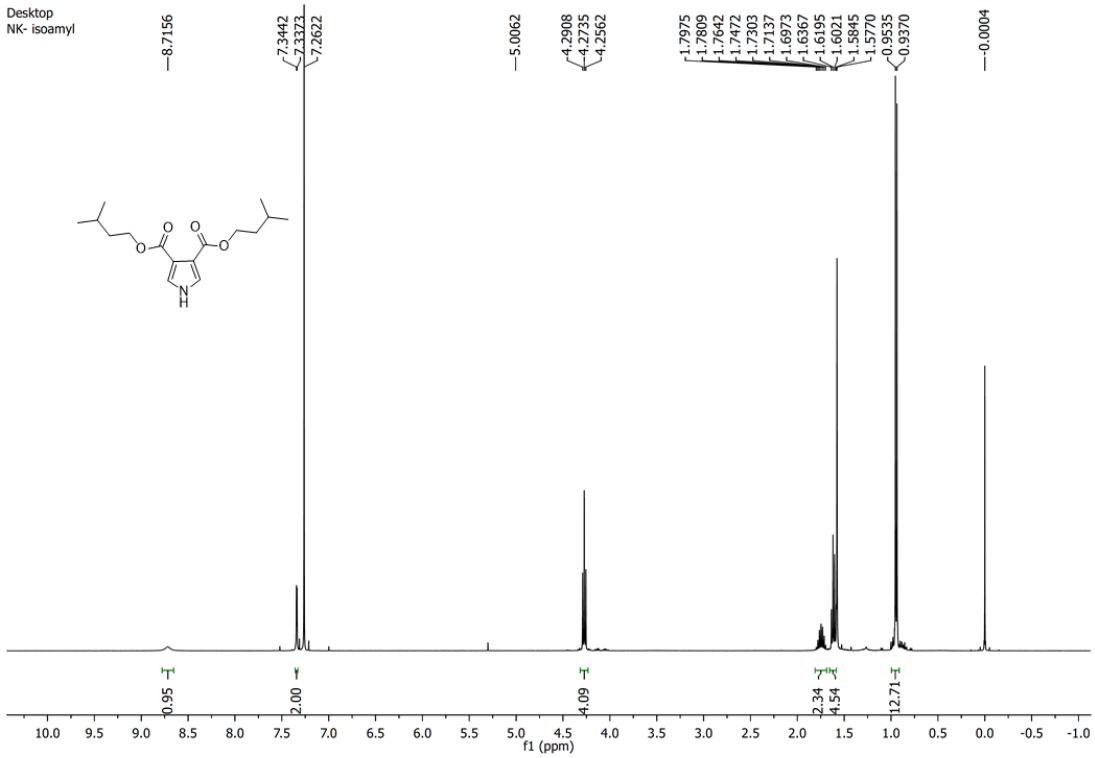

Figure 4.25 ^{1}H NMR spectrum of **4.28** in $CDCl_3$.

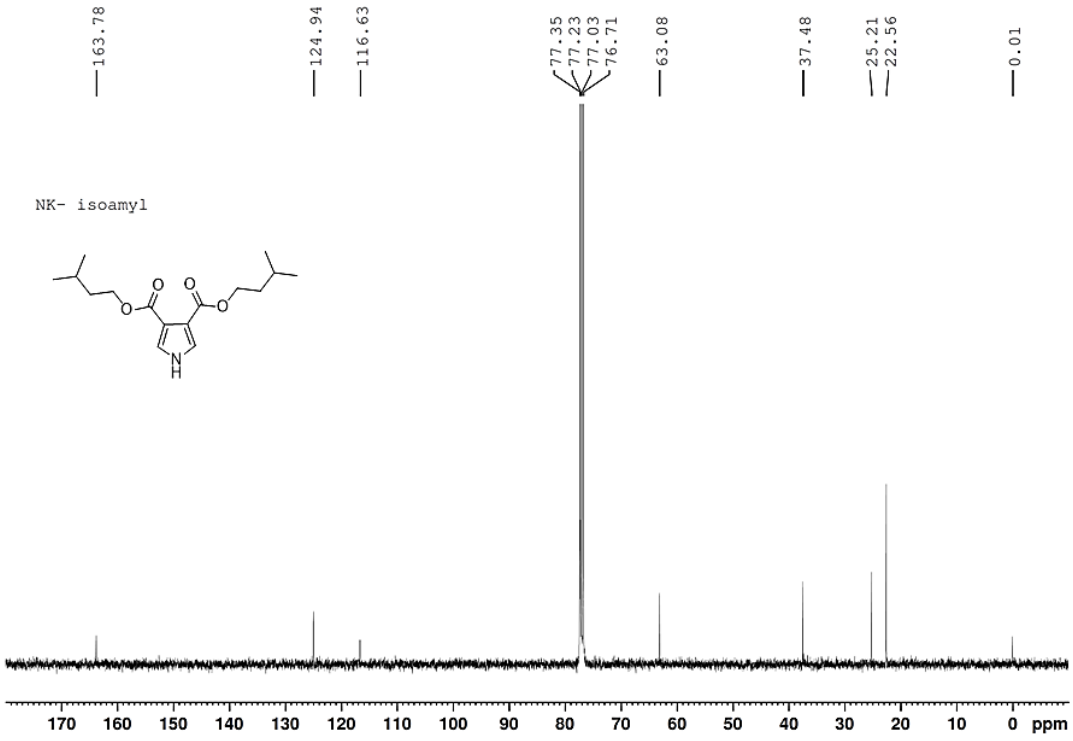

Figure 4.26 ^{13}C NMR spectrum of **4.28** in $CDCl_3$.

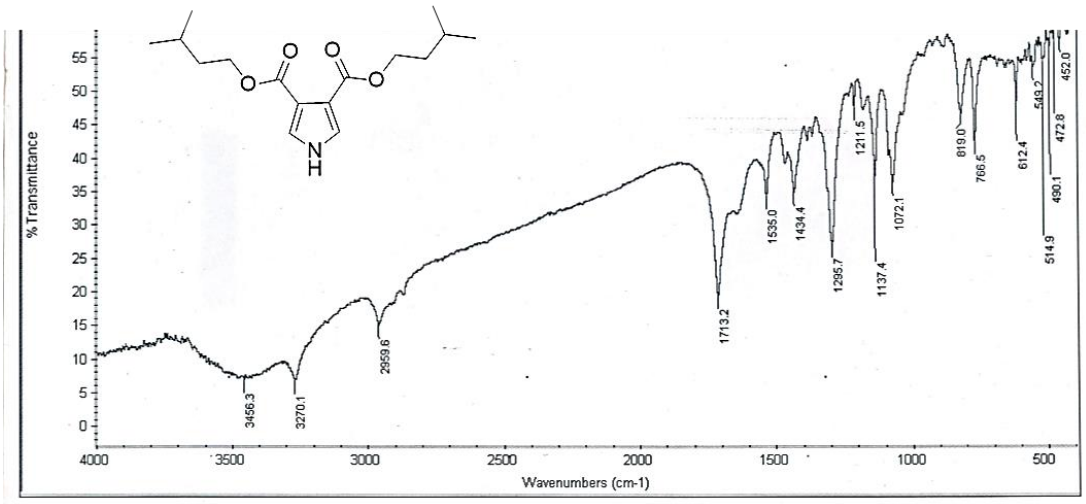

Figure 4.27 IR spectrum of **4.28**.

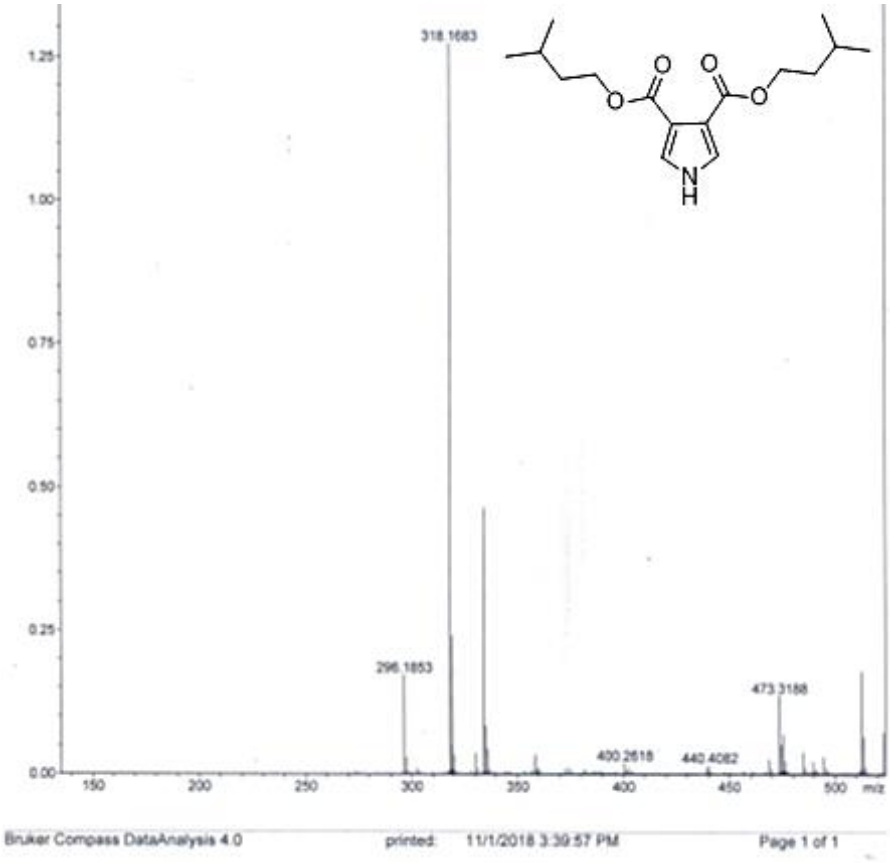

Figure 4.28 HRMS spectrum of **4.28** $[M+Na]^+$ $C_{16}H_{25}NO_4Na$: 318.1681, found 318.1683.

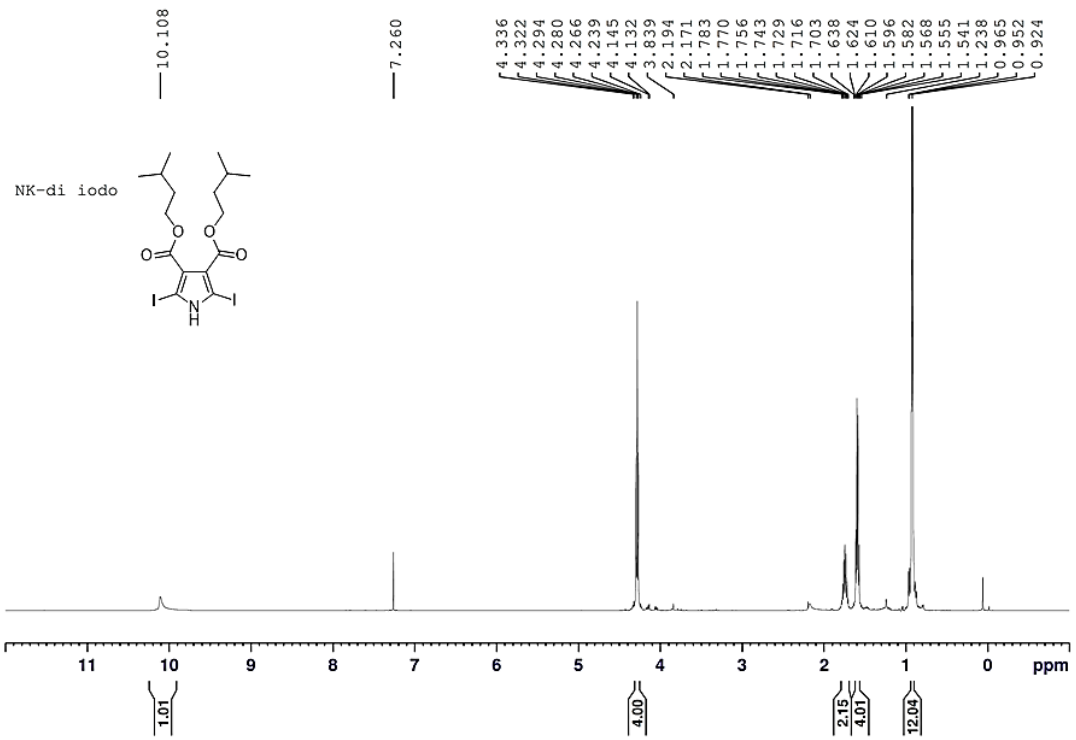

Figure 4.29 ^{1}H NMR spectrum of **4.29** in $CDCl_3$.

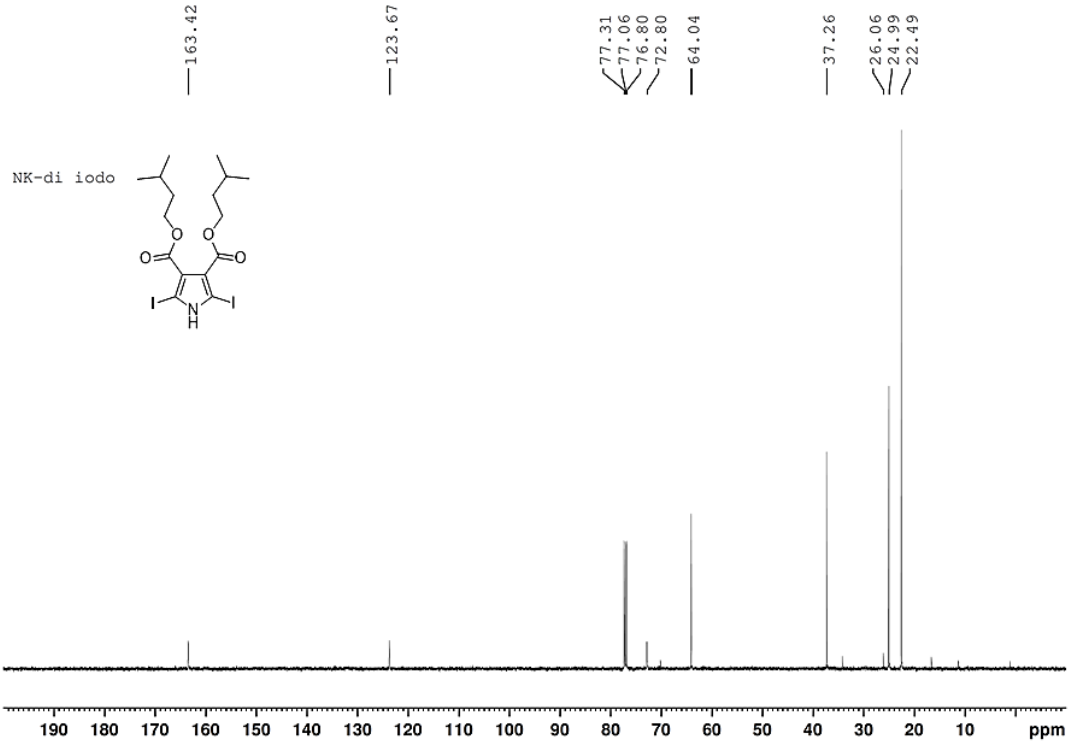

Figure 4.30 ^{13}C NMR spectrum of **4.29** in $CDCl_3$.

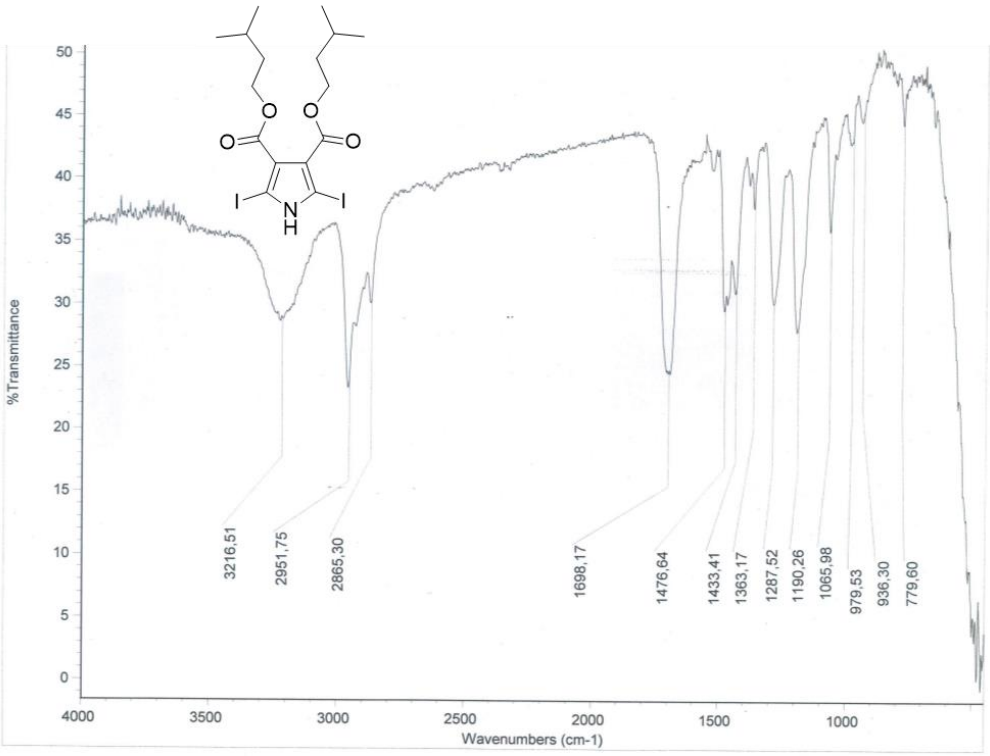

Figure 4.31 IR spectrum of **4.29**.

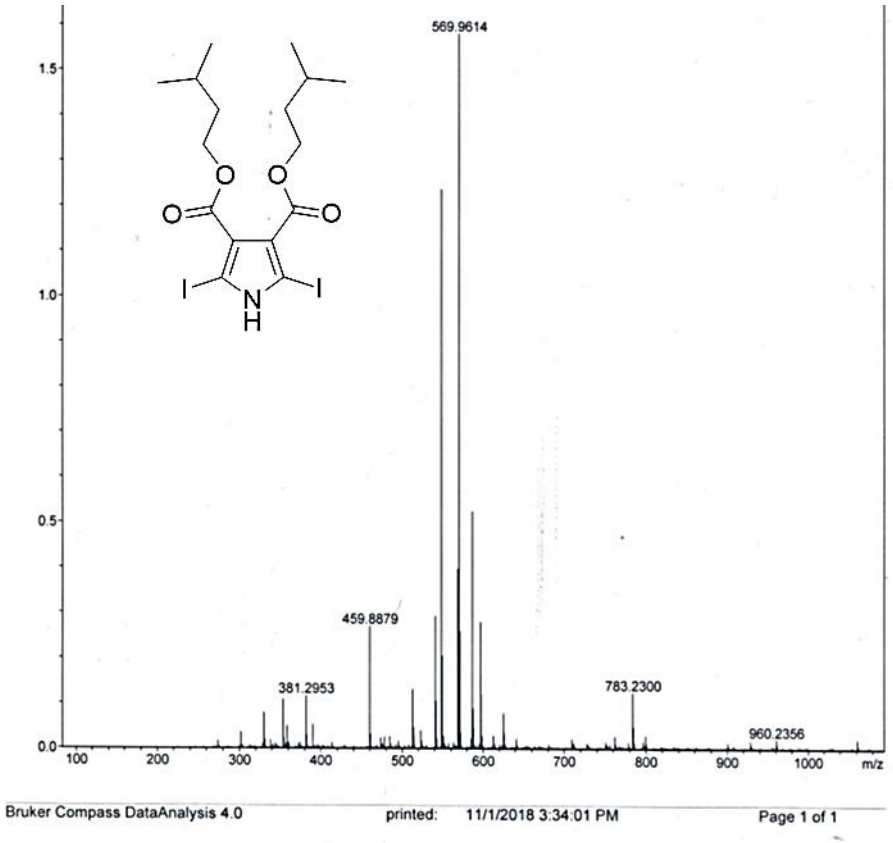

Figure 4.32 HRMS spectrum of **4.29** $[M+Na]^+$ $C_{16}H_{23}I_2NO_4Na$: 569.9614, found 569.9614.

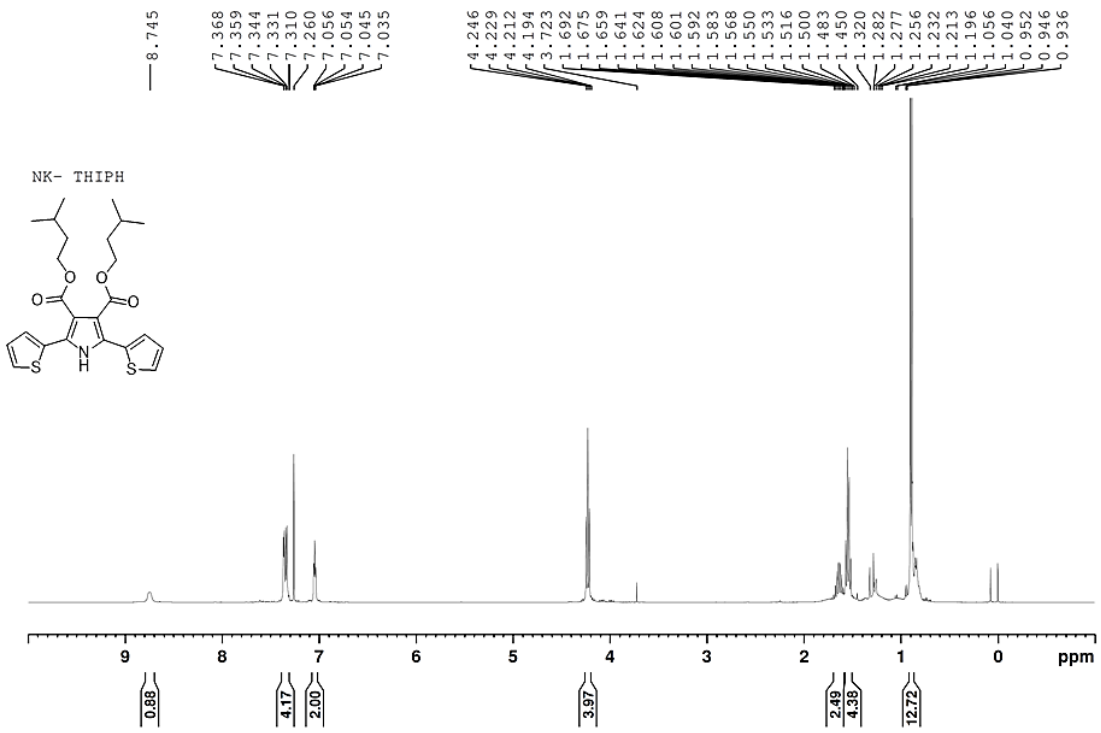

Figure 4.33 ^{1}H NMR spectrum of **4.31** in $CDCl_3$.

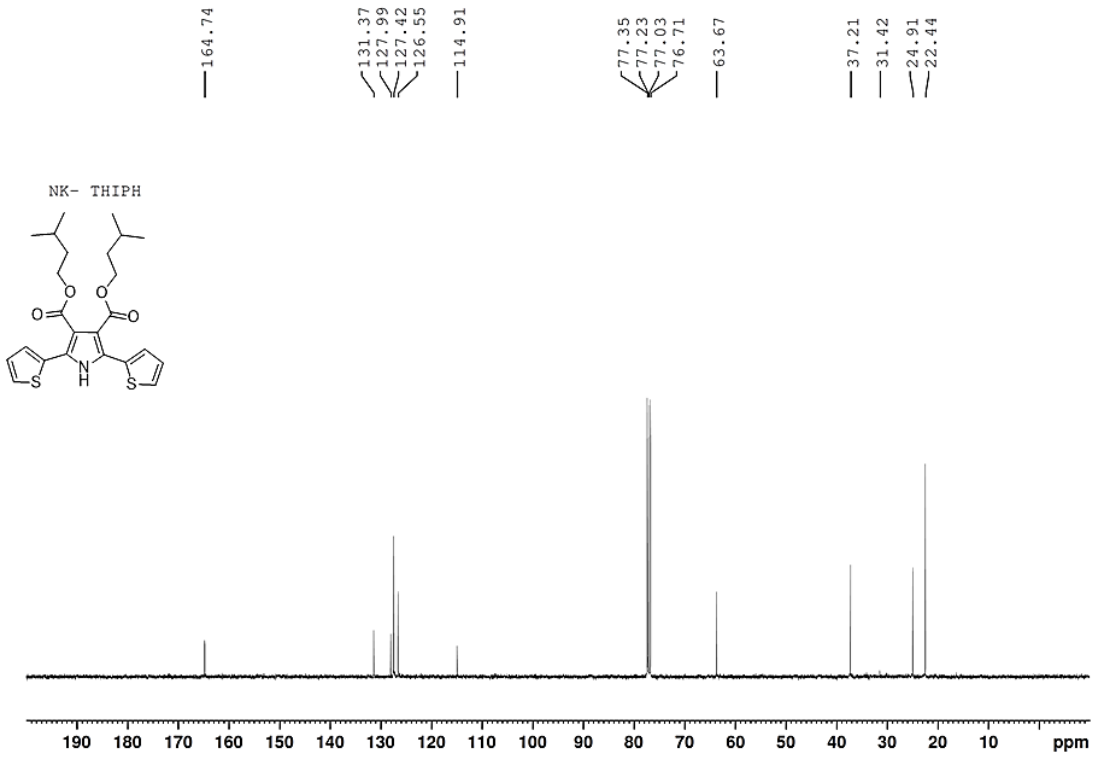

Figure 4.34 ^{13}C NMR spectrum of **4.31** in $CDCl_3$.

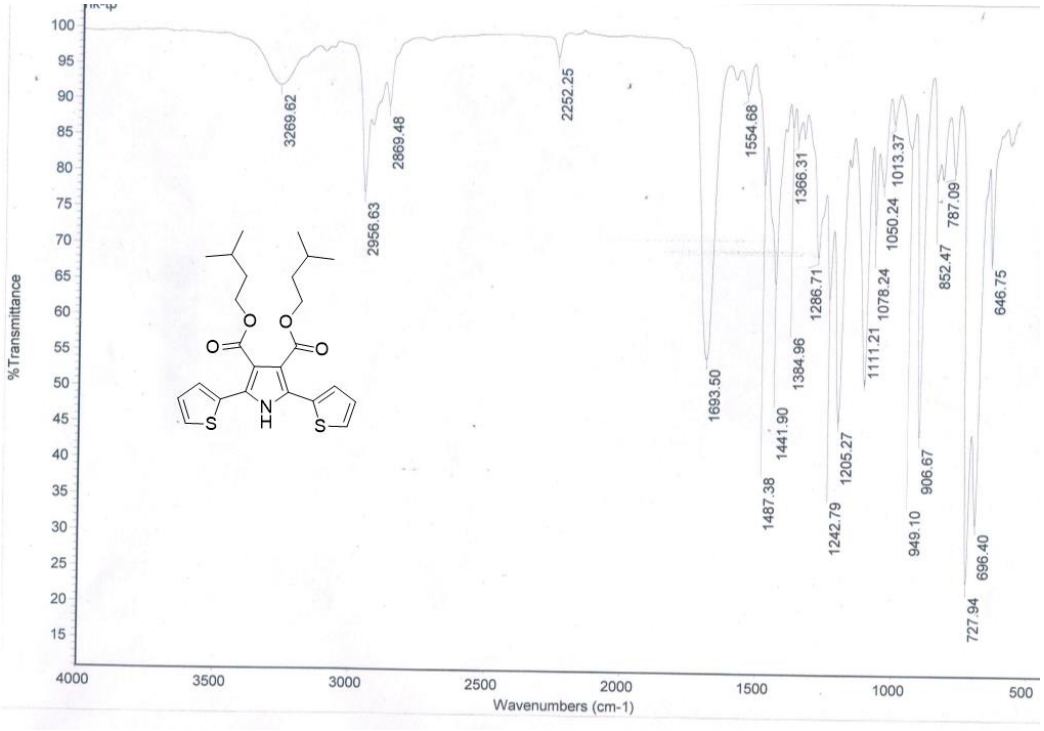

Figure 4.35 IR spectrum of **4.31**.

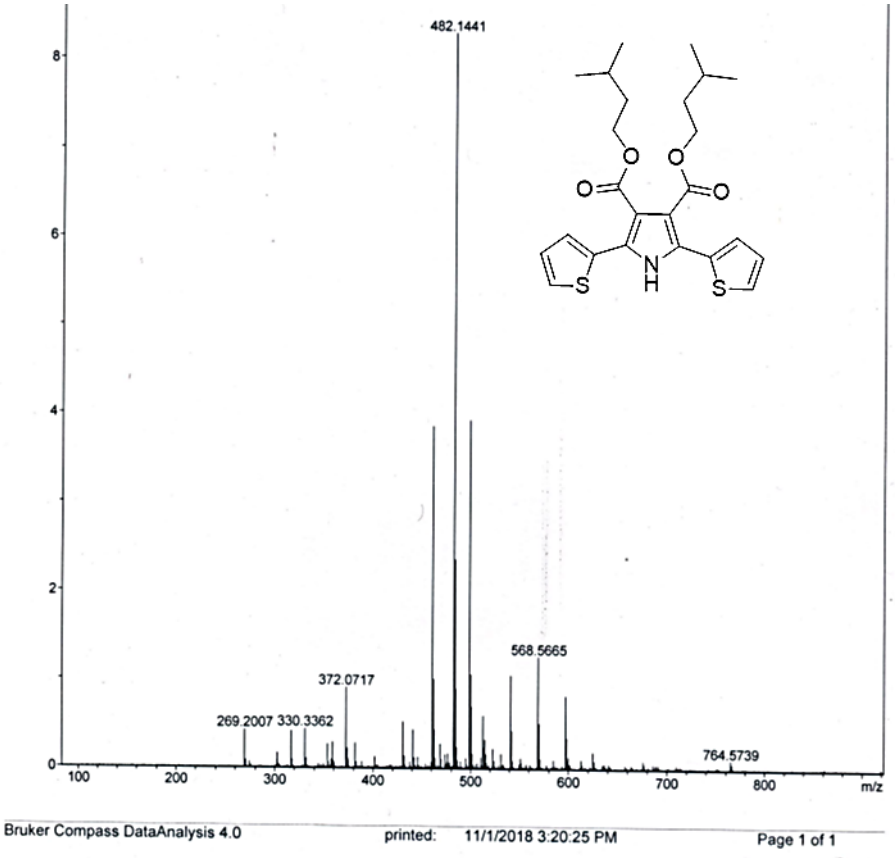

Figure 4.36 HRMS spectrum of **4.31**$[M+Na]^+$ $C_{24}H_{29}NO_4S_2Na$: 482.1435, found 482.1441.

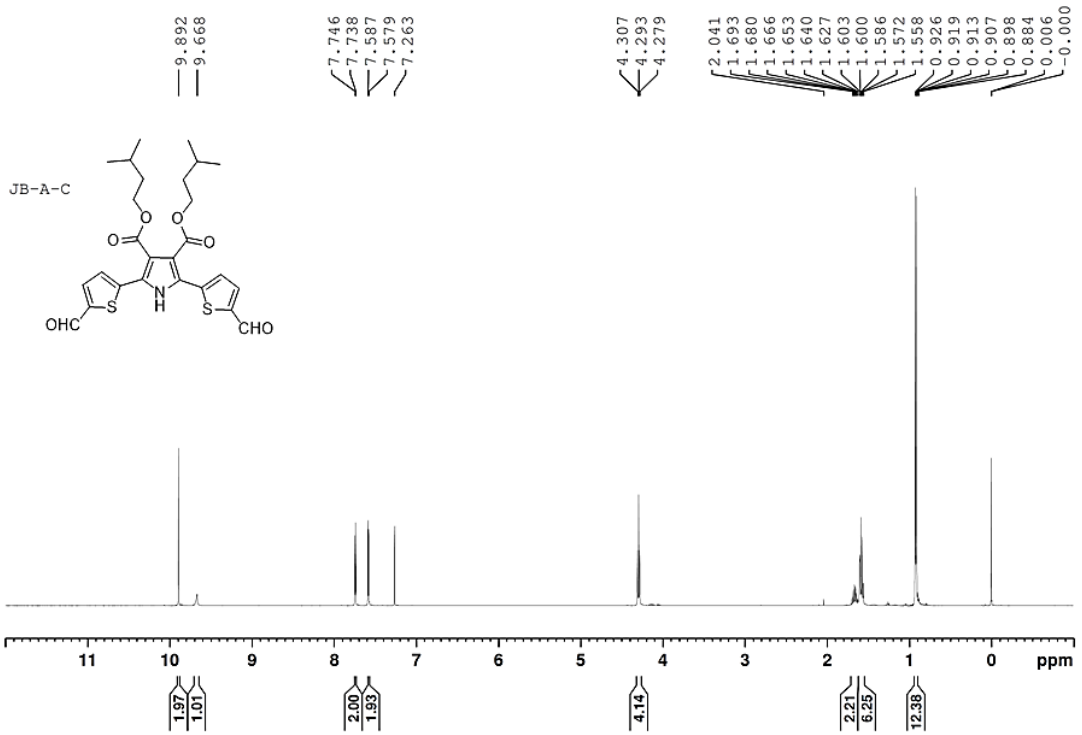

Figure 4.37 ^{1}H NMR spectrum of **4.32** in $CDCl_3$.

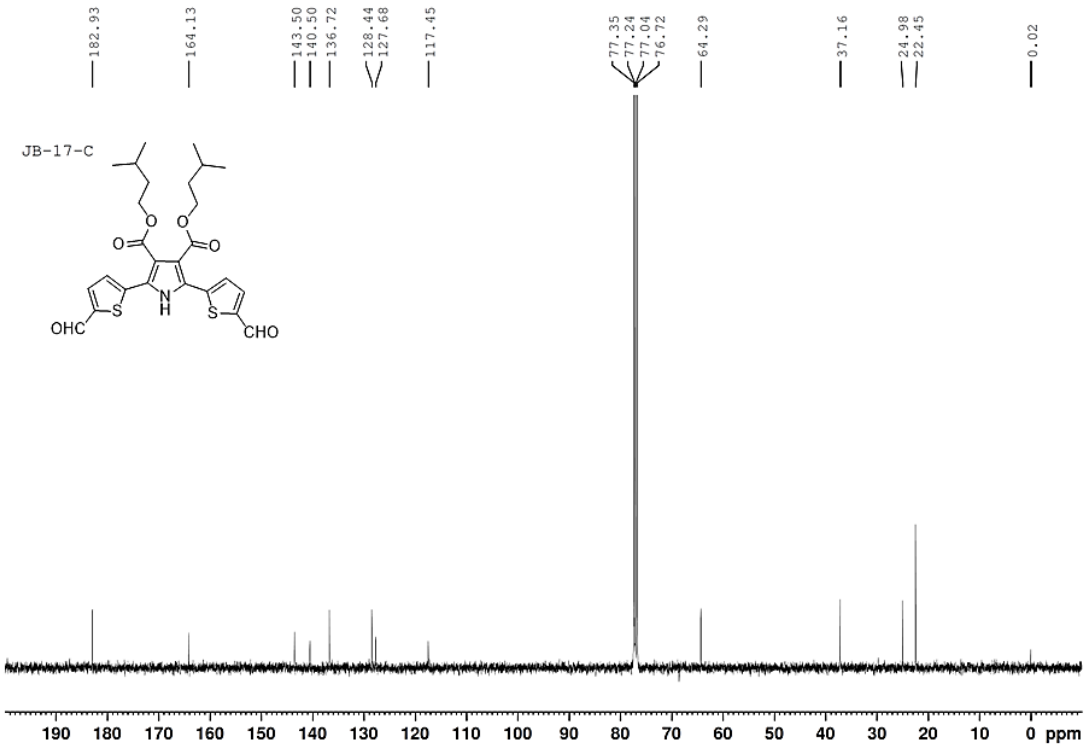

Figure 4.38 ^{13}C NMR spectrum of **4.32** in $CDCl_3$.

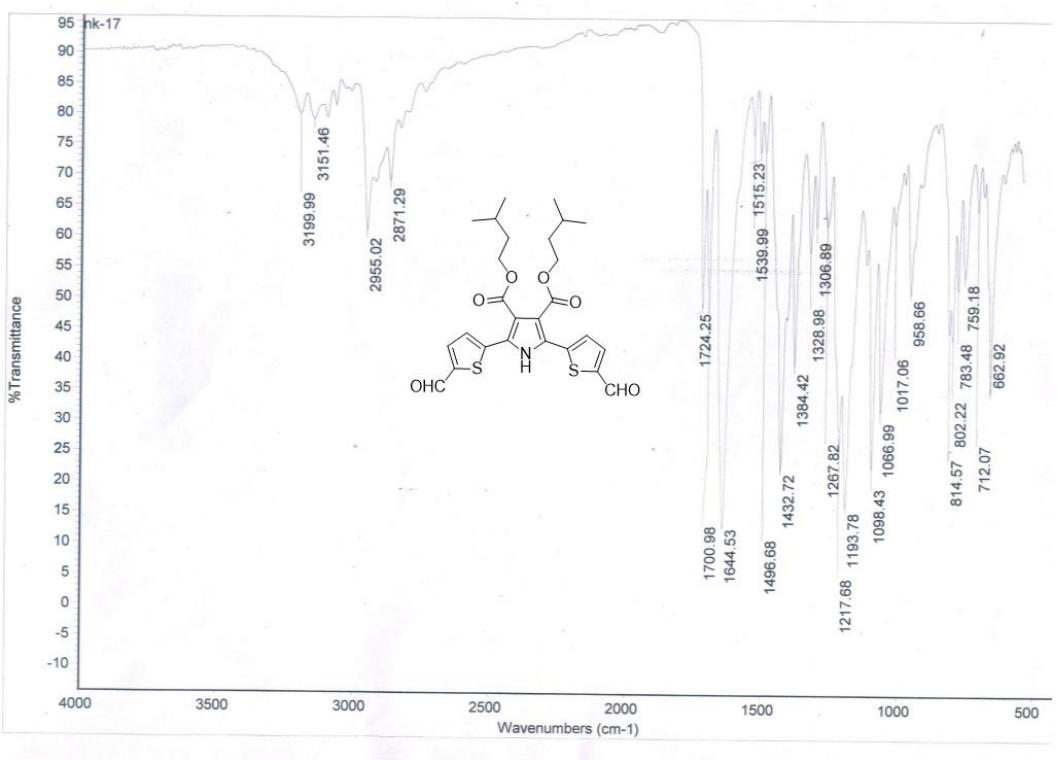

Figure 4.39 IR spectrum of **4.32**.

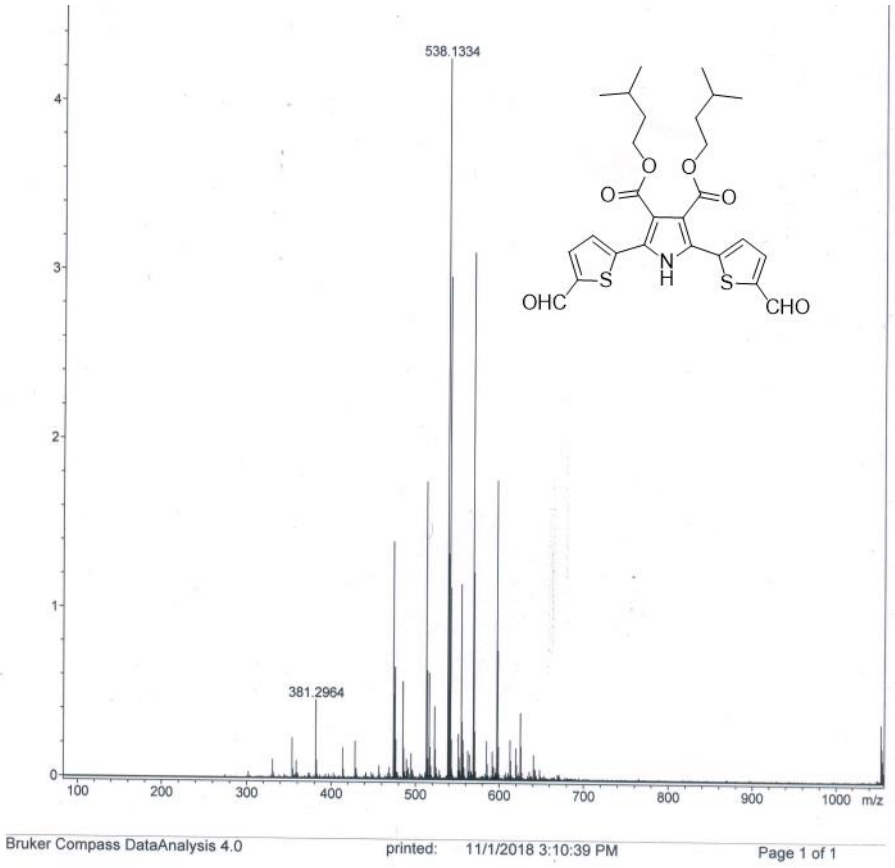

Figure 4.40 HRMS spectrum of **4.32** $[M+Na]^+$ $C_{26}H_{29}NO_6S_2Na$: 538.1334, found 538.1334.

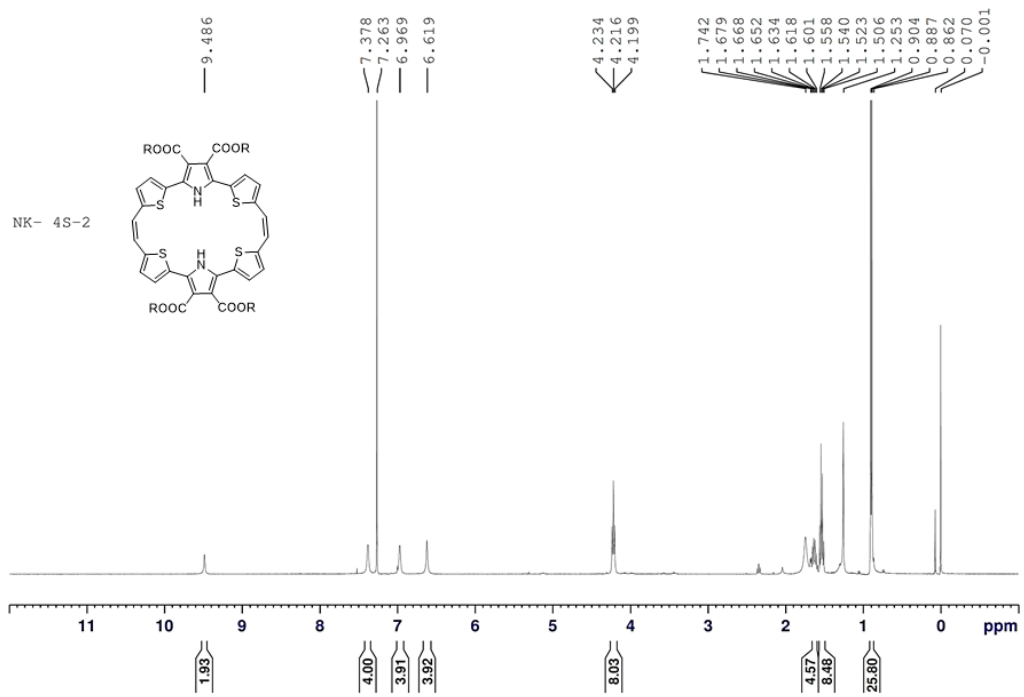

Figure 4.41 ^{1}H NMR spectrum of **4.33** in $CDCl_3$.

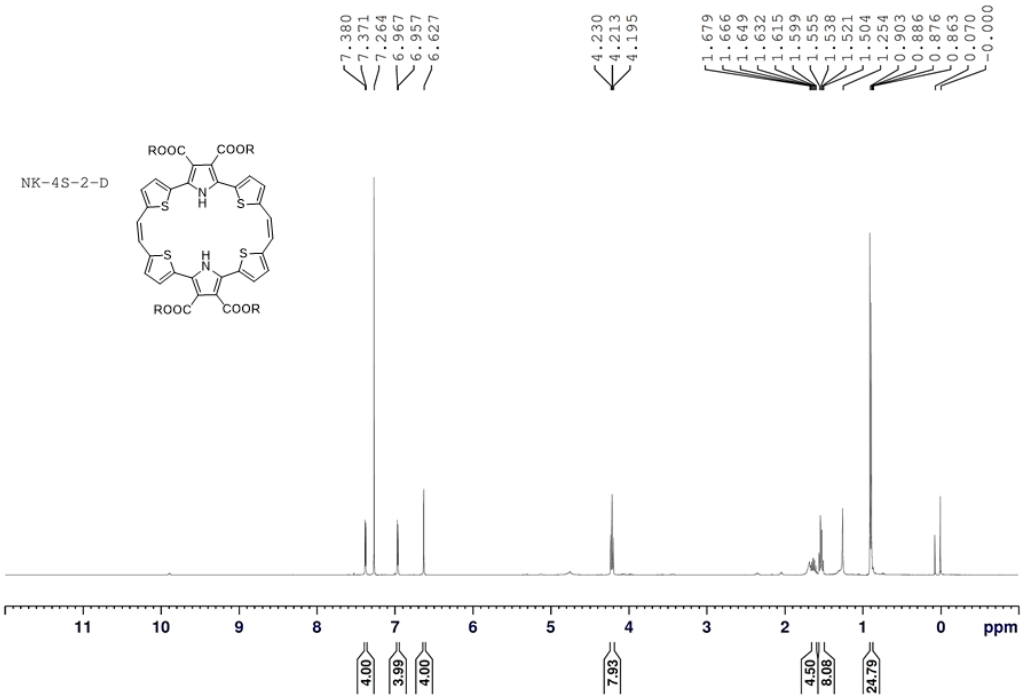

Figure 4.42 ^{1}H NMR spectrum of **4.33** in $CDCl_3$ + D_2O.

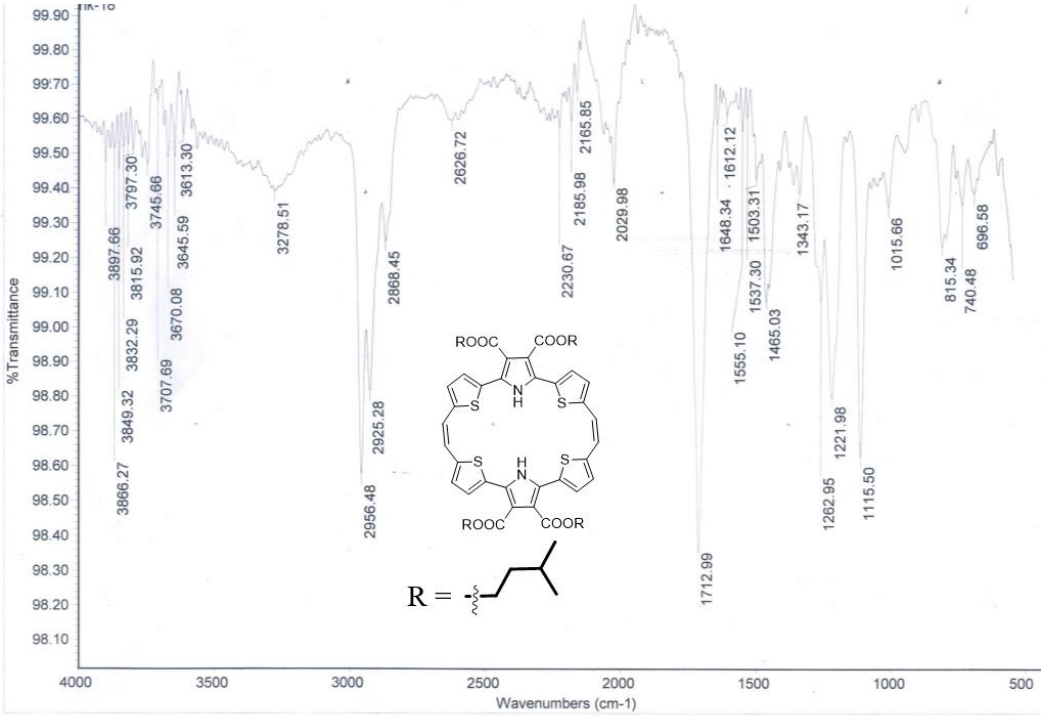

Figure 4.43 IR spectrum of **4.33**.

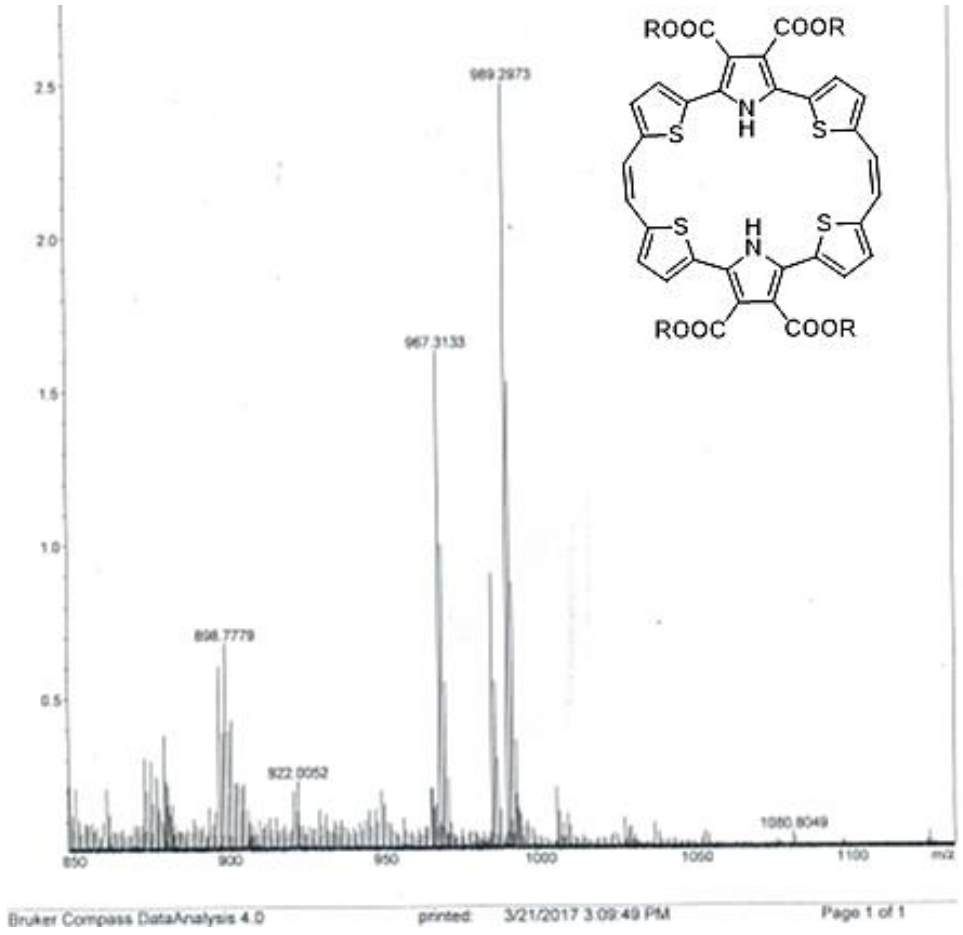

Figure 4.44 HRMS spectrum of **4.33** $[M+Na]^+$ $C_{52}H_{58}N_2O_8S_4Na$: 989.2974, found 989.2973.

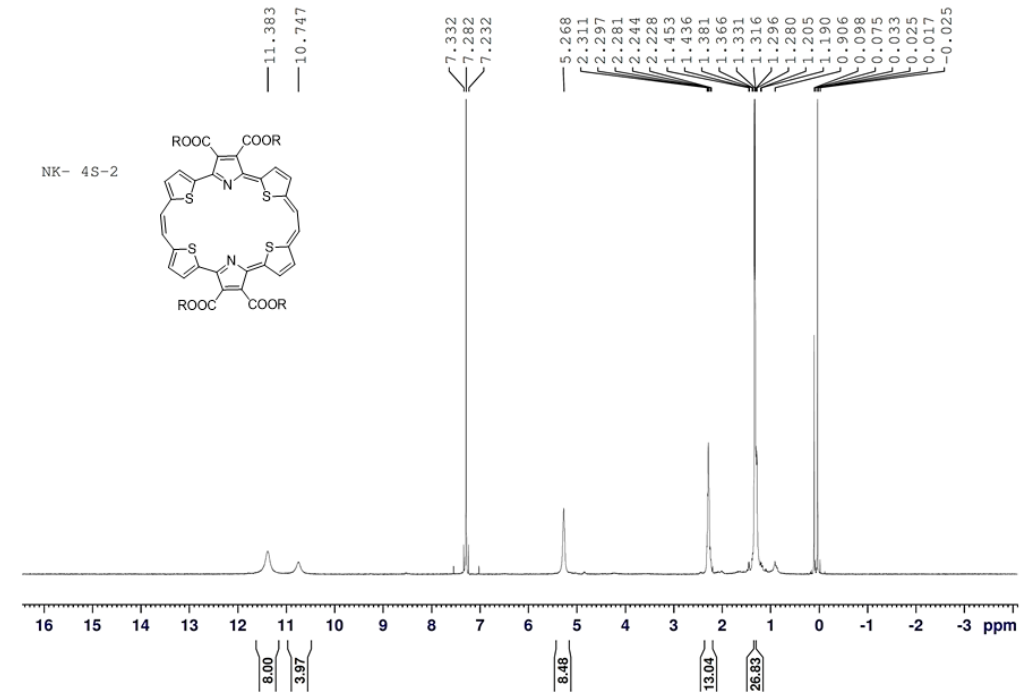

Figure 4.45 ^{1}H NMR spectrum of **4.34** in $CDCl_3$.

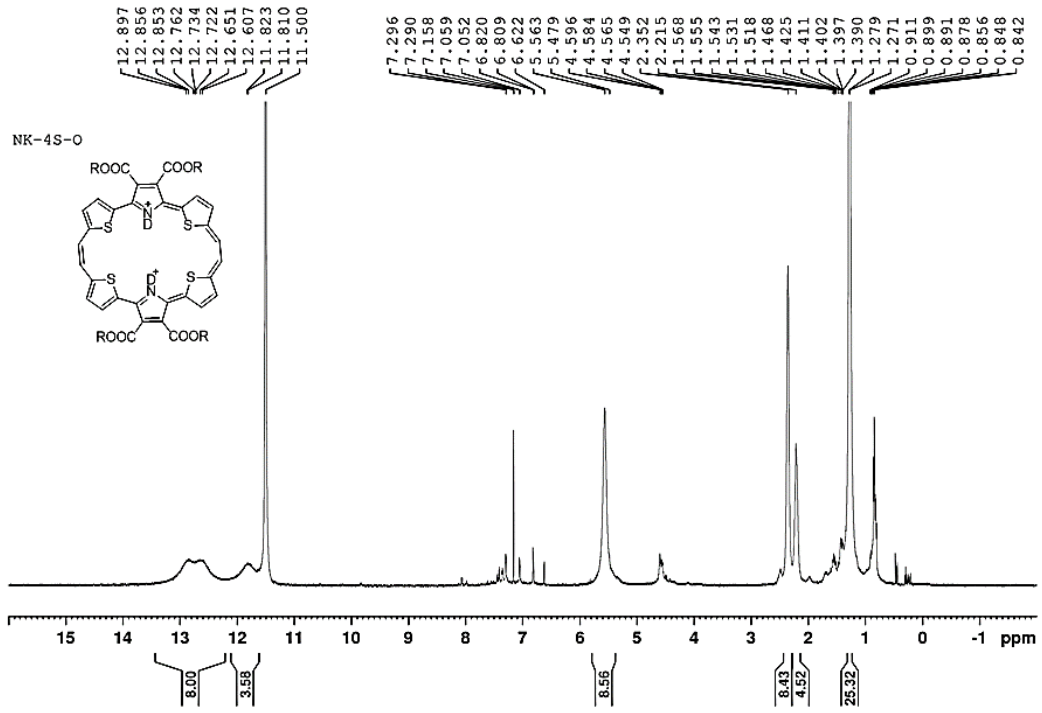

Figure 4.46 ^{1}H NMR spectrum of **4.34** in TFA-*d*.

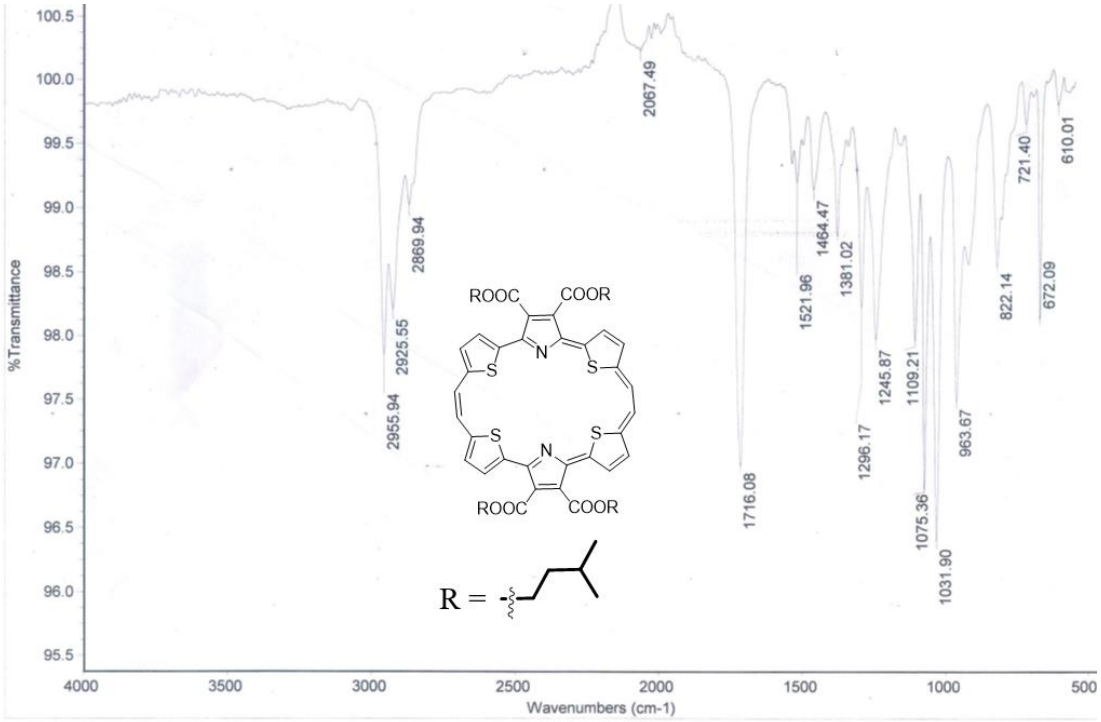

Figure 4.47 IR spectrum of **4.34**.

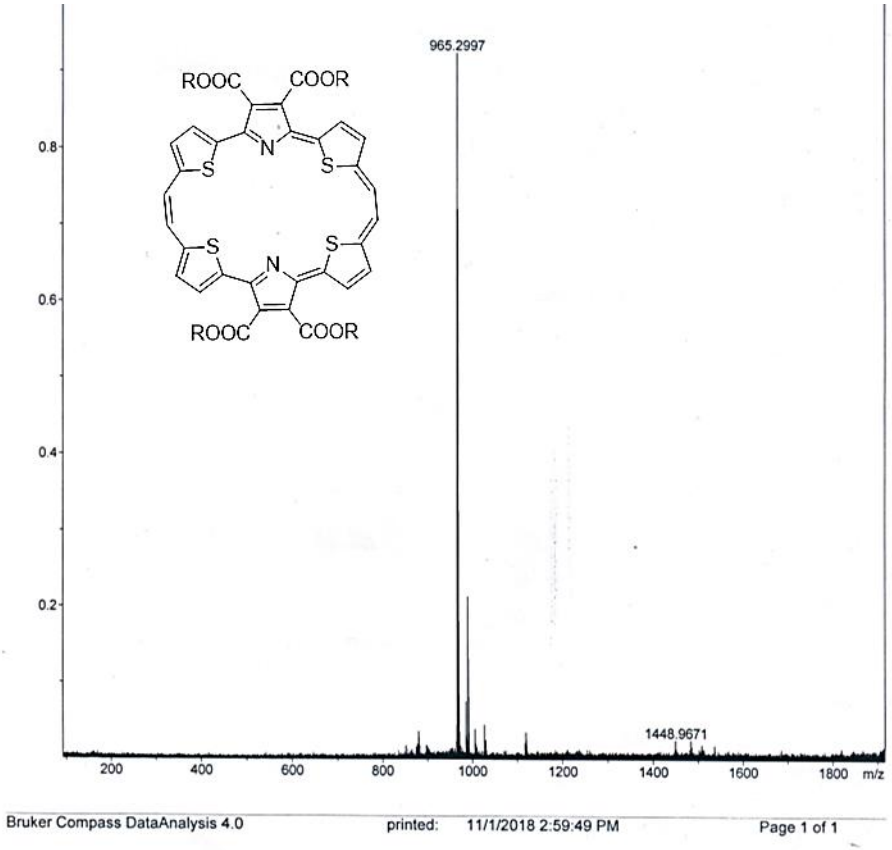

Figure 4.48 HRMS spectrum of **4.34** $[M+H]^+$ $C_{52}H_{57}N_2O_8S_4$: 965.2998, found 965.2997.

CHAPTER 5

Conclusion

5.1 Summary

The thesis entitled "*Exploration of bronzaphyrin – A 26π hexaphyrin(2.0.0.2.0.0) near infrared dye: Synthesis, structure and aromatic switching*" which consists of five chapters. The first chapter provides brief overview about the importance of expanded porphyrins along with various synthetic methodologies, photophysical properties and applications. The second chapter deals with materials and methods employed during the course of the research work. Subsequently, there are two chapters, which provides detail information about facile synthesis, structural diversities, photophysical aspects and aromaticity of bronzaphyrins. Finally, the current chapter provides overall summary of the research work carried out.

5.1.1 Introduction

Expanded porphyrins came to limelight by showcasing their wide range of applications ranging from biomedical science to sensing and material to optoelectronics. Although different kinds of expanded porphyrins pertaining to the number of pyrroles and/or meso positions and their combinations are well explored, there is still much scope in their effective synthesis, analyzing photophysical aspects, understanding structural diversities and investigating their NLO properties. In this aspect, we chose to revisit the bronzaphyrin,[1] a 26π-aromatic expanded porphyrin displaying intense near infrared absorption, which was ignored for more than two decades in spite of its early promise. A glimpse at its early chemistry revealed tedious synthetic procedures and little known structural and photophysical aspects. This chapter highlights the hassle-free synthesis of several novel bronzaphyrins through different approaches along with major findings regarding their structural, aromaticity and photophysical aspects.

5.1.2 Synthetic achievements

We have demonstrated a simple one pot approach in synthesizing acetylene and butadiyne bridged bipyrroles, utilizing a modified Sonogashira coupling in good to moderate yields.[1] One of the butadiyne bridged bipyrrole was employed in achieving terpyrroles by converting the butadiyne bridge to the corresponding heterocycles, which were further utilized in the synthesis of dithiabronzaphyrin[2] and first all-aza bronzaphyrin,[3] providing a much facile route in achieving these macrocycles. We have also synthesized stable α-free and N-unprotected terpyrrole endowed with β-ester groups through Suzuki coupling. This terpyrrole was subsequently utilized in synthesizing the first aromatic tetrathiabronzaphyrin in good yield.[4]

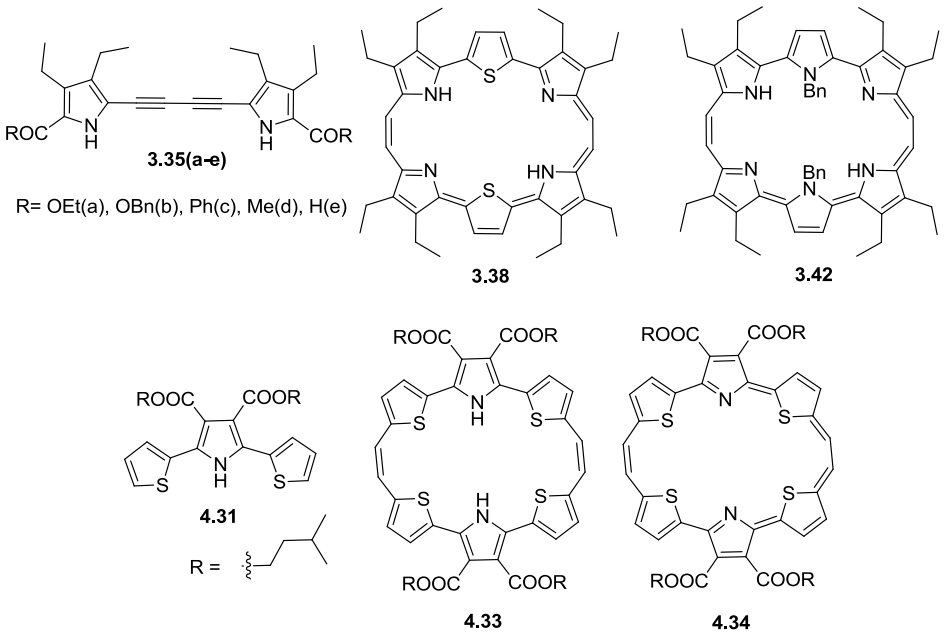

5.1.3 ^{1}H NMR studies

Assignment of peak positions of NH and other aromatic/antiaromatic protons of expanded porphyrins is always an ardent task due to flexible geometries. In case of dithiabronzaphyrin **3.38**, due to the strong hydrogen bonding effect, NH protons were deshielded akin to pophycenes[5] and the inversion of thiophene moieties led to an upfield shifting of the *β*-protons of thiophene which resonated in the negative region. This conformation remained stable even at 80°C, indicating the structural rigidity of the macrocycle. However, the protonation of dithiabronzaphyrin **3.38** shifted NH protons to upfield region and resonated along with the *β*-protons of thiophene due to lack of hydrogen bonding.[2] In case of diprotonated all-azabronzaphyrin **3.42**, a trans conformation led two of the meso protons to resonate in the negative region along with the benzylic protons, due to the strong aromatic ring current.[3] Tetrathiabronzaphyrin **4.34** displayed a ^{1}H NMR spectral pattern similar to aromatic macrocycles in which both the meso and *β*-protons of thiophene were downfield shifted indicating a normal conformation.[4]

5.1.4 Structural aspects

Solid state structural characterization done for the first time for this class of macrocycles revealed intriguing structural diversities. Dithiabronzaphyrin **3.38** crystallized both in freebase and protonated forms confirmed the inversion of thiophene rings, which might have occurred probably owing to the presence of inner ethyl groups on the neighboring

pyrroles at the periphery of the macrocycle. As a consequence, thiophene rings reside with a dihedral angle of 22° with respect to (w.r.t.) the mean plane of the two pyrroles of the terpyrrolic moiety (excluding Hs and ethyl Cs). The protonated dithiabronzaphyrin, in its crystal packing displayed binding to four open hydrogen bridged dimeric TFA ions, $[(CF_3COO)_2H]^-$ in a unique anion coordination mode to form a stacked network, having

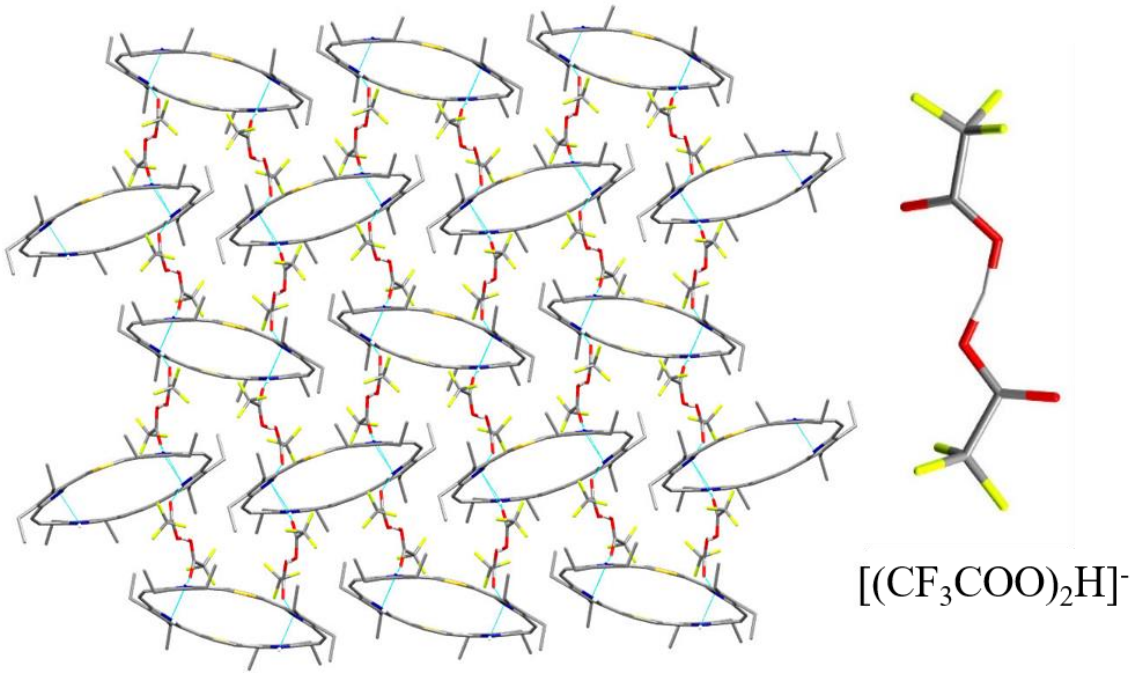

no precedence in porphyrin chemistry.[2] Furthermore, the all-azabronzaphyrin **3.42** crystallized as both dichloride and monochloride salts and revealed *trans*-alkene bridged meso double bonds indicating rich structural diversities that this class of macrocycles could adopt, which is a rare phenomenon in expanded porphyrin chemistry.[3] The reduced tetrathiabronzaphyrin **4.33** displayed three conformations in a single asymmetric unit probably due to hydrophobic interactions of long alkyl chains present in ester groups.[4]

5.1.5 Photophysical properties

All the bronzaphyrins display intense absorption in the NIR region making them unique among the hexaphyrins endowed with meso bridges. Dithiabronzaphyrin **3.38** exhibits strong sensitivity towards substituents e.g. presence of four additional inner β-ethyl substituents led to 45 nm red shift in the lowest energy absorption band. Further, the lowest energy Q-band is quite sharp (almost 80%) compared to the higher energy Soret band. Due to strong hydrogen bonding between the pyrroles across the meso bridges, dithiabronzaphyrin **3.38** required large quantity of acid for achieving the diprotonation and resulted in enhancement of intensity of the peaks probably due to lack of tautomerism

with red-shifted Soret and slightly blue-shifted sharp Q-band.[2] On the other hand, the all-azabronzaphyrin **3.42** exhibits an intense broad Soret band owing to merger of two bands along with intense NIR Q-bands, whose tail reaches up to 1100 nm. Interestingly, the all-azabronzaphyrin doesn't undergo much changes upon protonation except a blue shift of the lowest energy band, indicating possibly its core is not much affected during the process.[3] Tetrathiabronzaphyrin **4.34** exhibited much red shifted absorption when compared to dithiabronzaphyrins, tail reaching up to 1050 nm. Surprisingly, protonation study with HCl generated back the 28π-electron system i.e. the reduced bronzaphyrin **4.33** via a radical intermediate 27π-electron system. Though the intermediate can be converted back to freebase by quenching with triethylamine, the completely reduced species remained unaffected by triethylamine. The 26π-aromatic bronzaphyrin **4.34** can be directly reduced to the corresponding reduced derivative **4.33** in presence of sodium dithionite or potassium superoxide and again reverted back to oxidized species employing MnO_2, indicating a redox switch between all the three states.[4]

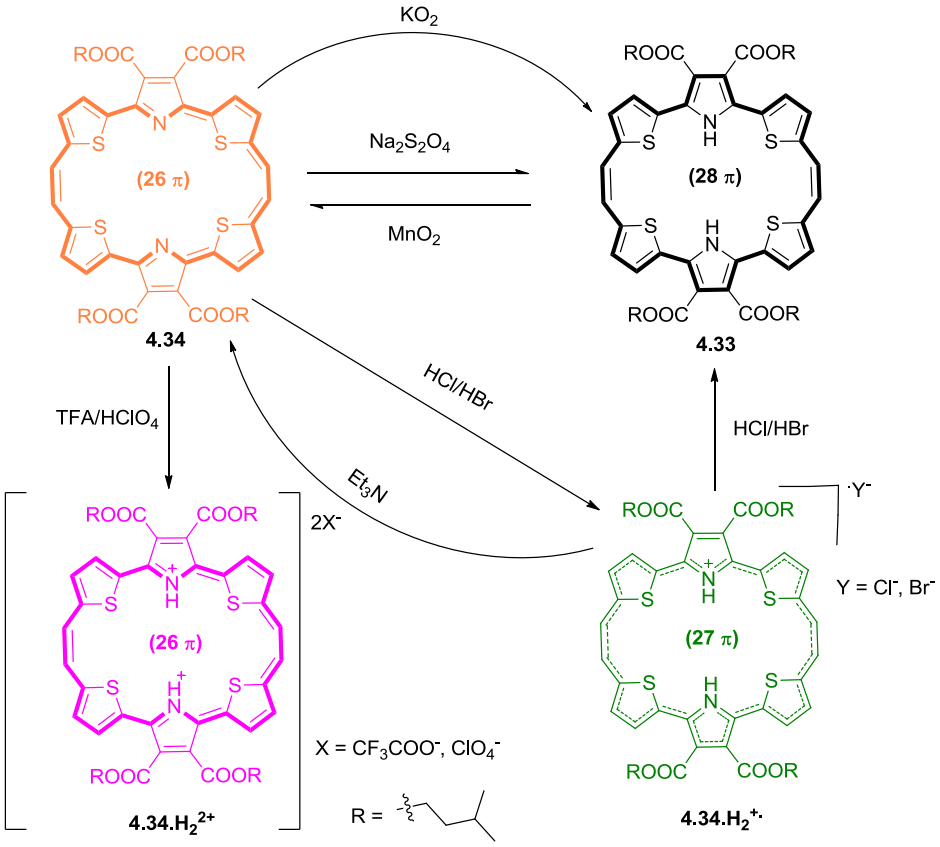

5.1.6 DFT studies

The DFT studies clearly revealed that the inverted structure possessed minimum energy in case of dithiabronzaphyrin **3.38**, but maximum energy in case of previously reported dithiabronzaphyrin **3.18**, accounting for the steric effect of the inner four ethyl substituents. The theoretical studies also showed that the peak arising in the negative region of ^{1}H NMR spectrum to be the β-protons of thiophene ring and the NH protons are much more deshielded.[2] Studies also demonstrate the stability of trans conformation in case of protonated all-azabronzaphyrin.[3] The TD-DFT studies revealed that the simulated absorption spectra coincide well with the steady state absorption spectra. It further confirmed the aromaticity of all bronzaphyrins with the help of NICS and HOMA calculations.

We believe, the two facile routes developed in attaining the bronzaphyrins will attract other researchers in developing this class of macrocycles. Interestingly, all the bronzaphyrin derivatives displayed intriguing structural diversities and photophysical properties indicating the subtle effects of substitution on the periphery and the inner core of the macrocycles. Hopefully, with this work, we have created again a great scope and enthusiasm in this class of macrocycles and at present our efforts are directed to further broaden its scope and utility.

5.2 References

1. Kishore, M. V. N.; Panda, P. K. *Eur. J. Org. Chem*. **2017**, 5197.
2. Kishore, M. V. N.; Panda, P. K. *Chem. Commun.* **2018**, *54*, 13135.
3. Kishore, M. V. N.; Panda, P. K. (manuscript under preparation)
4. Kishore, M. V. N.; Kang, S.; Kim, D.; Panda, P. K. (manuscript under preparation)
5. Waluk, J. *Chem. Rev*. **2017**, *117*, 2447.

Research Publications (Thesis)

1. One-Pot Synthesis of Butadiyne-Bridged Bipyrrole Derivatives and Bisporphyrin, **Kishore, M. V. N.**; Panda, P. K. *Eur. J. Org. Chem*. **2017**, 5197-5203.
2. Revisiting the intense NIR active bronzaphyrin, a 26-π aromatic expanded porphyrin: Synthesis and structural analysis, **Kishore, M. V. N.**; Panda, P. K. *Chem. Commun.* **2018**, *54*, 13135-13138.
3. Conformational flexibility of an intense NIR active first all-aza bronzaphyrin, **Kishore, M. V. N.**; Panda, P. K. (Manuscript under preparation).
4. Aromaticity switching in first 26π-tetrathiabronzaphyrin, **Kishore, M. V. N.**; Panda, P. K. (Manuscript under preparation).

Conference presentations

1. Oral presentation on "Facile synthesis of Dithiabronzaphyrin – A [26]hexaphyrin(2.0.0.2.0.0), with an intense near infrared absorption", **Andhra Pradesh Science Congress (APSC-2018)**, Yogi Vemana University, Kadapa, Andhra Pradesh, India, November 9-11, **2018**.
2. Poster presentation on "First synthesis of 26π-aromatic tetrathiabronzaphyrin – An Expanded Porphyrin with intense Near Infrared Absorption", **International Collaborative & Cooperative Chemistry Symposium (ICCCS-8)**, School of Chemistry, University of Hyderabad, Hyderabad, India, December 18-19, **2017**.
3. Oral and poster presentation on "Bronzaphyrin – A 26π-aromatic expanded porphyrin: Synthesis and photophysical properties", **12th Annual in house symposium** (**Chemfest-2015**), School of Chemistry, University of Hyderabad, Hyderabad, India, February 20-21, **2015**.
4. Poster presented on "Synthesis of diacetylene bridged bipyrrole and its application in the synthesis of Bronzaphyrins", **New Directions in Chemical Sciences**, Department of Chemistry, Indian Institute of Technology Delhi, New Delhi, December 7-9, **2012**.
5. Poster presented on "Synthesis of 1,2(4)-dipyrrolyl, 1,2(4)-bisporphyrinyl ethynes and butadiynes", **9th Annual in house symposium** (**Chemfest-2012**), School of Chemistry, University of Hyderabad, Hyderabad, India, February 25-26, **2012**.
6. Poster presented on "Synthesis of mono- and diacetylene bridged bipyrrole derivatives: Building blocks for the syntheses of porphyrinoid derivatives", **New**

Dimensions in Chemical Sciences, Department of Chemistry, P. G. College of Science, Saifabad, Osmania University, Hyderabad. India, January 30, **2010**.

Exploration of bronzaphyrin – A 26π hexaphyrin(2.0.0.2.0.0) near infrared dye: Synthesis, structure and aromatic switching

by M. V. Nanda Kishore

Exploration of bronzaphyrin – A 26π hexaphyrin(2.0.0.2.0.0) near infrared dye: Synthesis, structure and aromatic switching

ORIGINALITY REPORT

19%	2%	19%	2%
SIMILARITY INDEX	INTERNET SOURCES	PUBLICATIONS	STUDENT PAPERS

PRIMARY SOURCES

1	Nanda Kishore M V, Pradeepta Panda. "Revisiting the intense NIR active bronzaphyrin, a 26-π aromatic expanded porphyrin: Synthesis and structural analysis", Chemical Communications, 2018 Publication	8%
2	Shohei Saito. "Expanded Porphyrins: Intriguing Structures, Electronic Properties, and Reactivities", Angewandte Chemie International Edition, 05/02/2011 Publication	2%
3	Takayuki Tanaka, Atsuhiro Osuka. " Chemistry of -Aryl-Substituted Expanded Porphyrins: Aromaticity and Molecular Twist ", Chemical Reviews, 2016 Publication	2%
4	M. V. Nanda Kishore, Pradeepta K. Panda. "One-Pot Synthesis of Butadiyne-Bridged Bipyrrole Derivatives and Bisporphyrin", European Journal of Organic Chemistry, 2017	2%

	Publication	
5	M. V. Nanda Kishore, Pradeepta K. Panda. "Revisiting the intense NIR active bronzaphyrin, a 26-π aromatic expanded porphyrin: synthesis and structural analysis", Chemical Communications, 2018 Publication	1%
6	Bartosz Szyszko, Michał J. Białek, Ewa Pacholska-Dudziak, Lechosław Latos-Grażyński. "Flexible Porphyrinoids", Chemical Reviews, 2016 Publication	1%
7	www.rsc.org Internet Source	1%
8	Shin, Jae-Yoon, Kil Suk Kim, Min-Chul Yoon, Jong Min Lim, Zin Seok Yoon, Atsuhiro Osuka, and Dongho Kim. "Aromaticity and photophysical properties of various topology-controlled expanded porphyrins", Chemical Society Reviews, 2010. Publication	<1%
9	Submitted to University of Hyderabad, Hyderabad Student Paper	<1%
10	repositories.lib.utexas.edu Internet Source	<1%